

# **Investigating the characteristics of drug binding to the inner cavity of hERG potassium channels**

Thesis submitted for the degree of  
Doctor of Philosophy  
at the University of Leicester

by

Michael Woun Yein Chang BSc  
Department of Cell Physiology and Pharmacology  
University of Leicester

February 2010

## Abstract

### **Title: Investigating the characteristics of drug binding to the inner cavity of hERG potassium channels**

Michael Woun Yein Chang

The human Ether à-go-go Related Gene (hERG) channel makes up the pore forming subunit of the  $I_{Kr}$  channel. This channel is involved in the repolarisation of the cardiac action potential. Reduction in  $I_{Kr}$  may cause the prolongation of the action potential, leading to fatal arrhythmias. A large variety of potentially therapeutic compounds inhibit the  $I_{Kr}$  channels, leading to acquired long QT syndrome. Therefore characterisation of the channel and improvements to *in silico* models are needed to accurately predict potential hERG side effects.

The aim of this project was to use a series of analogues to block the hERG  $K^+$  channel, using them as molecular rulers to measure the size of the inner cavity. The phenotype of block was examined to see whether increasing length, results in a change in the phenotype of block from a drug trapping type to a foot in the door one. This would have given an estimate of the size of the hERG inner cavity.

Excised inside-out patches of hERG channels display a significant rundown with time after excision. The project also investigated the region of hERG responsible for rundown. A chimeric channel between hERG and bEAG, a closely related channel that does not display rundown, was produced. The aim was to produce a channel with hERG properties, but without the rundown characteristic. This chimeric channel could then be used in excised inside-out patch recordings.

The series of derivatives were found to have high affinity to the hERG channel. However, they displayed unusual blocking characteristics, inhibiting the channel in the open state, yet unbound in the closed state. It was also found that the C-terminus of hERG appears to be responsible for the rundown characteristic. The exchange for that of bEAG resulted in a channel that had attenuated rundown.

## **Acknowledgements**

I would like to sincerely thank my supervisor Dr John Mitcheson for giving me the opportunity to work in his research laboratory and for his constant support, patience, guidance and encouragement throughout the duration of this project.

I particularly want to thank Dr Rachael Hardman, Dr Matt Perry, Dr Sarah Nelson for their contributions and guidance to some of the recordings and other technical aspects of the project. I also extend my thanks to my research colleagues both past and present in the department with whom I had many fruitful discussions with throughout the course of this work.

I am grateful to the Medical Research Council and Martin Gosling at Novartis for providing the funding in order to carry out this project.

Final thanks go to my partner, friends and family who have followed me on this journey, offering their love, faith and support.

## Abbreviations

APD	Action potential duration
AMP-PCP	Adenosine 5'-monophosphate, monoanhydride with (phosphonomethyl)-phosphonic acid
ATP	Adenosine triphosphate
BAPTA	1,2-bis(2-aminophenoxy)ethane-N,N,N',N'-tetraacetic acid
bEAG	Bovine ether à-go-go
BHS16	hERG channel with the N- and C-terminus exchanged with bEAG
cAMP	Cyclic adenosine monophosphate
cfu	Colony forming unit
CHO cells	Chinese hamster ovary cells
CNBD	Cyclic nucleotide binding domain
DEPC	Diethylpyrocarbonate
DMSO	Dimethyl sulphoxide
DNA	Deoxyribonucleic acid
EAD	Early after depolarisation
EAG	Ether à-go-go
ECG	Electrocardiogram
EGTA	Ethylene glycol tetraacetic acid
ELK	Ether à-go-go like potassium channel
HEK-293 cells	Human embryonic kidney cells
hERG	Human ether à-go-go related gene
KAT1 channel	Hyperpolarisation activated K <sup>+</sup> channel
LB	Lysogeny broth
LQT	Long QT
LQTS	Long QT syndrome
MES	2-[N-morpholino]ethanesulfonic acid
MESA	MOPS-EDTA-sodium acetate

MiRP1	MinK related peptide
MLS-9 cells	rat microglia cell line
MOPS	3-(N-morpholino)propanesulfonic acid
NBHHC	hERG channel with the N-terminus exchanged with bEAG
NHHBC	herG channel with the C-terminus exchanged with bEAG
NTK hERG	hERG channel with a truncated N-terminus
PIP2	Phosphatidylinositol bisphosphate
PKC	Protein kinase C
RNA	Ribonucleic acid
SOC	Super optimal broth with catabolite repressant
TEVC	Two electrode voltage clamp
UTR	Untranslated region
WT	Wild type

# Contents

<b>Abstract .....</b>	<b>ii</b>
<b>Acknowledgements .....</b>	<b>iii</b>
<b>Abbreviations .....</b>	<b>iv</b>
<b>Contents .....</b>	<b>vi</b>
<b>Chapter 1: Introduction .....</b>	<b>2</b>
<b>Ions and ion channels.....</b>	<b>2</b>
<b>The cardiac action potential .....</b>	<b>5</b>
<b>IK<sub>r</sub> channel structure.....</b>	<b>9</b>
<b>The hERG channel structure .....</b>	<b>10</b>
<b>The hERG drug binding site .....</b>	<b>12</b>
<b>Long QT syndrome.....</b>	<b>14</b>
<b>Predicting LQT potential.....</b>	<b>16</b>
Use of cell lines to predict LQT potential .....	16
The use of animal models to predict LQT potential .....	18
In silico predictions of LQT potential.....	20
<b>Drug trapping in hERG.....</b>	<b>24</b>
<b>Foot in the door.....</b>	<b>26</b>
<b>Rundown.....</b>	<b>27</b>
<b>Chapter 2: Materials and methods .....</b>	<b>30</b>
<b>Molecular Biology .....</b>	<b>30</b>
Creation of chimeras.....	30
Sequencing .....	30
Restriction digests.....	31
Gel extraction.....	34
DNA ligation .....	34
Bacteria transformation.....	36

In vitro transcription.....	38
Xenopus Oocyte isolation and injection with cRNA.....	39
<b>Electrophysiological recordings .....</b>	<b>40</b>
Two Electrode Voltage Clamp of Xenopus oocytes .....	40
Recording solutions .....	44
<b>Patch Clamping .....</b>	<b>44</b>
The patch clamp setup.....	48
Solutions for patch clamp recordings.....	49
Excised inside-out patch clamp recordings .....	51
Data analysis of the electrophysiological recordings.....	52
Voltage dependence of activation.....	52
Fitting exponential functions .....	53
Concentration-response relationships .....	54
<b>Chapter 3: Characterising the voltage dependant properties of hERG/bEAG chimeras .....</b>	<b>55</b>
<b>Introduction .....</b>	<b>55</b>
<b>Results .....</b>	<b>56</b>
Characterisation of the Chimeras .....	56
Characterisation of current-voltage relationships .....	59
Time dependent kinetics of activation.....	61
The chimeras deactivate rapidly compared to WT hERG .....	66
Voltage dependence of recovery from inactivation.....	70
<b>Discussion .....</b>	<b>72</b>
The N- and C-termini are required for normal deactivation gating in hERG.....	72
The N- and C-termini interact to modify activation .....	74
Activation kinetics of the chimeric channels .....	74
Inactivation is present in hERG/bEAG chimeras .....	76
<b>Chapter 4: Characterising the pharmacological properties of hERG/bEAG chimeras .....</b>	<b>79</b>

<b>Introduction .....</b>	<b>79</b>
<b>Results .....</b>	<b>81</b>
E-4031 potency to chimeric channels.....	81
Propafenone potency to chimeric channels.....	84
What is the mechanism for difference in propafenone potency? .....	89
<b>Discussion .....</b>	<b>92</b>
<b>Chapter 5: Excised inside-out patch clamp experiments on hERG/bEAG</b>	
<b>chimeras .....</b>	<b>98</b>
<b>Introduction .....</b>	<b>98</b>
<b>Results .....</b>	<b>99</b>
Rundown of hERG/bEAG chimeras.....	99
Characterisation of the deactivation in patches.....	113
<b>Discussion .....</b>	<b>117</b>
hERG channel deactivation is unchanged on excision.....	120
<b>Chapter 6: Characterising hERG channel block with varying length drug</b>	
<b>molecules .....</b>	<b>123</b>
<b>Introduction .....</b>	<b>123</b>
<b>Results .....</b>	<b>128</b>
Pharmacology of drug intermediates .....	128
Pharmacology of further derivatives of E-4031.....	130
Concentration-response experiments.....	131
Kinetics of drug block.....	137
Do the derivatives exhibit a foot in the door phenotype?.....	143
Pharmacology of hERG channel mutants.....	150
<b>Discussion .....</b>	<b>154</b>
The methanesulphonamide intermediates have lower potency .....	154
E-4031 derivatives bind with high affinity within the inner cavity.....	155
The drugs bind to the channel inner vestibule .....	156
The E-4031 derivatives display an unusual phenotype of block.....	157

Faster deactivating channels do not display foot in the door phenotype.....	160
The derivatives block the hERG channel with an alternative model of block .....	162
<b>Chapter 7: General discussion and further experiments .....</b>	<b>165</b>
<b>The termini of hERG and bEAG interact to alter the gating of hERG .....</b>	<b>165</b>
hERG deactivation gating .....	166
hERG activation gating .....	167
hERG Inactivation .....	168
<b>Exchange of the C-terminus slows the rate of rundown .....</b>	<b>169</b>
<b>hERG binding site .....</b>	<b>171</b>
hERG channel inhibitors block hERG/bEAG chimeric channels in a similar fashion ...	171
E-4031 derivatives have high potency for hERG .....	173
<b>The derivatives block hERG with an unusual phenotype.....</b>	<b>175</b>
<b>Overall summary .....</b>	<b>179</b>
<b>Appendix .....</b>	<b>181</b>
<b>Bibliography.....</b>	<b>184</b>

# Chapter 1: Introduction

## Ions and ion channels

The voltage across the plasma membrane of cells (membrane potential) is caused by a difference in the number of charged ions inside and outside of the cell. This is mainly controlled by various ion pumps and exchangers that use energy to move ions across the membrane against the concentration gradient as well as passive diffusion of ions through ion channels. The passive flow of the ions is determined by the electrochemical gradient for that particular ion; which is determined by the concentration difference and electrical potential across the membrane.

Ion channels have several physiological roles. In inexcitable cells, they have effects on osmolarity, apoptosis, cell size and cell division. And in excitable cells they can regulate resting membrane potential, depolarisation and repolarisation of the cell membrane, refractoriness and action potential firing frequency. The control of passive diffusion of ions is mainly controlled by a diverse set of ion channels. Due to the unequal distribution of  $K^+$  ions across the membrane in most cells,  $K^+$  ions usually have an equilibrium potential that is negative at around -90 mV in excitable cells.  $K^+$  channels are important in the control of membrane potential. This is reflected in the diversity and size of the potassium channel family.

$K^+$  channels are membrane spanning proteins. They are typically composed of four subunits with a series of transmembrane alpha helices and linkers that assemble to create a pore through which ions can flow. Different members of the potassium channel family also have additional functional domains that

regulate the flow of ions through the pore. Our understanding of the principles underlying  $K^+$  channel permeation has increased dramatically since the crystallization of bacteria  $K^+$  channels such as KcsA and MthK by Rod Mackinnon's group.

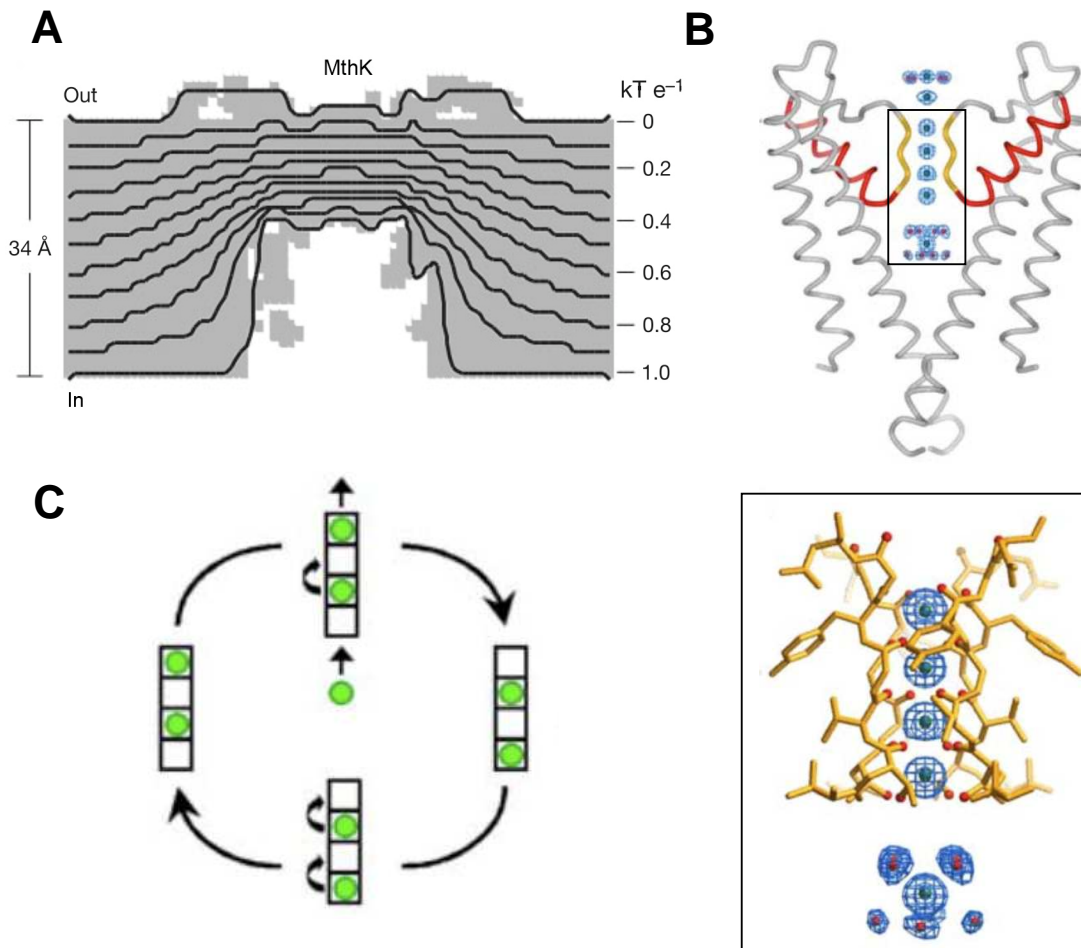


Figure 1.1: A model of the permeation of  $K^+$  ions through the pore of the bacterial potassium channels. **A**, computation of the potential difference across the pore of the MthK channel, showing how the barrier of potential difference is compressed across the pore. **B**, the permeation of potassium through the pore. The top diagram is the tertiary structure of two pore forming subunits of KcsA with potassium ions in 6 configurations around the pore, indicated by the green balls in blue mesh. Water molecules are indicated by the red balls in blue mesh. The lowest one is still fully hydrated in the inner cavity of the channel, and then there are 4 dehydrated ions in the selectivity filter. Finally there is the potassium ion at the extracellular mouth, which is in the process of reacquiring the hydration shell. The lower diagram is an expanded view, of the dehydrated ions in the 1-4 positions in the selectivity filter, with a hydrated potassium ion below it. **C**, The cycle of permeation steps of potassium ion conduction, two ions move through the selectivity filter at one time, going from the 4, 2 configuration to the 1, 3 configuration, then one of the ions will exit the filter and reacquire its hydration shell. (Modified from Jiang *et al.* 2002 and Mackinnon *et al.* 2003)

The central pore is formed by two transmembrane helices from each subunit, connected by a linker that forms a short pore helix and selectivity filter. The transmembrane helices form an inverted teepee structure that can form the intracellular activation gate, this gate controls the ion flow by opening and closing. The narrow selectivity filter is only 12 Å long and this compresses the diffusion distance and energy barrier that the ions have to cross in order to get to the other side of the membrane (Doyle *et al.*, 1998; Jiang *et al.*, 2002). The selectivity filter consists of carbonyl oxygen atoms that are suitably spaced for coordinating dehydrated K<sup>+</sup> ions so that they can selectively permeate the pore (see Figure 1.1). For K<sup>+</sup> channels the highly conserved 'signature' sequence is usually TVGYG or TVGFG (Jiang *et al.*, 2002; Bichet *et al.*, 2003; Holyoake *et al.*, 2004; Shrivastava & Bahar, 2006). The ion is required to lose its hydration shell, to compensate for this energetic cost, the carbonyl oxygen atoms of the selectivity filter take the place of the oxygen in water molecules (see figure 1.1). On passing through the selectivity filter, the K<sup>+</sup> ion then reacquires its hydration shell.

The open probability of the channels is controlled by various external factors, which act directly on the pore or additional structural domains that regulate the flux of ions through the pore. These structures have evolved to respond to these external factors. The response to external stimuli can cause a structural change at the selectivity filter or cytoplasmic end of the inner helices that influences the opening or closing of the pore (gating). hERG is an example of a voltage gated K<sup>+</sup> that has a voltage sensing domain of four transmembrane helices, coupled to the pore domain. The voltage sensing domains contain a series of charged amino acids that sense voltage and cause conformational

changes in the subunits in response to changing membrane potential. Channels can also be affected by ligands, such as  $\text{Ca}^{2+}$ , binding to the channel, by pH or by activation by internal signaling molecules such as G-proteins, cyclic nucleotides or ATP. The structural basis for hERG channel gating will be covered in more detail in a later section.

## **The cardiac action potential**

An action potential is a wave of electrical excitation that propagates across a cell membrane, and is caused by the controlled alterations in conductance of ion channels. Depolarisation is most commonly due to the fast opening of voltage-gated sodium channels. Repolarisation is mostly due to opening of potassium channels.

In the heart, the cardiac action potential synchronises the contraction of the muscle in order for the heart to pump blood efficiently. It starts at the sino-atrial node, which spontaneously depolarizes to the threshold potential for firing action potentials. The action potential then spreads through the myocardium from cell to cell via gap junctions. The propagation of the action potential through the heart can be detected as small voltage signals on the body surface electrocardiogram (ECG) (figure 1.2A). The P wave correspond to the depolarisation of the sino-atrial node, the QRS complex represents the depolarisation of ventricle and the T wave represents the repolarisation of the ventricle.

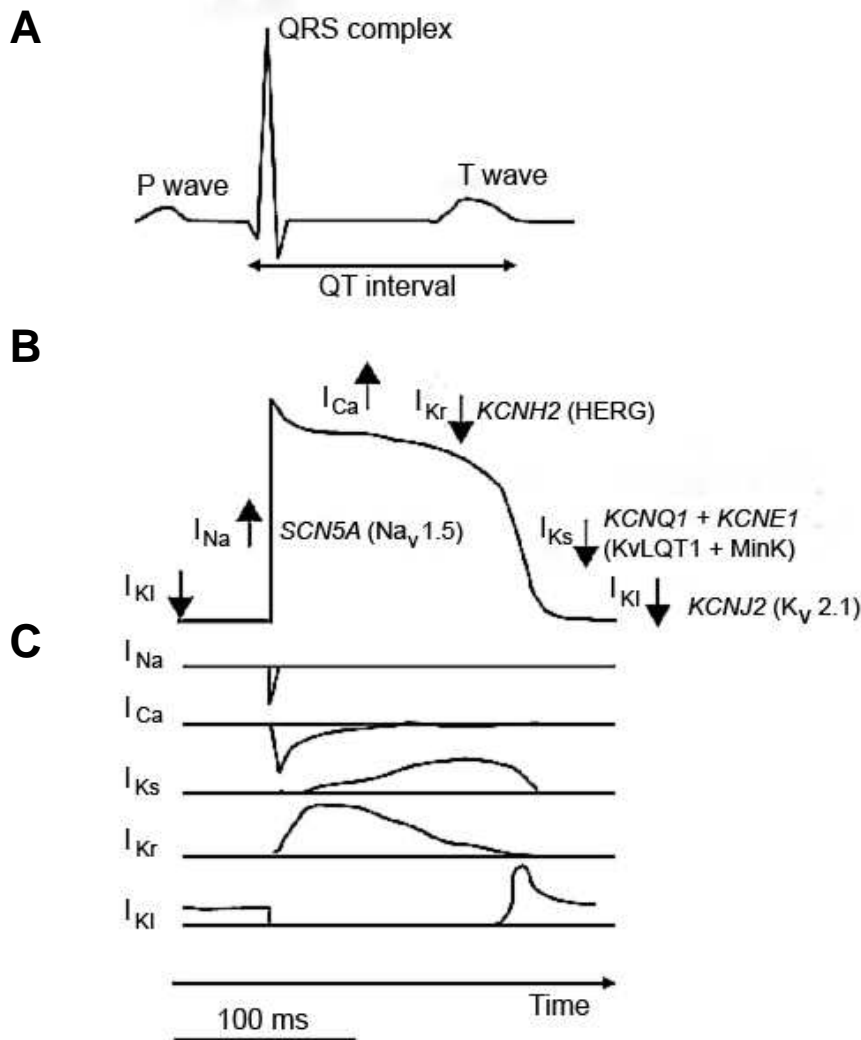


Figure 1.2: A schematic of the cardiac action potential recording. **A**, a representation trace of an ECG recording. This records the relative changes in electrical potential across the body as the heart beats. Each wave recorded indicates a different part of the cardiac cycle. The QT interval indicates the length of the ventricular action potential, where the Q wave indicates the ventricular depolarization and the T wave indicates the ventricular repolarisation. **B**, A representative trace of a ventricular action potential, with the main currents that summate to create the trace. **C**, Schematic representation of the individual currents that pass to give the action potential its characteristic shape. The timing of the currents passed are due to the gating characteristics of the channels. (modified from Roden *et al.* 2002 and Modell *et al.* 2006)

The ions involved in creation of the action potential can be split into excitatory and inhibitory, with sodium and calcium ions acting to excite the cells and potassium and chloride ions to inhibit them.

The ventricular action potential can be split into five phases (Roden *et al.*, 2002; Tamargo *et al.*, 2004; Sanguinetti & Tristani-Firouzi, 2006) (see Figure

1.2). The resting membrane potential of the cell is close to the equilibrium potential of  $K^+$  ( $E_K$ ) due to a relatively high resting conductance for  $K^+$  ions through inwardly rectifying ( $K_{ir}$  2.1) channels. Phase 0, where the cell is rapidly depolarised by the activation of voltage gated sodium channels ( $Na_v1.5$ ). This depolarises the cells to around +40 mV, which is close to the equilibrium potential for sodium ions.

Phase 1 is a brief partial repolarisation, as the sodium channels inactivate and also as repolarising current is passed by the transient outward  $K^+$  current ( $I_{to}$ ) and to a smaller extent the ultra rapid potassium current ( $I_{Kur}$ ).  $I_{to}$  is composed of a transient outward potassium current ( $I_{to1}$ ) mediated by  $Kv4.2$ ,  $Kv4.3$  and  $Kv1.4$  and a calcium activated chloride current ( $I_{Cl(Ca)}$ ).  $I_{Kur}$  is a delayed rectifier current mediated by  $Kv1.5$ . The cell is repolarised to about 0 mV. The timing and size of the repolarisation has influence on the duration of the cardiac action potential, as it alters the plateau potential and the voltage-gated calcium channels which are responsible for the inward L-type calcium current ( $I_{Ca,L}$ ) in phase 2.

Phase 2 is the plateau phase of the action potential, which can last for over 100 ms, and is due to the delicate balance of inward and outward currents. The main inward current is the  $I_{Ca,L}$ , the pore forming subunit being  $Ca_v1.2$ . The outward currents are mainly delayed rectifier potassium currents which were named according to their relative kinetics of activation ( $I_{Kur}$ ,  $I_{Kr}$  and  $I_{Ks}$ , standing for ultra rapid, rapid and slow activation respectively). The main potassium current during the early stages of phase 2 is  $I_{Kur}$ . This current is small in amplitude and so contributes to slow repolarisation. The calcium channels are slower activating and inactivating than sodium channels. The

slow, calcium-dependent inactivation means the current is long lasting and this is critical to the long duration of ventricular action potentials. The entry of  $\text{Ca}^{2+}$  ions cause the activation of ryanodine receptors in the sarcoplasmic reticulum, which causes the calcium induced calcium release, this causes the contraction of the cardiac myocyte.

The termination of phase 2 and the start of phase 3 is due to the shift in balance between  $I_{\text{Ca,L}}$  and the delayed rectifier  $\text{K}^+$  currents.  $I_{\text{Ks}}$  is a slowly activating potassium current, which is also a small amplitude current under basal conditions. It is carried by Kv7.1 $\alpha$  subunits coassembled with KCNE1 auxiliary subunits. The  $I_{\text{Kr}}$  current (carried by Kv11.1, also known as hERG) is larger than  $I_{\text{Ks}}$  current. During the initial depolarisation, it undergoes slow voltage dependent activation, but also fast voltage dependent inactivation, which limits the initial impact during the early phases of the action potential. During the late plateau phase the  $I_{\text{Kr}}$  channels start to recover from the inactivation as repolarisation by other  $\text{K}^+$  currents occurs, resulting in an increase of  $I_{\text{Kr}}$  amplitudes. The rapid repolarisation phase is due to the inwardly rectifying  $\text{K}^+$  current ( $I_{\text{K1}}$ ) rapidly increasing in amplitude as the channels recover from block by polyamines and divalent cations. The increasing repolarisation creates a positive feedback loop to accelerate the repolarisation to the resting potential. The open probability of the potassium channels is high during phase 3, but the current amplitudes decline as the driving force on the potassium ions decreases as the membrane potential approaches  $E_{\text{K}}$ . With repolarisation, the voltage dependent channels also deactivate.

## **I<sub>Kr</sub> channel structure**

The  $\alpha$ -subunit of the I<sub>Kr</sub> channel is encoded by the *human ether-à-go-go related gene* (hERG) (Trudeau *et al.*, 1995; Mitcheson *et al.*, 2000a). The hERG channel is a voltage sensitive, inwardly-rectifying potassium channel. It is a member of the ether-à-go-go (EAG) family of potassium channels which also include EAG (Kv10) and EAG like (ELK, Kv12) channels (Trudeau *et al.*, 1995).

The hERG channel currents do not quite have the same properties as I<sub>Kr</sub>. It is thought that it may coassemble with a  $\beta$ -subunit to modify its characteristics. The modification makes subtle changes, the main differences being a positive shift in the  $V_{1/2}$  of activation (-15 mV compared to -22 mV for hERG and guinea pig I<sub>Kr</sub> respectively), a reduction of the single channel conductance, a reduction in the sensitivity to regulation by external potassium concentrations and a reduction in the potency of block (obtaining an IC<sub>50</sub> of 1.0  $\mu$ M for E-4031 inhibition of hERG compared to 0.4  $\mu$ M when inhibiting guinea pig I<sub>Kr</sub>) (Sanguinetti *et al.*, 1995; Abbott *et al.*, 1999; Weerapura *et al.*, 2002).

A  $\beta$ -subunit is as yet not clearly defined. There is some published data that suggest that it associates with MinK or MinK related Peptide 1 (MiRP1) (McDonald *et al.*, 1997; Abbott *et al.*, 1999). The data on this is not conclusive, as it is mainly based on co-precipitation data. Many other studies have found the  $\beta$ -subunits do not alter the channel to have I<sub>Kr</sub> channel like characteristics. The MiRP1 subunits are mainly expressed in the conduction system of the heart and not the atria or ventricles. The mutations to MinK that cause long QT syndrome cause the reduction of I<sub>Ks</sub> rather than I<sub>Kr</sub>. Coassembly of full length hERG (hERG1a) with a splice variant of hERG (hERG1b, which has a

much shorter N-terminus) or post translational modifications may underlie differences in  $I_{Kr}$  and hERG currents.

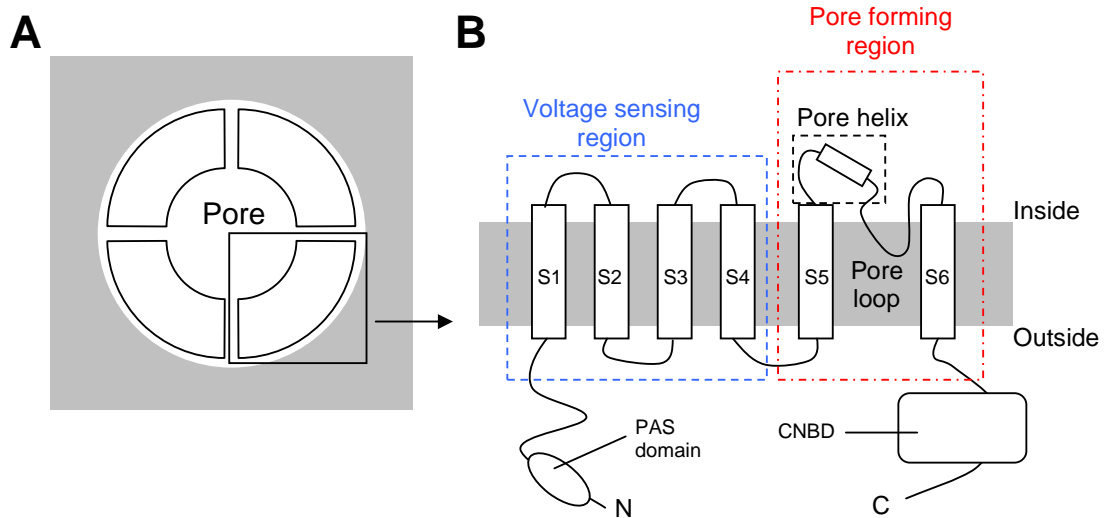


Figure 1.3: A schematic of the structure of the hERG channel. hERG channel is made up of 4 subunits (A). Each subunit containing 6 transmembrane helices plus a pore forming loop, with intracellular termini (B).

## The hERG channel structure

hERG channels like most other potassium channels, are tetramers formed from four subunits. Each subunit has 6 transmembrane  $\alpha$ -helices and intracellular N- and C- termini (see figure 1.3). Each of the subunits has a Per-Arnt-Sym (PAS) domain on the N-terminus and a cyclic nucleotide binding domain (cNBD) on the C-terminus (Trudeau *et al.*, 1995; Morais Cabral *et al.*, 1998). The PAS domain has a specific sequence of amino acids which has been implicated in protein-protein interactions and acting as light and chemical sensors. In hERG, it does not appear to have a single function, the slowing the deactivation of the channels, possibly by binding to the S4-5 linker region and stabilising the open state of the channel (Morais Cabral *et al.*, 1998; Chen *et al.*, 1999). The cNBD appears to have a minor modulatory role,

through the binding of cyclic nucleotides (Cui *et al.*, 2000), this affects the voltage dependence of activation of the channels. The cNBD is likely to be a structural domain necessary for folding and trafficking of the channel to the cell membrane. Key residues for binding cyclic nucleotides are different in hERG from known cNBD proteins and it is unlikely that cAMP directly binds to the C-terminus to modulate function.

The first four transmembrane helices correspond to the voltage sensing domain. Like other voltage sensitive channels, they contain a number of positively charged arginine residues in the fourth transmembrane helix (Trudeau *et al.*, 1995). This forms an important part of the mechanism converting the change in membrane potential into gating of the pore. Movements of the voltage sensor are coupled to the pore via the S4-S5 linker region.

The S5-S6 region forms the pore of the channel and is thought to have similar structural architecture to the pores of other K<sup>+</sup> channels. The S6 transmembrane helices form an intracellular gate that regulates the flow of ions through the channel. This opens and closes in response to voltage via interactions with the S1-4 region. The pore structure also contains the structure for voltage dependent inactivation. The turret region of the pore is thought to collapse into the pore and inhibits the flow of ions (Jiang *et al.*, 2005). The selectivity filter may also twist and thereby disrupt the ability to coordinate the K<sup>+</sup> ions, so making the pore non-conducting (Stansfeld *et al.*, 2008).

## The hERG drug binding site

The binding site of hERG is quite unique, as it is able to bind a large number of compound molecules, which have a wide variety of chemical structures (Cavalli *et al.*, 2002; Ekins *et al.*, 2002). The structure of the hERG inner cavity appears to be uniquely suited to bind these molecules. Mutagenesis studies on the residues that line the inner cavity have shown the Phe656 and Tyr652 residues are particularly important to high affinity binding (Lees-Miller *et al.*, 2000; Mitcheson *et al.*, 2000a; Fernandez *et al.*, 2004; Kamiya *et al.*, 2006). Fernandez *et al.* (2004) examined this further with the use of a series of amino acid substitutions at position 652 and showed that an aromatic residue is required, which indicates that it interacts with compounds by  $\pi$  stacking with the phenyl ring and forming cation- $\pi$  bonds with the hydroxyl groups. Similar experiments at the Phe656 position indicated a hydrophobic residue was required for high affinity binding at this position. Therefore it is likely to interact with the compounds through van der Waals forces to produce high affinity binding.

There are also further residues in the pore region of hERG that have also been found to be important to the binding (Kamiya *et al.*, 2006; Perry *et al.*, 2006). In particular, Thr623 and Ser624 close to the pore helix are important for some compounds. These residues have been less extensively studied, but it appears that the binding to these residues is dependent on the drug molecule itself. The use of alanine mutations of these residues show differing reductions to inhibition with different compounds, such as dofetilide, E-4031, fluoxetine and ibutilide. (Mitcheson, 2003; Perry *et al.*, 2004; Kamiya *et al.*, 2006; Perry *et al.*, 2006).

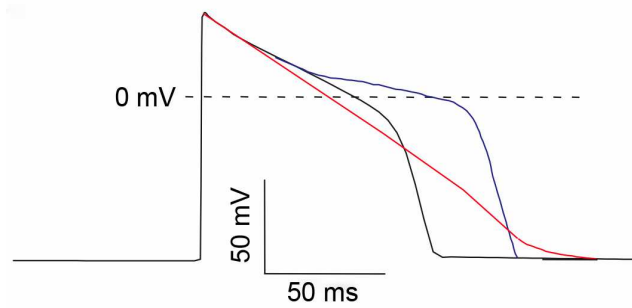
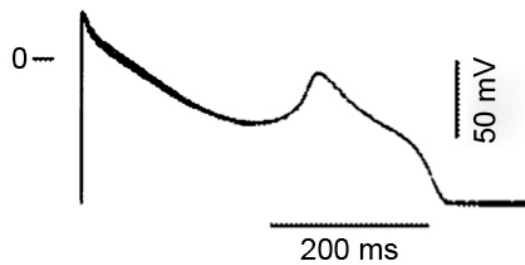
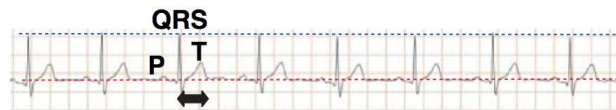
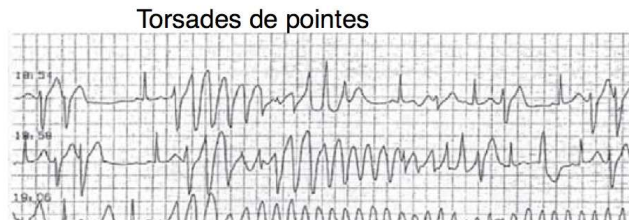
**A****B****C****D**

Figure 1.4: The reduction in repolarising currents can prolong the length of the cardiac action potential and cause arrhythmias. **(A)** a cartoon of a normal cardiac action potential is shown in black. The alteration of the currents due to congenital defects or by drug block can cause a change in the length of the action potential. In the case of hERG channel block, a parallel shift (blue) or a triangulation of the current (red) can occur. **(B)** This alteration of the action potential could increase the likelihood of EADs. **(C)** The shape of the cardiac action potential can be inferred from the analysis of ECG traces. **(D)** When there is an alteration in the balance of the currents, it may lead to life threatening arrhythmias such as Torsade de pointes, a condition where the QRS complex oscillates across the isoelectric field (Modified from Sanguinetti *et al.* 2005 and Fenichel *et al.* 2004).

## Long QT syndrome

The cardiac action potential is subject to a balance of the currents through different ion channels as highlighted in the section above. These are modulated by a variety of mechanisms in response to different physiological requirements. For example, sympathetic stimulation causes an increase in cardiac output. This occurs by increasing heart rate and contractile force. The amplitude of the calcium transients and  $\text{Ca}^{2+}$ -reuptake are enhanced. Alterations to kinetics and voltage dependence of  $I_{\text{Ca,L}}$  and  $\text{K}^+$  currents, and rates of extrusion of calcium, decreases the length of the cardiac action potentials and shortens refractory periods.

The importance of balancing the different currents is further emphasised in people who suffer from inherited heart disorders, such as Romano-Ward and Jervell-Lange-Nielsen syndrome (Abbott *et al.*, 1999; Haack *et al.*, 2004; Sanguinetti & Tristani-Firouzi, 2006). These are conditions that mostly cause a decrease in the repolarising currents, particularly the  $I_{\text{Kr}}$  and  $I_{\text{Ks}}$  currents, and cause a lengthening of the cardiac action potential (see Figure 1.4A). The ECG shows a lengthening of the QT interval (see Figure 1.4B), which indicates the time between ventricular depolarisation and repolarisation.

The reduction of the  $I_{\text{Ks}}$  or  $I_{\text{Kr}}$  currents is caused by mutations that affect the characteristics of the channels that pass the currents. Mutations can be either in the KCNQ1 and hERG subunits, which form the pore of the  $I_{\text{Ks}}$  and the  $I_{\text{Kr}}$  channels respectively (Trudeau *et al.*, 1995; Barhanin *et al.*, 1996; Sanguinetti *et al.*, 1996; Tristani-Firouzi & Sanguinetti, 1998; Roden *et al.*, 2002), or in the  $\beta$ -subunits, MinK and MinK related peptide 1 (MiRP1) (Sanguinetti *et al.*, 1996). If the lengthening of the QT interval is extreme, this can predispose

individuals to early after depolarisations (EADs), where a second, unsynchronized depolarisation occurs before the initial action potential has terminated. This can potentially lead to cardiac arrhythmias and sudden cardiac death.

Unfortunately LQTS is not just seen as an inherited disorder. The symptoms can be acquired through the use of drugs. Class III antiarrhythmic drugs were developed to block cardiac ion channels, with the aim to elongate the cardiac action potential and reduce re-entrant arrhythmias in some patients by increasing the refractory periods. However, many of these class III antiarrhythmic drugs were subsequently taken off the market due to the observation that they were frequently pro-arrhythmic. Moreover, it rapidly became apparent that drug-induced LQTS was also caused by non-cardiac drugs and that a very large number of drugs could cause this potentially lethal side-effect. The other striking finding was that virtually all these drugs caused this side effect by blocking  $I_{Kr}$ . This unintended block of the  $I_{Kr}$  channels was leading to the lethal arrhythmias.  $I_{Kr}$  channels have the potential to bind a large number of drug molecules with relatively high affinity (De Ponti *et al.*, 2000, 2001; Cavalli *et al.*, 2002). This is a major problem for drug companies developing new drugs, as there have already been large numbers of drugs that were released which were then found to have lethal side effects involving the blockade of  $I_{Kr}$  channels; these were subsequently either taken off the market or had warning flags placed on them, controlling their use. Examples of which are cisapride, haloperidol, and clarithromycin, which have warnings placed on them (De Ponti *et al.*, 2000, 2001) (see also [www.torsades.org](http://www.torsades.org)).

This highlights the need for further research in this area to characterise the channel and drug molecules so that the side-effects profile can be predicted earlier in the design of drugs and eliminated or reduced as the development progresses. It may also reduce the likelihood of false positives, allowing for the development of drugs that can be therapeutically useful and safe.

### **Predicting LQT potential**

There are a number of tests that are now present which are used to predict LQT potential. Each has its own advantages and also their drawbacks. Pharmaceutical and biotechnology companies usually employ a combination of them in order to investigate potential drug targets and the drug molecules (see figure 1.5). The order for these tests is dependent on the cost and complexity of the experiments involved.

#### ***Use of cell lines to predict LQT potential***

These include binding studies and electrophysiological recordings from cell lines over-expressing LQT causing channels. These are useful in the early stages of research, where the focus will be finding potential targets for compounds, examining the specificity of the compound to a target and mode of action. These can also be used to investigate LQT potential. Carrying out binding studies of drugs to hERG channels through competition binding assays can give a quick indication of the LQT potential of many drugs, as it can be carried out in a high throughput system. However, the main limitation to this method is the conformational state of the hERG channel is not changed so the state dependence of the binding cannot be examined.

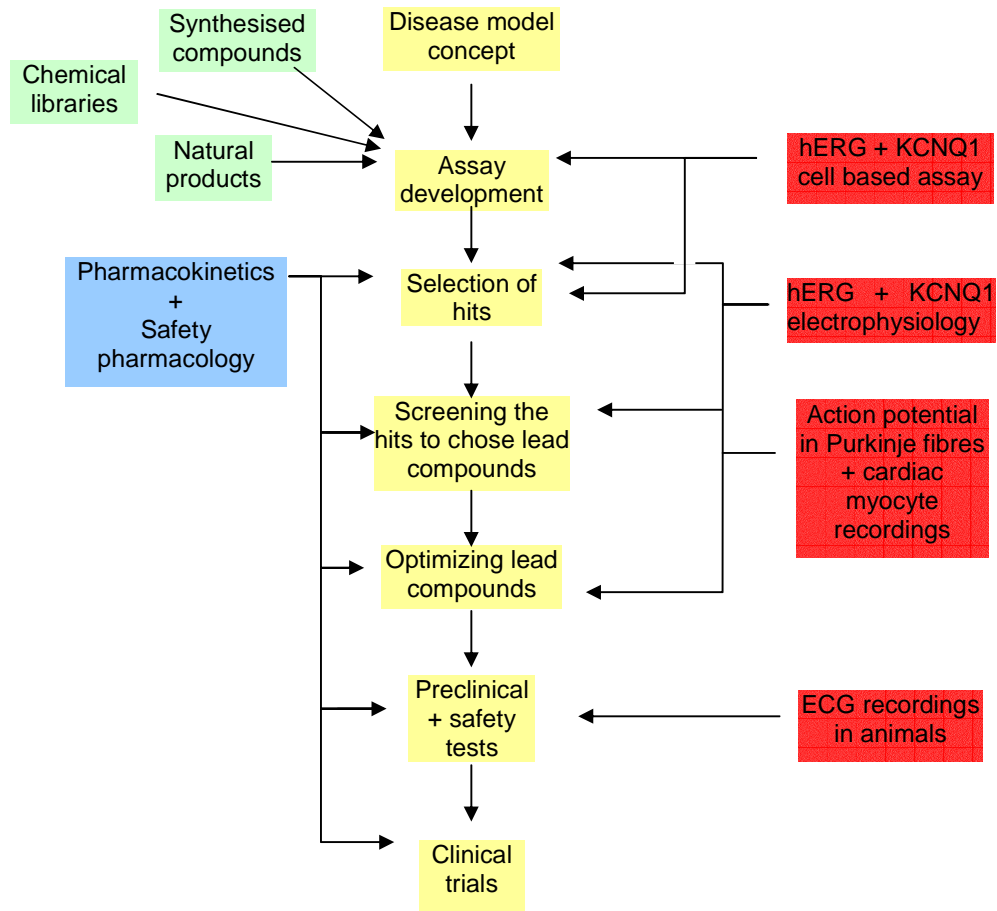


Figure 1.5: A schematic of the steps taken to get a drug to clinical trials used by pharmaceutical companies. This displays the steps at which the different tests for cardiotoxicity are carried out. This is due to the cost and complexity of the recordings involved. (modified from Netzer *et al* 2001 and Novartis website.)

Recordings from cells expressing the channels of interest give a direct indication of whether the drug acts on the channel. For the investigation of LQT potential, mammalian cells transfected with hERG are usually used. This is usually predicted from the percentage block of the hERG channel currents. The recording method can be used to look at the state dependence of the drugs. The drawback of this technique is that it looks at individual channel types and cannot predict the dispersion of repolarisation which can affect the likelihood of EADs. Dispersion of repolarisation occurs due to the difference in the expression level of channels in different regions of the heart for example

from epi- to endocardium or the base to apex (De Ponti *et al.*, 2000; Brunner *et al.*, 2008). This affect leads to alterations in the shape of the cardiac action potential in differing areas of the heart due to the differential expression of channels in the different regions, and has been indicated as a possible cause of cardiac arrhythmias because it increases the opportunity for reentrant currents. Also, the use of hERG channels do not have exactly the same characteristics as the  $I_{Kr}$  channels, as will be discussed later in the chapter. Therefore, the results from these tests can give a good indication of the LQT potential, however, they need to be combined with further tests to give a definitive result. Nevertheless, many compounds are discarded from further development on the basis of hERG inhibition.

### ***The use of animal models to predict LQT potential***

Animal studies are also used to investigate LQT potential (De Ponti *et al.*, 2001; Arnaout *et al.*, 2007) (see also the US Food and Drug Administration <http://www.fda.gov/RegulatoryInformation/Guidances/ucm129121.htm> (2005) and European medicines evaluation agency for guidelines <http://www.emea.europa.eu/pdfs/human/ich/042302en.pdf> (2005)). A model will be selected based on traits that are similar to the specific human condition. Models can be used to test compounds that have potential to treat conditions of interest, as well as looking at potential side effects. The model, if selected with care, can give a comparable reaction to that found in humans. Animals that are presently used to investigate LQT potential are usually guinea pigs, rabbits and dogs.

Recordings from isolated cardiac myocytes can be used to study the effect of different compounds on the channels. This gives a more accurate indication of

LQT potential compared to mammalian cell lines transfected with hERG channels, as the cells express the channels that are involved in the cardiac action potential. However, careful choice of animal from which to isolate the myocytes has to be made as different animal species express the channels and  $\beta$ -subunits to varying levels (Watanabe *et al.*, 2007). This could alter the susceptibility of the tissue to possible arrhythmias caused when the compound blocks the channel, due to the relative differences in the currents that contribute to the repolarisation.

An isolated perfused heart and heart wedge preparation can be used to monitor heart rate (Choi *et al.*, 2007; Hillman *et al.*, 2007). The perfused heart can also be used to optically trace the conduction of the action potential across a section of the heart. These methods can be used to study if there is a chance the compounds cause cardiac arrhythmias and if there is an effect on conduction in the heart.

In some cases a whole animal is used. The studies can give an indication of how the drug affects other systems in the body apart from the one of interest. It may highlight possible side effects from using the drug, due to metabolites or by direct drug action. The disadvantage is that the animal models may not use the same molecular pathways to metabolise the drug or express the same proteins as those of the human condition.

Therefore, careful selection is needed to get a model that closely represents the condition that is being studied. The cardiac activity is monitored in the presence and absence of drug, however, there are differences in the channels expressed in the different organism. In guinea pigs, the  $I_{T_o}$  channels are not highly expressed. Rabbit cardiac muscle appears to express channels that

are more like human cardiac channels. Dog is the species that is most frequently used in preclinical safety tests.

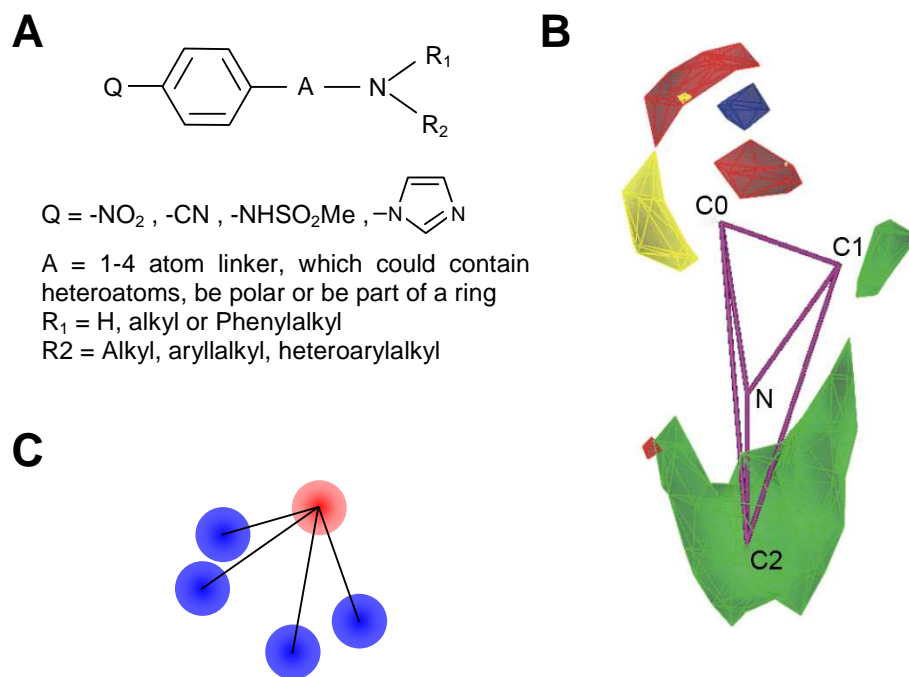


Figure 1.6: Creation of a hERG blocking pharmacophore. Comparisons of several known chemical structures that are able to block the hERG channel were used to create a pharmacophore which displays the common characteristics of the drugs analysed. **A**, A class III antiarrhythmic pharmacophore model based on commonly found chemical structures by Morgan and Sullivan 1992. **B**, A model developed by Cavalli *et al.* 2002, this gives a template of a centrally charged nitrogen (N) with aromatic groups that can be in two of three centroids (C0-2). Red and blue contours indicate increased activity with the presence of a positive or a negative charge respectively. Green regions indicate where molecular volume increases cause a rise in the ability to block hERG channels; yellow regions indicate where volume decreases cause a drop. **C**, A pharmacophore template by Ekins *et al.* 2002 with centres of positive (red) and hydrophobic nature (blue).

### ***In silico predictions of LQT potential***

The use of *in silico* modelling has become a method increasingly used by companies to gain an idea of how compounds bind to their targets. This is with the aim of reducing the cost, time taken and variability of results that presently occur when carrying out experiments. The approach can be ligand or target based. The ligand based approach uses experimental data and

ligand structures to derive quantitative structure-activity relationship (QSAR) models. If structural information on the targets is available (e.g. 3D structures from crystallography and nuclear magnetic resonance (NMR) spectroscopy) then in silico structural models can be developed into which compounds can be docked to investigate target-ligand interactions.

The ligand-based approach has been used to create a pharmacophore model of hERG channel blockers (figure 1.6). This is a structure that takes into account common features from compound structures in a bank of known hERG blockers, it uses these features to predict the spatial distribution of domains that makes a high affinity hERG blocking compound. New compounds can be fitted to this template in order to predict the probability of hERG binding and the strength (Morgan & Sullivan, 1992; Cavalli *et al.*, 2002; Ekins *et al.*, 2002; Coi *et al.*, 2006; Garg *et al.*, 2008) (see figure 1.6). As can be seen there are differing templates that have been created, these can be used to fit a new compound and predict hERG binding. As can be seen in figure 1.6A, the model is a basic chemical structure used for predicting hERG block, this used model was obtained by analyzing the chemical structures of a set of hERG blockers. The other two are 3D QSAR models of a pharmacophore of hERG blockers; these model common features that are found in hERG blockers in a 3D space. The features include positive charged and hydrophobic groups that are found in many hERG blockers. The model in figure 1.6B also adds regions where presence of positive, negative charges or change in volume would cause an increase or decrease in the affinity of the compound to hERG.

This method may give indications of whether it is a hERG blocker. However, the method at present does not accurately predict binding affinity.

The target based approach to predicting LQT potential creates a homology model of the hERG channel and then models the binding of compounds this channel. This method relies on having accurate structures of similar proteins,

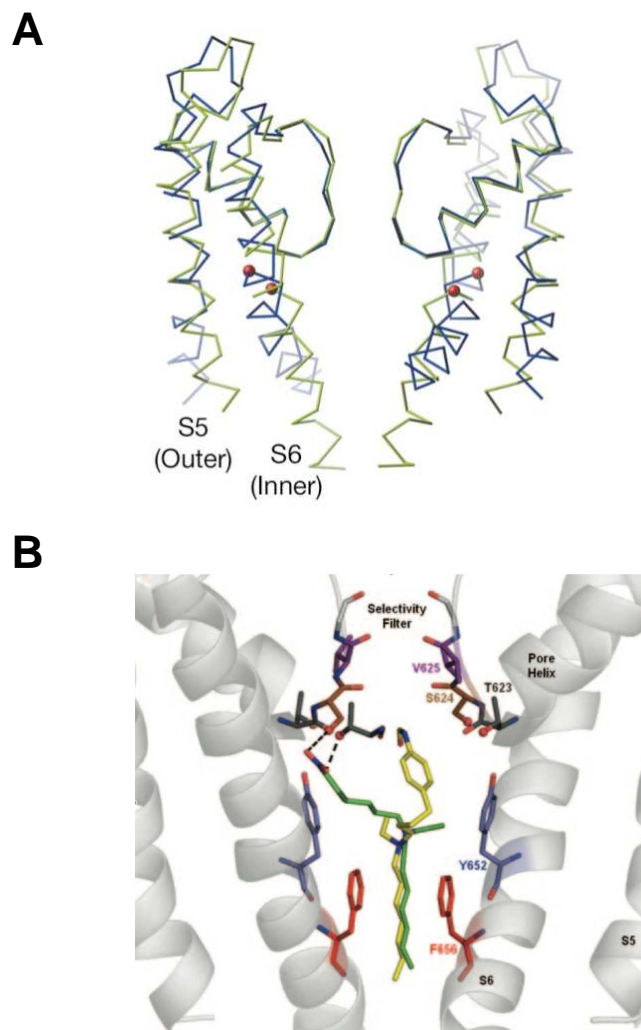


Figure 1.7: Modelling structures of protein based on homologous structures. The crystal structure of the pore forming inner (S6) to outer (S5) helices of channels such as KcsA (green) and KvAP (blue) (A) (modified from Jiang *et al.* 2003) can be used as a template to create a model of the pore structure of a channel. The amino acids of F656 and Y652 are highlighted in red as important to drug binding. B, Two clofilium analogues (green and yellow) docked into a homology model of the hERG inner cavity based on KcsA. The pore shown in cross-section perpendicular to the membrane, with two of the four subunits shown. The carbon backbone of the protein is represented in grey, with key residues of S6 and pore region. It shows how the compound tails may hydrophobically interact with Phe656 residues,  $\pi$ -stack with Tyr652 and form hydrogen bonds with Tyr632 and Ser624 (modified from Perry *et al.* 2006).

obtained from X-ray crystallography and NMR (Doyle *et al.*, 1998; Jiang *et al.*, 2002; Long *et al.*, 2007). At present there are few crystallographic models of ion channels due to difficulty crystallising them as they are in the membrane.

The structures are used as a template to model the structure of hERG. First the amino acid sequences are aligned and the 3D structure is produced based on this alignment. This structure is then optimised relative to the amino acid backbone (Pearlstein *et al.*, 2003; Osterberg & Aqvist, 2005; Farid *et al.*, 2006; Stansfeld *et al.*, 2007). This model can be further tested using experimental data such as cysteine scanning experiments. If the model is accurate, it can be tested by attempting to dock drug molecules into the channel and see if they are able to bind. The binding can also be quantified and compared with experimental results. The binding can be used to see which parts are predicted to bind to particular amino acids, these can be cross checked with experimental data such as the mutational work, so the models and experimental work can feedback both ways to further understand the mechanisms of binding.

Therefore this method is a powerful tool that can help researchers bring together results from studies and aid in the visualisation of the binding of compounds in the cavity. This can lead to further hypotheses which can be tested and used to refine the model. Thus far the models have not been successful as accurate predictive tools. The present models of hERG have some limitations the need to be addressed. The models are based on a limited number of crystal structures of voltage-gated potassium channels. So far only two have been resolved, KvAP a bacterial channel from *Aeropyrum pernix* (Jiang *et al.*, 2003) and Kv1.2 from rat brain (Long *et al.*, 2005). Due to

differences in amino acid structures, the hERG channel may not be modelled accurately, particularly the S5-S6 linker, which is involved in the fast inactivation of hERG (Herzberg *et al.*, 1998; Dun *et al.*, 1999; Tseng, 2001, 2006), as there is difficulty resolving the loops in the aqueous solution. Therefore more experimental data is needed to help model these.

This work will use a series of hERG channel inhibitors of varying length to try to characterise the size of the hERG channel inner vestibule. The phenotypes of block will be looked at to try to gain an insight into the structure and function of inhibition. The hypothesis is that as the channels are inhibited by compounds of increasing length, the phenotype will change from a drug trapped phenotype to a foot in the door one.

### **Drug trapping in hERG**

The size and /or structure of the inner cavity of hERG appears to influence the ability to retain a wide range of compounds within it. It may be due to the proportions of the inner cavity permitting it to accommodate large molecules compared to other channels. hERG lacks a Pro-X-Pro motif in the S6 helix (Fernandez *et al.*, 2004), this sequence of amino acids is present in a lot of other channels and is thought to introduce a kink in the helix (del Camino *et al.*, 2000). This may reduce the volume of the inner cavity, introduction of this motif reduces drug sensitivity (Fernandez *et al.*, 2004). However this is not conclusive, as the mutation also alters the channel gating.

Drug trapping is a phenotype of block that has been reported in many studies into hERG channels (Mitcheson *et al.*, 2000b; Perry *et al.*, 2004; Witchel *et al.*, 2004). This is where drugs can be retained in the inner cavity of the hERG channel while in the closed state. The channels will activate, opening the

intracellular gate and allowing the drug to bind blocking the current flow. Upon repolarisation, the channel is able to close and the drug is retained in the inner cavity.

The characteristics for the onset and recovery of block have a series of notable characteristics. In the first instance, the currents are not inhibited when drug is applied at the holding potential, as the channels are closed. During a depolarisation, current activation is similar to control currents, but with prolonged depolarisations, onset of block is observed. This indicates that the drugs can only gain access to their binding site when the channels open (open channel block). Upon repolarisation, channels deactivate. The hallmark of drug trapping is that even when the drug is washed off, with the channels in the closed state, the current remains inhibited when applying the next depolarisation. In addition, there is no change to the deactivation kinetics. The interpretation of these results is that upon deactivation and closure of the channels, the drug is able to be retained in the inner cavity of the channel. The drug does not interfere with the closure of the channel, so the apparent deactivation rate should not be significantly different compared to controls (figure 1.8), as the currents recorded will only be from channels that are not blocked.

The block of the channels remains if they are kept closed, and so it will affect the rate of wash off of the drug. If they are closed, the recovery from channel block is slow as the intracellular gate stops the drug from exiting the channel. Only when the channels are opened up again will they recover. However, if the channel is opened while the drug is washed off, over the same time period, there will be greater recovery from block. This is seen in previously reported

data on hERG and other potassium channels (Armstrong, 1971; Mitcheson *et al.*, 2000b; Perry *et al.*, 2004; Witchel *et al.*, 2004).

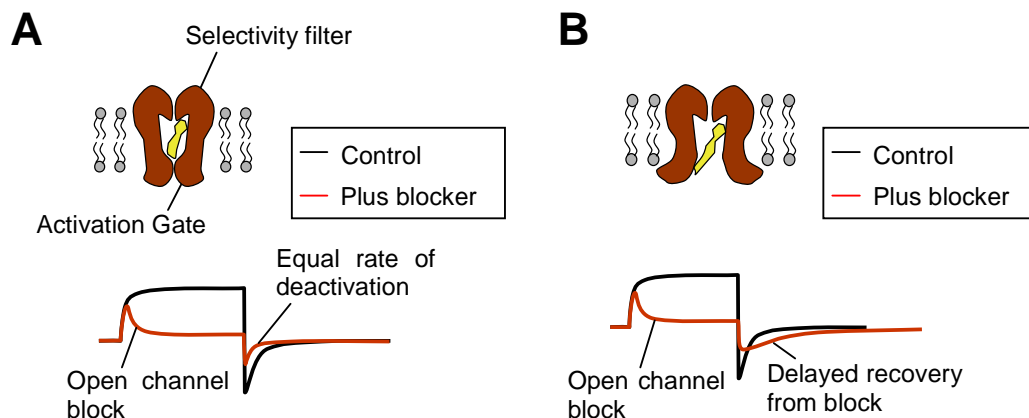


Figure 1.8: The characteristics of drug block. **A**, Drug trapping, the channel is able to close around the drug molecule preventing compounds leaving the channel and recovering from block. The kinetics of the current traces should be the same as those without drug present. **B**, foot in the door, the channel is unable to close around the drug molecule. The currents will show the open channel block, but the currents of deactivation may appear to be slowed due to the currents from channels that recover from block.

Evidence of drug trapping is further confirmed with the use of a mutant hERG channel, D540K (Mitcheson *et al.*, 2000b). This is a mutant that opens at positive potentials, much like WT hERG. However, the channels are able to reopen at potentials negative to -90 mV. It was seen that the drugs MK-499 were able to inhibit the channels at positive membrane potentials, much like WT hERG, but when applying voltage steps to -160 mV, the D540K channels displayed almost complete recovery. This shows that MK-499 is retained in the cavity of WT hERG when the intracellular gate of the channel is closed, trapping the drug in the channel.

### Foot in the door

This effect is seen in experiments on most  $K^+$  channels, some compounds cause open channel block, but recovery from block is rapid and the kinetics of

deactivation are slowed (figure 1.8B). Armstrong (1971) first described this phenomenon with quaternary amines (QA) and showed that it was dependent on blocker length. Large QA, slowed the kinetic of deactivation because the blocker prevents closure of the activation gate. The channels are unable to deactivate until the drug has unbound. This was subsequently referred to as foot in the door type block. Smaller QA allowed channels to close 'silently' with no slowing of deactivation and channels remained blocked after drug washout, features characteristic of drug trapping. These findings were consistent with channels having an inner cavity of a sufficient size that small QA molecules could be accommodated, even with the closure of the activation gate. But larger drug molecules are unable to be trapped within the inner cavity. These models of drug block suggest that drug molecules can be used as molecular rulers to measure the size of the inner cavity. Drug molecules which are smaller than the inner cavity would exhibit drug trapping phenotype of block, whereas drugs larger than the inner cavity would exhibit foot in the door type block. One of the aims of my thesis was to use this approach, by using a series of varying length analogues based on E-4031 to estimate the size of the hERG channel inner cavity.

## **Rundown**

Changing the length of chemical structures can change the membrane permeability, this can have affects on their potency. To remove this potentially limiting factor, the hERG channels can be recorded using the excised inside-out patch clamp technique. This allows the compounds to be perfused directly to the intracellular side of the membrane. However, the hERG channels exhibit significant rundown when they are excised from the membrane.

Rundown is a phenomenon where the activity of the channels decreases over time in patch clamp experiments. This has been reported to occur with hERG (McNicholas *et al.*, 1994; Bian *et al.*, 2001; Cayabyab & Schlichter, 2002; Du *et al.*, 2004), either in whole cell patch clamp or excised inside-out patches. The reasons for this rundown are not clear. The rundown can be due to changes in the open probability and voltage dependent characteristics

There have been reports on this phenomenon in several papers, but this has not been studied in great detail. Reports previously published, involving studies of the hERG or other channels, suggest that the loss of function is due to one or more modulatory factors (McNicholas *et al.*, 1994; Bian *et al.*, 2001; Cayabyab & Schlichter, 2002; Du *et al.*, 2004; Hirdes *et al.*, 2004). These studies added reagents to the intracellular recording solutions and observing the slowing or acceleration of hERG current rundown.

Bian *et al.* (2001) investigated whether PIP<sub>2</sub> had effects on the hERG activity, addition of PIP<sub>2</sub> to the intracellular solution was found to cause a hyperpolarising shift in the voltage dependent activation and a slowing of the inactivation of hERG. In excised patches a slower rundown was observed in the presence of PIP<sub>2</sub> compared to control solutions. This effect is not due to a change in the single channel conductance, as it is not greatly affected in the presence of PIP<sub>2</sub>. However, the concentrations of PIP<sub>2</sub> was high (10 µM). Comparing to the basal levels of PIP<sub>2</sub> that was calculated in the orders of femtomoles per cell in an assay by Willars *et al.* (Willars *et al.*, 1998). This may not however indicate the local distribution of the factor in the cell membrane.

Hirdes *et al.* (2004) and Cayabyab *et al.* (2002) observed an increase in the rundown rate for hERG currents when they applied broad spectrum kinase inhibitors in the intracellular solution. Addition of 2 or 3 mM ATP reduced the rate of rundown. Hirdes *et al.* (2004) also added a non-hydrolysable ATP analogue to the intracellular solution as a replacement of ATP and observed an increase in the rate of the rundown of hERG currents. This indicates that the hERG channel requires some phosphorylation to stay active.

Rundown studies on calcium and other potassium channels have also shown that the channels have to be phosphorylated in order to remain active (Armstrong & Eckert, 1987; Tang & Hoshi, 1999). Tang *et al.* (1999) showed that KAT1 channels display changes to voltage dependent activation once they were excised.

These results indicate that there may be different modulatory pathways affecting the rate of rundown in hERG channels. The loss of activity may be due to a shift in the voltage dependence of activation and open probability and not the channel conductance.

The second aim of this project is to investigate the region responsible for the rundown through the creation of a hERG/bEAG chimeric channel.

## **Chapter 2: Materials and methods**

### **Molecular Biology**

#### ***Creation of chimeras***

The aim was to create a set of chimeras by exchanging the intracellular amino- (N) and carboxyl- (C) termini of bEAG and hERG. These would be based on a chimera that was produced by Eckhard Ficker (Ficker *et al.*, 1998). These chimeras were produced with the aim to create a channel that does not rundown. This was with the view to create a channel with the hERG pharmacology, but lacks the property of rundown. This would allow prolonged recordings in the inside-out patch conformation, allowing application of drugs to the intracellular surface to study their affinity to the hERG channel. This would eliminate the factor of membrane permeability of drugs.

#### ***Sequencing***

A set of chimeras were provided to us as a generous gift from Eckhard Ficker in a pSP64 vector (figure 2.1), they were sequenced using the in house sequencing service (Protein and Nucleotide Acid Chemistry Laboratory, University of Leicester) who used an automated DNA sequencer (ABI PRISM Model 377). The resulting sequence was used to confirm the particular constructs that were sent. The sequencing primers were designed to be approximately 100 bp up or downstream from the region of interest. The analysis was focused on the regions where the DNA sequences had been ligated. The primers were also designed so that they had an approximate length of 21 bp, which began with a G or a C, with a melting temperature of

more than 55 °C, a GC content around 60 % and resistance to forming dimers or hairpin loops. The primers were synthesised by Sigma Genosis (Poole, UK)

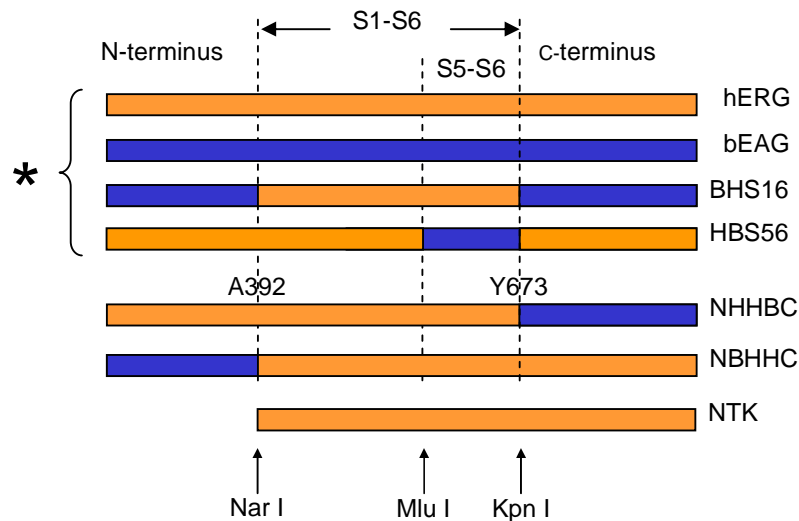


Figure 2.1: A schematic of the channels provided by Ficker *et al.* as indicated by the \*. The cDNA was provided subcloned between BamH I and HinD III of the pSP64 vector. These were used to create the single terminus exchanged chimeras. As indicated in the lower two chimeras. A N-terminus truncated (NTK) hERG mutant would also be studied. The hERG sequence is shown in orange and bEAG sequence in blue. The pore and voltage sensing domains (S1-S6) of hERG was retained in all chimeric channels studied. The position of the Nar I, Mlu I and Kpn I are indicated by the dashed lines.

The resulting sequence was then put into a sequence alignment programme (Vector Nti, Sigma), and aligned against the published database sequences (hERG: Q12809, bEAG: O18965) to check that they were correct. When the resulting sequence was identical to the expected one, the constructs were used to produce the set of chimeras.

### **Restriction digests**

As hERG and bEAG did not share unique restrictions sites in order to produce the single N- or C-terminal exchanged chimeras (NHHBC and NBHHC), the chimeras of BHS16 and HBS56 were used. BHS16 was a hERG channel subunit with both of the intracellular termini exchanged for bEAG ones. HBS56 was a hERG channel subunit with the S5-S6 transmembrane regions

exchanged with that of bEAG. These chimeras shared a series of restriction sites (*Hind* III, *Bam*HI, *Mlu* I and *Kpn* I) (See fig. 2.2).

The restriction sites chosen to make the digests were unique to the inserts. They were also chosen so that the resulting digests had sticky ends to allow for annealing and easier ligations. The digests were run in accordance to the

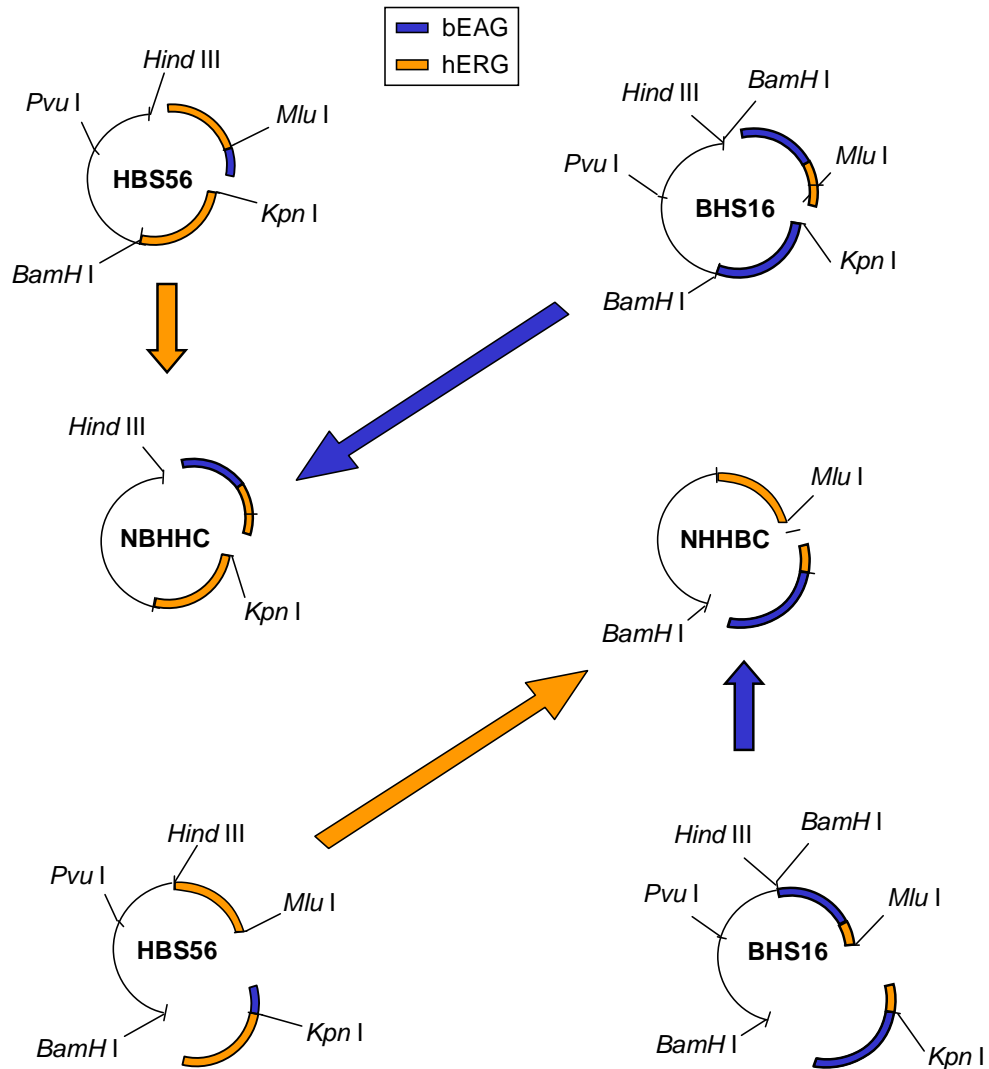


Figure 2.2: Schematics of the restriction enzyme cuts needed to create a single terminus exchanged chimera. The chimeric DNA in pSP64 vectors were cut with the restriction enzymes indicated. The cuts ensured that there was an intact hERG S1-S6 domain. The hERG containing sections of the HBS56 were ligated to the remaining part of the channel obtained from BHS16 to obtain a continuous DNA plasmid.

manufacturers' protocols. Single digests were run before any double digests were carried out to ensure none of the enzymes displayed any non-specific cuts (star activity). To minimise this, the volume of enzyme was controlled, so that the glycerol concentration of the reaction did not exceed 5 % of the total reaction volume. The time duration of the incubation was limited it to 1-2 hrs. 1 unit of enzyme digests 1 µg of DNA in an hour. The enzyme units did not go above a 30 fold overdigestion.

To create the chimera with the N-terminal of hERG exchanged with bEAG, the HBS56 and BHS16 chimeric DNA (1 µg) were digested simultaneously with 20 units of *Hind* III and 15 units of *Kpn* I (New England Biolabs, Hertfordshire, UK) in buffer 2 plus BSA, making the final volume 15 µl. A double digest was used as the enzymes were compatible together and it allowed for potentially greater yields of DNA. To create the C-terminal exchanged chimera, the HBS56 and BHS16 chimeric DNA (1 µg) were digested sequentially with *Bam*HI (New England Biolabs, USA) in its unique buffer and then *Mlu* I (New England Biolabs) in buffer 3. The digests were run sequentially, as *Bam*HI was not compatible with the other buffer solutions. Between the digests the DNA was purified using a QIAquick gel extraction kit (Qiagen, Chatsworth, USA). The digests were left at 37 °C for two hours. The fragments were then electrophoresed on a 1 % weight per final volume agarose gel containing 0.003 µg/ml ethidium bromide to look at the size and number of the cuts. The gels were viewed on a UV light box to confirm that the restriction enzymes had completely cut the vector to give fragments with the expected size.

On digestion with *Hind* III a second restriction site was found to be present on the vector which contained the HBS56 insert. This was not predicted from the

plasmid sequence, indicating that there was an extra mutation in this plasmid. The digestion resulted in the DNA being cut into 2 fragments. From further diagnostic digests, the site was found to be in the vector region. With the second *Kpn* I restriction digest there were smaller fragments produced running lower on the gel, allowing good separation on a gel. Therefore the relevant DNA fragments could be extracted and used to create the chimeras (Figure 2.3).

### ***Gel extraction***

The required fragments were then cut out from the gel using a scalpel and the DNA was purified using a QIAquick gel extraction kit (Qiagen) using the manufacturer's protocol. The kit uses a resin that is able to bind DNA depending on the salt concentration, this means that by controlling the salt concentration the DNA can be bound, washed and eluted in order for it to be purified.

### ***DNA ligation***

The DNA fragments were ligated together using a Quick Ligation Kit (M2200, New England Bioscience). The DNA fragments were diluted in a 1:1 ratio with volumes that result in a DNA concentration less than 20 ng/μl as per the manufacturer's protocol. The ligations were run alongside a set of negative controls, where either the enzyme or one of the fragments is left out of the reaction. These were run to test for the presence of self ligation of the individual DNA fragments or contamination by other vectors, such as those from the restriction digest. The reaction was carried out at room temperature

for 5 min and then placed on ice before the reaction was used to transform competent bacteria.

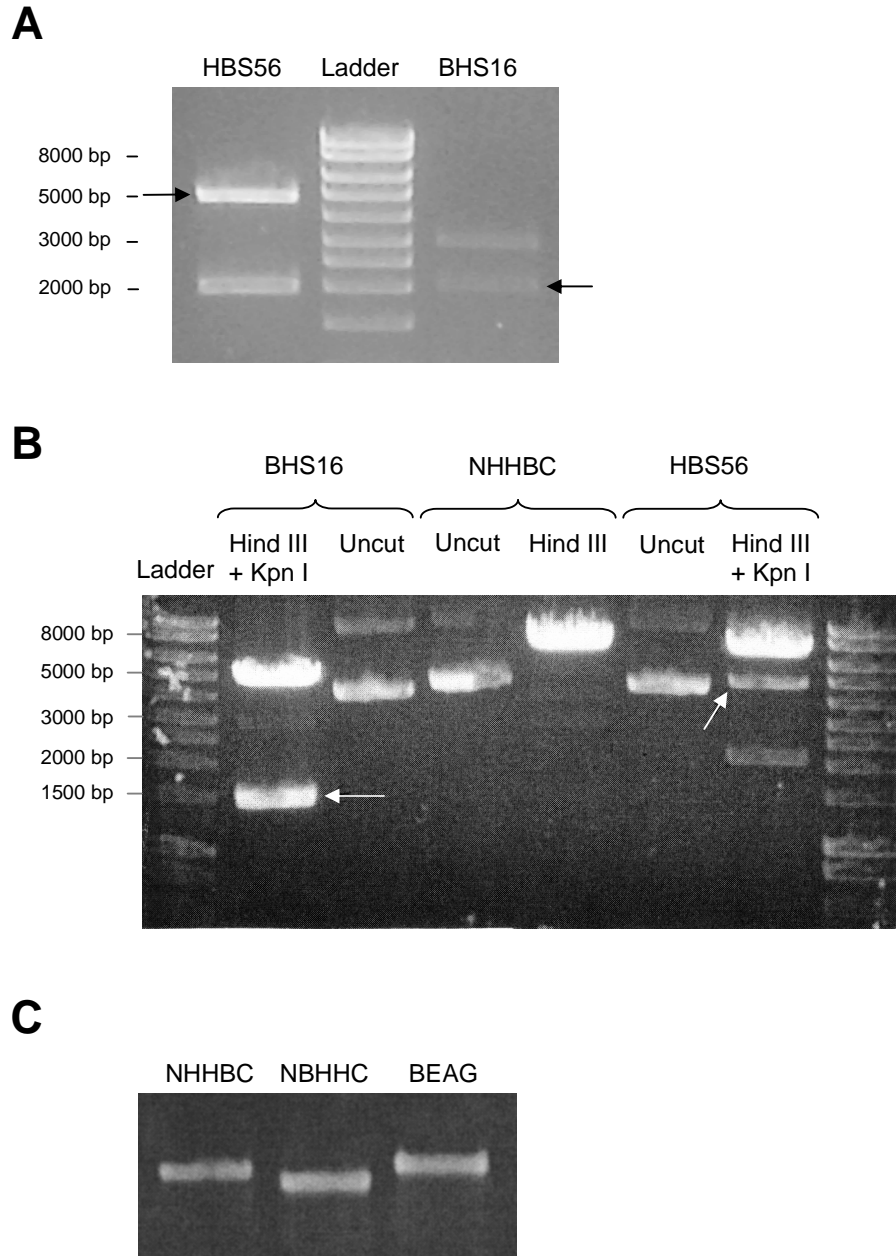


Figure 2.3: Creation of the single terminus exchanged chimeras NHHBC and NBHHC. **A**, A DNA gel of HBS56 and BHS16 cut by Mlu I and BamH I. These produced fragments (indicated by the arrows) that would be used in order to produce the C-terminus exchanged chimera (NHHBC). **B**, DNA gel of HBS56 and BHS16 cut by Hind III and Kpn I in order to produce fragments for the N-terminus exchanged chimera (NBHHC). **C**, A gel of the RNA produced from in vitro transcription reactions. The gel shows the RNA runs as a single band with no degradation products that would indicate contamination by RNase.

### ***Bacteria transformation***

The act of transformation is the insertion of DNA plasmid into bacterial cells that have been treated to permeabilise the membrane, allowing them to absorb DNA. This is an efficient way of replicating the DNA plasmids by using the bacterial machinery, the plasmids can then be purified to be used further. The transformation reactions were carried out using a standard protocol, using DH5 $\alpha$  competent cells which had a transformation efficiency of  $>1 \times 10^9$  cfu/ $\mu$ g.

The transformations are carried out in falcon 2059 tubes and incubated for at least 30 mins before the start of the protocol. The DH5 $\alpha$  cells were slowly thawed and the 50  $\mu$ l of cells were gently placed into the falcon 2059 tubes. 5  $\mu$ l of the ligation reactions were then added to the bacteria and incubated for 30 mins on ice. A positive control (pUC 18) vector was run alongside to measure transformation efficiency.

The bacteria was then heat shocked at 42 $^{\circ}$ C for 45 s and then returned to ice for 2 mins. 0.9 ml S.O.C. media that was warmed to 37 $^{\circ}$ C was added and placed in a shaker incubator for an hour, set at 37 $^{\circ}$ C, shaking at 220-250 rpm. After one hour, the 200  $\mu$ l of bacterial culture was spread on LB agar plates containing 100  $\mu$ g/ $\mu$ l of ampicillin.

The bacteria were grown up overnight at 37  $^{\circ}$ C on LB agar plates with 100  $\mu$ g/ml ampicillin as the selection antibiotic. The resulting colonies were then compared with the positive and negative controls. This was to check first for transformation efficiency and whether there were errors in the ligation as explained before.

If a ligation had occurred, where the plasmid contains the hERG fragment and ampicillin resistance gene, colonies grew on the experimental plate and none on the negative controls. Three or four of the colonies were picked to be grown up for a miniprep. Single colonies were grown in 10 ml of LB broth with 100 µg/ml ampicillin overnight in a shaker incubator at 225-250 rpm at 37 °C. 0.5 ml of bacterial culture was mixed with 0.5 ml of glycerol and stored in a -80 °C freezer. The remaining culture was then centrifuged at 3000 rpm at 4 °C to pellet the bacteria and the plasmid DNA was purified using a miniprep kit from Qiagen (Qiagen). The resulting DNA was tested with a diagnostic digest to further check if the DNA ligation had been successful. The DNA was sent to be sequenced, with particular focus on the ensuring there were no mutations introduced into the ligated regions.

With the DNA validated from the sequencing data, the clones were further amplified using a midiprep kit (Sigma-Aldrich). The bacteria were grown in a shaker incubator for over 24 hrs at 37 °C in LB broth plus 100 µg/µl ampicillin, as the pSP64 vector has a fairly low copy number in the bacteria, thus giving a low yield. First, the colonies were grown in 10 ml broth with 100 µg/ml ampicillin during the day, before the media was centrifuged at 3000 rpm at 4 °C for 5 min to pellet the bacteria and the pellet was resuspended in 40 ml broth with 100 µg/ml ampicillin and placed in the shaker incubator again overnight. The next day the resulting culture was pelleted by centrifugation. The plasmid DNA was purified were then extracted using a midi prep kit (Sigma-Aldrich) using the manufacturer's protocol. The purified DNA was quantified against a DNA Hyperladder I (Bioline, London) on a 1% weight to final volume agarose gel, and stored at -20 °C.

### ***In vitro transcription***

Having produced the chimeric DNA constructs, the next step was to study their expression and voltage dependent characteristics compared to wildtype channels.

First the plasmid had to be linearised to allow for the transcription to occur efficiently. The chimeric vectors were cut at a position beyond the 3' UTR using EcoR V (New England Biolabs). The WT hERG vector was cut with EcoR I restriction enzyme (New England Biolabs). The linearisations were carried out with these enzymes as the bEAG gene has several EcoR I restriction sites in its sequence. The DNA was then purified with the Qiaquick gel purification kit and quantified. Steps were taken to prevent contamination with RNase, which would digest any RNA produced. The template DNA was stored at  $-80\text{ }^{\circ}\text{C}$  for future use to reduce the chance of it degrading.

Template DNA was then transcribed to RNA using an SP6 mMessenger mMachine kit (Ambion Inc.) using the manufacturer's protocol.

The reaction mix was made up, 10  $\mu\text{l}$  of 2xNTP/CAP, 2  $\mu\text{l}$  of 10x reaction mix and 2  $\mu\text{l}$  of enzyme. Then 1  $\mu\text{g}$  of DNA template was added to the reaction and the volume was made up to 20  $\mu\text{l}$ . The reaction was incubated for 2 hours at  $37\text{ }^{\circ}\text{C}$ . DNAase I (Ambion Inc.) was then added to digest the DNA template, incubating again at  $37\text{ }^{\circ}\text{C}$  for 15 mins.

To check that the kit had successfully transcribed RNA that was free of contamination by RNase, 0.5  $\mu\text{l}$  sample of the transcription reaction was loaded on a 1 % agarose-formaldehyde gel. As a control the RNA was also ran alongside RNA of hERG that had been quantified and had been

successfully transcribed. This was to help quantify the RNA and ensure the molecular weight of the RNA was similar.

The gel was made up of 1% weight for volume agarose, MESA buffer (containing (in mM): 40 MOPS, 10 sodium acetate, 1 EDTA pH 8.3 with NaOH, made up with DEPC treated water) and 5% volume of formaldehyde (Sigma). The gel was electrophorised in MESA buffer at 80 mV for 50 minutes. The MESA buffer inhibits RNase, to prevent the breakdown of RNA in the samples as the gel is run. The gel was then viewed on a UV light box, if the RNA was viewed as a single band which had a molecular weight that was similar to the control RNA, it was quantified.

The resulting RNA was then quantified on a UV spectrometer (Genequant, Pharmacia) and aliquoted out so that each had a concentration of 500 ng/ $\mu$ l.

### ***Xenopus Oocyte isolation and injection with cRNA***

The oocytes were isolated from *Xenopus laevis* frogs. The frogs were euthanised by anaesthesia and decapitation. The ovaries were dissected out and placed in OR2<sup>-</sup> buffered solution containing (in mM): NaCl 82.5, Na<sub>2</sub>PO<sub>4</sub> 1, KCl 2.5, HEPES 5, buffered to pH 7.2 with NaOH. This was to reduce the possible degradation of the oocytes by hypoxia and necrotic factors. The ovary lobes were then separated in clumps of 20-30 oocytes for digestion by type IA collagenase (1mg/ml, Sigma). The oocyte clumps were digested for approximately 30 minutes and then washed with Barth's solution containing (in mM): 88 NaCl, 1 KCl, 0.4 CaCl<sub>2</sub>, 0.33 Ca(NO<sub>3</sub>)<sub>2</sub>, 1 MgSO<sub>4</sub>, 2.4 NaHCO<sub>3</sub>, 10 HEPES, buffered to pH 7.4 with NaOH. The digestion of the follicular cell layer weakens it and allows for its manual removal using forceps without much damage to the oocyte. The oocytes that were selected were of stage IV-V

maturity, where the dark and light pole were well defined and may have a light banding on the equator. The isolated oocytes were then stored in Barth's solution at 18 °C ready for injection with cRNA.

The oocytes were usually left overnight to recover from the handling that occurred during the isolation. They were then injected with cRNA using a nanolitre 2000 injector (World Precision Instruments Inc., UK). Glass micropipettes were made of TW120-3 glass (World Precision Instruments) pulled on a Flaming-Brown puller (Sutter instruments) and broken to a tip diameter of 5-8 µm with fine forceps. The RNA was diluted to the required concentration and drawn up into the micropipette. Oocytes were injected with 20 to 60 nl of cRNA, which equated to 1.25 to 30 ng of RNA per oocyte according to expression requirements. The oocytes were cultured for 2-4 days in order for them to express functional channel protein at the plasma membrane.

## **Electrophysiological recordings**

### ***Two Electrode Voltage Clamp of Xenopus oocytes***

This technique uses two electrodes to control and record the voltage and ionic currents across the cell membrane. The voltage has to be clamped in order to accurately record currents flowing through channels, these currents will affect the voltage if they were not clamped. The technique uses sharp glass electrodes to gain access to the cell interior (figure 2.4). The bath is clamped at 0 mV and is used as the reference for the voltage sensing electrode which measures the membrane potential. The other is used to inject current into the cell to control the membrane potential. This is controlled by an amplifier,

which contains a series of feedback amplifiers which controls the current injected to control the voltage (figure 2.4B). It is linked to a computer via an analogue to digital converter. The computer controls the amplifier using stored voltage protocols; and records the responses from the cell onto hard disc for offline analysis.

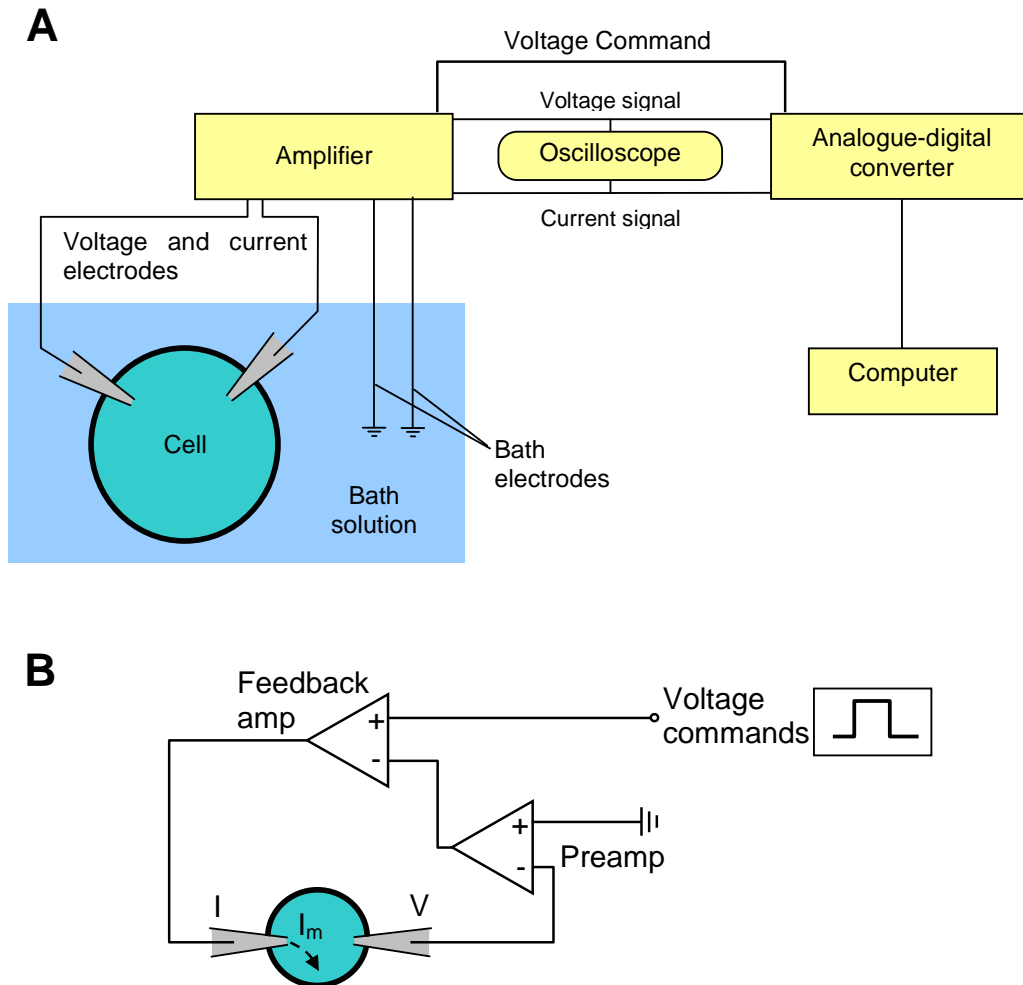


Figure 2.4: A schematic diagram of the two electrode voltage clamp (TEVC) setup. **A**, shows a basic cartoon of the connections for the recording equipment. **B**, The basic configuration of the amplifier in a voltage clamp mode, where the circuit forms a feedback loop to control the membrane potential via commands from the computer. (Modified from *Microelectrode Techniques- The Plymouth Workshop Handbook*)

The Axon 500B Geneclamp amplifier (Molecular Devices, USA) was used to control and record from the cell. The cell was placed in a bath and viewed under a low power microscope. The bath was perfused using a gravity fed perfusion system, connected to an electronic flow control device, allowing control of the solutions perfusing the cell. The flow of solutions was set at ~2 ml/min.

Sharp glass electrodes broken to a resistance of 1.1-2.0 M $\Omega$  were used to penetrate the oocyte membranes to record and control the membrane potential. The amplifier was linked to the computer via a 1322A series digitizer (Molecular Devices), an analogue to digital converter; this allows the analogue signal from the amplifier to be coded into a digital signal for the computer to record. The amplifier was controlled by the computer using voltage protocols that were designed and run using pCLAMP 9.0 software (Molecular Devices), these will be discussed in further detail in later chapters. The resulting current was recorded and written to the hard disc.

There are several practical advantages to this technique over the use of mammalian cells. The oocytes are large, robust and easy to culture without fear of infection. The protein expression levels from cell to cell are reproducible and easily controlled, compared to stable mammalian cell lines by regulating the amount of cRNA injected into them. The recording method using the sharp electrodes does not appear to alter the intracellular contents of the cell by dialysis as much as whole cell patch clamp recordings from mammalian cells. The disadvantage to the system is that the cells are not mammalian. This may mean that there are differences in the processing of proteins, and modulation by intracellular signalling pathways. When inhibition

by drugs is investigated, there is usually around a ten fold increase in the  $IC_{50}$  values compared to mammalian cells. This affect can be partly due to the presence of yolk inside the cells sequestering drugs thereby reducing the drug concentration at the membrane and so shifting the concentration-response curves. As it is not a mammalian cell, the way the protein is processed may not be the same as those seen in native cells, for instance having differential phosphorylation or glycosylation.

The technique is not suitable for recording rapid events, due to the large size of the cells, the capacitance of the membrane is high. Therefore it is slow to clamp the membrane potential to a command potential. This can lead to loss of voltage control if the cell membrane passes large amounts of current and therefore artefacts in the recordings. The large currents can also change the local concentration of ions, in hERG currents there may be potassium accumulation. This effect can be augmented by the fact the oocytes also have a second vitelline membrane around them, this can impede the diffusion of ions. The hERG channel conductance is also regulated by external potassium concentration (Sanguinetti *et al.*, 1995), so an increase in current due to ion accumulation can cause artefacts in the recordings.

In order to minimise artefacts caused by large currents, a sufficiently powerful amplifier was employed to clamp the membrane potential and the electrodes are broken to an ideally low resistance. This allows enough current to pass to retain voltage control, but to also create the least damage when the cell is impaled. This damage can introduce a non-selective leak current that needs to be considered when carrying out recordings. However in many cases, the membrane seals up around the electrode after it is impaled. The size of the

currents is controlled by titrating the amount of cRNA so that the cells express an optimum level of channels in the membrane. The ideal current amplitude for recordings was 1-5  $\mu$ A. To reduce the amount of potassium accumulation the perfusion system outlet, with a sufficient solution flow rate, was placed adjacent to the cell, this ensures good solution exchange around the cell.

### ***Recording solutions***

A low chloride extracellular bath solution was used, where MES (2-[N-morpholino]ethanesulfonic acid) largely replaced the chloride ions to reduce contamination of the recordings by endogenous chloride currents found in oocytes. The solution contained (in mM) 96 NaMES, 2 KMES, 2 CaMES<sub>2</sub>, 5 HEPES, 1 MgCl<sub>2</sub> adjusting to pH 7.6 with NaOH.

For two electrode voltage clamp, the glass electrodes made of filamented glass (TW150F-4, World Precision Instruments) were pulled using a Flaming-Brown puller (Sutter instruments) filled with 3 mM KCl solution.

Compounds were first made into a stock solution by dissolving in DMSO. The drugs were then dissolved in the bath solution to the required concentration. The dilutions were carried out to ensure that the concentration of DMSO did not exceed 1%, due to the possibility that it induce non-specific effects on cells.

### **Patch Clamping**

This technique of electrophysiological recording is a more specialised and technically challenging recording method compared to the two electrode voltage clamp technique. It differs in several ways:

- It uses one electrode for simultaneously controlling voltage and recording current. (figure 2.5 and 6)
- A different amplifier circuit is used to record the current elicited from the voltage commands (figure 2.6B).
- It uses blunt fire polished glass electrodes to attach to the cell membrane and this forms a high resistance seal, electrically isolating the patch of membrane so the currents recorded are mostly through the patch. It also allows for low noise recordings to be achieved as the variance of noise is related to the resistance.
- The end of the patch pipette needs to be kept clean to form a gigaseal, therefore the electrode is used only once with each attempt at gaining a seal.
- It uses smaller cells and is sensitive to smaller currents.
- This increase in the sensitivity means that the equipment is more susceptible to both vibrational and electrical noise. Careful insulation from external influences is needed to get a good signal to noise ratio. This is usually through use of an air table to minimise vibrations and faraday cage to isolate the apparatus from electrical fluctuations.
- The technique is also able to record channel activity in a variety of configurations: Cell attached, whole cell, excised inside-out and outside-out patch configurations (figure 2.5).

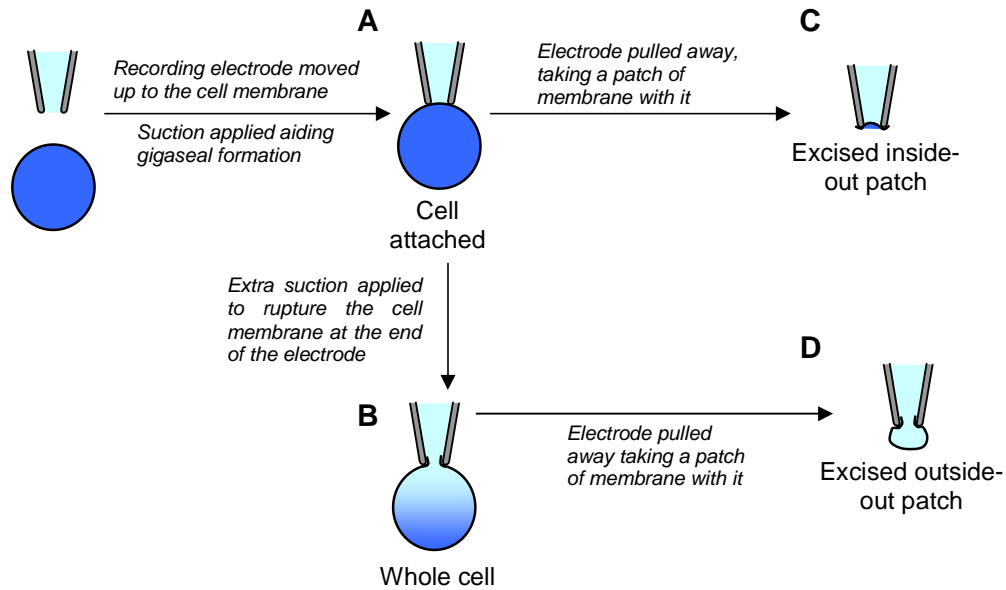


Figure 2.5: The possible configurations of patch clamp experiments. A diagrammatic explanation of the recording configurations that can be achieved by a patch clamp setup.

The technique relies on the glass being able to bond to the cell membrane to create a mechanically stable high resistance (gigaohm) seal. This isolates the patch from the bath solution allowing for low noise recordings to be made. The different conformations have different uses. Cell attached recordings (figure 2.5A) are used mainly to characterise the biophysical properties of single channels. The channels may be activated by application of a suitable concentration of agonist into the pipette solution. In the case of voltage-gated channels a voltage step is applied. However, the internal conditions are unknown, therefore the membrane potential can not accurately set unless the cell membrane is ruptured and a voltage measurement is taken.

Whole cell recordings (figure 2.5B) are used for a majority of biophysical and pharmacological studies. This configuration records from the whole population of channels in the cell, which allows simple electrophysiological experiments to be made. In most cases they are used for observing cellular response to

the application of ligands or channel inhibitors. It also gives access to the intracellular contents of the cell, so solutions can be dialysed into the cell, thereby controlling the intracellular contents.

Excised patch clamp recordings are more technically challenging than recording whole cell currents, as there is a higher likelihood of losing the high resistance seal when the patches of membrane are pulled away by the glass pipette. This technique is used for studying single or multiple channels, with no guarantees of the number of channels in the patch. There are two types of excised patch conformations: excised inside-out (figure 2.5C) and excised outside-out patch clamp (figure 2.5D).

This study will mainly use the inside-out patch clamp technique. The technique gives access to the inner surface of the cell membrane, allowing direct application of ligands and channel blockers to this surface. This is advantageous if they are not permeable to the membrane.

## The patch clamp setup

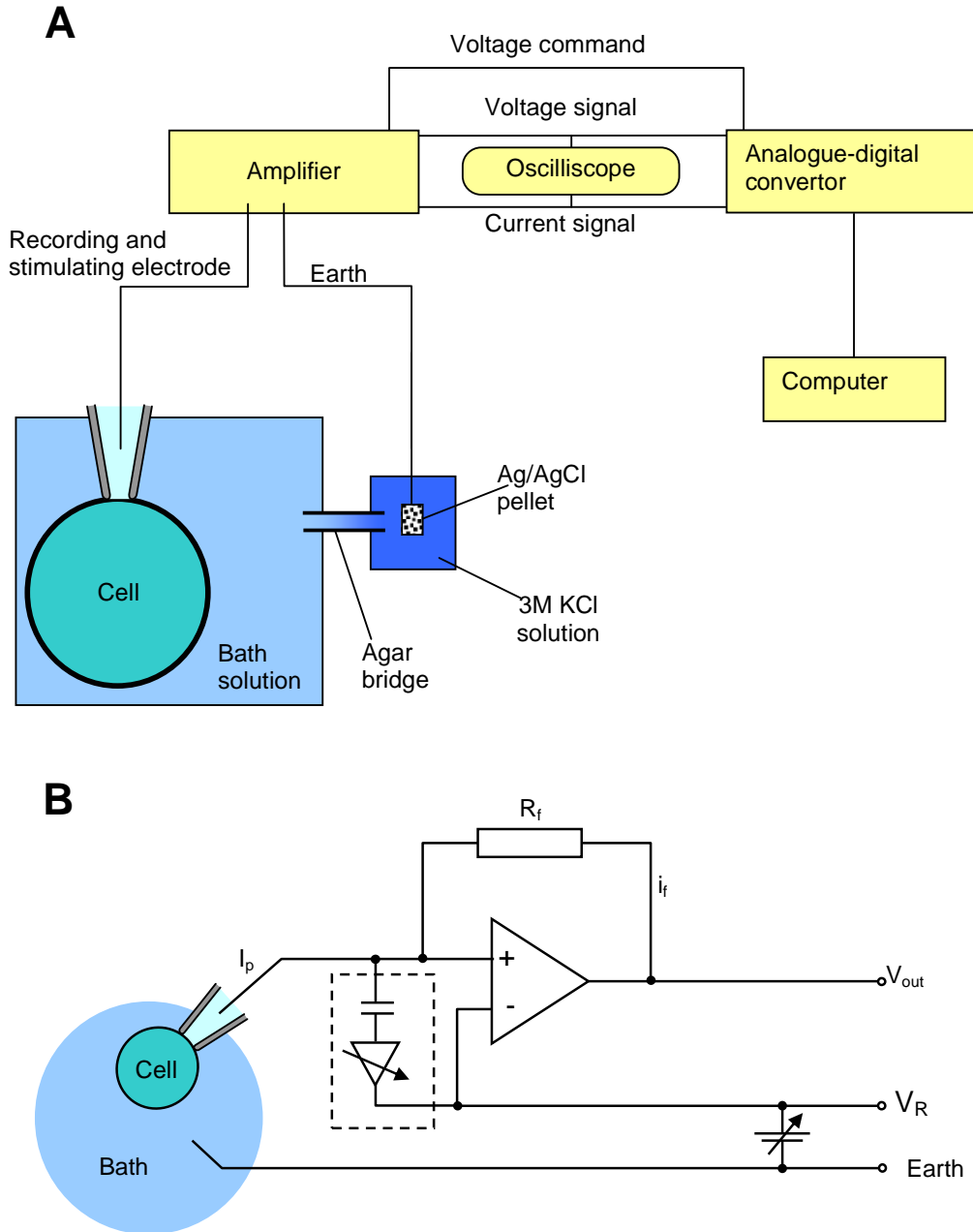


Figure 2.6 A schematic of the patch clamp setup. **A**, shows a cartoon of the connections for the electronic data. Note the differences in the setup compared to the TEVC technique. **B**, A basic representation of the patch clamp circuitry. The voltage of the electrode is controlled by the feedback amplifier, which injects current via the recording electrode to control voltage. The dashed box shows an extra circuit used to inject current that compensate for series resistance and capacitance of the pipette and cell membrane. (Modified from *Microelectrode Techniques-The Plymouth Workshop Handbook*)  $I_p$  is the patch membrane current.  $R_f$  is the feedback resistor,  $i_f$  is the feedback current.  $V_R$  is the reference voltage.  $V_{out}$  is the voltage output that is proportional to the current injected into the pipette  $V_{out} = -V_R \cdot i_p \cdot R_f$ .

An Axopatch 200B amplifier (Molecular devices, USA) was used in the patch clamp recordings, linked to the computer via a Digidata 1322A (Molecular devices). The amplifier was controlled by the computer using voltage protocols that were designed and run using pCLAMP 8.2 software (Molecular Devices), these will be discussed in further detail in later chapters. The resulting current was recorded and written to the hard disc. In our recording conditions, membrane current and voltage data were filtered at 1 kHz and recorded to the hard disc at a sampling frequency of 10 kHz.

The cells were placed on coverslip on an inverted microscope (Zeiss Axiovert, Germany). The microscope was used, in conjunction with a micromanipulator (Siskiyou MX7600, USA), to move the glass microelectrode up to the cell membrane in order for the pipette to seal against the membrane. Before sealing against the cell the capacitance and voltage offset of the glass electrode were compensated for using the amplifier. In cell attached mode, recordings can be made if the patch was to be excised. This was to check the number of channels in the actual patch and get a steady state value of the amplitude of the currents passed through the patch. Then the patch would either be excised or ruptured to gain an inside-out patch or whole cell configuration in order to begin recordings.

### ***Solutions for patch clamp recordings***

The oocytes were prepared as described previously. However, before patch clamp recordings could be carried out, a second membrane had to be stripped from the cell. This is membrane, which helps protect the plasma membrane from damage, would interfere with access to the channels on the cell surface and has to be removed. The cells were shrunk in hypertonic

solution containing (in mM) 200 NaCl, 20 KCl, 1 mM MgCl<sub>2</sub>, 10 HEPES, 1 EGTA adjusted to pH 7.4 using NaOH. This separates the cell membrane from the vitelline membrane, allowing it to be broken and pulled away using fine forceps. Care was taken in stripping the membrane, as the cell membrane can be quite viscid, this can adhere to the vitelline membrane, any surfaces the cells touch, such as the dish in which the cells were stripped and the plastic bulb pipette that was used to transfer the cells. Therefore the cells were stripped using a glass dish and pipette, these have much smoother surfaces than the plastic dishes that they are usually stored in. The equipment was cleaned thoroughly to reduce the chance that the cell would stick to any of the surfaces. Care was also taken to ensure that the cell did not touch the liquid-air interface, as the surface tension on the cell was likely to cause tears in the cell membrane. The stripped cells were then transferred to the recording chamber which was mounted on the stage of an inverted microscope.

To record bEAG currents, a low potassium, extracellular solution was used, containing (in mM) 103.6 NaAsp, 11.4 KCl, 10 HEPES, 1.8 CaCl<sub>2</sub> adjusted to pH 7.2 using NaOH, and a high potassium intracellular recording solution containing (in mM) 120 KAsp, 15 KCl, 10 EGTA, 10 HEPES adjusted to pH 7.2 using KOH (Gessner & Heinemann, 2003). These solutions set the equilibrium potential for potassium to ~-60 mV, creating a large driving force on the potassium ions at positive potentials during test depolarisations to +20 mV. Aspartate based solution was used to reduce any endogenous chloride current that may be present.

To record the currents that were elicited from the hERG and bEAG/hERG chimeras, solutions with a symmetrical potassium concentration was used. This set the equilibrium potential for potassium at 0 mV, creating a larger driving force on potassium ions at negative potentials. Tail currents were measured at -120 mV following a test pulse to +20 mV. High extracellular potassium concentrations also reduce the inactivation of the hERG channels. The extracellular solution was composed of (in mM) 140 KCl, 5 HEPES, 1 CaCl<sub>2</sub> adjusting to pH 7.2 with KOH and the intracellular recording solution contained (in mM) 140 KCl, 1.63 CaCl<sub>2</sub>, 5 EGTA, 5 MgATP, 10 HEPES, pH was adjusted to 7.4 using HCl). In this intracellular solution, Ca<sup>2+</sup> was buffered to 30 nM (estimated with WEBMAXCLITE software [www.stanford.edu/cpatton/webmax](http://www.stanford.edu/cpatton/webmax)).

In some of the recordings carried out on the WT hERG and hERG/bEAG chimeric channels, EAG intracellular recording solution was used in conjunction with the hERG extracellular solution. This was done as the success of the excised patches with the other solution was low. A junction potential of -9.7 mV would be produced between the intracellular and extracellular solutions (calculated on pClamp software), this was corrected for by dialling in a voltage offset on the amplifier. Comparisons of the voltage-dependence of the channels in either solution showed that they were unchanged. The cells that were recorded with these solutions will be marked out.

### ***Excised inside-out patch clamp recordings***

Glass electrodes were pulled using GC150F-10 borosilicate filamented glass (Harvard Apparatus Inc.) using a Flaming-Brown puller (Sutter instruments).

They were fire polished to create blunt electrodes that had a resistance of between 1-3 M $\Omega$ . The electrodes were back filled with extracellular recording solution. The recording chamber was filled with the extracellular recording solution at room temperature. The cell was introduced into the solution and intracellular recording solution was then perfused on for 2 minutes to allow the solution to exchange.

The patch pipette was moved toward the cell so that it could seal and form the cell-attached conformation. Seals below 1 G $\Omega$  were discarded. The membrane potential was pulsed to +20 mV for 500 ms then repolarised to –120 mV for 1 s, and the protocol repeated every 8 s. The recordings were taken if the cell displayed a stable current in the cell attached configuration. Once a set of traces were recorded, the patch pipette was moved away from the cell to acquire an excised inside-out patch. The recordings were then resumed, taking the time of excision as zero time.

### ***Data analysis of the electrophysiological recordings***

The traces recorded were analysed using Clampfit 8.2 software (Molecular devices, USA). The methods of analysing the traces will be explained in the relevant results chapters.

Statistics and curve fitting were carried out on the resulting data using Clampfit 8.2 (Molecular Devices) and Graphpad Prism 4.0 (Graphpad Software, San Diego California, USA).

### ***Voltage dependence of activation***

The voltage dependence of activation (chapter 3) was analysed by taking the peak tail currents and normalising them against the maximum peak tail

current recorded in that protocol. These normalised values were then plot against the test potential. The points were then fit with a Boltzmann function (see below) using Graphpad Prism 4.0 (Graphpad Software, San Diego California, USA) to obtain values for half maximal activation ( $V_{1/2}$ ) and slope, which is an indication of the voltage sensitivity of the channel.

$$Y = \frac{I_{\min} + (I_{\max} - I_{\min})}{\left(1 + e^{\left(\frac{V_{1/2} - x}{\text{slope}}\right)}\right)}$$

Where:

- Y is the conductance
- $I_{\min}$  is minimum value on the curve
- $I_{\max}$  is the maximum value on the curve
- $V_{1/2}$  is the midpoint of the curve
- Slope is the curves gradient
- $x$  is the test potential

### ***Fitting exponential functions***

Data were fitted with first and second order exponential functions (see below) using clampfit 8.2 or 9.0. Single exponentials were fit to points to measure the time constant for activation and estimate the amount of inhibition when it reaches steady state block. A double exponential was used to fit the deactivation and inactivation time course in order to obtain a time constant for the decay.

$$f(t) = \sum_{i=1}^n A_i e^{-t/\tau_i} + C$$

Where:

- $t$  is the time
- $A$  is the component amplitude
- $i$  is the component
- $\tau$  is the time constant
- $C$  is the constant y-offset

### ***Concentration-response relationships***

In order to obtain the IC<sub>50</sub> and Hill slope values of compounds, concentration-response experiments were carried out, where increasing concentrations of compound was used to inhibit the channel currents. The concentrations of compounds were chosen in half log<sub>10</sub> increments so they flanked the IC<sub>50</sub> value, which would allow for accurate fitting of the Hill function (see below) by Graphpad prism 4.0 (Graphpad Software). The current amplitudes were normalised to current recorded when there was an absence of compound, these were then plotted against the log<sub>10</sub> concentration.

$$Y = \frac{[B]^n}{IC_{50} + [B]^n}$$

Where:  $Y$  is the Inhibition

$[B]$  is the concentration of inhibitor

$n$  is the Hill slope

Each of the individual concentration response experiments were fit with the Hill function and then the IC<sub>50</sub> and Hill slope values were averaged to get the mean and standard error of the mean.

All data are presented as mean  $\pm$  the standard error of the mean (S.E.M.) unless otherwise stated. Statistical comparisons were made by one-way Anova with Dunnett's post test for multiple comparisons. This test determines if there are any significant differences between group means with a reference group. A significant difference between two data sets was classed as significantly different for  $p \leq 0.05$ .

## Chapter 3: Characterising the voltage dependent properties of hERG/bEAG chimeras

### Introduction

Recording from excised inside-out patches of hERG channels can be difficult, as the channels display a rundown in activity. This is where the activity of the channels in the patches decreases so that they fail to pass current. Rundown can be a serious obstacle in recording currents from excised inside-out patches of hERG, due to the limited number of channels in the patch. It has been noted in many articles using whole cell and excised patch clamp recordings, but the phenomenon has not been extensively studied (Bian *et al.*, 2001; Cayabyab & Schlichter, 2002; Du *et al.*, 2004). It is thought to be due to some internal modulatory factors, such as PKC, PIP<sub>2</sub> and tyrosine kinases (Bian *et al.*, 2001; Cayabyab & Schlichter, 2002; Thomas *et al.*, 2003), although a clear picture has not yet been put forward.

bEAG channels, a close relative of hERG, do not display significant rundown on excision of patches (Gessner & Heinemann, 2003; Gessner *et al.*, 2004). The channels share a sequence homology of 59% between each of the transmembrane domains; the main differences lie in the cytoplasmic tails and the turret regions of the channels, where they share 28% homology (see appendix for the structures and alignments).

The cytoplasmic N and C termini would be the most likely structures that affect the rundown, as they are large structures positioned on the cytoplasmic side of the membrane, and so could be influenced by internal modulatory factors. The cytoplasmic domains of many channels are known to have a

regulatory role. As with HCN channels, the hERG and bEAG channels have a cyclic nucleotide binding domain on the C-terminus of the channel, although it does not appear to be directly regulated by the binding of cyclic nucleotides, such as cAMP (Curran *et al.*, 1995; Sanguinetti *et al.*, 1995; Frings *et al.*, 1998; Cui *et al.*, 2001). The two channels also have a PAS domain on the C-terminus (Morais Cabral *et al.*, 1998; Vilorio *et al.*, 2000), this interacts with the pore to slow the rate of channel deactivation. The aim of this study was to exchange the individual WT hERG termini with that of WT bEAG and study whether the rundown of these channels has been altered in any way. The intention was to create a channel that has the inactivation and pharmacological properties of the WT hERG channel, but one that can be recorded from in excised patches without rapid rundown. Therefore, before making excised patch recordings, the chimeras had to be characterised to see if there was any alteration in voltage dependent properties from WT hERG channels (the focus of this chapter). The pharmacological properties of the chimeric channels will be covered in the next chapter.

This study used the two electrode voltage clamp technique to examine the voltage and time dependent properties of the chimeric channels (see page 40).

## **Results**

### ***Characterisation of the Chimeras***

The cRNA for the BHS16, NHHBC and NBHHC chimeric constructs were expressed in *Xenopus* oocytes and the currents that were recorded were compared to WT hERG, bEAG and a NTK mutant, in which the N-terminus of

hERG has been deleted. The expression levels of the chimeras are much lower than WT hERG, bEAG and NTK, with the WT channels 5-10 ng cRNA

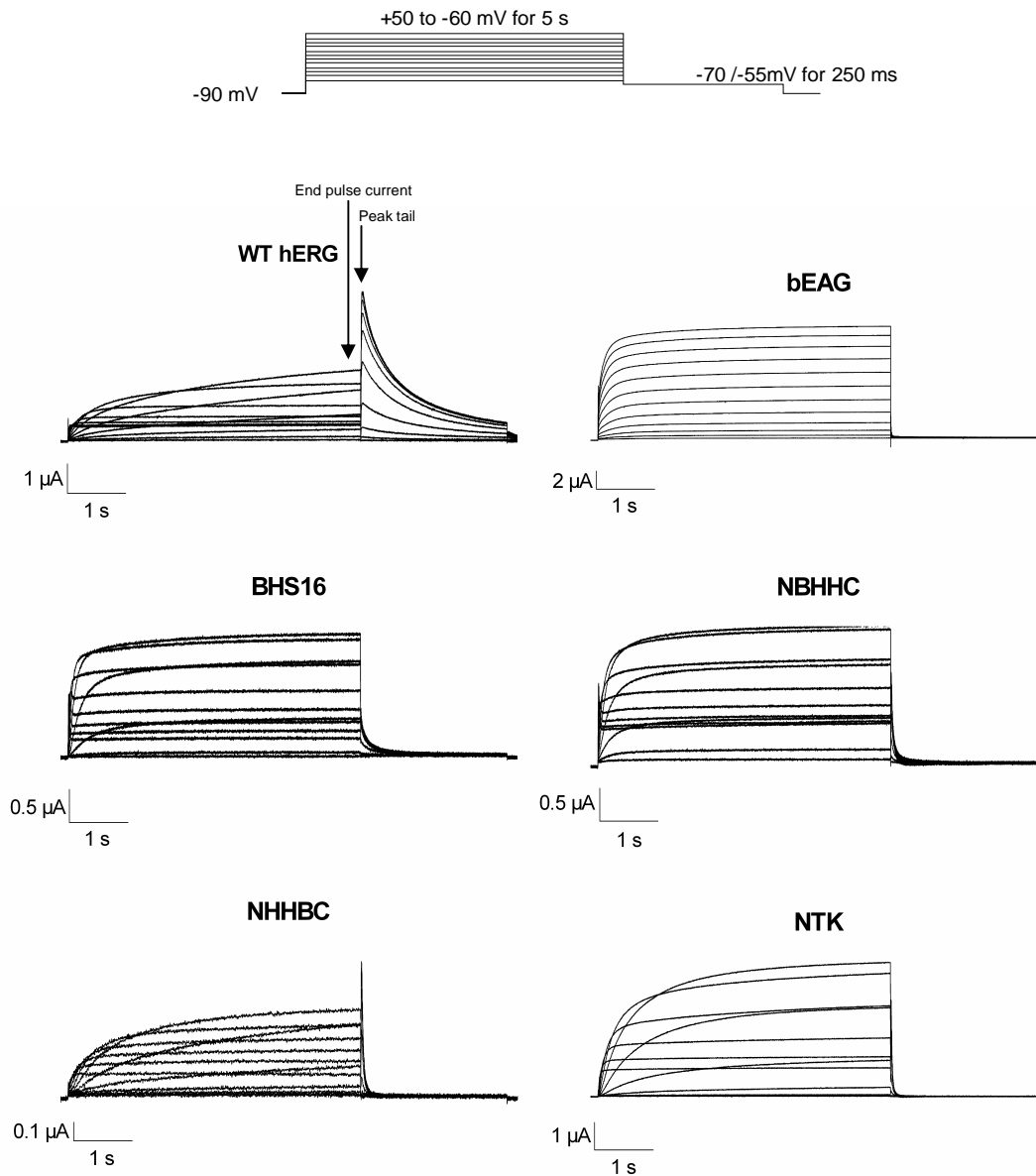


Figure 3.1: Comparison of the I-V relationships of hERG/bEAG chimeras with WT hERG and bEAG and NTK channels. Representative current traces are shown in response to the voltage protocol illustrated in the inset. **A** and **B**, are the WT hERG and bEAG currents. **C-E**, are the chimeric channel currents. **F**, currents from hERG channels with a truncated N-terminus. The horizontal arrow indicates the zero current line. Vertical lines indicate the time points where the measurements of currents amplitudes were taken and used in subsequent analysis of the I-V relationships. Tail currents for A, B, C, D and F were measured at -70 mV, whilst E was measured at -55 mV.

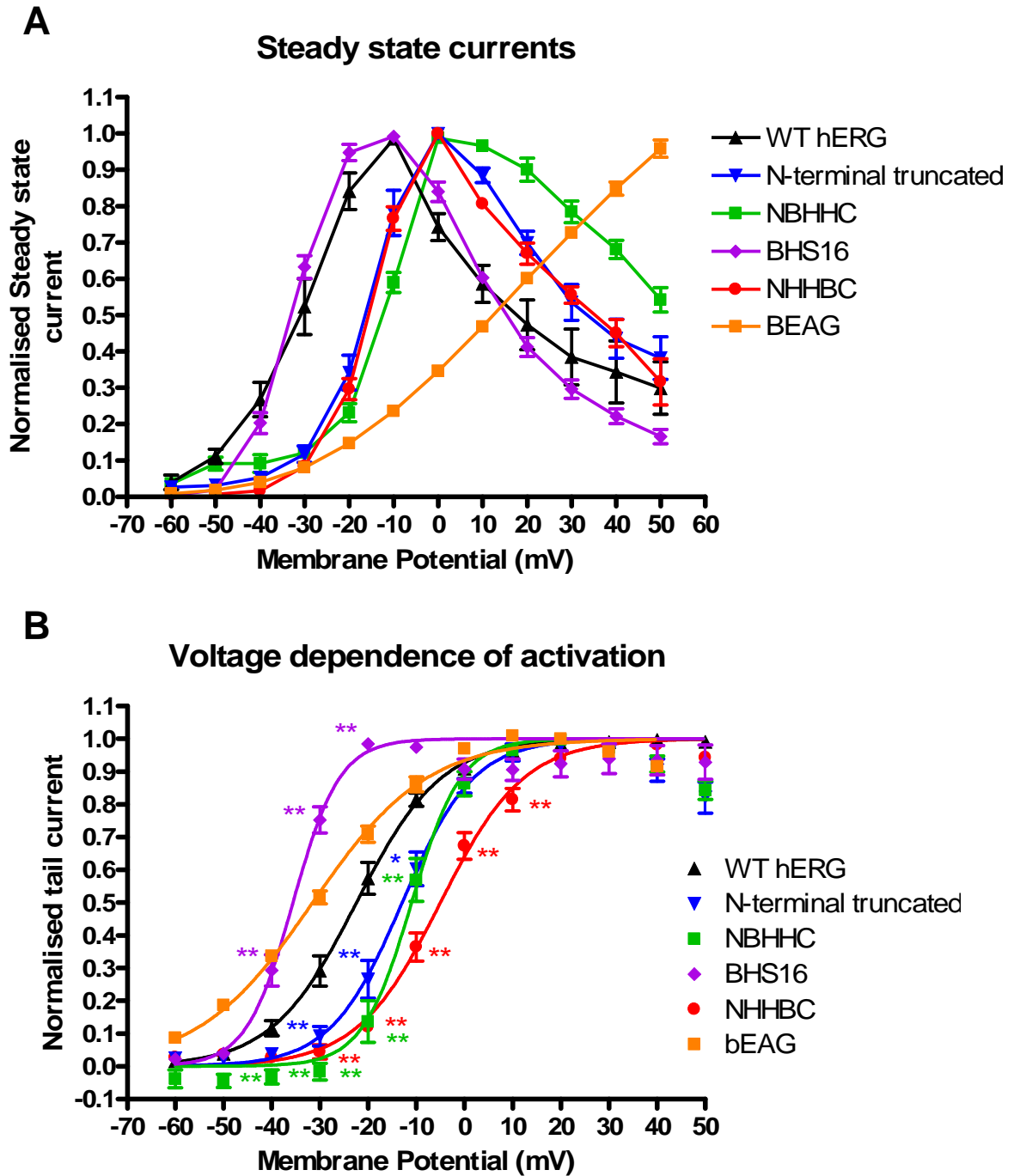


Figure 3.2: Voltage dependent relationship of hERG/bEAG chimeras. A, Mean end pulse currents normalised to the maximum current elicited and plotted against the test potential. B, Mean peak tail current amplitudes, normalised to the maximum current elicited and plotted against test pulse potential. Data were fitted with a Boltzmann function to obtain values for  $V_{1/2}$  and slope.  $n=5$ . \* indicates  $p<0.05$  and \*\* indicates  $p<0.01$  for the respective chimeras compared to the WT hERG value at the same voltage.

was injected, with NTK, 10-15 ng was injected, these elicited currents that had a peak amplitude of between 1 - 5  $\mu$ A, 2 days after the injections were carried out. This is compared to injections of 30 - 60 ng of the chimeric cRNA eliciting peak current amplitudes of less than 1.5  $\mu$ A (figure 3.1).

### ***Characterisation of current-voltage relationships***

The voltage dependence of activation was studied using the standard I-V protocol, as described in the methods (figure 3.1). In comparison with bEAG, the hERG currents increase with relatively slow time courses in response to test depolarisations at potentials positive to the threshold value of -60 mV. The WT hERG end pulse current amplitudes reach a maximum at -10 mV and then show a reduction in amplitude at more positive potentials due to increasing proportions of channels inactivating. This is a characteristic window current, which is defined by the voltage dependence of activation and inactivation (figure 3.2A). This negative slope in end pulse I-V relationship is not displayed by bEAG channels, due to the fact that it does not display inactivation.

The WT hERG currents have a characteristically large tail current, which decays in amplitude with a slow time course. This occurs due to the fast recovery from inactivation and the slower deactivation. In contrast bEAG tail currents are small and deactivate with relatively rapid time courses.

	WT hERG	WT bEAG	NTK	NBHHC	BHS16	NHHBC
$V_{1/2}$ (mV)	$-22.4 \pm 0.5$	$-31.5 \pm 0.6$ **	$-12.9 \pm 0.9$ **	$-11.0 \pm 0.7$ **	$-35.6 \pm 0.7$ **	$-5.0 \pm 0.6$ **
Slope	$8.8 \pm 0.4$	$11.9 \pm 0.5$ **	$7.4 \pm 0.8$ **	$5.1 \pm 0.6$ **	$4.9 \pm 0.6$ **	$8.7 \pm 0.5$
	n=5	n=4	n=4	n=5	n=5	n=5

Table 3.1: Comparing voltage dependence of activation of the chimeras and mutant channels with the WT channels. The data is presented as the mean and the S.E.M. \*\* represents  $p < 0.01$  when compared to the WT hERG value.

The chimeric and NTK channels display similar activation characteristics to WT hERG; they show slow activation starting at approximately -60 mV. The inactivation of the channels is retained by the chimeric and NTK channels, which is indicated by the negative slope seen at potentials positive to 0 mV.

The deactivation of the bEAG/hERG chimeric channels have tail currents that deactivate much quicker than WT hERG; this is not as rapid as bEAG, but similar to NTK channels. Therefore, measurements of the peak tail current give an indication of the voltage dependence of activation. WT hERG is maximally activated at +10 mV. The plot of peak tails can be fitted with a Boltzmann sigmoidal function (figure 3.2B). This gives you the voltage where the channels are half maximally activated ( $V_{1/2}$ ) and a slope value that indicates the channels sensitivity to voltage. The data is summarised in table 3.1.

From my data, WT hERG channels have a  $V_{1/2}$  of  $-22.4 \pm 0.5$  mV with a slope of  $8.8 \pm 0.4$  (n=5). bEAG currents do not display any inactivation. Deactivation is so rapid, tail currents cannot be reliably analysed. Instead the steady state currents were used to derive the voltage dependence of activation, by calculation of the gradient of the activation curve, normalising to the maximum gradient and plotting this against voltage. The results indicate that the channels have a mean  $V_{1/2}$  of  $-31.5 \pm 0.6$  mV and a slope of  $11.9 \pm 0.5$  (n=4). Thus, bEAG channels can activate at slightly more negative potentials than WT hERG, but are less sensitive to voltage changes.

The BHS16 chimera displays a negative shift in the  $V_{1/2}$  of -13.2 mV, compared to WT hERG (figure 3.2B). The other channels studied have a positive shift:

with a 10.5, 11.4 and 17.4 mV shift in the  $V_{1/2}$  by NTK (n=4), NBHHC (n=5) and NHHBC (n=7) respectively. These were all significantly different to WT hERG. The slopes of the chimeras are similar to the WT hERG, these were found to be significantly different to WT hERG. However, NTK was not significantly different.

The difference in the activation properties of all the chimeras and the NTK mutant suggests that the N- and C-termini are important in activation gating. Only BHS16 showed a negative shift of the activation curve. The hERG N- and C-termini may exert a negative shift on the voltage dependence of activation, destabilising the open state. While the bEAG termini interact to increase the activation rate, by increasing the coupling between the voltage sensor and the intracellular gate.

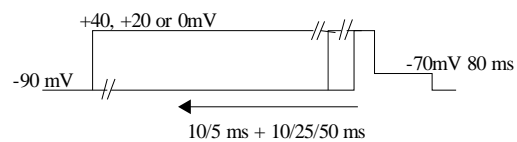
### ***Time dependent kinetics of activation***

To look at the activation of current with time, an envelope of tails protocol was used (figure 3.3). The length of the test depolarisation step was varied and channel activation determined from the increase in amplitude of tail current measured at -70 mV. The test pulse durations were chosen to get an accurate range of activation from just active to fully active. Tail current amplitudes were measured, normalised to the maximum current elicited, plotted against the test pulse duration and fitted with a single exponential function to give time constants for activation. The initial activation is delayed and this was particularly noticeable for NBHHC and NHHBC.

The activation of wild type hERG is relatively slow, with a mean time constant of  $241.4 \pm 4.6$  ms at 0 mV  $154.6 \pm 1.9$  ms at +20 mV and  $43.8 \pm 1.1$  ms at +40 mV (figure 3.4). bEAG activates at a similar rate as WT hERG. However,

unlike WT hERG, the rate of activation of bEAG does not change as greatly with voltage. This reflects what is seen in the I-V relationships of each of the channels, that hERG channels have a steeper slope value than bEAG channels, indicating more voltage sensitivity.

**A**



**B**

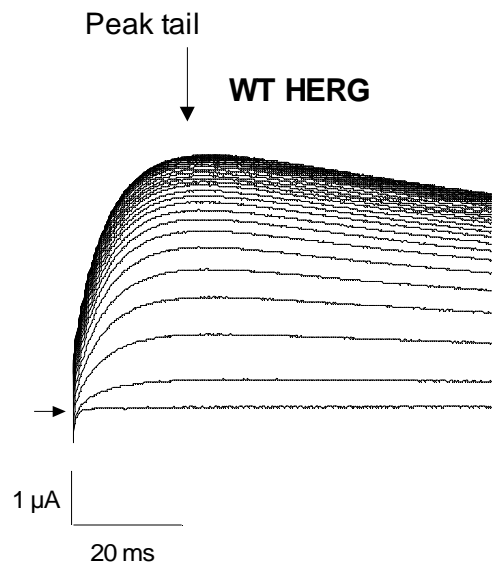


Figure 3.3: Time dependence of activation of WT and chimeric channels. **A**, The envelope of tails protocol used to record the activation time course of channels. The cells were depolarised to either 0, +20 or +40 mV. The duration of the depolarising pulse was started at either 5 or 10 ms and then extended by 10, 25 or 50 ms steps. Tail currents were recorded at -70 mV. **B**, representative family of tail currents of WT hERG showing the increase of tail current amplitudes as activation accumulates with the increasing length of the test pulse. The currents during the test pulse are not shown.

0 mV

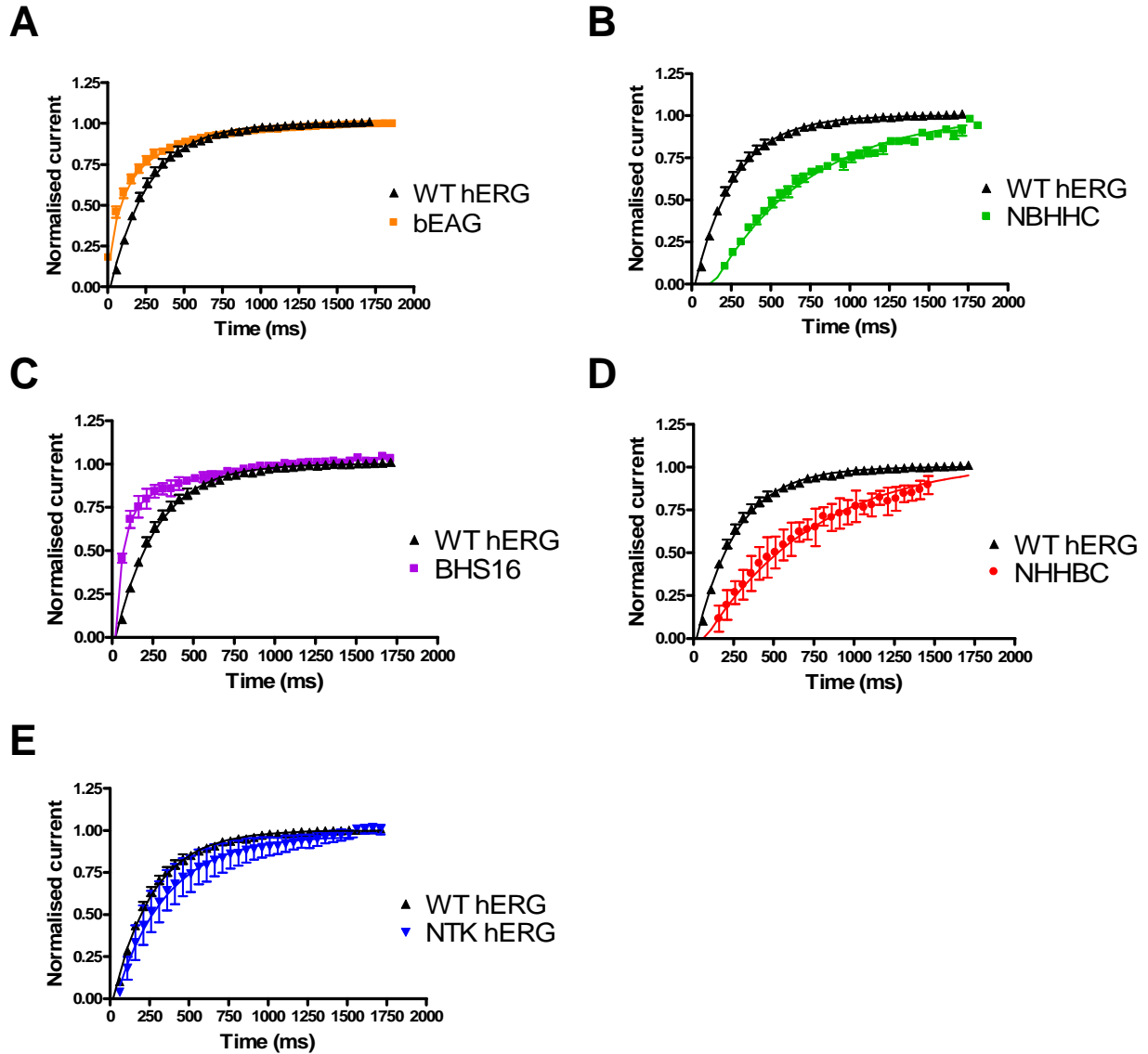


Figure 3.4: Time course of activation at 0 mV. Plots of the peak tails against test depolarisation duration to show the activation of the channels when depolarised to 0 mV. Comparisons are made with WT hERG. The results were fitted with a single exponential to get a time constant of activation. WT hERG n=6, bEAG and chimeras n=3-5 oocytes.

+20 mV

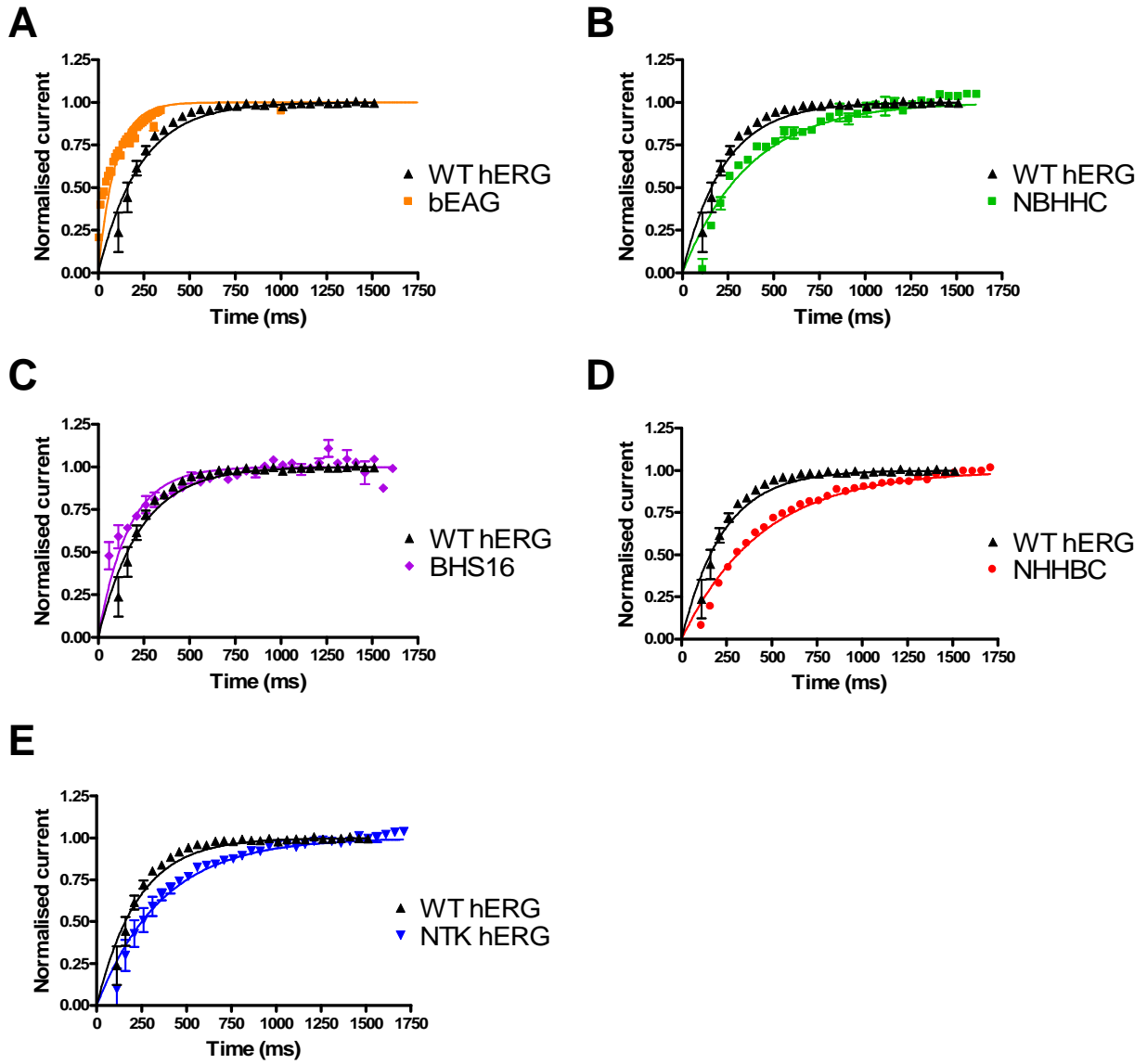


Figure 3.5: Time course of activation at +20 mV. See figure 3.4 for details. WT hERG, bEAG and chimeras n=3-4 oocytes.

+40 mV

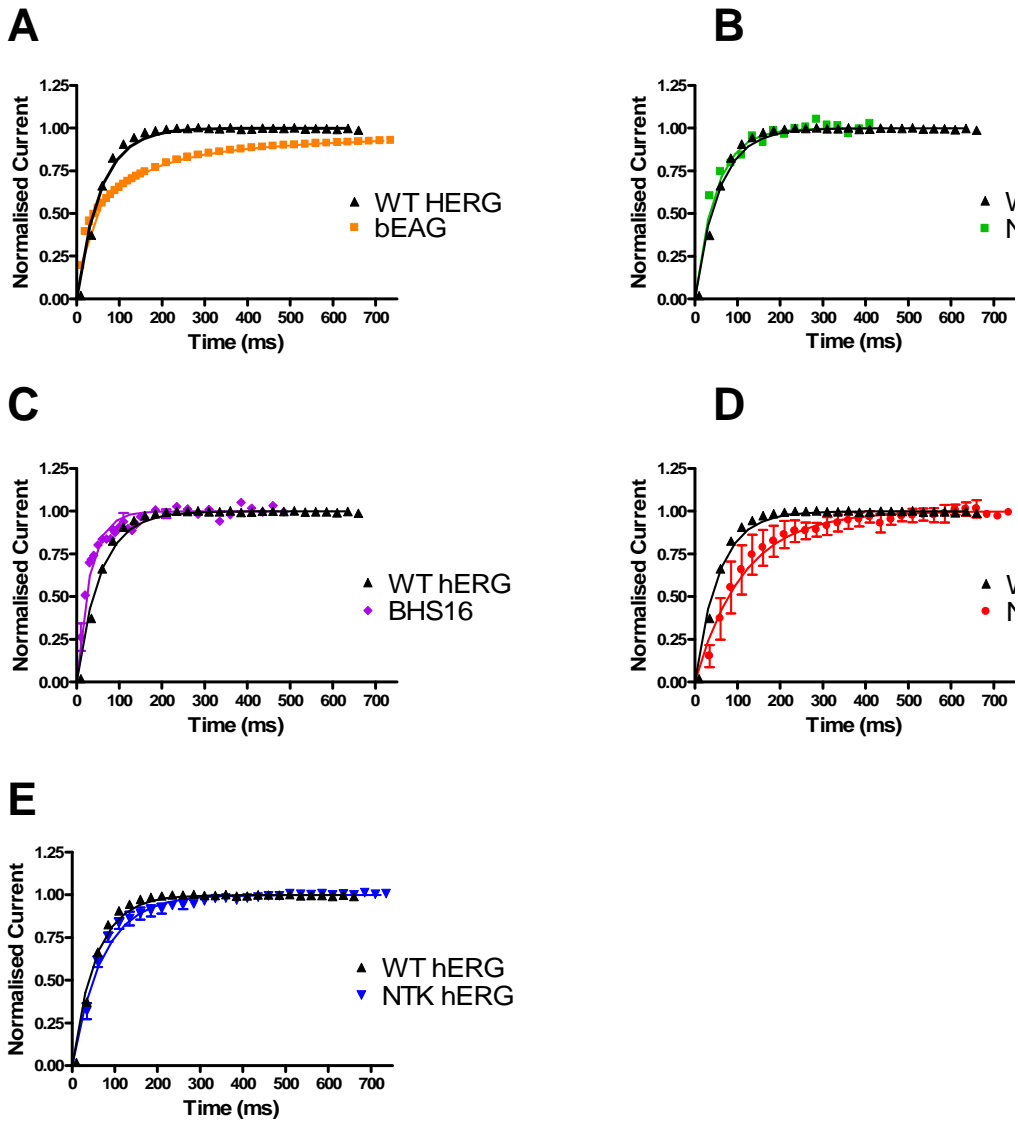


Figure 3.6: Time course of activation at +40 mV. See figure 3.4 for details. WT hERG n=3, bEAG n=3, NTK n=5, chimeras n=3 oocytes.

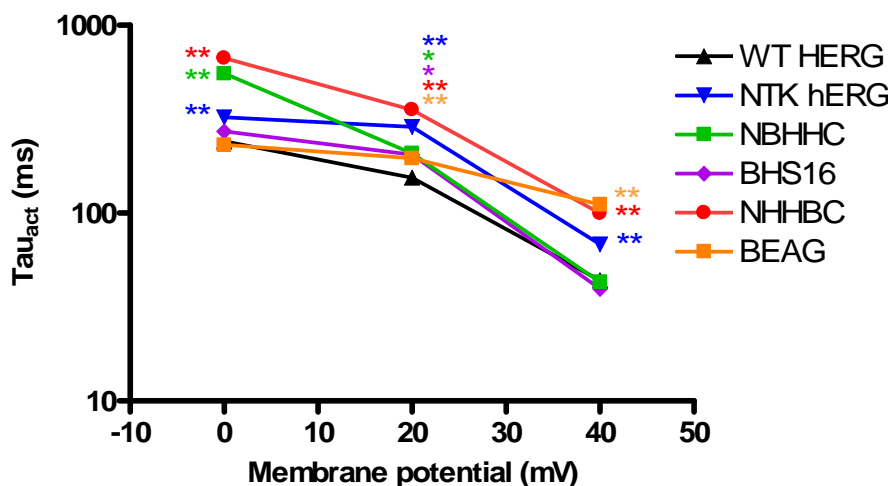


Figure 3.7: Mean time constants for activation of hERG and the chimeras are voltage dependent. bEAG shows less voltage sensitive activation. \* indicates  $p < 0.05$ , \*\* indicates  $p < 0.01$  for the respective chimeras compared to the WT hERG value at the same voltage.

Studying the chimeras, all chimeras are significantly slower than WT hERG except for BHS16 (figure 3.5-7). The voltage sensitivity of activation of these chimeras also follows the trend of hERG by increasing the rate of activation as the voltage becomes more positive. The activation of the N-terminal swapped chimera (NBHHC) appears the most voltage sensitive (figure 3.7). The rate of activation for this current increased the most over the voltage range studied. This again reflects what is seen from the I-V relationship, where the slope of the N-terminal swapped chimera is steeper than other channels. The swapping of the termini has varied effects on the activation of the channel. Though these changes are significant, they are unlikely to have a pronounced effect on open channel block by pharmacological inhibitors.

### ***The chimeras deactivate rapidly compared to WT hERG***

Time constants for deactivation were determined from the decrease of tail currents elicited with a fully activated I-V protocol (see material and methods).

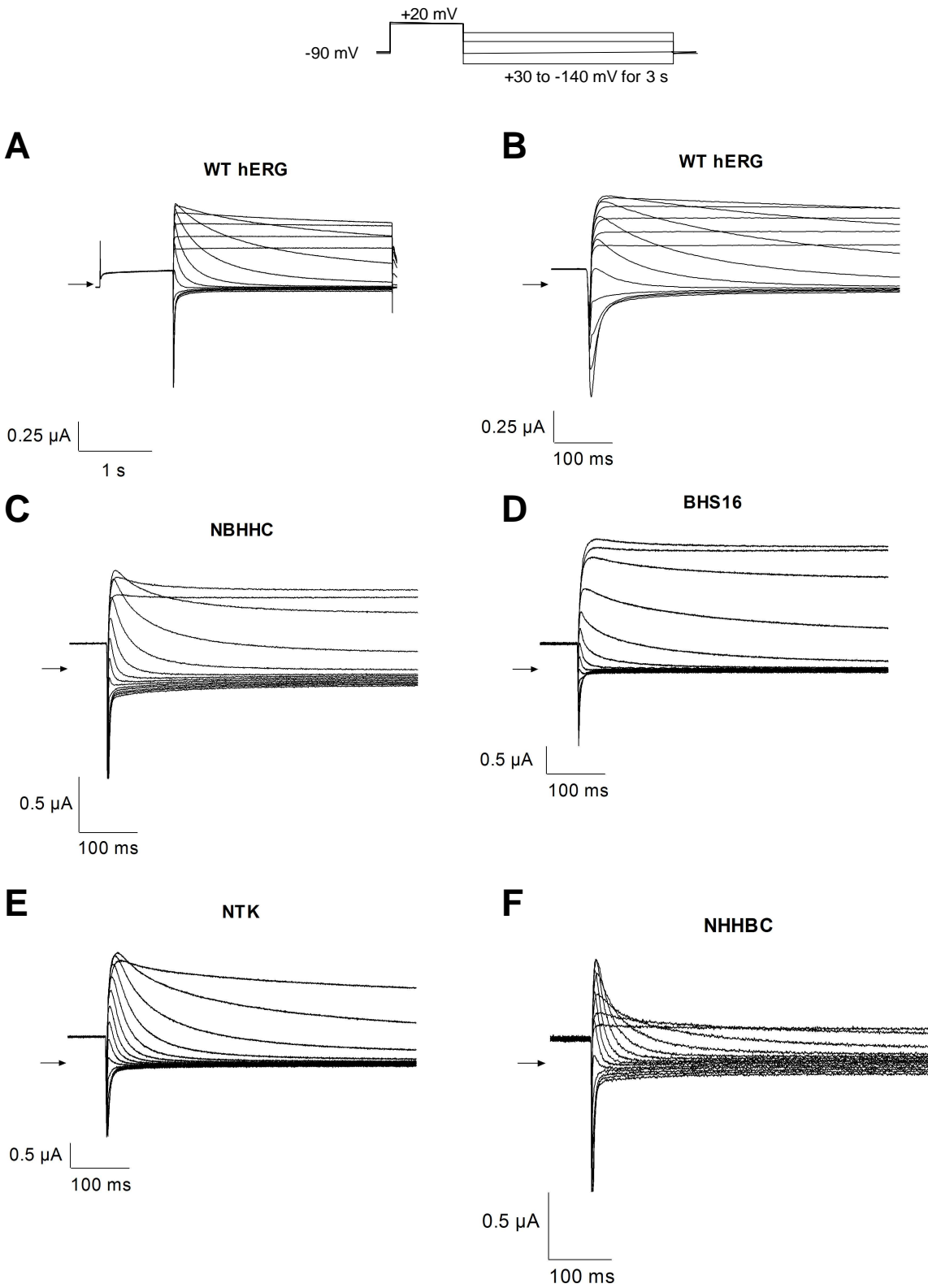


Figure 3.8: Substitution or deletion of the hERG N-terminus causes accelerated rates of deactivation. **A**, Representative traces of WT hERG recorded using the above protocol. **B-F**, Representative tail currents of WT hERG and other currents.

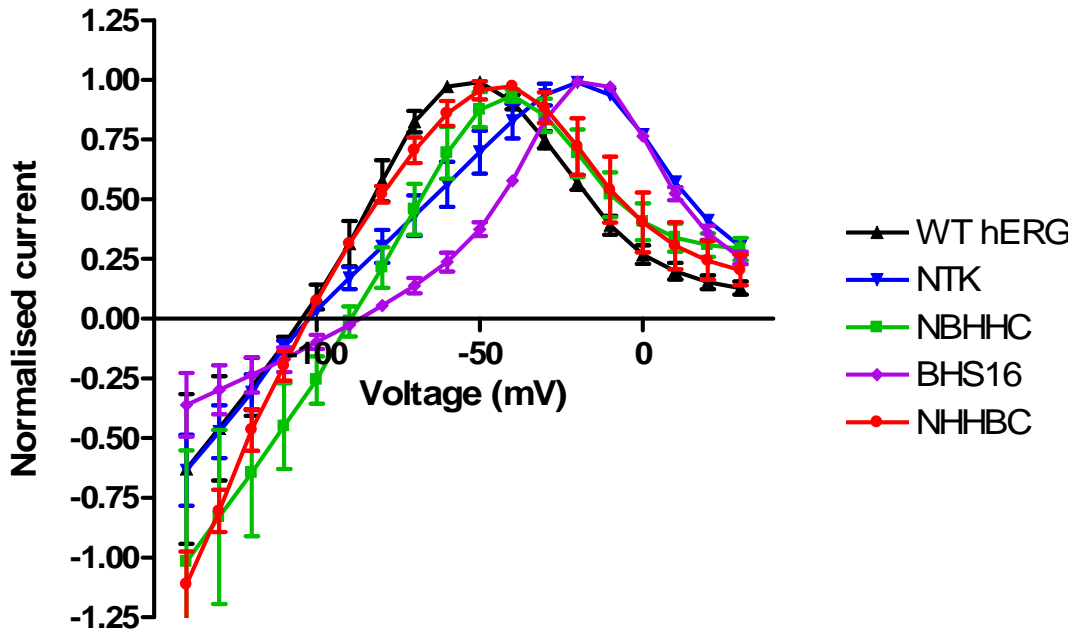


Figure 3.9: Plot of the peak tail currents recorded from the fully activated I-V protocol. The currents were normalised to the greatest peak outward tail. The plots show the weak inward rectification of the channel and also the reversal potential for these channels which can indicate the ion selectivity of the channels n=4-5.

Figure 3.8 shows representative traces from recordings taken using the fully activated protocol. The first step pulse fully activates the channels at +20 mV and then the membrane potential was stepped to varying repolarising potentials to record the fast recovery from inactivation and then the decay of the tails currents, as the channels deactivate. The increase in the tail current amplitude seen on repolarisation is due to the recovery from inactivation, these decreases in amplitude as the repolarising voltage step approaches the reversal potential of potassium. The current will then reverse when the voltages become negative to this.

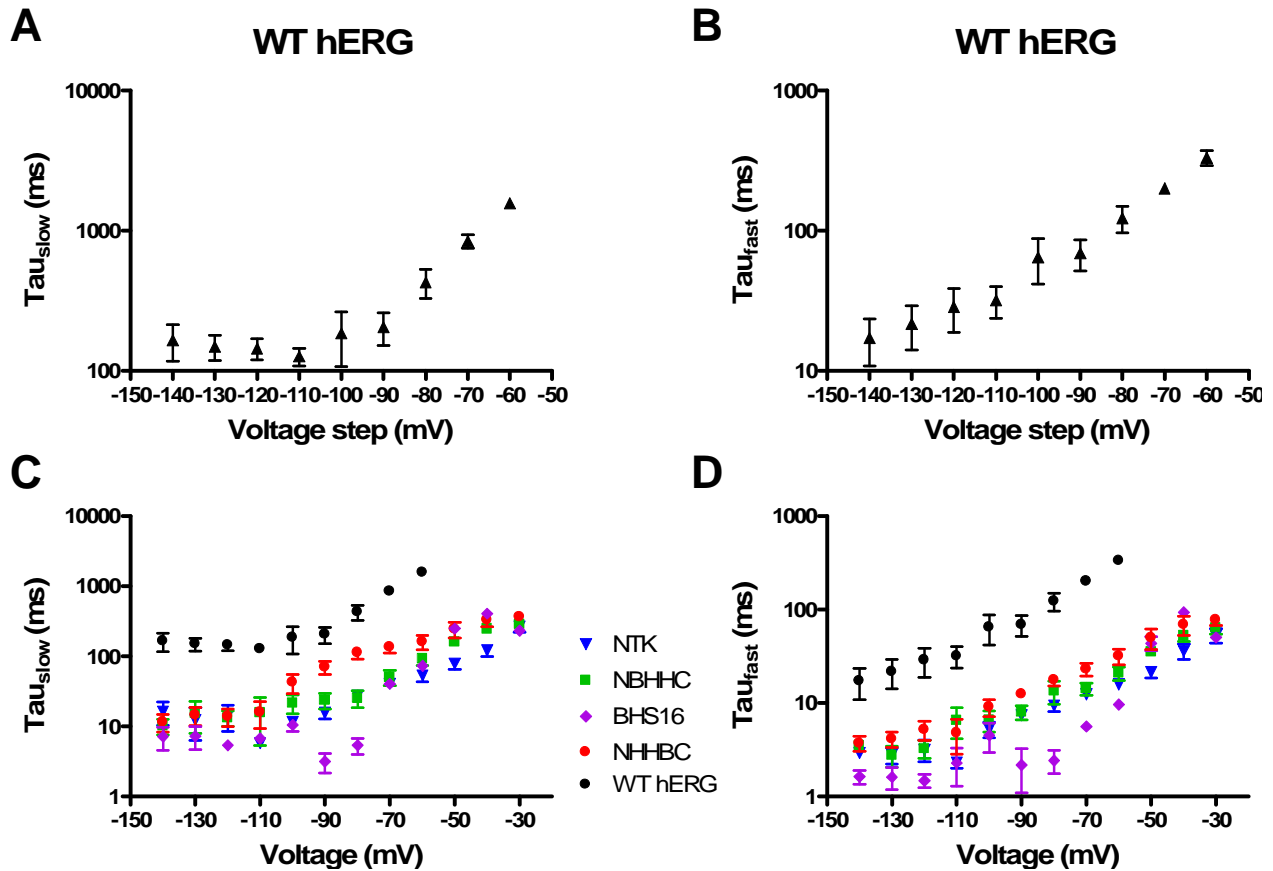


Figure 3.10: Comparing the voltage dependence of deactivation between WT hERG and the chimeras. A and B, Plots of the time constants of deactivation of WT hERG channels. C and D, Plots of the time constants of deactivation of the chimeras. The deactivation in all chimeras were faster than WT channels, much like the N-terminal truncated hERG mutant n=5.

The decrease of tail current amplitudes with time is due to current deactivation. This phase of the tail currents were best fit with a double exponential function, which separates the deactivation into fast and slow components (figure 3.10). This would indicate that there are at least two closed states that the channels go through in order to deactivate. The mean tau values were then plotted against the membrane potential. Deactivation of WT hERG was strongly voltage dependent and significantly slower ( $p < 0.01$ ) than the chimeric and NTK hERG channels at voltages positive to -80 mV. The deactivation is

slowed by almost one  $\log_{10}$  unit. As the membrane potential becomes more negative the voltage dependence of the channels reduces, as the gradient of the lines in figure 3.10 gets shallower.

The peak tail current amplitudes were plotted against the test potential (figure 3.9). The reversal potential was close to -105 mV for WT hERG, NTK and NHHBC, which suggests that these channels are highly selective for potassium ions. The equilibrium potential for potassium ions was estimated at approximately -110 mV based on an estimate of the intracellular potassium concentration and an extracellular concentration of 2mM. The other chimeras displayed a small positive shift in the reversal potential to approximately -90 mV indicating possible reduction in selectivity for potassium ions. The fully activated I-V relationship also showed the degree of inward rectification, as indicated by the negative slope at the positive potentials (figure 3.9).

### ***Voltage dependence of recovery from inactivation***

The next step was to investigate the voltage dependence of inactivation. To investigate the recovery from inactivation, a triple pulse protocol was employed. First the cell was depolarised to +40 mV for 3 s, then the membrane potential was stepped to a series of potentials ranging from -140 to +30 mV for 5/10 ms, then stepping back to a potential of +40 mV, before returning to a holding potential of -90 mV. The brief repolarising step allows the channels to recover from inactivation, but not significantly deactivate, and the decay of current after the start of the third pulse records the onset of inactivation. This decay in current was fitted with a double exponential and extrapolated to start of the third voltage step. The amplitude of this point indicates the degree of recovery from inactivation. However, the resultant

graph (figure 3.11) differs from that of published data (Wang *et al.*, 1997; Yang *et al.*, 2004), suggesting that there were problems with the recording. The results appear to show a linear relationship, where in previous studies a sigmoidal relationship was seen. The recordings appear to be contaminated by artefacts resulting from ringing and loss of voltage control.

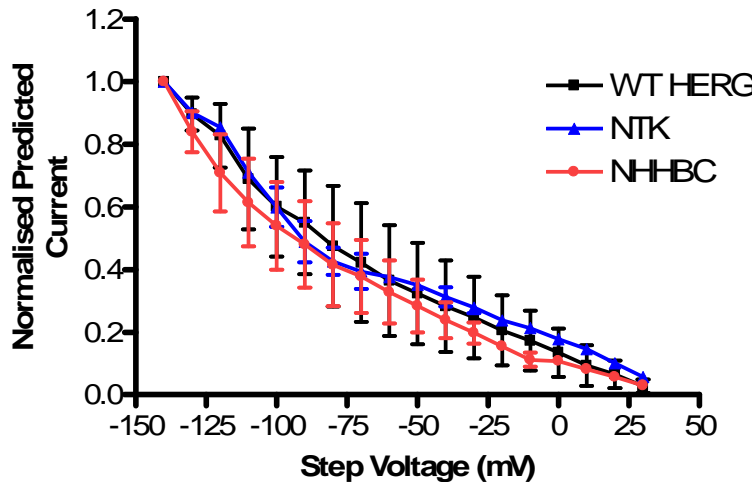


Figure 3.11: Plot of the peak current from the fits. The currents recorded during the third pulse of the protocol were fitted with a double exponential which was extrapolated to the start of the pulse. This peak current was used to plot this graph, normalising them to the peak current. WT hERG (n=5), NTK and NHHBC (n=2).

However there were difficulties recording other chimeras as there was such a shift in the deactivation. This led to some deactivation that occurred during the second repolarising pulse, leading to re-onset of activation during the pulse. This led to currents that could not be accurately fitted. Shortening the duration of the repolarising pulse was not an option, as the amplifier could not clamp the cell accurately at shorter durations. Further recordings need to be done to try to overcome these problems, by recording from smaller oocytes than those presently used and impaling them with lower resistance electrodes.

Even though the inactivation can not be quantified, it can be observed in the I-V, where the current from WT hERG and hERG/bEAG chimeric channels can

be seen to inactivate during the test pulses as they become more positive; this was not seen in the BEAG recordings. It is also seen in the tail currents of the fully activated I-V graphs, where the currents show a recovery from inactivation before deactivation occurs.

## **Discussion**

In this chapter the voltage and time dependent properties of gating of hERG/bEAG were investigated to compare the characteristics to those of WT hERG and bEAG. This was to identify whether they were similar enough to be comparable to WT hERG channels when used for concentration-response experiments. It was found the exchanging of the N- and/or C-termini of hERG with bEAG significantly altered the gating characteristics. It activates slower, deactivates faster. These differences will be discussed further now.

### ***The N- and C-termini are required for normal deactivation gating in hERG***

Characteristic features of hERG channels consist of a Per-Arnt-Sym (PAS) domain that is conserved with EAG and related channels. The hERG channels also have an addition sequence of amino acids between this PAS domain and the channel designated the proximal domain (Viloria *et al.*, 2000; Gomez-Varela *et al.*, 2002). Previous investigations into the fast inactivation that is seen in hERG showed that the N-terminus was not responsible for this effect (Schonherr & Heinemann, 1996; Spector *et al.*, 1996b). Through these studies it was observed that it was responsible for the slowing of the deactivation. Truncations to the N-terminus were carried out in these studies and resulted in the increase in the rate of deactivation (Schonherr &

Heinemann, 1996; Wang *et al.*, 1997; Morais Cabral *et al.*, 1998; Wang *et al.*, 1998). Further investigations showed that the PAS domain was responsible for slowing the deactivation, when fragments of the N-terminus were applied to the intracellular side of the channels, it caused a slowed deactivation of N-terminal truncated mutants (Morais Cabral *et al.*, 1998; Wang *et al.*, 1998). The PAS domain is thought to bind to positive residues on the S4-S5 linker to slow the closure of the channel, as mutations of residues such as Asp540, Glu544 in the region increases the deactivation rate of the channel (Wang *et al.*, 1998; Sanguinetti & Xu, 1999). As the EAG channels have the PAS domain on the N-terminus and lack a proximal domain present in hERG, deletions of this region, which would make the channel more EAG like, resulted in faster deactivation of the channels (Gomez-Varela *et al.*, 2003)}. This reflects what was seen in the deactivation of channels with the N-terminus exchanged with that of bEAG, with or without exchanging the C-terminus.

The C-terminus of hERG is quite similar to that of EAG, it contains a cyclic nucleotide binding domain (CNBD) which shares a large degree of homology with the C-terminus of HCN channels. This domain has a modulatory role and little to do with the gating of the hERG channels; however, it is required for functional channels. There is also a putative tetramerisation site which may be important to assembly of hERG. There are several putative phosphorylation sites as predicted by Prosite (<http://www.expasy.ch/prosite/>), these may modify the activity of the channels and be important to rundown. Previous studies focused again on the truncation of the terminus (Aydar & Palmer, 2001). The truncation of the last 236 residues caused the increase in

deactivation rate by almost one  $\log_{10}$  unit. This compliments the result obtained in the present study, the exchange of the C-terminus with hERG also increases the rate of deactivation by almost one  $\log_{10}$  unit. These results suggest that the N- and C-termini are important for normal deactivation, and that they interact together in order for the N-terminus to bind to the channel and stabilise the open state.

### ***The N- and C-termini interact to modify activation***

The activation of the hERG channel was also affected by the termini. Valoria *et al.* (2000) made deletions of the proximal domain between residues 138 and 373, which led to a hyperpolarised shift of 21 mV in the  $V_{1/2}$ . However, truncations of the N-terminus caused a positive shift in the  $V_{1/2}$ . From the I-V experiments, exchanging just the N-terminus shifts the  $V_{1/2}$  of activation to positive potentials compared to the WT hERG channels. So it behaved like the NTK hERG channel. But the BHS16 chimera has a ~13 mV negative shift in the  $V_{1/2}$  making it behave more like the proximal deleted mutant and bEAG.

The C-terminal deletions carried out by Aydar *et al.* (2001) did not display a shift in the  $V_{1/2}$ . Which contrasts to when the C-terminus was exchanged, the  $V_{1/2}$  is shifted ~17 mV to positive potentials, this suggests an alteration of the activation that is similar to the NTK hERG channel.

### ***Activation kinetics of the chimeric channels***

The examination of time course of activation shows that there was a sigmoid shape which was seen in other papers, this indicates possible complex closed states which the channels have to go through in order to activate (Wang *et al.*, 1997; Vilorio *et al.*, 2000; Gomez-Varela *et al.*, 2002). There appears to be at

least two closed states that the channel has to go through in order for it to activate. As the rate that channels move from each closed state would vary it appears that compared to hERG, the chimeras NHHBC and NBHHC have similar or slightly slower activation kinetics. This reflects results by Aydar *et al.* (Aydar & Palmer, 2001), where they deleted 357 amino acids from the N-terminus and see a slight slowing of the activation. But it also disagrees with research done in other labs, where the NTK hERG channels are seen to have a faster activation compared to WT hERG (Schönherr & Heinemann, 1996; Spector *et al.*, 1996a; Vilorio *et al.*, 2000), where they deleted parts of the region of 2-373 on the N-terminus. They see a small increase in the rate of activation rather than a slow down, this maybe due to my low number of experiments and further experiments are required. BHS16 was slightly faster at activating than hERG, this was also seen in the experiments of Vilorio *et al.* and Gomez-Valera *et al.* (Vilorio *et al.*, 2000; Gomez-Varela *et al.*, 2002). They create hERG channels with deletions of the proximal domain and observe that there was an increase in the rate of activation depending on the amount that is deleted. The deletions would make the N-terminus more EAG like, as hERG has the largest N-terminus in the EAG family, this was not seen in results from NBHHC chimera recordings. The difference maybe due to how the EAG terminus interacts with the hERG terminus, slowing the rate of activation in some way through different bonds with intracellular parts of the channel. This slowing was also seen in NHHBC, which may also be the reason for the slow down.

### ***Inactivation is present in hERG/bEAG chimeras***

The hERG exhibits fast voltage dependent C-type inactivation. It is thought to be due to the 'collapse' of the pore region, making it non-conducting (Smith *et al.*, 1996; Liu *et al.*, 2002). The outer pore region of the hERG channel is much larger than other voltage gated K<sup>+</sup> channels (43 amino acids compared to 14-23 amino acids long). Other channels in the EAG channel family have similar pore regions, however they do not show this inactivation. The mechanism of inactivation has been investigated through the mutations and structural analysis of the pore regions of the channel and using molecular dynamic simulations (Schönherr & Heinemann, 1996; Herzberg *et al.*, 1998; Ficker *et al.*, 2001; Torres *et al.*, 2003; Clarke *et al.*, 2006; Stansfeld *et al.*, 2008). The studies indicated that the region between the S5 helix and the pore region (S5-P) that creates the selectivity filter is responsible for the inactivation characteristic. Initial point mutation to the S5-P region showed that the Ser631 (Ficker *et al.*, 2001) and S620 (Schönherr & Heinemann, 1996; Herzberg *et al.*, 1998) residues were able to reduce the hERG inactivation. Further mutations to other residues in the S5-P region, through cysteine scanning experiments, found other residues that also affected the inactivation (Liu *et al.*, 2002). These mutations were also seen to affect the K<sup>+</sup> selectivity as well, indicating their involvement with the stability of the selectivity filter. It is thought that the S5-P region forms an amphipathic helix that interacts with the voltage sensing region of the channel and causes the 'collapse' of the pore. EAG channels do not have some of these residues (for instance Ser631, Ser620, and Asp591) therefore they do not display inactivating characteristics. The conformation of the inactivation mechanism is

important for high affinity block of hERG (Herzberg *et al.*, 1998; Ficker *et al.*, 2001).

The mechanism of inactivation is much faster than the C-type inactivation that is seen in other voltage dependent K<sup>+</sup> channels. The reason for this is not entirely clear, it maybe due to the aromatic residue within the selectivity filter, most K<sup>+</sup> channels have a GYG sequence while the hERG channels have a GFG sequence. The tyrosine is thought to form hydrogen bonds with two tryptophan residues, which stabilise the pore (Doyle *et al.*, 1998). A mutation of the tyrosine in the selectivity filter to a phenylalanine causes an increase in the rate of C-type inactivation (Ranganathan *et al.*, 1996). Conversely, if the Kir6.2 channel, which has a GFG sequence in the selectivity filter and has a gating process that is similar to C-type inactivation (Proks *et al.*, 2001), has the phenylalanine mutated to a tyrosine, the channel becomes inactive. This shows that the residue is important for the functional conformation of the selectivity filter. The structure of the hERG channel selectivity filter has been modelled using molecular dynamic simulation (Stansfeld *et al.*, 2008), it shows that carboxyl group on the phenylalanine (Phe627) is able to flip away from the centre of the conduction pore, which would make the channel non-conducting. In contrast when the non-inactivating mutants were modelled, the flipping occurs less frequently.

As the inactivation mechanism is localised to the voltage sensing domain and the selectivity filter region, the intracellular termini are unlikely to have a major effect on inactivation gating. Contrasting this to the activation gating which occurs on the cytoplasmic side of the channel, this would make it more likely to be affected by alterations in the intracellular termini. This is what is

reflected in the results from my experiments, the inactivation is still present in the chimeric channels, as can be seen in the I-V experiments. However this has not been properly quantified, due to the difficulties in obtaining recordings that were not contaminated with artefacts. Further recordings will have to be done to quantify the inactivation properties of the chimeric channels. The cut open oocyte method (Costa *et al.*, 1994) may be used to record these characteristics. The technique gains greater access to the intracellular side of the membrane, making it easier to voltage clamp large fast changing currents. The chimeric channels can also be transfected into a mammalian cell line to see if it alters the voltage dependent properties with the different cell background.

From the present data, it can be seen that all the hERG/bEAG chimeras were functional. They all displayed inactivation characteristics, which is important for high affinity hERG channel block. There were observable differences in the activation and deactivation kinetics, where the activation rate was slowed, while the deactivation rate increased. This reflects the reduced stability of the open state of the channels. The next question is whether these changes to the activation and inactivation alter the pharmacological properties.

## Chapter 4: Characterising the pharmacological properties of hERG/bEAG chimeras

### Introduction

Most compounds that block hERG channels bind to the inner cavity, usually acting by binding to the open channel. Numerous studies have been carried out to show that the pore cavity has a specific arrangement of amino acid residues, which allows it to bind a wide range of drug molecules (Mitcheson *et al.*, 2000a; Kamiya *et al.*, 2001; Chen *et al.*, 2002; Perry *et al.*, 2004). From alanine scanning experiments residues are found to be important are Phe656 and Tyr652 on the S6 transmembrane domain. Further studies which replaced these residues with aromatic and hydrophobic residues showed that they bind to the aromatic and charged amine groups on compounds by hydrophobic and electrostatic interactions (Fernandez *et al.*, 2004). There are other residues that are less important to binding, such as Ser624, Val625 and Thr652 on the S5-S6 linker, as well as the Ile662 on the S6 transmembrane domain (Kamiya *et al.*, 2001; Ishii *et al.*, 2003; Perry *et al.*, 2004). These residues display a lower impact on potency when the amino acid is substituted. The impact that the residue has on binding also is dependent on the compound that binds the channel, they may be affected by one residue substitution, but not another. The important residues are characterised mainly using alanine scanning to see which residues caused a large shift in the  $IC_{50}$  or  $10\times IC_{50}$  of a particular drug.

Another characteristic of hERG that appears to be important for compound potency is channel inactivation. Mutants that do not inactivate or have shifted

voltage dependence of inactivation to positive potentials display a significant reduction in compound potency (Ficker *et al.*, 1998; Herzberg *et al.*, 1998; Ficker *et al.*, 2001). It may be that the act of the channel transitioning from the activated to inactivated state will move the residues on S6 transmembrane helix, creating a more favourable site for high affinity binding to the channels (Chen *et al.*, 2002). In the previous chapter, the voltage dependence of bEAG/hERG chimeras was studied and showed that they have relatively similar properties to WT hERG; they display similar voltage and time dependent properties of activation and inactivation. However, they also display an accelerated rate of deactivation. The next step is to investigate how the pharmacological properties are affected by exchanging the termini with those of bEAG. The prediction was that since the chimeras retain the same S1-S6 domains that form the voltage sensing and pore forming domains, the pharmacology of the chimeras should not be greatly affected when compared to WT hERG (Ficker *et al.*, 1998; Herzberg *et al.*, 1998).

This chapter uses two electrode voltage clamp recordings, as described in the Materials and Methods chapter (see page 40), to investigate the effects on inhibition by two inhibitors, E-4031 and propafenone, when exchanging the intracellular termini of the hERG channels with bEAG termini. These two drugs have differing structures, potency and kinetics of block. This is with the view to identifying a chimera with WT hERG pharmacological characteristics but also low rundown on excision of an inside-out patch.

## Results

### *E-4031 potency to chimeric channels*

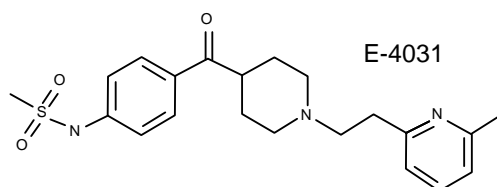
First the pharmacology of the methanesulphonanilide E-4031 was studied. This is a well characterised compound that blocks hERG with a high affinity and would be the template for analogues used in subsequent investigations into the characteristics of the hERG inner cavity. Concentration-response experiments were carried out by depolarising the membrane potential from -90 to +20 mV for 5 s and tail currents were recorded with a 400 ms duration step to -70 mV. The depolarising potential was set at +20 mV to ensure the chimeric channels were maximally activated. This protocol was repeated every 6 s ensuring the channels were predominantly in the open and inactivated states. To get a control set of recordings, the protocol was carried out in the absence of compound and traces were recorded when the tail current amplitudes were stable. After recording stable control current traces, the first concentration of E-4031 was perfused on for 2 min, before the recordings were restarted. This allowed the drug to equilibrate across the cell membrane. Repetitive pulsing was continued until steady state inhibition was reached. This was repeated with higher concentrations of compound at half  $\log_{10}$  molar concentrations.

Representative current traces for WT hERG current inhibition by E-4031 are shown in figure 4.1. E-4031 inhibited both the current during the test depolarisations and the tail currents. Oocytes express small endogenous currents during the test pulse, which are not usually observed in the tail current. This, and the fact that tail currents are large for hERG, was the

reason for analysing tail current amplitudes to determine the relative inhibition. The onset of the drug block in the chimeras was slow, much like the WT channel (figure 4.2). Inhibition was not observed until pulsing was resumed, indicating open state block.

The peak tail current amplitudes in the presence of E-4031 were normalised to the control values, plotted against time and the resulting plots were fitted with a single exponential function to obtain a value where the current reaches steady state. These values from individual cells were plotted against the  $\log_{10}$  of E-4031 concentration and then fitted with a Hill function. Mean concentration-response relationships are shown in figure 4.3, Data from the fits are summarised in table 4.1.

**A**



**B**

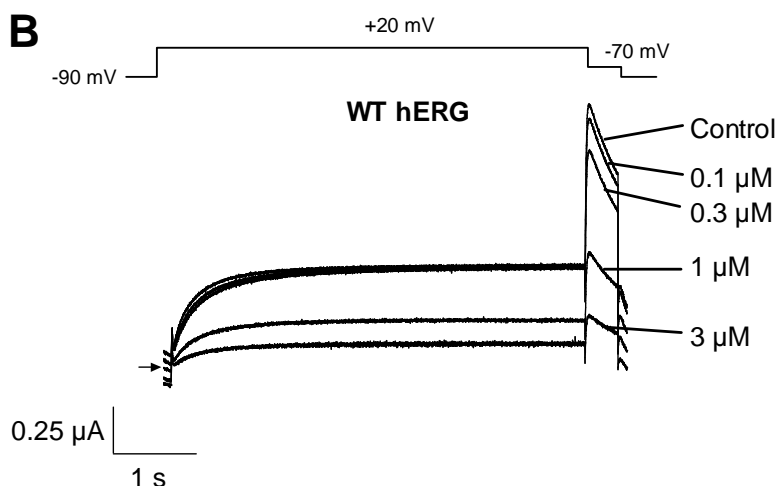


Figure 4.1: Concentration dependent inhibition of WT hERG by E-4031. **A**, The chemical structure of E-4031. **B**, The membrane potential was pulsed to +20 mV for 5 seconds followed by a repolarisation to -70 mV for 400 ms and the protocol was repeated every 6 s. Representative traces of WT hERG current inhibited by increasing concentrations of E-4031. The traces shown are where steady state amplitudes have been attained. The arrow indicates zero current.

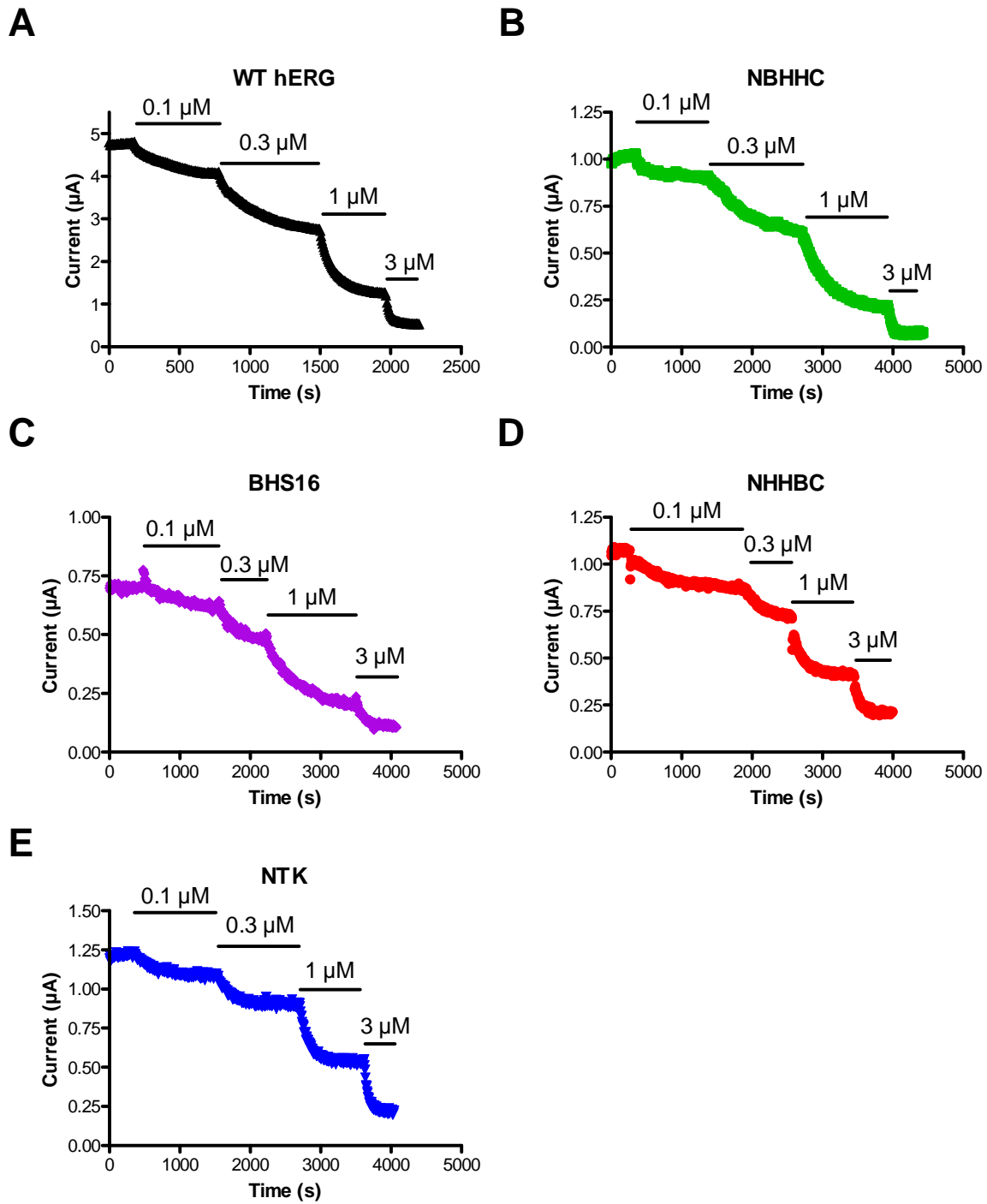


Figure 4.2: Concentration dependent inhibition of hERG, NTK hERG and chimeric channels by E-4031. Representative plots of the peak tail current amplitudes by indicated concentrations of E-4031, showing the time dependence for onset of block. The time (~2 mins) between the switch in E-4031 concentration and first of the step depolarisations is not shown.

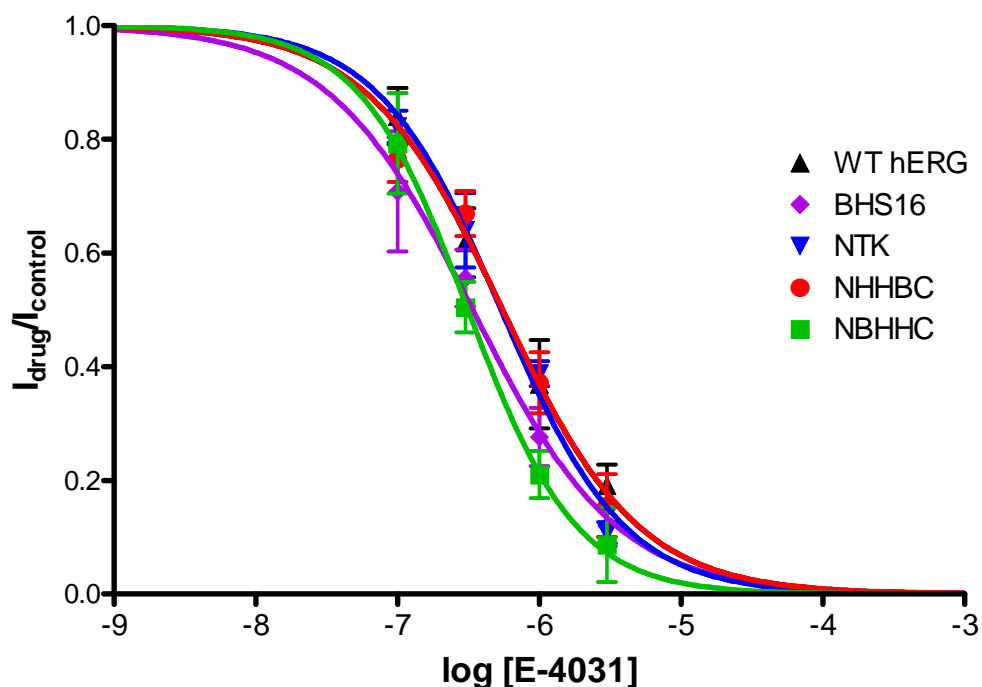


Figure 4.3: Concentration-response curve of channels dosed with E-4031. The peak tail amplitudes of the inhibited channels were normalised against the control value and plotted against the concentrations used. There is no significant difference between WT channels and chimeras. n=5

Channel	IC <sub>50</sub>	Hill slope	
WT hERG	532.5 ± 1.1 nM	-1.00 ± 0.05	n=6
NTK hERG	296.5 ± 1.0 nM	-1.14 ± 0.06	n=4
NHHBC	601.5 ± 1.1 nM	-1.07 ± 0.15	n=4
BHS16	551.8 ± 1.2 nM	-1.03 ± 0.17	n=4
NBHHC	330.2 ± 1.2 nM	-0.92 ± 0.14	n=4

Table 4.1: Comparison of IC<sub>50</sub> and Hill slopes of channel inhibition by E-4031. The data are presented as the mean and S.E.M.. p>0.05

The IC<sub>50</sub> values of E-4031 inhibition of the chimeric currents were not significantly different to that of WT hERG, analysis with a one way ANOVA test resulted in p>0.05. This was an indication that the pore region of the chimeras was not affected by the exchanging of the bEAG N- or C- termini.

### ***Propafenone potency to chimeric channels***

Having shown that E-4031 was just as potent an inhibitor of the chimeric currents as WT hERG; the inhibition by propafenone, a non-

methanesulphonamide drug, was investigated. Propafenone is a lower potency drug compared to E-4031, it has a fast rate of block on WT hERG (Witchel *et al.*, 2004). The experiments were carried out as described with E-4031. First the inhibition of WT hERG and bEAG channels was investigated. Representative current traces are shown in figure 4.4. The relative inhibition of hERG currents was determined from tail currents. However, bEAG currents deactivated too rapidly to analyse and so current amplitudes from the +20 mV test pulse were analysed.

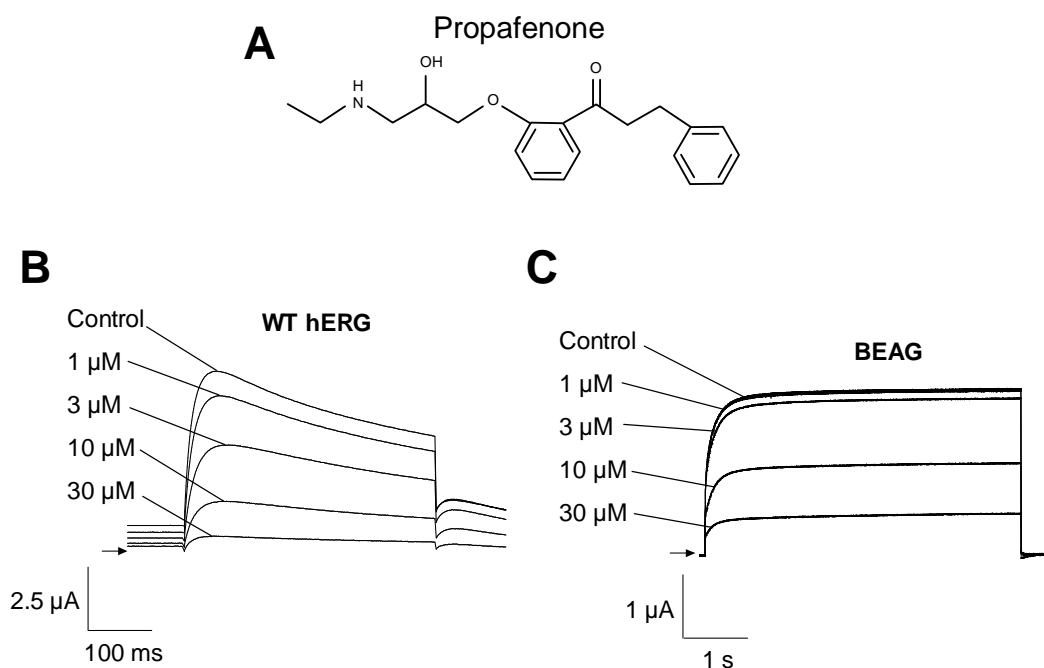


Figure 4.4: Representative traces of WT hERG and bEAG inhibition by propafenone. **A**, The chemical structure of propafenone. **B**, Tail currents inhibited by increasing concentrations of propafenone. **C**, bEAG channels blocked by increasing propafenone concentrations during the depolarising pulse. The arrows indicate the zero current line.

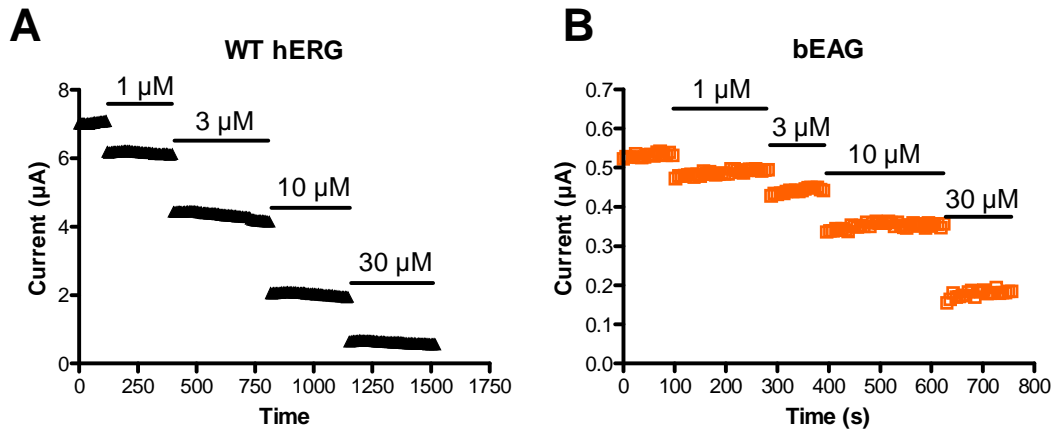


Figure 4.5: Inhibition of hERG and bEAG current by propafenone is rapid and concentration dependent. Representative plots of the peak tail current amplitudes of hERG (A) and test pulse current amplitudes of bEAG (B) with increasing concentrations of propafenone. The onset of block is much faster than with E-4031.

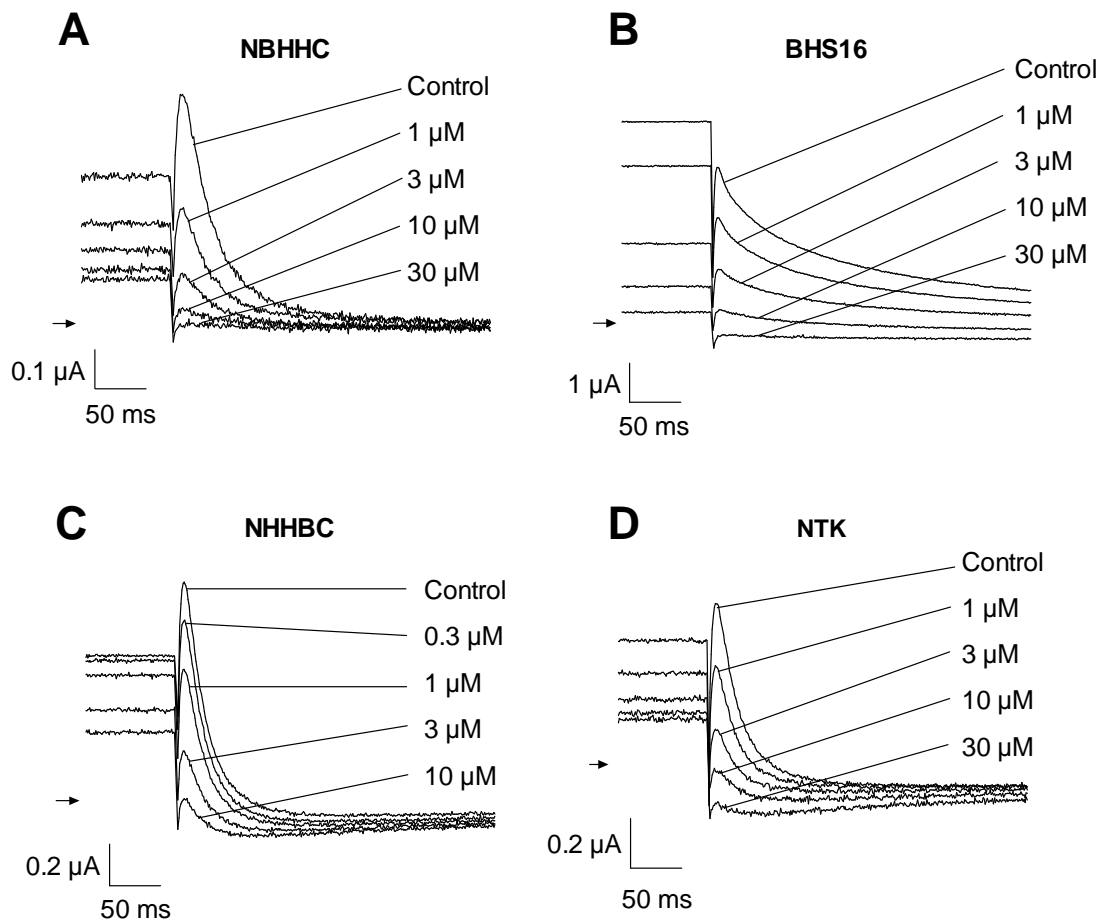


Figure 4.6: Representative traces of the tail currents of chimeric and NTK hERG currents inhibited by propafenone. The experiments were run as described for WT hERG (figure 4.1). The currents were inhibited in a concentration dependent manner. The arrow indicates zero current.

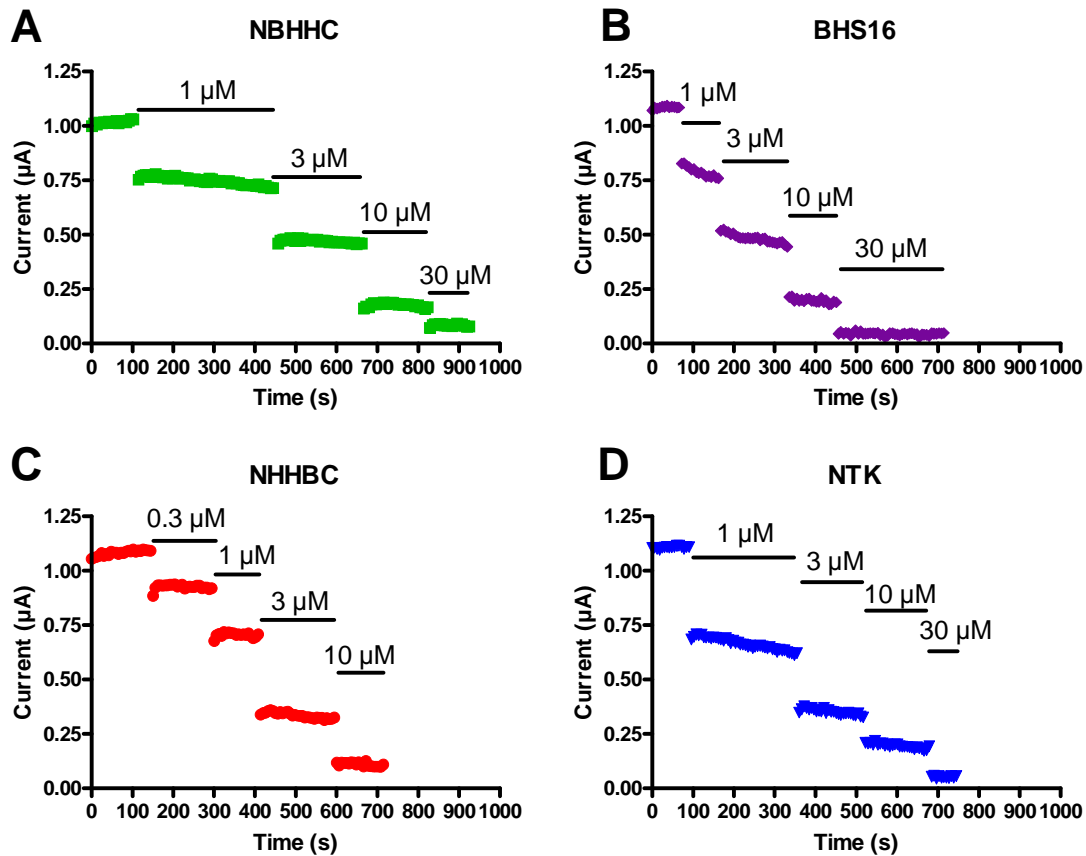


Figure 4.7: The mutant channels are inhibited by propafenone in a concentration dependent manner. Representative plots of the peak tail current amplitudes with in cumulative concentrations of propafenone, showing the time dependence of block. The amount of block was also greater than the wildtype channels.

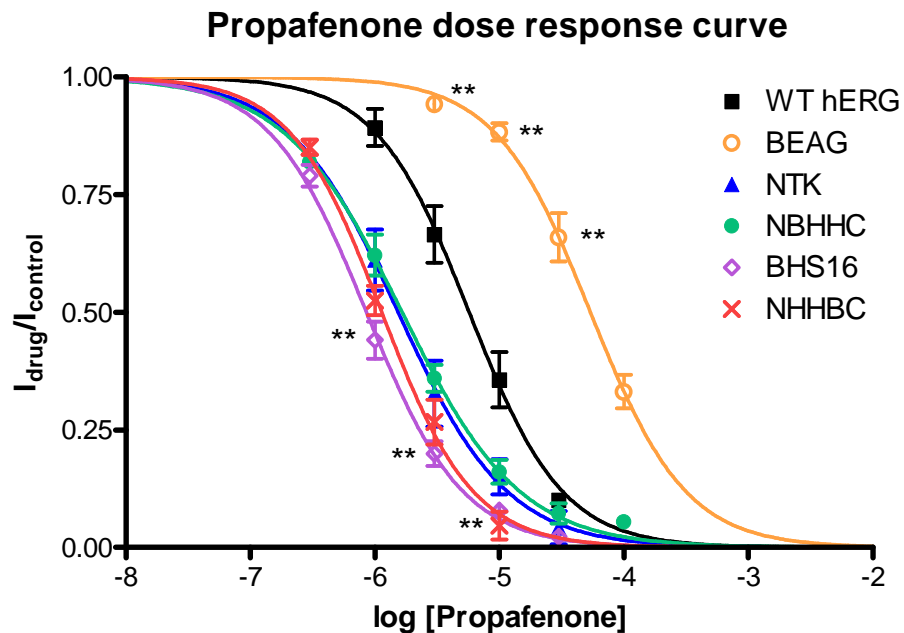


Figure 4.8: NTK and chimeras are blocked by propafenone with a higher affinity compared to WT hERG. Concentration-response experiments were carried out as detailed before. They all had  $IC_{50}$  values significantly different to WT hERG.  $n=4-6$  \*\* indicates  $p<0.01$  to WT hERG.

A much higher concentration of propafenone was needed to get the equivalent block to E-4031. The time course for the onset of block is shown in figure 4.5. Block was rapid and reached steady state during the first test pulse. The propafenone IC<sub>50</sub> of WT hERG was 5.5 ± 0.4 μM and 48.2 ± 1.8 μM with bEAG. The WT channels have a difference of almost one log unit, with bEAG displaying a lower potency to propafenone compared to hERG. However, both of the WT channels did get inhibited at a fast rate (figure 4.5).

Channel	IC <sub>50</sub>	Hill slope	
WT hERG	5.5 ± 0.7 μM	-1.19 ± 0.09	n=5
WT bEAG	48.2 ± 1.8 μM **	-1.03 ± 0.08	n=4
NTK hERG	1.6 ± 0.2 μM*	-1.04 ± 0.08	n=4
NHHBC	1.1 ± 0.2 μM**	-1.26 ± 0.02	n=6
BHS16	0.9 ± 0.3 μM**	-1.15 ± 0.05	n=6
NBHHC	1.6 ± 0.3 μM**	-0.97 ± 0.16	n=6

Table 4.2: Comparing the IC<sub>50</sub> and Hill slopes of WT hERG to chimeric channels when blocked by propafenone. The data are presented as mean ± S.E.M.. \* indicates p<0.05, \*\* indicates p<0.01.

The next step was to investigate if the chimeric channels displayed an IC<sub>50</sub> different from either of these channels (figure 4.6 and 4.7). Using the same protocol as described before, it was noted that in some of the oocyte recordings, the deactivating tail currents displayed inward currents on repolarising the membrane potential to -70 mV (figure 4.6C and D). These inward currents appeared to activate after a depolarisation step and the amplitude of this current decayed after the membrane potential was repolarised. This current was not present when just a step to -70 mV was applied, to measure non specific leak current and they were not inhibited by the propafenone or E-4031. The occurrences of the current were oocyte batch specific. There were some batches of cells that did not display these currents. Therefore it seems to be an endogenous current. These inward currents are evident in the oocytes with lower channel expression and fast deactivating

currents and became apparent as the exogenously expressed channels were blocked. As a control, results from recordings with this inward current were compared to those that did not display this endogenous current. The  $IC_{50}$  values and Hill slope were similar (with a mean  $IC_{50}$  of 1.53 compared to 1.57  $\mu$ M in both batches of NTK hERG channels) and therefore the data were grouped together.

It was found that all the N-truncated and chimeric channels still displayed the fast onset of block, but displayed a higher potency to propafenone than WT hERG channels. The  $IC_{50}$  was reduced by over half a log unit (Figure 4.8), these were found to be significantly different from WT hERG.

### ***What is the mechanism for difference in propafenone potency?***

The chimeras and NTK hERG all have the same pore structure. Therefore differences in propafenone potency are likely to be due to allosteric effects on the binding. As a first step to investigating the mechanism behind the differences in potency, we compared the kinetics for onset and recovery from inhibition of NTK and WT hERG. The time course for onset of block between WT and NTK hERG channels was studied during long (30 s) depolarisation to 0 mV. After measuring the control current, 5  $\mu$ M propafenone was then perfused on for 2 min before the protocol was repeated. Propafenone was then washed off for 2 min and the protocol was repeated (figure 4.9). Relative block was calculated by normalising the current in the presence of propafenone against the control current and subtracting from one. This was plotted against time and fit with a single exponential to get the time constant for the onset of block (figure 4.10). The percentage inhibition, and percentage inhibition after wash off, was calculated by taking the relative block at the end

of the 30 s test pulse and multiplying by 100. The mean results are summarised in Table 4.3.

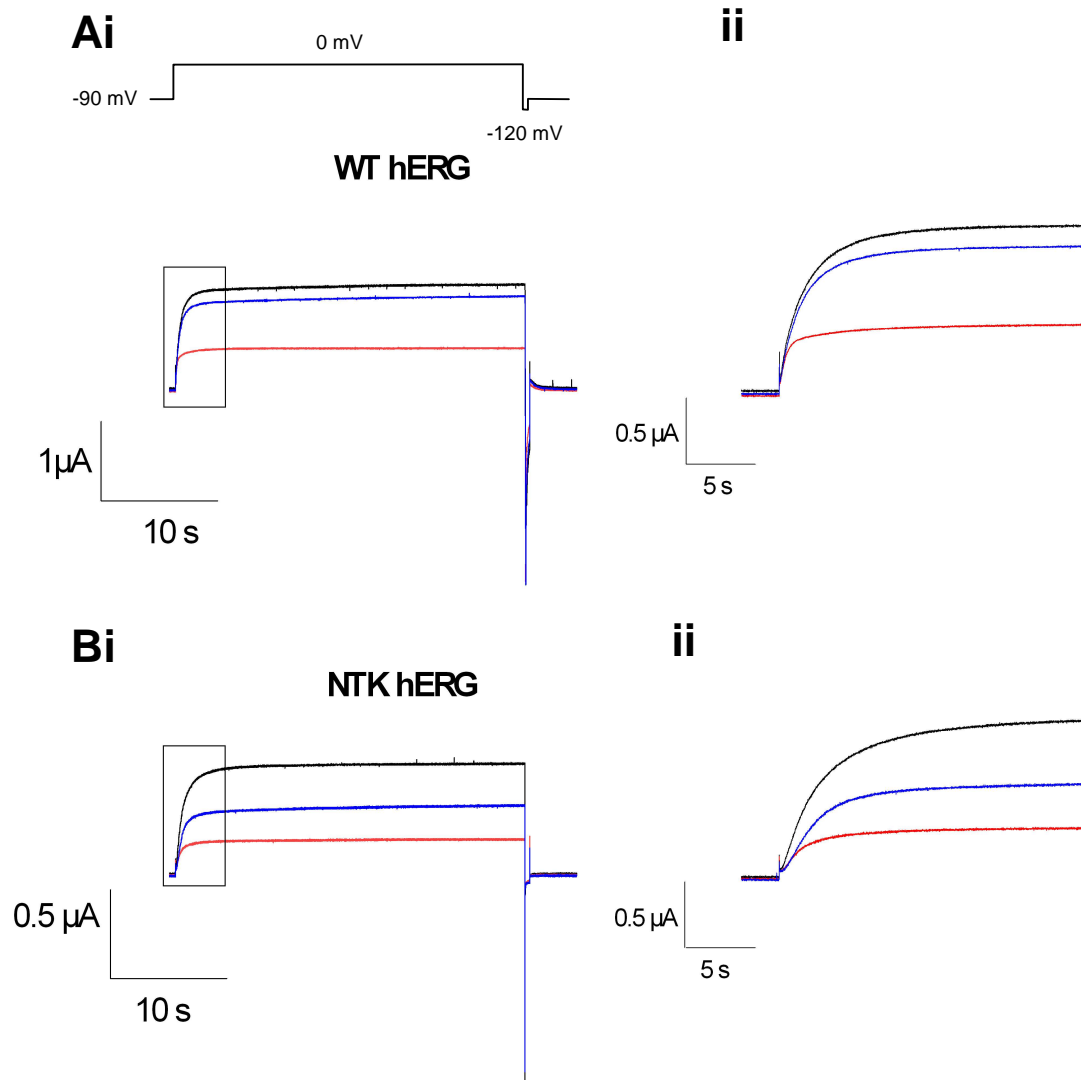


Figure 4.9: Onset of block and recovery with propafenone wash-off are faster in WT than NTK hERG. Representative traces of WT and NTK hERG channels in response to the voltage protocol shown above. **Ai** and **Bi**, in absence of drug (black), in presence of 5  $\mu$ M propafenone (red) and after 2 min wash out (blue). **Aii** and **Bii**, An expanded view of the currents on activation of the channels shown in **i**.

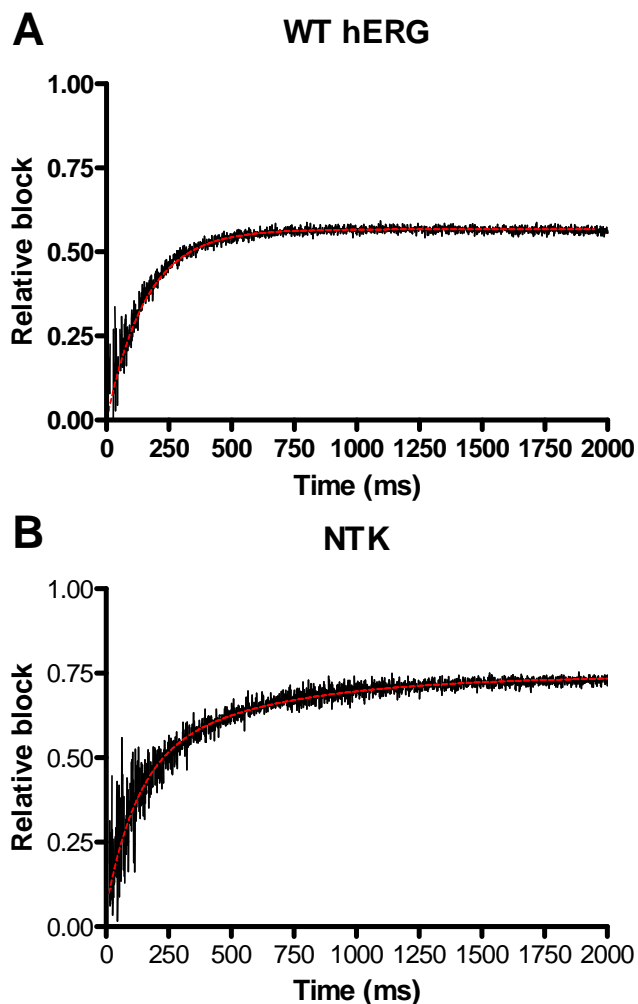


Figure 4.10: WT hERG displays more rapid onset of block than NTK hERG. Relative block at each time point was calculated by dividing the current in presence of 5  $\mu\text{M}$  propafenone by the control current amplitude and subtracting from 1. The curve was fitted with a single exponential (dashed red line) to get a time constant for the onset of block. Zero time is when the test pulse began.

	Time constant of block	% inhibition	%inhibition washout
WT hERG	$165.6 \pm 4.4$ ms	$51.3 \pm 4.2$ %	$17.3 \pm 2.6$ %
NTK hERG	$390.5 \pm 3.7$ ms** n=4	$68.0 \pm 1.8$ % ** n=4	$42.5 \pm 2.8$ % ** n=4

Table 4.3: Comparison of the time constants and degree of block by 5  $\mu\text{M}$  propafenone between WT and NTK hERG channels. The time constant of block and the normalised steady state level is shown. The normalised level of inhibition after 2 minutes of washout is also shown. The values are expressed as the mean  $\pm$  S.E.M. \*\* indicates  $p < 0.01$ .

From the traces in figure 4.9, the onset of block by propafenone is very fast, occurring during the 30 s test pulse. The percentage block is greater in NTK

hERG channels than WT hERG, reflecting findings from the concentration-response experiments examined earlier.

Fitting exponential curves to the time courses of block indicate that the rate of onset of block is faster when propafenone is applied to WT hERG channels than when applied to NTK hERG channels. The rate of onset is over twice as fast as that of NTK hERG using the same concentration. This would indicate that the loss of the N-terminus slows the onset of drug block.

When propafenone was washed off, the degree of block that remained was much greater with NTK than with WT hERG (figure 4.9 and table 4.3). ~40 % of NTK hERG current was inhibited compared to ~15% inhibition remaining when cells containing WT hERG were washed off. This would indicate that the off rate of NTK was slower than that of WT hERG, which would explain the increase in potency of propafenone for NTK hERG channels.

Further study of the drug binding will have to be carried out in order to determine why propafenone has higher potency to faster deactivating channels.

## **Discussion**

My studies of E-4031 inhibition of chimeric channels suggest that it binds in the pore with similar potency to WT hERG. Inhibition occurs in a state dependent manner, propafenone and E-4031 inhibit the current when the channel is open. This is also indicated in other drug studies that look at related chimeric channels. One of these is the study carried out by the Ficker group (1998). Here another methanesulphonamide based drug, dofetilide, was used to investigate the site of drug binding by comparing the  $IC_{50}$  of hERG/bEAG chimeras. In this study, the  $IC_{50}$  did not greatly change, from

0.32 ± 0.04 µM with WT to 0.60 ± 0.22 µM in the BHS16 chimera. Similar results were obtained by Herzberg *et al.* (1998). They made a series of chimeras composed of varying parts of hERG and mouse EAG were used to study the structural determinants of inactivation. The study also looked into the effects on the E-4031 block. A chimera with the region from the pore to the first half of the S6 transmembrane domain of hERG was exchanged into the mouse EAG channel showed no significant change in E-4031 IC<sub>50</sub> compared to WT hERG (348 ± 34 nM with WT hERG and 346 ± 67 nM with the mEAG/hERG chimera). These results indicate that for methanesulphonamide drugs, the S6 and pore regions are the most important for the binding to the channel and that the termini play a very small role.

Propafenone has a markedly different structure to E-4031 and dofetilide. It contains 2 phenyl groups and a charged amine, but lacks the methanesulphonamide group plus has other structural differences. These differences in the drug's molecular structure results in an alteration in the binding, resulting in the lower potency compared to E-4031. A study by Witchel *et al.* (2004) used a series of pore lining mutants to investigate the residues that were important to binding. It was found that propafenone requires Phe656 for the majority of its binding and other residues lining the inner cavity such as Tyr652 and Ser624 have a minor influence. Comparing this to E-4031, the inhibition of hERG is affected by mutations to greater numbers of pore lining residues (Thr 623, Ser624, Val625, Gly648, Tyr652, Phe656, and Val 659) (Kamiya *et al.*, 2006). The greater numbers of significant residues may be the reason for the lower potency.

Concentration-response experiments carried out on chimeric and N-truncated channels all displayed an  $IC_{50}$  that is lower than that of WT hERG. This would indicate that the drug has a higher affinity for the altered channels compared to the wildtype channel. This is unexpected, as the consensus would be for the  $IC_{50}$  of the chimeras and NTK hERG channels to increase relative to WT hERG. An increase in  $IC_{50}$  was seen in another study involving propafenone (Madeja *et al.*, 2003), where the termini of the Kv2.1 channel which was sensitive to propafenone inhibition was exchanged for the termini of Kv1.2, which is insensitive to propafenone inhibition. The study showed that in the presence of 100  $\mu$ M propafenone, the chimeras were inhibited to a lesser extent compare to the WT Kv2.1 ( $59 \pm 2\%$  inhibition in WT Kv2.1 compared to  $41 \pm 3\%$  and  $45 \pm 2\%$  inhibition with the N- and C-terminal exchanged chimeras respectively).

Having noted that the higher potency of propafenone for the chimeric and NTK hERG channels, the kinetics of block were investigated using a few simple experiments, this was with the view to understanding the mechanism that underlies the increase in potency. The experiments were done to give indications of the rates of binding and dissociation of propafenone. The results showed that the rate of onset of the block by 5  $\mu$ M propafenone was much faster in the WT hERG channel than with NTK hERG ( $165.6 \pm 4.4$  ms compare to  $390.5 \pm 3.7$  ms). However, the NTK hERG current displayed greater inhibition. This suggests that the on rate of hERG is greater than that of NTK, but the off rate of WT hERG may also be greater.

In order to examine the off rate further, a wash off protocol was used. The propafenone was washed off for 2 minutes before recordings were resumed.

WT hERG currents recovered to a greater degree compared to NTK hERG, it indicates that the off rate of propafenone is slower in NTK hERG channels. This would explain the high potency of propafenone for NTK hERG.

The effect caused by the termini is likely to be an allosteric effect on the binding site, making it more favourable for the propafenone to bind, while leaving the binding site for E-4031 unchanged. The loss of the termini seems unlikely to have a great direct affect on the binding site of drugs, as their presence is outside the pore.

There are a few limitations to these experiments, stemming mainly with the whole cell recordings. The cells are quite large and they have a second membrane outside of the cell, the vitelline membrane, which may slow the exchange of solutions. They also contain yolk, which absorb compounds, further slowing the exchange of solutions. For a fast onset drug such as propafenone, this makes it difficult to get accurate values for the kinetics of block, as apparent on and off rates of drugs will be affected by this. The absorption of compounds by the yolk can cause it to accumulation in the cell and raise the local concentration of drug, this will also slow the washoff of the drug, making it difficult to investigate the on and off rate of the drugs. To try to minimise these factors, the perfusion system was set up to provide efficient exchange of solution around the cell.

Further experiments would have to be carried out in order for a conclusive reason for the higher affinity for the altered channels.

The study shows that drugs bind in different manners as displayed by the change in propafenone potency when blocking the chimeric channels, compared to the lack of change when inhibiting with E-4031. Reviewing these

results against previously published data, it indicates that the drugs from the same class of molecule can bind to the channels in a similar way, these are not affected by the alterations to the channel termini.

Further studies can be carried out to investigate which residues on the chimeric channels are important in the drug binding. This could help explain the small differences in the binding between E-4031 and propafenone, and uncover whether there are changes in the binding compared to wildtype hERG. Further drug classes can also be used to block the chimeric channels, this will confirm whether the effect of propafenone is a unique effect of that drug. The chimeras could be transfected into a mammalian cell line to see if there is a difference in the way that the drugs bind to the channels when compared to wildtype. If there is a difference, it would indicate that in mammalian cells the chimeric and mutant channel folding alters the drug binding site.

As a full crystal structure of the hERG channel has not been resolved, the closest structure resolved being the KvAP and Kv1.2 channel crystal structure (Jiang *et al.*, 2003; Long *et al.*, 2005), these also lack the intracellular regions. It is therefore difficult to model a mutant with altered intracellular regions, as there is no whole template to compare against. So far there are just crystal structures of the separate sections of the PAS domain, shaker transmembrane region and cyclic nucleotide binding domains (Morais Cabral *et al.*, 1998; Zagotta *et al.*, 2003; Long *et al.*, 2005). The linkages in the differing channels of EAG and ERG could also make the structure difficult to predict and model. They may fold differently and due to flexibility of structures in the aqueous environment the orientation and interactions could be difficult

to model. Therefore further study is needed in these fields and the experimental data is also needed to feed into this to help give an idea of where and how drugs bind to the channels.

## **Chapter 5: Excised inside-out patch clamp experiments on hERG/bEAG chimeras**

### **Introduction**

When currents in mammalian cells expressing the hERG channel are recorded they display a reduction in the activity with time; a rundown of the current. This is particularly apparent in excised patches.

This is mentioned in several articles (Bian *et al.*, 2001; Gessner & Heinemann, 2003; Du *et al.*, 2004). It is thought that the phenomenon of rundown is due to the modulation of the channels. The factors causing rundown in hERG channels are not well studied, but there have been some articles published on hERG and other channels where there was an attenuation of rundown when modulatory factors such as ATP, PIP<sub>2</sub> were added to the perfused solutions (Armstrong & Eckert, 1987; McNicholas *et al.*, 1994; Tang & Hoshi, 1999; Bian *et al.*, 2001; Cayabyab & Schlichter, 2002; Du *et al.*, 2004; Hirdes *et al.*, 2004). The actual domains responsible for the rundown have not been fully studied.

This chapter will investigate whether the intracellular amino and carboxyl domains are responsible for the rundown. bEAG is a channel that does not display any rundown, compared to hERG (Gessner & Heinemann, 2003). A set of chimeras between WT hERG and WT bEAG were produced and these have been characterised in the previous chapters. Analysing the sequence for potential modulation sites using Prosite (<http://www.expasy.ch/prosite/>) identified several putative modulation sites for hERG and bEAG. These sites are concentrated within the termini (figure 5.1). There are a few that are

present in the extracellular and transmembrane regions, but these are not likely to be involved in modulation as it is unlikely that intracellular regulatory factors will reach them. Therefore the focus was on the intracellular termini of the channels. The termini are also the regions where the two channels differ most. They both share the Per-Arnt-Sim (PAS) domain on the N-terminus and a Cyclic Nucleotide Binding Domain (CNBD) on the C-terminus, the differences lie in length and sequence of the proximal N-terminus and distal C-terminus regions, these lead to possible differences in the regulatory sites and may therefore influence the rate of rundown.

In this study, the rate of rundown of channels was investigated using the excised inside-out patch clamp technique as described in the Materials and Methods chapter (see page 44). This was with a view to determining if exchanging one or both of the termini of hERG with bEAG will reduce the degree of rundown.

## **Results**

### ***Rundown of hERG/bEAG chimeras***

The first thing that needed to be done was to classify how quickly the wildtype hERG and bEAG channels rundown. This would give a basis for comparison with the chimeras.

Recordings were made first in cell attached mode, to get a measure of the amount of current from the micropatch. The patch was depolarised to +20 mV for 0.5 s to activate the channels and then repolarised to -120 mV for 1 s to record the deactivating tail currents. The start to start interval was set to 8 s.

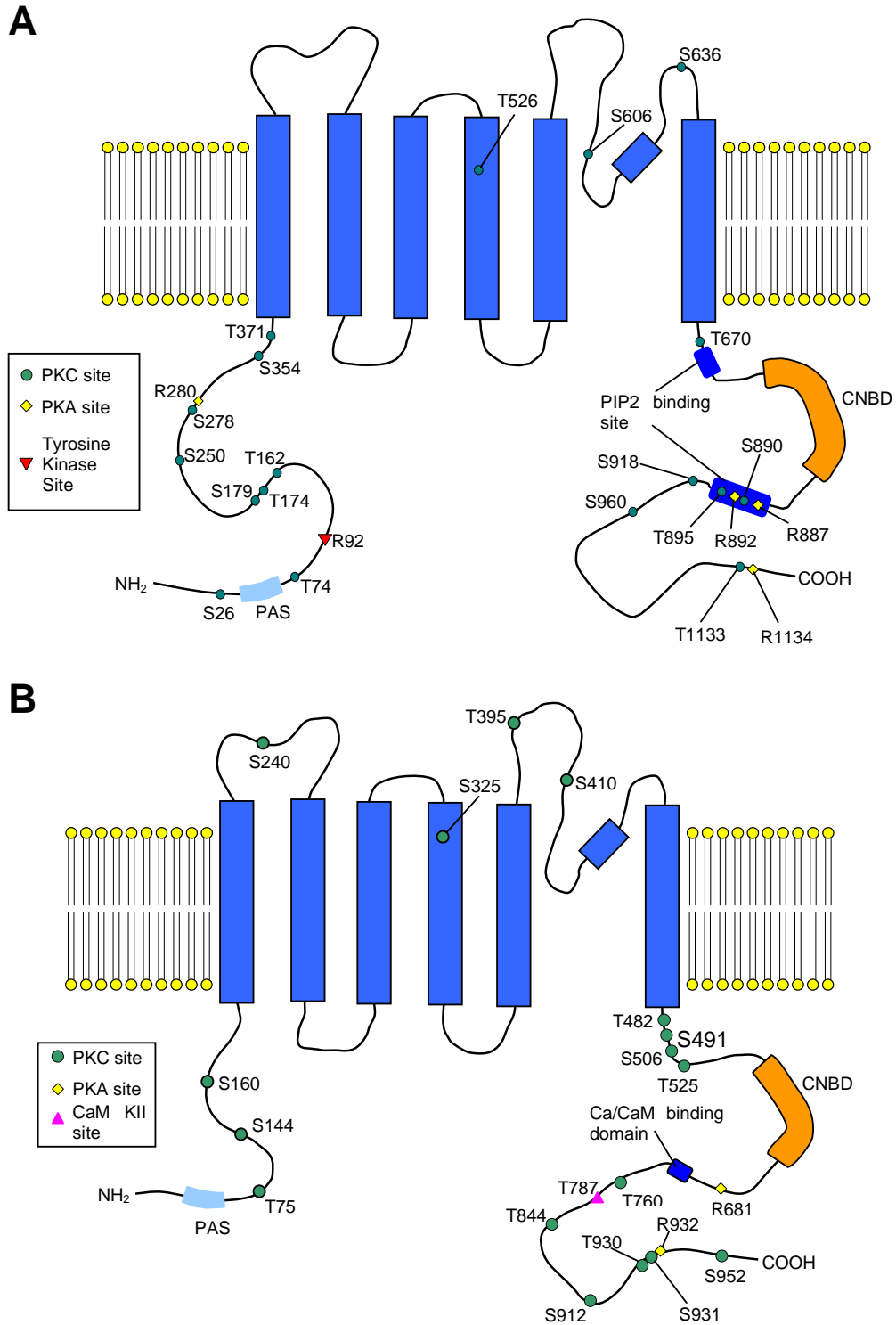


Figure 5.1: Predicted putative modulation sites of hERG and bEAG. Schematic representation of the putative modulation sites of (A) hERG and (B) bEAG predicted by Prosite. The location of the PAS and CNBD are also shown. This shows that the majority of modulation sites are on the intracellular termini of the channels.

The tail currents were measured to show the activity of the channels in the patch, as the channels are in a mostly inactivated state during depolarisation. In the case of WT bEAG, the steady state current at the end of the depolarising pulse was measured. If the currents recorded from the cell-attached patch did not stabilise, it was discarded. On stabilisation, it was excised. The pulsing was started again and the currents were recorded. To confirm any decrease of activity was not an artefact of the patch sealing up on itself and forming a vesicle, the patch was also removed from the solution through the bath-air interface and returned. If the patch had vesiculated, it would not conduct current. The temporary removal from the bath solution of the pipette should cause the vesicle to break back into a patch so that a current would then be recorded. However, the process runs the risk of causing the loss of the seal between the pipette and membrane. Figure 5.2 shows representative traces of WT hERG currents from 5 different patches. The amplitude of the currents in the cell attached configuration varied from ~500 to 50 pA. The coloured traces show the recordings from inside-out patches at different times after excising the patch. All 5 recordings showed significant decreases in current amplitude with time. However, the time courses and finally current amplitudes varied substantially (figure 5.3). In some cases, current amplitudes were relatively stable for a period of time following excision (figure 5.3 A and C) and then declined rapidly. In another, there was a steady decline directly from excision (figure 5.3D) and in one patch (figure 5.3B), excision caused an initial rapid decrease in amplitude, but the current amplitudes then stayed relatively constant for more than 10 mins.

However all displayed a significant reduction in the currents, averaging ~30 % over the 10 mins of recording.

Figure 5.4 shows representative recordings from bEAG expressing cells. Compared to WT hERG, the WT bEAG patches display very little rundown (figure 5.4 and 5.5), in one case there is run up of the WT bEAG current (figure 5.5A). There was only one WT bEAG expressing patch that displayed rapid rundown (figure 5.5D). Removal and replacement of the patch from the solution did not cause a return of the current indicating that there may still be some modulation of activity occurring. These results seem to reflect what has been reported before that, where bEAG currents exhibit little rundown in excised inside-out patches (Gessner & Heinemann, 2003).

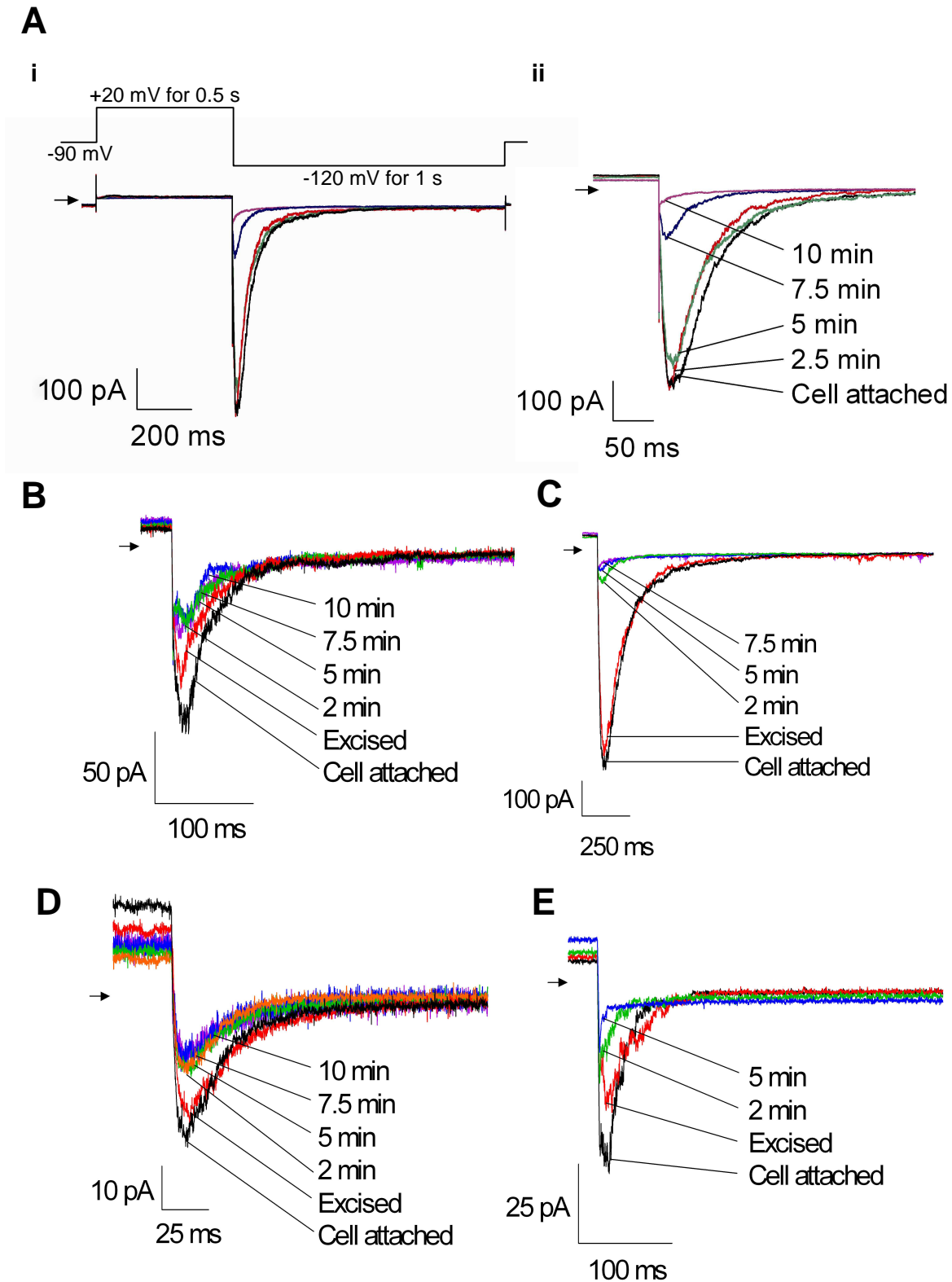


Figure 5.2: Excised inside-out patches of WT hERG current display rundown. The currents were recorded using the voltage protocol in **Ai**. **Aii-F**, expansion of the tail currents traces at indicated time points after excision from 5 different patches. These show that the activity of the channels decreased after excision and that the time course of rundown onset is variable. Zero current is indicated by the arrow.

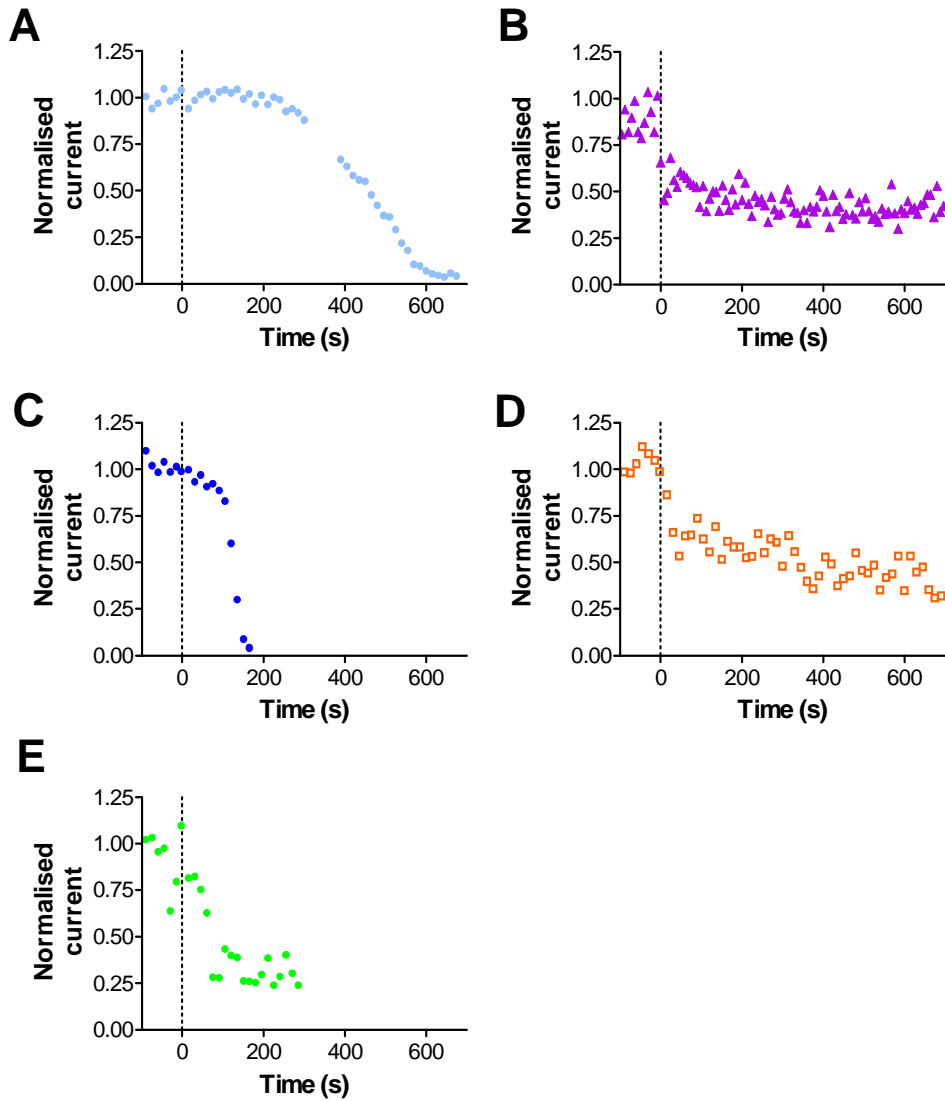


Figure 5.3: The rate and time of rundown onset is highly variable. (A-E) The amplitudes of the tail currents from every fifth trace were plotted against time. The degree of rundown is quite rapid but the start of onset is variable. In the case of C and D, the experiment was cut short as the currents had either rundown or stabilised. The dotted line indicates the time of excision, set at time zero. B, C and E were carried out with the EAG intracellular recording solution in conjunction with the hERG extracellular recording solution.

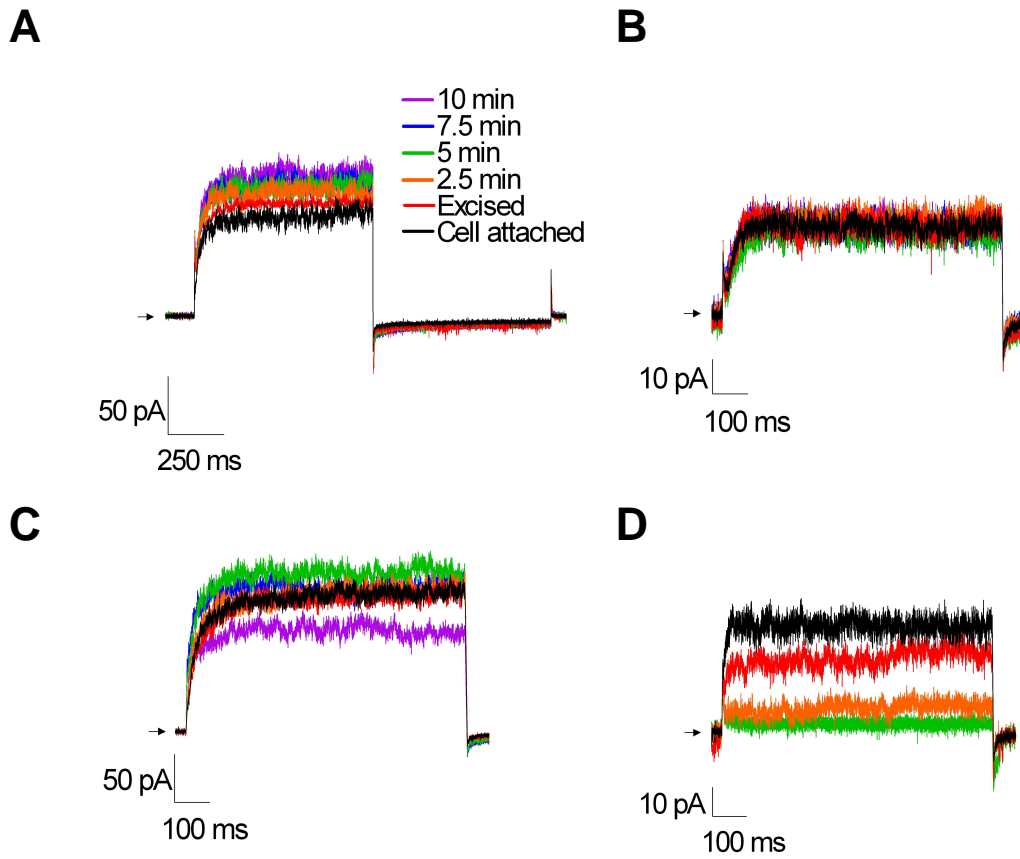


Figure 5.4: Excised WT bEAG channels do not rundown. **A**, full trace of the current elicited by the protocol shown in figure 5.2 at different points before and after inside-out patch excision. **A-D**, representative traces from four different cells expressing bEAG channels at differing times after excision. The arrows indicate zero current.

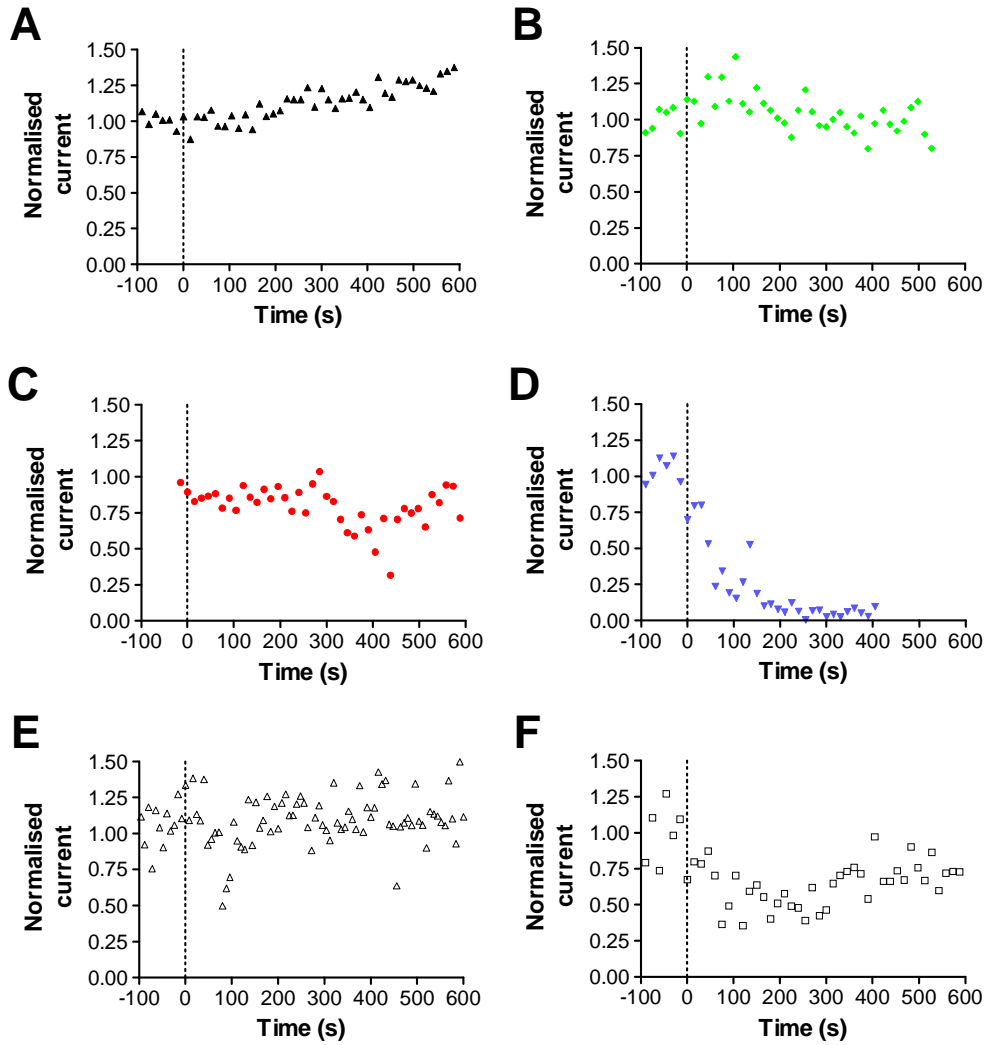


Figure 5.5: Time course of bEAG currents in inside-out patches. Plots of the amplitude of currents during the test depolarisations from excised inside/out patches of WT bEAG channels plotted against time. Time 0 (dotted line) indicates when the patch was excised from a cell attached patch.

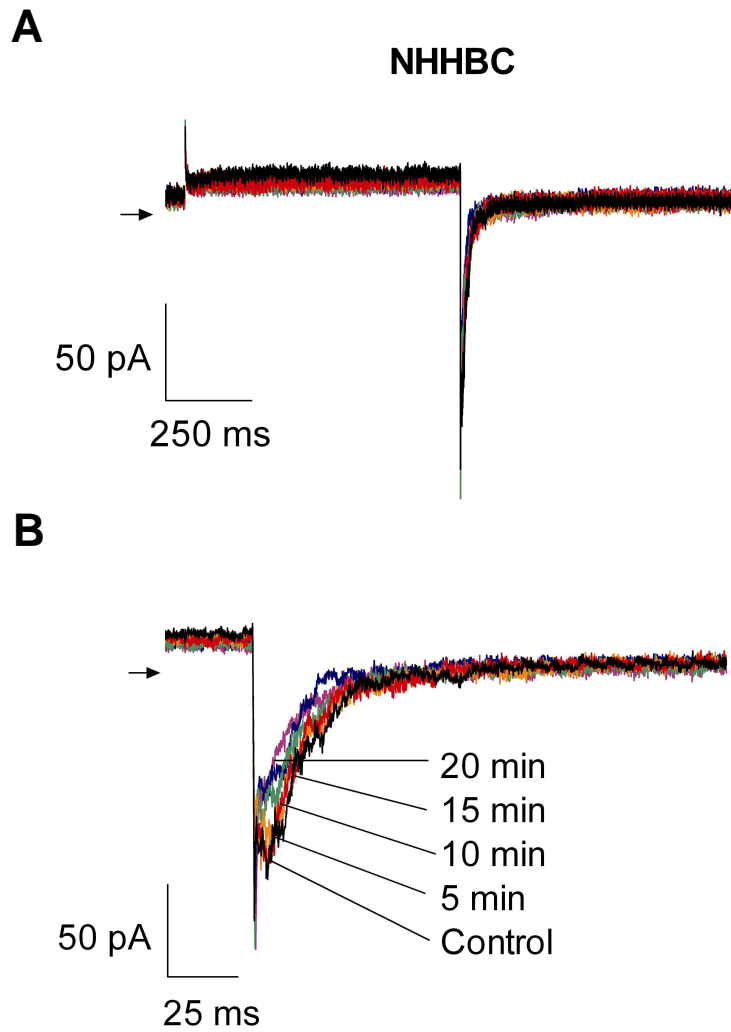


Figure 5.6: Representative traces of C-terminal swapped chimeric channel rundown in excised inside-out patches. **A**, Full trace of the currents elicited by the protocol in figure 5.2 over a 20 min time period. **B**, Detail of the tail currents at different time points after excision. There appears that there is little rundown. The arrow indicates the zero current line.

Next the rundown of the chimeric channels was investigated. These had a much lower expression level, with a mean peak tail current amplitude of 65.8 pA, compared to an average of 301.5 pA for the WT hERG channels, and so it was much harder to obtain recordings from the cells which had any discernable current.

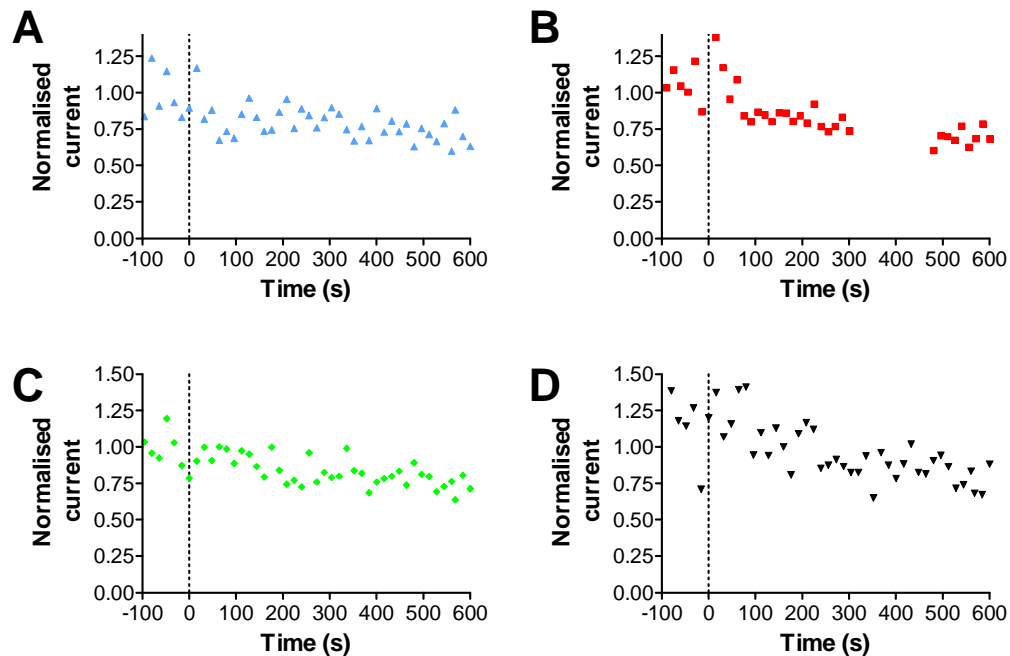


Figure 5.7: C-terminal swapped chimeras display a slowed rundown relative to WT hERG when excised from the cell. (A-C) The peaks of the tail currents were plotted against time to record the degree of channel rundown. The rundown onset occurs at a constant rate. The dotted line represents the point of excision. Results are shown from four different patches recorded in the EAG intracellular solution in conjunction with the hERG extracellular recording solution.

The C-terminus swapped mutant (NHHBC) had a rundown that was significantly lower than WT hERG over 10 minutes (figure 5.6, 7 and 11). The tail current amplitudes declined to approximately 75% of the original amplitude, compared to ~30 % remaining with WT hERG. This also shows that the NHHBC channel is not as resistant to rundown as WT bEAG, but could be to a manageable level.

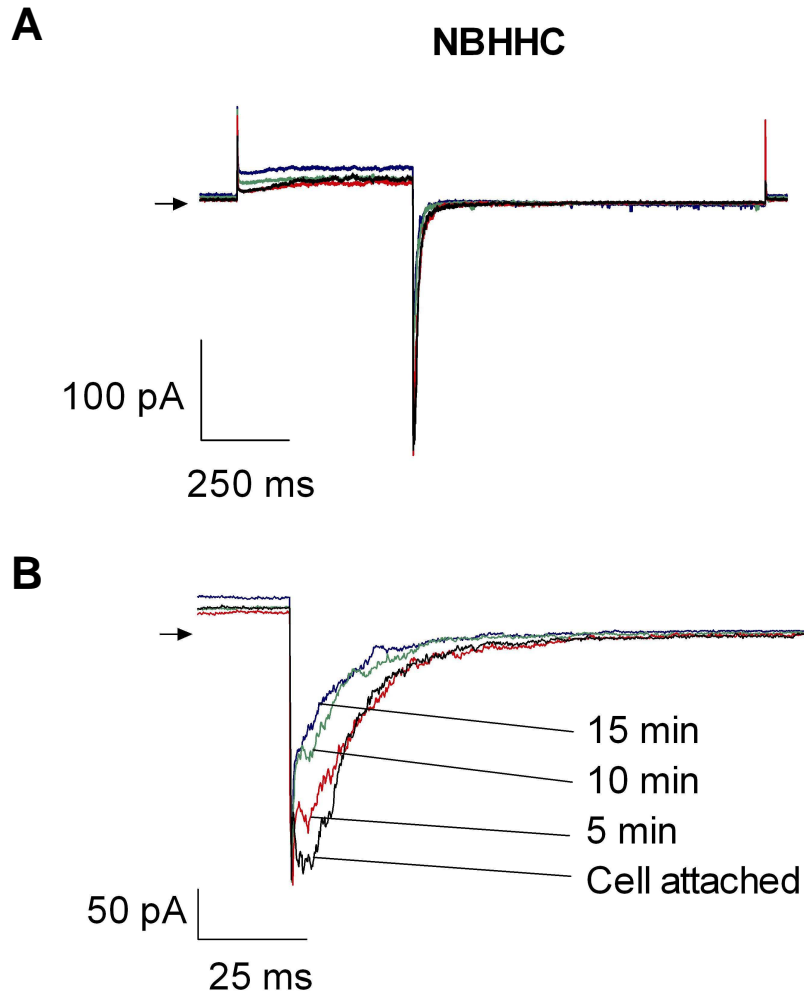


Figure 5.8: Representative traces of N-terminal swapped chimeric channel rundown in excised inside-out patches. **A**, Full trace of the currents elicited by protocol in figure 1 at set time points before and after the excision of the patch. **B**, an expanded view of the family of tail currents recorded to show the degree of rundown. The arrow indicates zero current.

Figure 5.8 shows the current traces from the N-terminal swapped chimera (NBHHC). These currents displayed a rapid decline after patch excision that was very similar to WT hERG (figure 5.8-5.9). The rate of rundown was again quite variable, but there was less of a delay in the onset of rundown in patches studied.

Finally, the BHS16 chimera, in which both termini are from bEAG, was studied. Expression of this channel was poor and only one recording was achieved. The results are shown in figure 5.10. Over 10 minutes after the excision of the

patch, there was a steady decline in the tail current amplitudes, with over 50 % of the current remaining. It indicated that there was a much slower rate of rundown compared to WT hERG (figure 5.10C). Unfortunately, from just one recording, it is hard to confidently compare rundown with bEAG or NHHBC. Further recordings will have to be carried out in order to see if this is a significant effect.

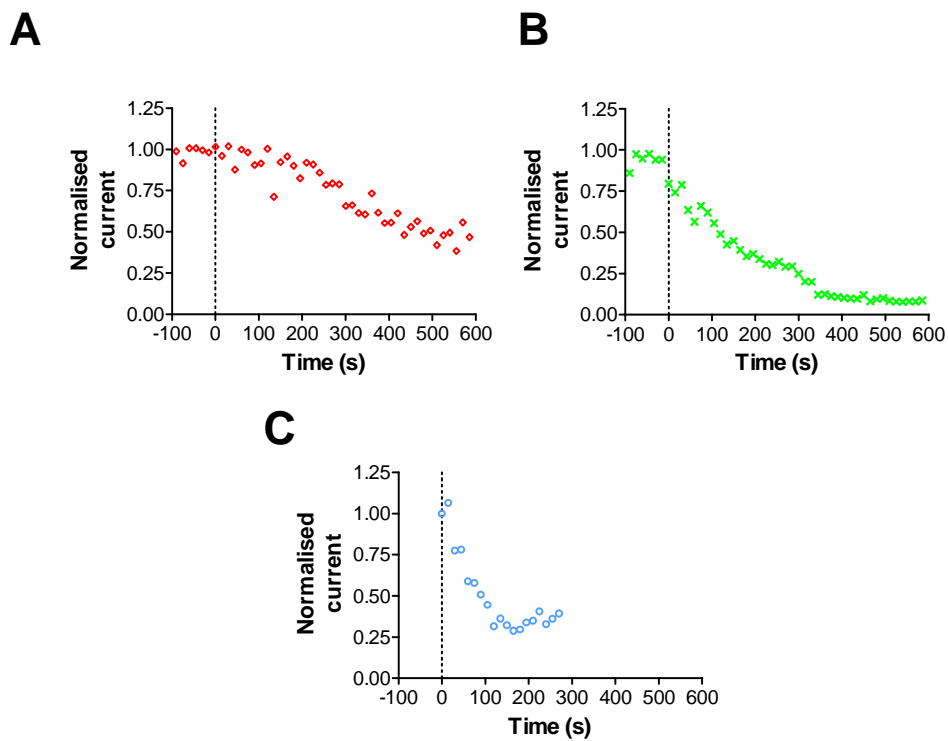


Figure 5.9: The time course of NBHHC chimera current rundown. **A-C**, Plots of the peak tail currents of three separate patches before and after excision. The dotted line represents the time of excision.

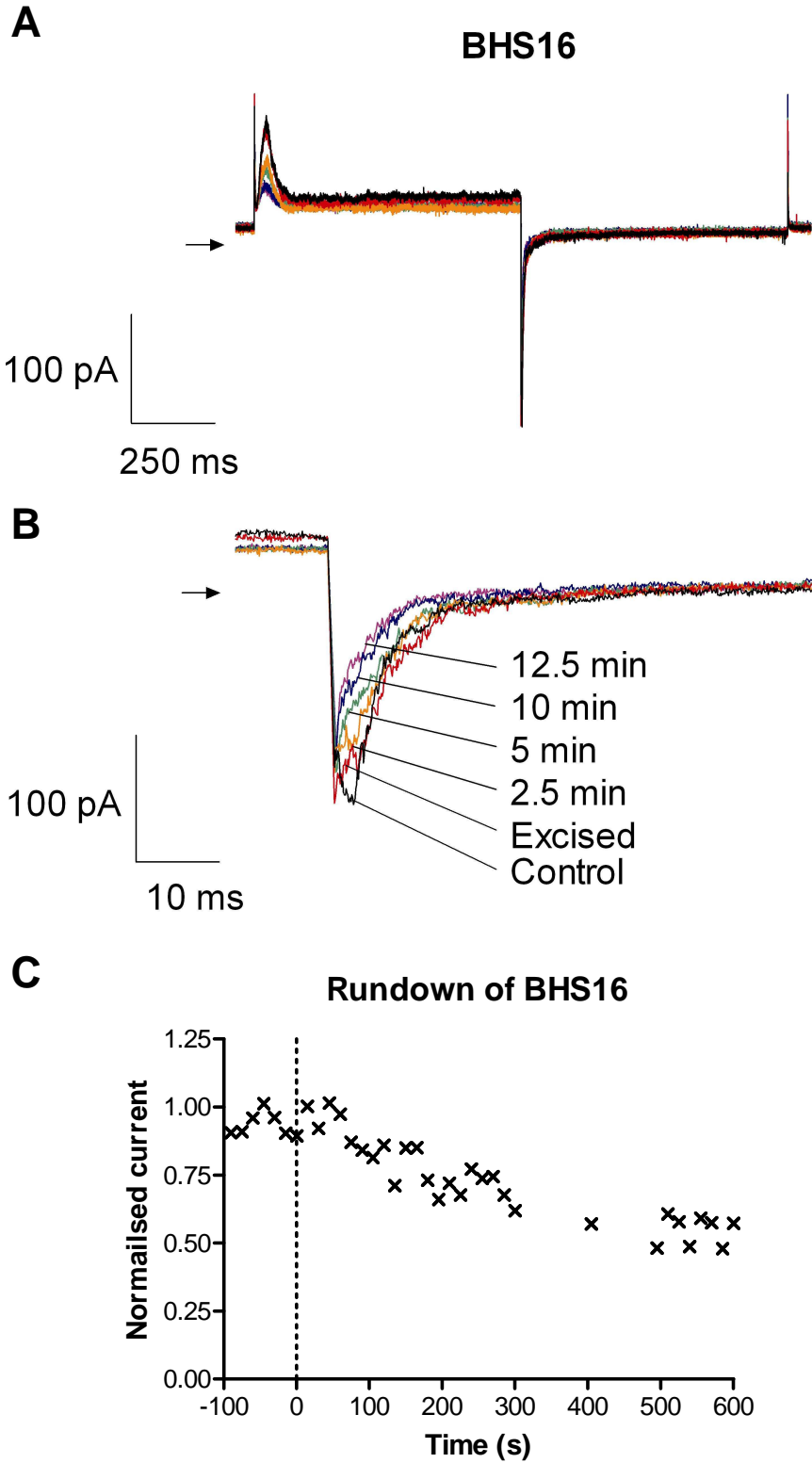


Figure 5.10: Double terminal swapped chimera displays rundown. **A**, representative current traces of the chimeric channel at differing time points before and after excision of an inside/out patch. **B**, detail of the deactivating tail currents at different time points. **C**, Plot of the peak tail currents before and after excision.

The results of the rundown experiments are summarised in figure 5.11 and table 5.1. On average WT hERG currents decrease to 51% of the cell attached value after 5 mins and to 30% after 10 mins. Although this is not a particularly rapid rundown, the problem is that the rate is unpredictable and variable from one patch to another. Exchanging the hERG N-terminus for a bEAG one does not significantly reduce rundown. However, exchange of the C-terminus slowed rundown. The NHHBC currents were 81% of the cell attached current amplitudes after 5 minutes and decreased by only another 8% over the next 5 mins. Thus, the C-terminus may contain the sites that are sensitive to modification upon excision. When both the N- and C-termini are swapped, the slowing of rundown affect is less than with just the single C-terminal exchange. But further experiments would have to be carried out to confirm this.

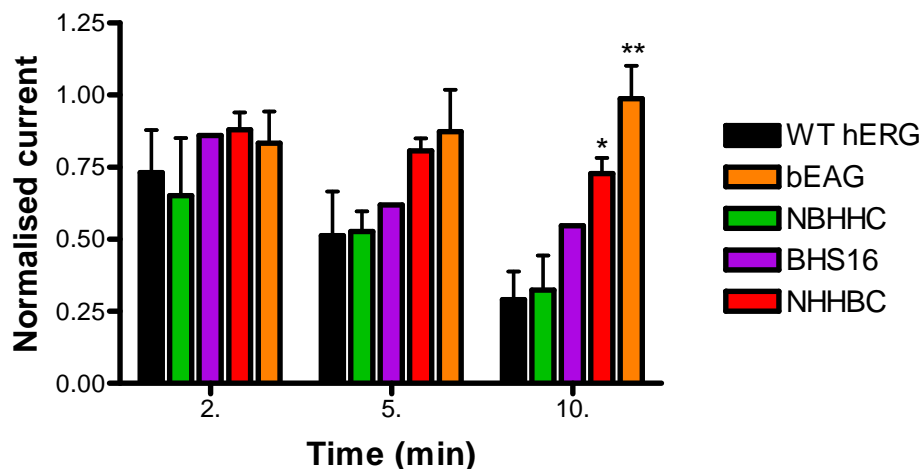


Figure 5.11: NHHBC appears to be the channel that has the lowest amount of rundown. A summary of the degree of rundown after 2, 5 and 10 minutes of excision. The data are presented as means  $\pm$  S.E.M. WT hERG n=6, WT bEAG n=7, NHHBC n=4, NBHHC n=3, BHS16 n=1. \* indicates  $p < 0.05$ , \*\* indicates  $p < 0.01$  for respective chimeras compared to WT hERG at the same time point.

Time from excision	WT hERG	BEAG	NBHHC	BHS16	NHHBC
2 min	0.73 ± 0.15	0.83 ± 0.11	0.65 ± 0.20	0.86	0.88 ± 0.06
5 min	0.51 ± 0.15	0.87 ± 0.14	0.53 ± 0.07	0.62	0.81 ± 0.04
10 min	0.30 ± 0.10	0.99 ± 0.11**	0.32 ± 0.12	0.55	0.73 ± 0.05*
	n=6	n=7	n=3	n=1	n=4

Table 5.1: Summary of the rundown of WT and chimeric channels at set points after excision of the patch. The data are summarised as mean of current remaining ± S.E.M. \* indicates  $p < 0.05$ , \*\* indicates  $p < 0.01$ .

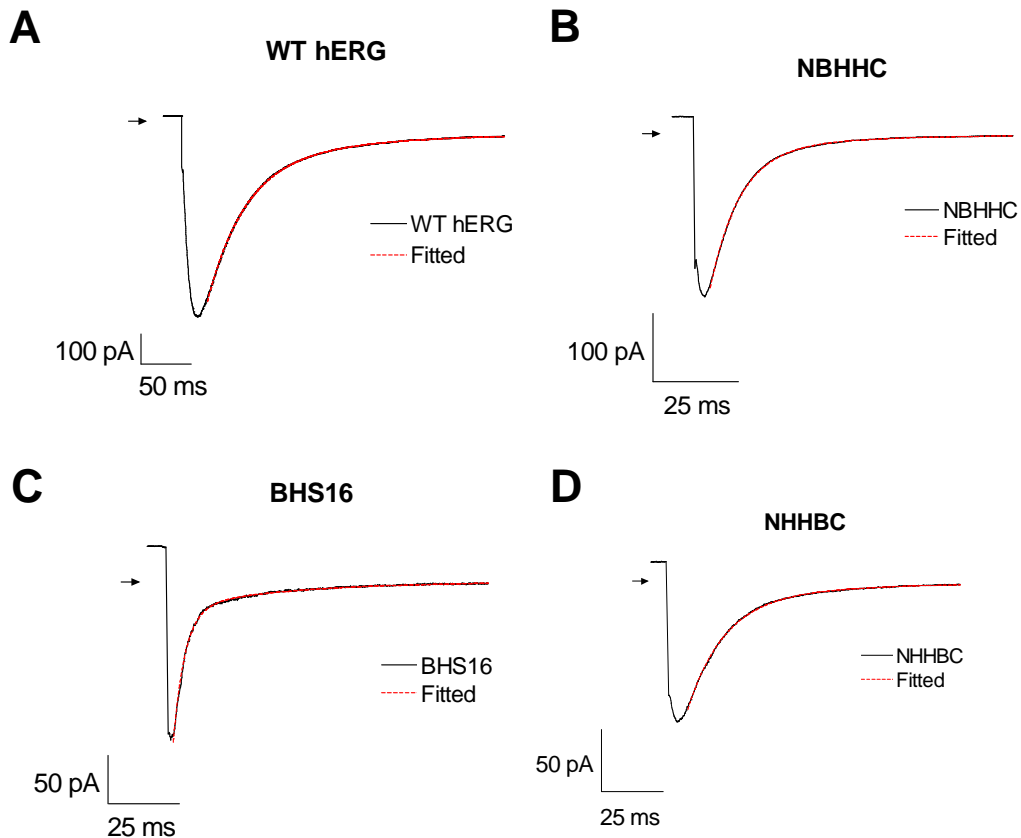


Figure 5.12: Inside-out patches of chimeric channels deactivate at a higher rate compared to WT hERG. The traces from inside-out patches were averaged (black line) and fitted with a double exponential curve (red line) to get a time constant for deactivation. The arrow indicates zero current

### ***Characterisation of the deactivation in patches***

Having examined the amplitudes of currents in inside-out patches, the tail currents were further analysed to see if deactivation differs from the results obtained from the two electrode voltage clamp (TEVC) technique.

To reduce the noise and to facilitate more precise curve fitting with exponential functions, five consecutive current traces were signal averaged.

Double exponential functions were then fitted to these signal average traces. Figure 5.12 shows representative traces resulting from this analysis. These currents are signal averaged from the first five recordings following excision. The procedure substantially reduces the noise and each of the traces is accurately fitted by the double exponential function. This analysis was done for currents recorded from cell attached patches (time = 1 mins) and immediately following excision (time = 0 mins) and at 2, 5 and 10 mins subsequent to excision. The mean results for the fast and slow time constants for deactivation are shown in figure 5.13. In general, the time constants for each channel type remain relatively constant at each time point, suggesting that deactivation is unaffected by changing the recording configuration. The large error bars for some of the values at the 10 minute time point are due to the small current amplitudes and sample numbers.

Looking at WT hERG, it can be seen that the time courses of deactivation, obtained from fitting a double exponential curve to the tail currents, are not significantly different to that found using the TEVC technique (figure 5.14). The results also indicate, as reported in the previous chapter, that the deactivation of the chimeric channels was faster than that of WT hERG (figure 5.13 and 5.14). From the fits, (figure 5.13 and 5.14) the two time constants of the chimeric channel deactivation recorded from inside-out patches are significantly slower compared to those recorded using the TEVC experiments. This can be seen when the tail currents are normalised and overlaid (figure 5.15). When analysing the contribution of the slow and fast components of deactivation, the results indicate that the slow component has less contribution than that of the fast.

The kinetics of the deactivation does not appear to vary greatly over the time after the patch is excised (figure 5.13). This is apparent with all of the patches studied, meaning that any modulation that occurs during the excision of the patch primarily influence the number of active channels rather than the voltage dependence.

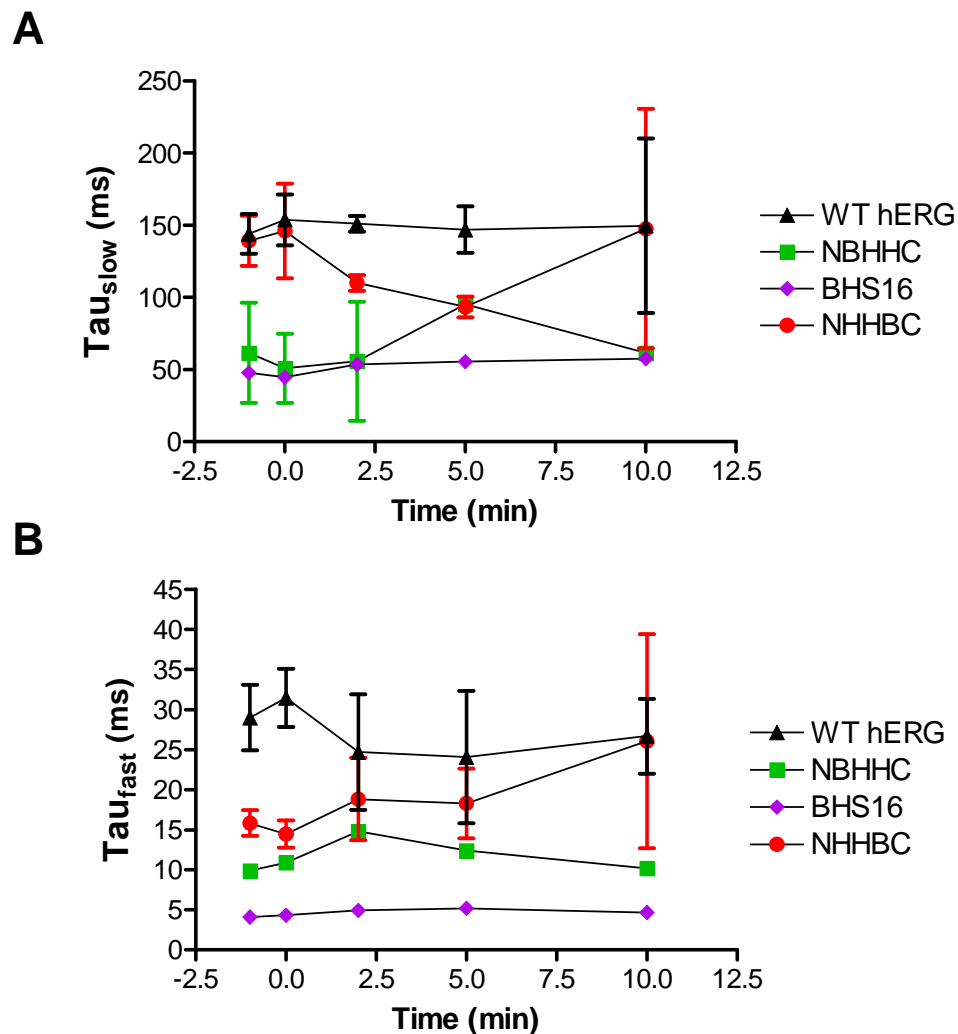


Figure 5.13: The deactivation rate of WT and chimeric channels does not change greatly after excision. The deactivating tail currents from inside-out patches at varying time points after excision were fitted with second order exponential functions and plotted against the elapsed time from excision. The data are presented as means and S.E.M. WT hERG n=6, NHHBC n=4, NBHHC n=3, BHS16 n=1.

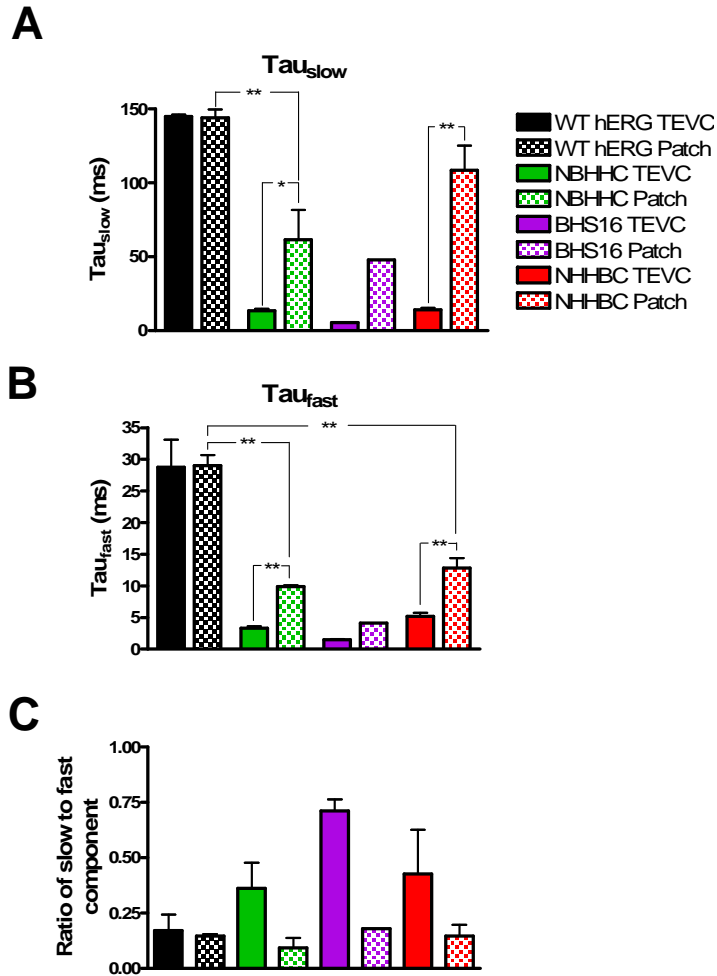


Figure 5.14: The time course of deactivation obtained from exponential fits for the chimeras is slower in the patch clamp recordings than in TEVC recordings. The results from WT hERG deactivation are similar to those in patch clamp as in TEVC recordings. The chimeric currents show fits with much slower time constants in both the slow and the fast components (A and B). However, the fast component has a higher contribution to the deactivation time course in the patches (C). The data are shown as mean and S.E.M. \* indicates  $p < 0.05$ , \*\* indicates a  $p < 0.01$  when compared to either the WT hERG patches or the TEVC equivalent. The patching data were taken from time 0, at the point of excision.

	WT hERG	NBHC	BHS16	NHHBC
Tau <sub>Slow</sub> (patch)	144.1 ± 13.7 ms	61.6 ± 34.7 ms**	47.8 ms	108.6 ± 33.1 ms
Tau <sub>Fast</sub> (patch)	29.0 ± 4.1 ms	9.9 ± 0.3 ms**	4.1 ms	12.8 ± 3.2 ms**
	n=6	n=3	n=1	n=4
Tau <sub>Slow</sub> (TEVC)	144.9 ± 24.7 ms	13.3 ± 3.2 ms^^	5.4 ± 0.3 ms	13.9 ± 3.2 ms^^
Tau <sub>Fast</sub> (TEVC)	28.7 ± 9.8 ms	3.3 ± 0.7 ms^^	1.5 ± 0.2 ms	5.2 ± 1.2 ms^^
	n=5	n=5	n=5	n=5

Table 5.2: The deactivation rate of the chimeric channels is slower when recorded from patches than in whole cell recordings. The Data are shown as mean ± S.E.M. \* indicates  $p < 0.01$  when compared to WT hERG. ^^ indicates  $p < 0.01$  when compared to patches from the same chimera.

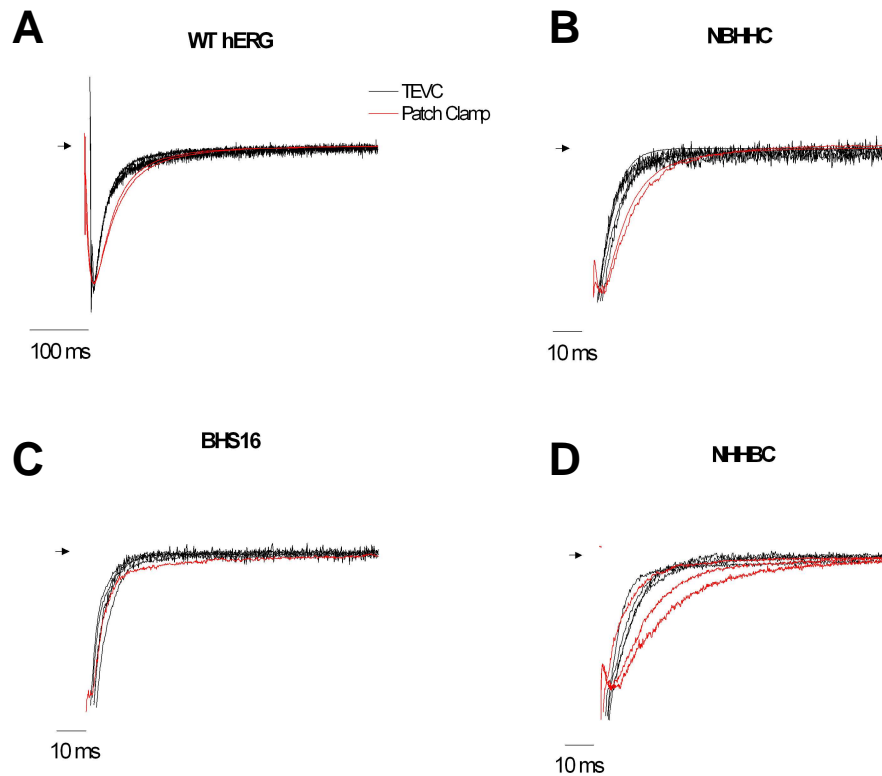


Figure 5.15: Deactivation is slower in excised patches. The tail currents from TEVC (black) and inside-out excised patch (red) recordings (at time 0, the point of excision) were normalised to peak amplitudes and overlaid. It can be seen that in general the deactivation of the channels in the excised patches were slower than those recorded from the TEVC experiments.

## Discussion

WT hERG channels in excised inside-out patches rundown. The reduction in channel activity occurs at variable rates in different patches. hERG current rundown has been reported in previous studies (Bian *et al.*, 2001; Gessner & Heinemann, 2003; Du *et al.*, 2004). It could be indicative of a modulatory factor that is present in the vicinity of the channels that keeps them active and either diffuses away on excision or is metabolised. The speed of the rundown would therefore, be dependent on the properties of individual patches. The mechanism for rundown is unclear. The size and/or shape of the membrane

patch within the pipette may affect the diffusion or regulatory factors that keep the channels active. There may also be patch to patch differences in cytoskeletal or cytoplasmic constituents that remain when the patches are excised.

From my recordings, it was clear that WT bEAG does not display much rundown compared to hERG. This has been reported in previously published data (Gessner *et al.*, 2004). This could indicate that the channel lacks the regulatory domain or that bEAG binds this regulatory factor with higher affinity and thus it does not unbind when the patch is removed from contact with the cytoplasm.

When the C-terminus of hERG is swapped for that of bEAG, there is a reduction in the rate of rundown in the excised patches. This indicates that the C-terminus contains a site that is important in the regulation of rundown, while exchanging the N-terminus appears to have little contribution to this. The rundown is not fully prevented, by either the C-terminal swapped or the double terminal swapped chimeras. Therefore, there may be further regions within S1-S6 that regulate the rundown or interactions of the termini with S1-S6 are altered to increase the susceptibility to rundown

The irregularity of the rundown of the channels appears to suggest that it could be due to a diffusible regulatory factor that binds to keep the channel active. Two possible modulatory factors could be PIP<sub>2</sub> or ATP, these have been used in previous studies (Bian *et al.*, 2001; Cayabyab & Schlichter, 2002; Bian *et al.*, 2004; Hirdes *et al.*, 2004), added to the recording solutions. Bian *et al.* (2001) recording hERG channels in CHO cells added a concentration (10 µM) of PIP<sub>2</sub> to the intracellular solution. They found that the rundown rate

was significantly reduced. Further experiments (2004) show that the PIP<sub>2</sub> is able to bind on the C-terminus of hERG. This indicates there may be involvement of PIP<sub>2</sub> binding in regulation the activity of the channels.

Hirdes *et al.* (2004) found that 3 mM ATP present in the recording solution was able to slow the rundown of hERG in human tSA-201 cells, when ATP was replaced by AMP-PCP, a non hydrolysable analogue of ATP, rundown rate was rapid. They also noticed that using kinase inhibitors caused an increased rates of rundown. Using a broad spectrum kinase inhibitor (1 μM staurosporin) and a protein kinase C (PKC) inhibitor (1 μM bisindoloylmaleimide I), they found that the kinase inhibitors increased the rate of rundown of rERG. Cayabyab *et al.* (2002) also found similar effects, when 2 mM ATP was present, the rate of rundown of hERG in MLS-9 cells was reduced compared to its absence. Over 45 mins, in presence of 2 mM ATP the rundown was 10-15%, while in its absence, was ~50%. They also used protein-tyrosine kinase (PTK) inhibitors to look for hERG regulation, they found that they increased the rundown rate to 35% with Lavendustin A and 65% with genistein over 20-30 mins, this is more than the 10% decline in their absence. These studies indicate there may be more than one type of regulation of activity, with the binding of PIP<sub>2</sub> to the C-terminus and the possible phosphorylation effects being important to the activity of the channels. From these studies it could be said that the rundown may be reduced if modulation factors bind to the channel with a higher affinity, as could be indicated by the comparison of bEAG and the C-terminal swapped chimera. It is also possible that there is a modification site, which may need substrates present to stay modified, on excision these substrates are not replaced as

there is insufficient concentration present in the solution, therefore the activity of the channel decreases. The rate of rundown would, therefore, appear to be irregular, as the patches are never identical and the quantity of intracellular factor that is excised with each patch will be dependent on several variables that are difficult to control. The rate of rundown may be dependent on the rate of decrease in these factors.

Further experiments to investigate possible modulatory factors, such as ATP and PIP<sub>2</sub> will need to be carried out to discover if they are able to reduce the rundown seen. The chimeric channels could be transfected into mammalian cell lines to attempt to see if the different cell background has any impact on channel activity.

### ***hERG channel deactivation is unchanged on excision***

From the results of the curve fitting of the deactivating tail currents, the deactivation of WT hERG channels is shown to be significantly slower than that of the chimeric channels. This is what is reflected in the TEVC experiments and previously published data in which the N- and C- termini were altered. Where, the N-terminus is truncated or shortening through deletions in the proximal N-terminus, accelerates the deactivation rate (Schönherr & Heinemann, 1996; Wang *et al.*, 2000; Aydar & Palmer, 2001; Gomez-Varela *et al.*, 2002). Deletions in the C-terminus also may increase the rate of deactivation (Aydar & Palmer, 2001). This further confirms that the termini of hERG channels have a role in the stabilisation of the open state.

It can be seen from the patches recorded, the deactivation rate did not change greatly over time after excision. This is in contrast to some other reports where calcium and KAT1 channels display some changes to the

gating properties of the channels once they were excised (Armstrong & Eckert, 1987; Tang & Hoshi, 1999). *Tang et al.* (1999) show that there is a shift in the voltage dependence of the KAT1 channels when the channels are excised from the membrane. In the case of the hERG constructs, it seems that there was no substantial change in the voltage dependent gating, such as a large positive shift to voltage dependent activation that would have reduced tail current amplitudes and accelerated deactivation. However there were differences between those recordings obtained from the TEVC experiments and those of the inside-out patches. The deactivation rate of the chimeric channels in the inside-out patch recordings were slower than those recorded from the TEVC experiments. This may be due to the differences in the recording solutions used in the recordings; the TEVC technique keeps the cell contents mostly intact, while the inside-out patch clamp technique will alter the solutions the channels are exposed to. The alteration of the solutions may therefore alter the kinetics of the chimeric channels in a similar way that EAG channel activation kinetics are altered by divalent ions (Terlau *et al.*, 1997; Schonherr *et al.*, 1999).

In summary, WT hERG currents exhibit a rapid rundown in excised inside-out patches that was not seen with WT bEAG. The NHHBC chimera containing the C-terminus of bEAG exhibited remarkably stable currents and could conceivably be used in inside-out patch clamp studies in which an exchange of intracellular solutions is required. This could be valuable for testing if compounds with different whole cell  $IC_{50}$  values have an altered affinity for the inner cavity binding site or altered access to the binding site due to differences in membrane permeability. The NHHBC construct might also be

suitable for cysteine accessibility studies on intracellularly located amino acid residue positions.

## Chapter 6: Characterising hERG channel block with varying length drug molecules

### Introduction

As described in the introduction, a structurally diverse and large number of compounds are potent blockers of hERG potassium channels (Cavalli *et al.*, 2002; Aronov, 2005; Zunkler, 2006). They mainly act by binding to inner cavity of hERG, gaining access when the channel opens and blocking the channel (Mitcheson *et al.*, 2000b).

There have been many attempts to try to predict which molecules will be able to block hERG channels. One way was through analysis of known libraries of hERG blocking drugs and creation of pharmacophore models. This looks at the structure of the different drugs and models what they have in common. The model can then use these pharmacophore features to predict whether a novel drug

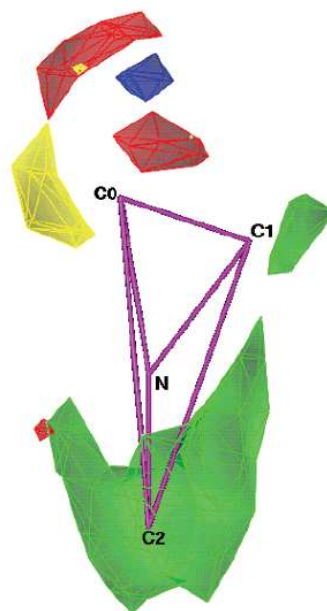


Figure 6.1: The Cavalli pharmacophore model. The model was created from the analysis and comparison of 31 drug molecules that block hERG with  $IC_{50}$  values that varied by >5 orders of magnitude. The model suggests that hERG blocking drugs mostly have a central charged nitrogen **N** and an aromatic group in two or three of the centroids **C0-2**. Green regions indicate where molecular volume increases cause a rise in the ability to block hERG channels; yellow regions indicate where volume decreases cause a drop. Red and blue contours indicate increased activity with the presence of a positive or a negative charge respectively. (Cavalli (2002) *J. Med. Chem.*, **45**, 4844-4853)

has the potential to be a hERG channel blocker. Cavalli *et al.* (2002) created a

template pharmacophore that contained characteristics commonly found in hERG blocking drugs. This consisted of a central tertiary amine group with three centres of mass coming off it at a specific angle and distance away (figure 6.1). These centres are hydrophobic aromatic groups and frequently the model includes physicochemical parameters that either increase or decrease the potency of the drug to hERG. The model can be used to predict whether a new chemical entity could be a possible hERG blocker. Several other pharmacophore models have been reported (Morgan & Sullivan, 1992; Ekins *et al.*, 2002) and this approach is widely used by the pharmaceutical industry. Although the models can predict the likelihood of binding to the hERG channel; at present, this can not be used to give an accurate quantitative figure on binding affinity. There will also be possible false positives being reported.

Another method used is homology modelling, where the channel is modelled using available crystal structures of open and closed channels, sequence alignments and refined using experimental data. These data were used to set the position of the transmembrane domains and amino acids (Osterberg & Aqvist, 2005). This can then be used to model binding to channels and highlight potential important interactions with amino acid residues. New experimental data can also be used to test refine the model and propose further experiments. The quality of the models initially depends on the homology between the template crystal structure and hERG. At present the channels that have been crystallised have greatly differing amino acid sequences to hERG. Shaker channels share ~13 % homology with hERG channels in the transmembrane region. The homology models are generally

rigid and although molecular dynamics simulations can investigate dynamic changes in structure, these are on time scales too short to relate to process such as activation gating.

It is thought that drugs bind with higher potency to the open channels than closed channels due to conformation changes involved in the gating of the channel (Mitcheson *et al.*, 2000b; Chen *et al.*, 2002). It is also thought that drug trapping may play an important role in the high potency block of hERG channels. Drug trapping is where a compound is retained in the inner vestibule of a channel, when in a closed state. Thus it is prevented from unblocking the channel (figure 6.2) (this is explained in further detail later). It has been observed that many high affinity

hERG channel blockers do not wash off when the channels are held in a closed state (Carmeliet, 1993). Use of the D540K mutant channel, a channel with unique gating properties, provides strong evidence for trapping. The D540K mutant is able to open at positive potentials much like the wildtype and

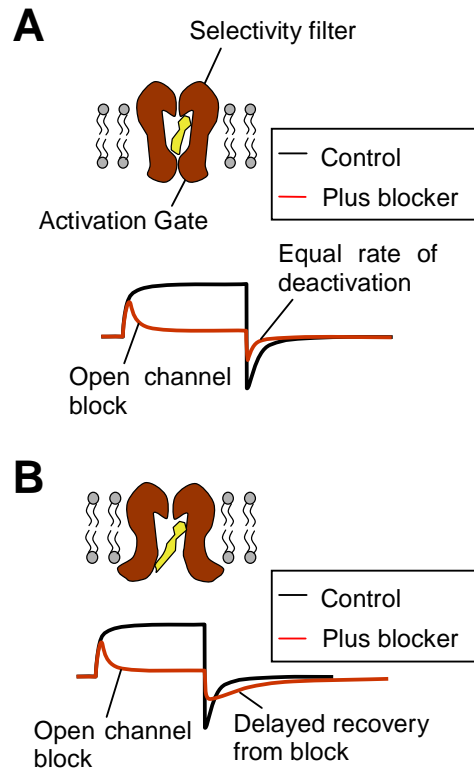


Figure 6.2: The characteristics of drug block. **A**, Drug trapping. The channel is able to close around the drug molecule preventing compounds leaving the channel and recovering from block. The kinetics of the current traces should be the same as those without drug present. **B**, foot in the door, the channel is unable to close around the drug molecule. The currents will show the open channel block, but the currents of deactivation may appear to be slowed due to the currents from channels that recover from block.

is mostly closed at -90 mV. However, at potentials negative of -90 mV, it is able to open. In presence of a blocker, the channel is blocked at positive potentials, but at the negative potentials when the channels are open, the drug is washed off relatively quickly compared to the wildtype channels. (Sanguinetti & Xu, 1999; Mitcheson *et al.*, 2000b; Perry *et al.*, 2004). The trapping of the drug molecules in the cavity of hERG may cause the channel to remain blocked for longer periods of time as it will inhibit the molecules diffusion away from the channel. There are also questions on the size of the actual inner cavity, as the channel is able to accommodate quite large drug molecules when it closes, which brings me to this study.

A series of compounds were designed with varying length based on the high potency blocker, E-4031 (figure 6.3 and 6.6). These analogues could be used as molecular rulers to measure the size of the inner cavity. By examining the characteristics of block of each of these analogues. The hypothesis was that the shorter drugs would be trapped in the inner cavity. As the length of the drug molecules was extended, we expected that the compound would no longer be trapped and instead would give a foot in the door type block (Armstrong, 1971; Holmgren *et al.*, 1997). The characteristics of the current traces would change as the compound interferes with channel closure and unbinding has to occur before channel closure, causing the apparent slowing of deactivation (Holmgren *et al.*, 1997). This would give an indication of the size of the channel cavity. The characteristic indicators of drug trapping are open channel block on the first pulse with no recovery from block between pulses. When drug block reaches equilibrium, the whole cell current traces in presence of drug should have reduced currents with similar activation and

deactivation kinetics to those in absence of drug (figure 6.2), since the only channels that pass current are the ones not blocked by drugs. There is little recovery from block upon wash off with the channels closed, as the drug is trapped in the cavity (Armstrong, 1971; Ficker *et al.*, 2001; Gessner *et al.*, 2004).

In contrast, ‘foot in the door’ type is characterised by open channel block, but upon repolarisation, deactivation appears to be slowed (figure 6.2B). The channels are unable to pass current when blocked, but upon repolarisation, when channels begin to close, there may be current passed as channels recover from block. The key difference is that the compound must unbind before the channel can close. For the short time the channels are open between recovery from block and closure of the channel, it will pass current. This current gives rise to the slowing of deactivation.

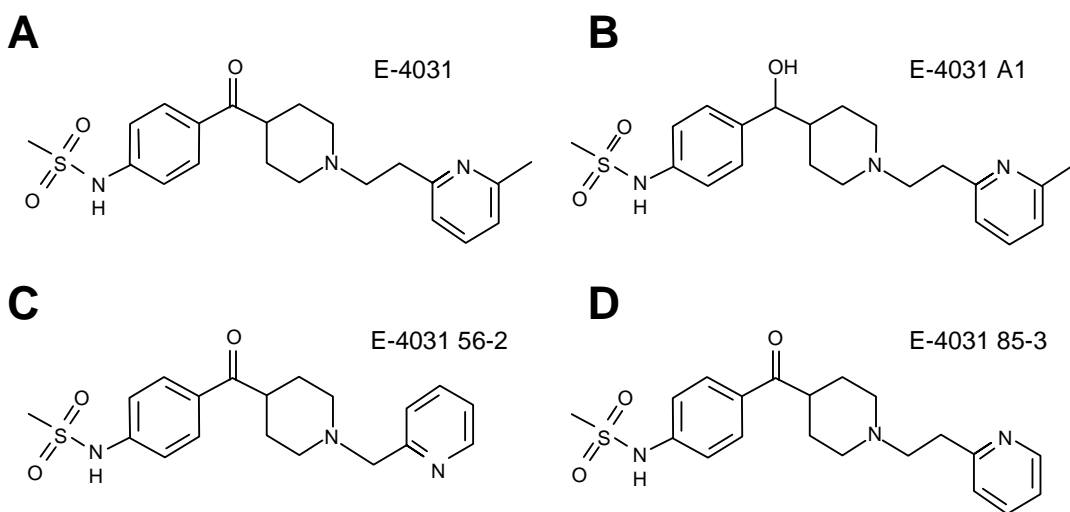


Figure 6.3: Chemical structures of E-4031 and some preliminary analogues. A set of analogues of E-4031 were produced as an initial test to see the potency of the drugs produced. **A**, E-4031, the drug molecule that the analogues were based on. **B**, was a possible intermediate structure to produce further analogues. **C** and **D** were analogues produced that were shorter than E-4031, where **C** is shortened by two carbon bonds and **D** is shortened by one.

This chapter investigates the use of the compounds in figure 6.3 and 6.6 to block hERG channels expressed in *Xenopus* oocytes. Using a series of experiments, the potency and the kinetics of block will be analysed to investigate whether the length changes the phenotype of block; so giving an estimate of the size of the inner cavity of hERG.

## Results

### *Pharmacology of drug intermediates*

In order to try to create a compound series, an intermediate based on E-4031 were synthesised at Novartis, Horsham and then tested for potency. E-4031 A1 had a hydroxyl group on the linker between the piperidine and

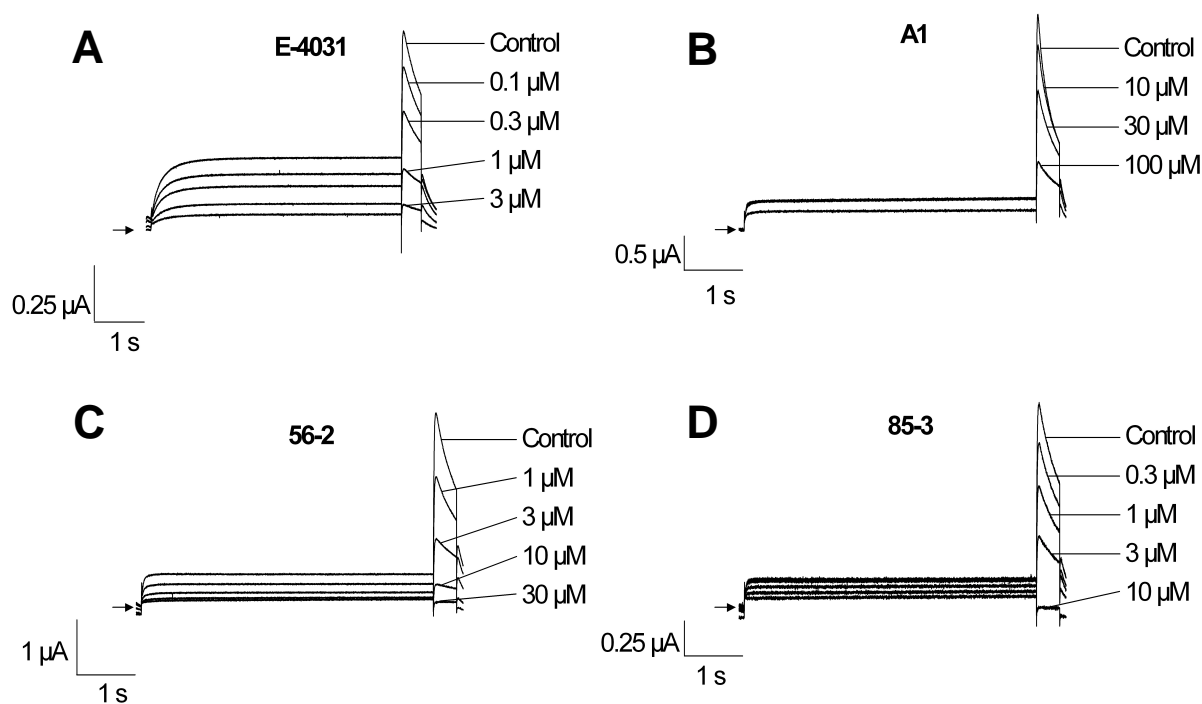


Figure 6.4: Small modifications to E-4031 structure can have a profound effect on the potency of hERG current inhibition. Inhibition of WT hERG currents by E-4031 and the indicated analogues. **A-D**, representative traces of currents recorded in absence of drug (control) and after achieving stable steady state block in presence of increasing compound concentrations, as indicated.

methylsulphonamide groups, instead of carbonyl group. Two shorter compounds based on E-4031 were also produced (figure 6.3). E-4031 56-2 had a shortened linker between the pyridine and piperidine groups, whereas E-4031 85-3 the methyl group was removed from the pyridine ring. Concentration-response experiments on WT hERG were carried out with the compounds to see the effect of the changes in structure on potency (figure 6.4 and 6.5). The membrane potential was depolarised to +20 mV for 5 seconds and tail currents were recorded with a 400 ms step to -70 mV to record the activity of the channels. The protocol was repeated every 6 seconds. The resulting concentration-response relationships (figure 6.5) indicated that there was an increase in the  $IC_{50}$  of the E-4031 derivatives compared to E-4031. This could be due to the decrease in the hydrophobicity of the 85-3 and 56-2 drugs, the 85-3 compound had the smallest change in the potency. The dramatic drop in potency of the E-4031 A1 drug, of over two log units was quite unexpected as the difference in the structure was subtle.

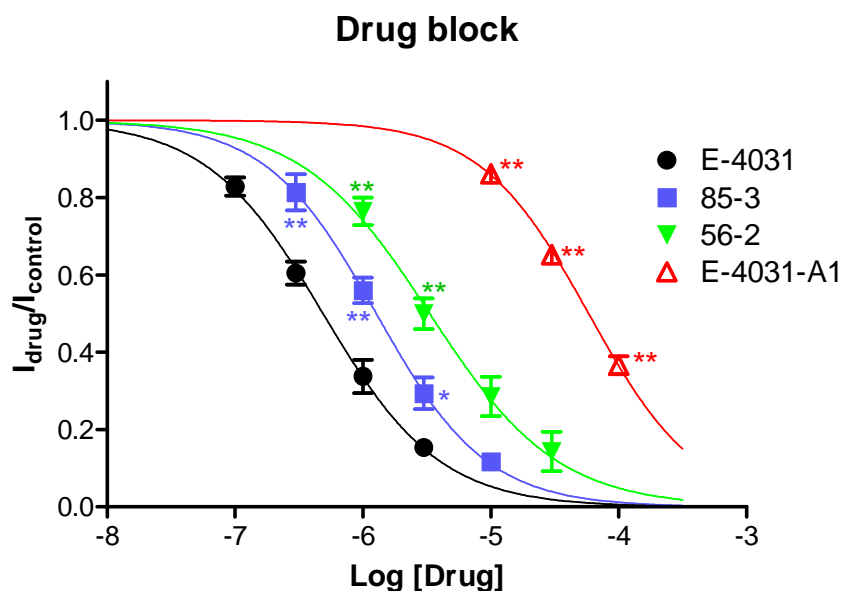


Figure 6.5: Mean concentration-response relationships for the block of hERG tail currents by E-4031 and its analogues. These all have reduced potency compared to E-4031. mean and S.E.M. are shown.  $n \geq 5$ , \* indicates  $p < 0.05$ , \*\* indicates  $p < 0.01$  compared to E-4031.

Drug	IC <sub>50</sub>	Hill slope	
E-4031	0.53 ± 0.11 µM	-1.00 ± 0.05	n=6
E-4031 A1	58.7 ± 0.6 µM**	-1.05 ± 0.01	n=5
85-3	1.1 ± 0.1 µM**	-0.92 ± 0.03	n=6
56-2	3.3 ± 0.2 µM**	-0.93 ± 0.05	n=5

Table 6.1: Comparisons of the IC<sub>50</sub> of E-4031 analogues. Concentration-response experiments with WT hERG channels when blocked by a series of drug molecules. The data are presented as mean and S.E.M. \*\* indicates p<0.01

### ***Pharmacology of further derivatives of E-4031***

As the actual process to produce elongations of E-4031 was time consuming and difficult, a set of molecules were created using E-4031 as the basic structure of the drug molecule (figure 6.6) but with some modifications. The methanesulphonamide group was substituted for a chlorine atom and a phenyl ring was substituted for a pyridine ring.

The chlorine atom substitution was predicted to have a minor impact on the potency, as other high potency hERG channel blockers, such as sertindole and clofilium, have the chlorine atom in this position. The effect of the removal of the nitrogen from the pyridine ring was unknown. The E-4031 derivatives differed from each other in the length of the linker between the piperidine and phenyl ring or the length of the length of the alkyl chain on the phenyl ring at the 'tail' of the molecule. Thus the length of the derivatives was increased in one of two different ways.

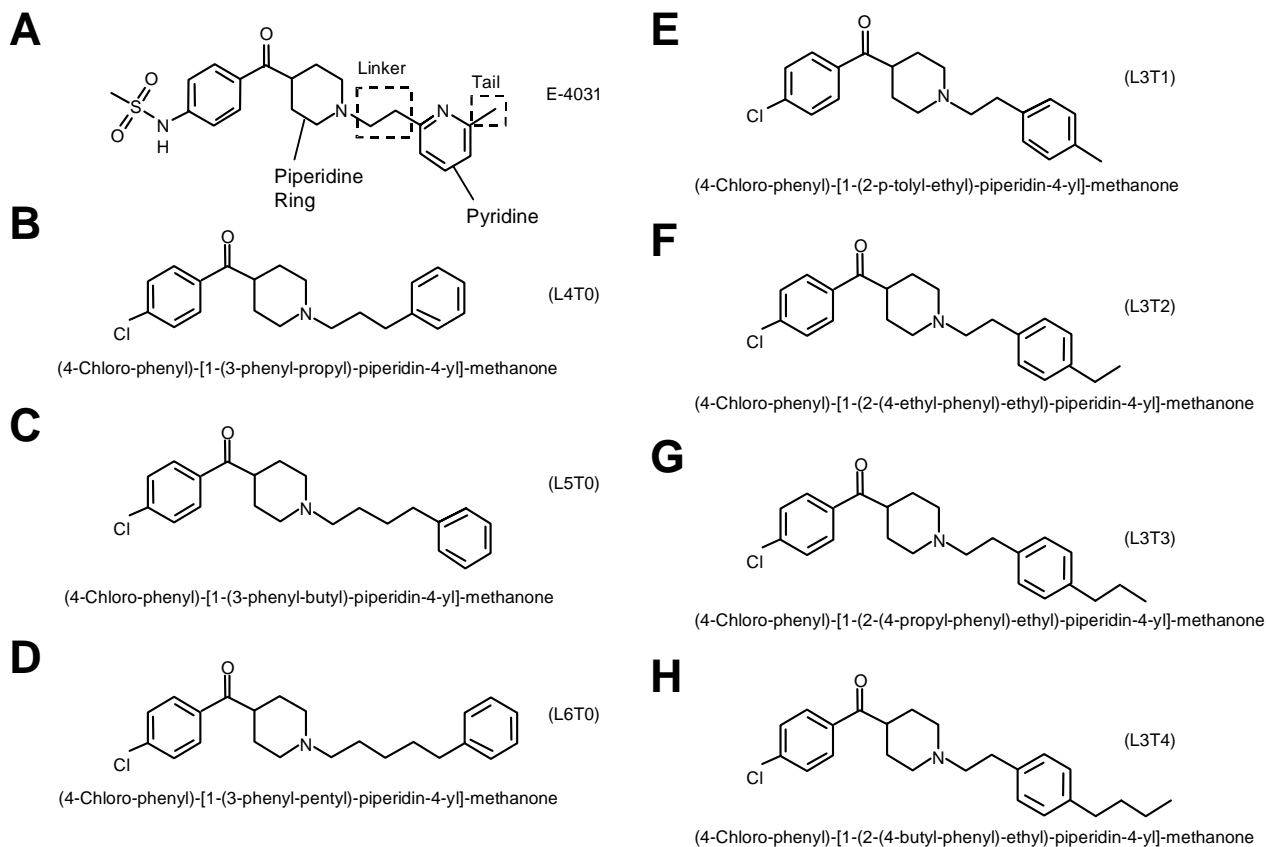


Figure 6.6: Chemical structures of E-4031 and its derivatives. The length of the molecule was increased by adding to the length of the alkyl chain in either the “tail” region (T) (**E-H**) or in the “linker” (L) region (**B-D**) as indicated on the E-4031 structure. The LxTy nomenclature relates to the number of carbons in the linker or tail.

### **Concentration-response experiments**

Experiments were carried out on oocytes expressing WT hERG to examine the potency and kinetics of block using the compound series. Figure 6.7 shows representative WT hERG currents before (control) and during application of the two largest molecules, L6T0 and L3T4. The time courses of block are shown in figure 6.8. Results show that the onset of block for all the drugs is much quicker than E-4031 and lower concentrations are required to produce equivalent current inhibition. The speed of this onset is quick, a large majority of the inhibition occurred during the initial pulses, much like that seen

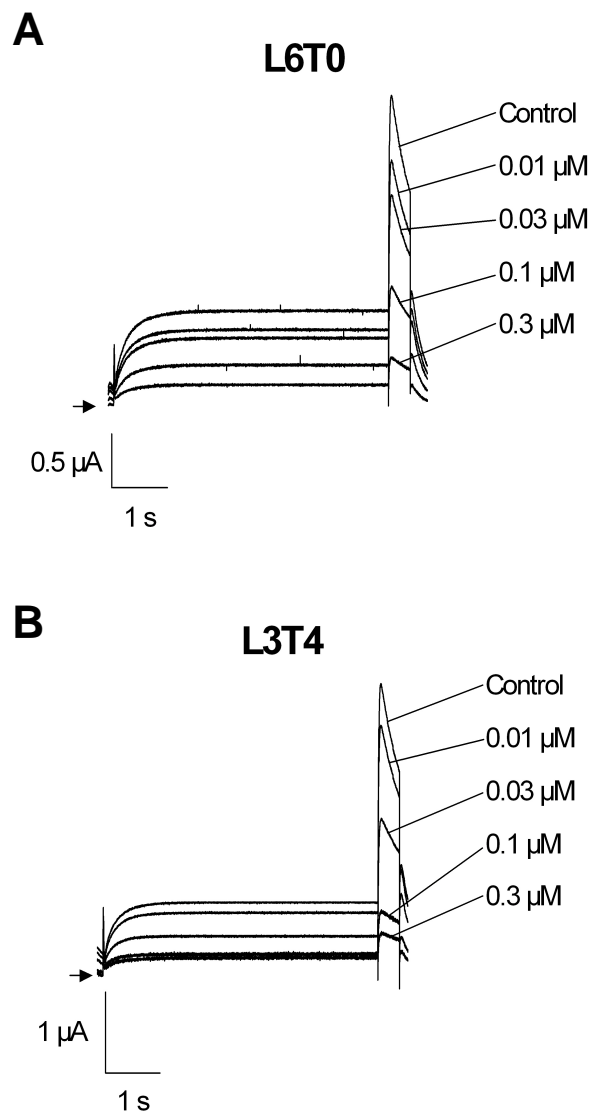


Figure 6.7: L6T0 and L3T4 are potent inhibitors of hERG channels. **A-B**, Representative currents were recorded in absence of drug (control) and after achieving steady-state block with the indicated concentrations.

with propafenone (figure 6.7-9). The inhibition of the channels occurs when it is open, as recovery from inhibition was observed during the interval when the pulsing had stopped, solution flow was being changed and pulsing was resumed (figure 6.8- 9). This suggests that the inhibition by these compounds is highly state dependent.

Figure 6.10 shows the mean concentration-response relationships for inhibition of hERG by the E-4031 derivatives. Data were analysed and fitted with a Hill function as described in the material and methods. There is a trend for the longer molecules to have a higher potency (figure 6.11 and table 6.2). However, this trend does not follow an obvious pattern with the results seen. The linker extended molecules show a decrease and then increase in potency as the length of the linker increases. While the tail extended molecules show an increase in potency up until the longest molecule, where there is a decrease in potency. This is summarised in figure 6.11, this is a plot of approximate carbon length against the mean  $IC_{50}$ . The length of the molecule was estimated by the number of bonds from one end to other end. The increase in potency could be due to an increase in the hydrophobicity of the drug, which follows the increasing length. But as the potency increase does not directly correlate with length, it would indicate that there could be other interactions that could be occurring.

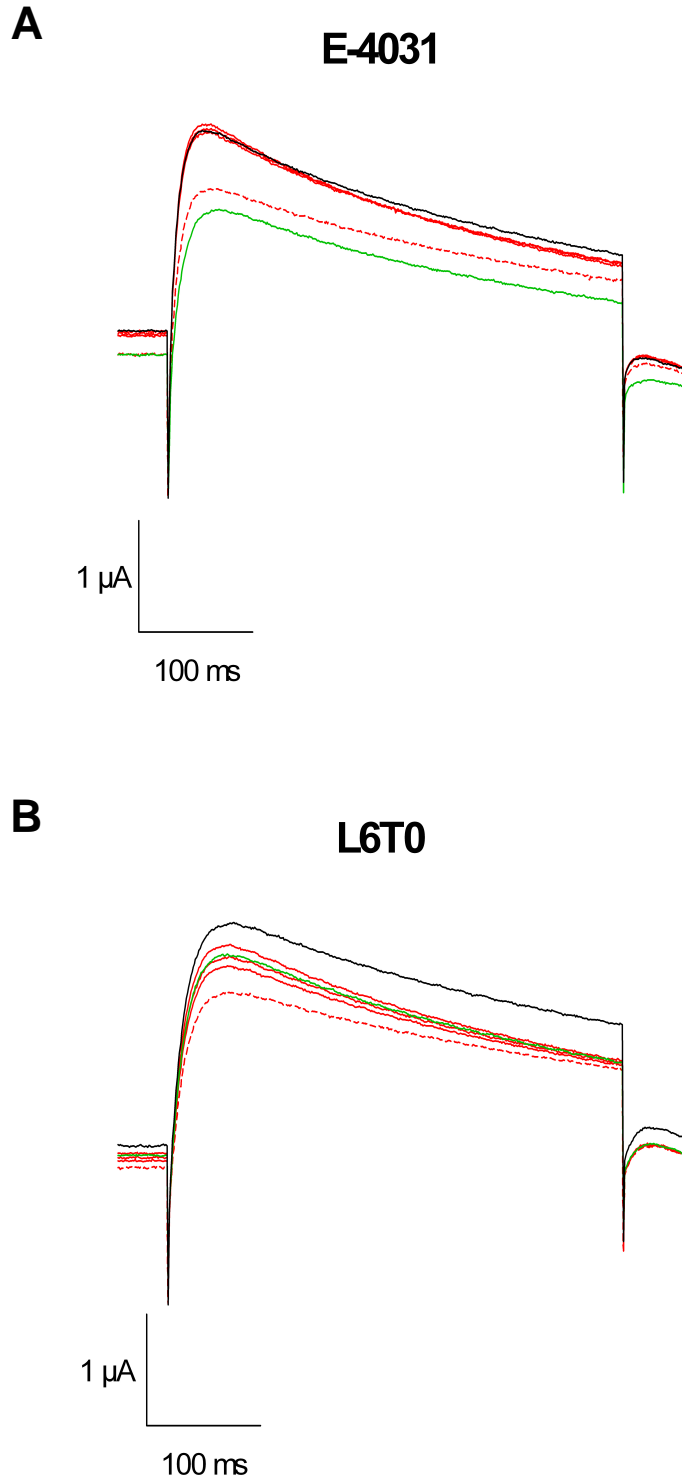


Figure 6.8: E-4031 derivatives block the open channel quickly, but recover when the channels are closed. Representative tail currents displaying hERG channel inhibition time course in the presence of E-4031 (**A**) or L6T0 (**B**) (red and green). The control trace in absence of compound is in black. The first three pulses in presence of 0.3  $\mu\text{M}$  E-4031 or 0.01  $\mu\text{M}$  L6T0 are shown as red solid lines; the dashed line represents the trace when steady state block is achieved. When the pulsing was resumed after a 2 minute pause, recovery is seen in presence of 0.03  $\mu\text{M}$  L6T0 (green trace), but not with 0.3  $\mu\text{M}$  E-4031 (Arrows indicate zero current line)

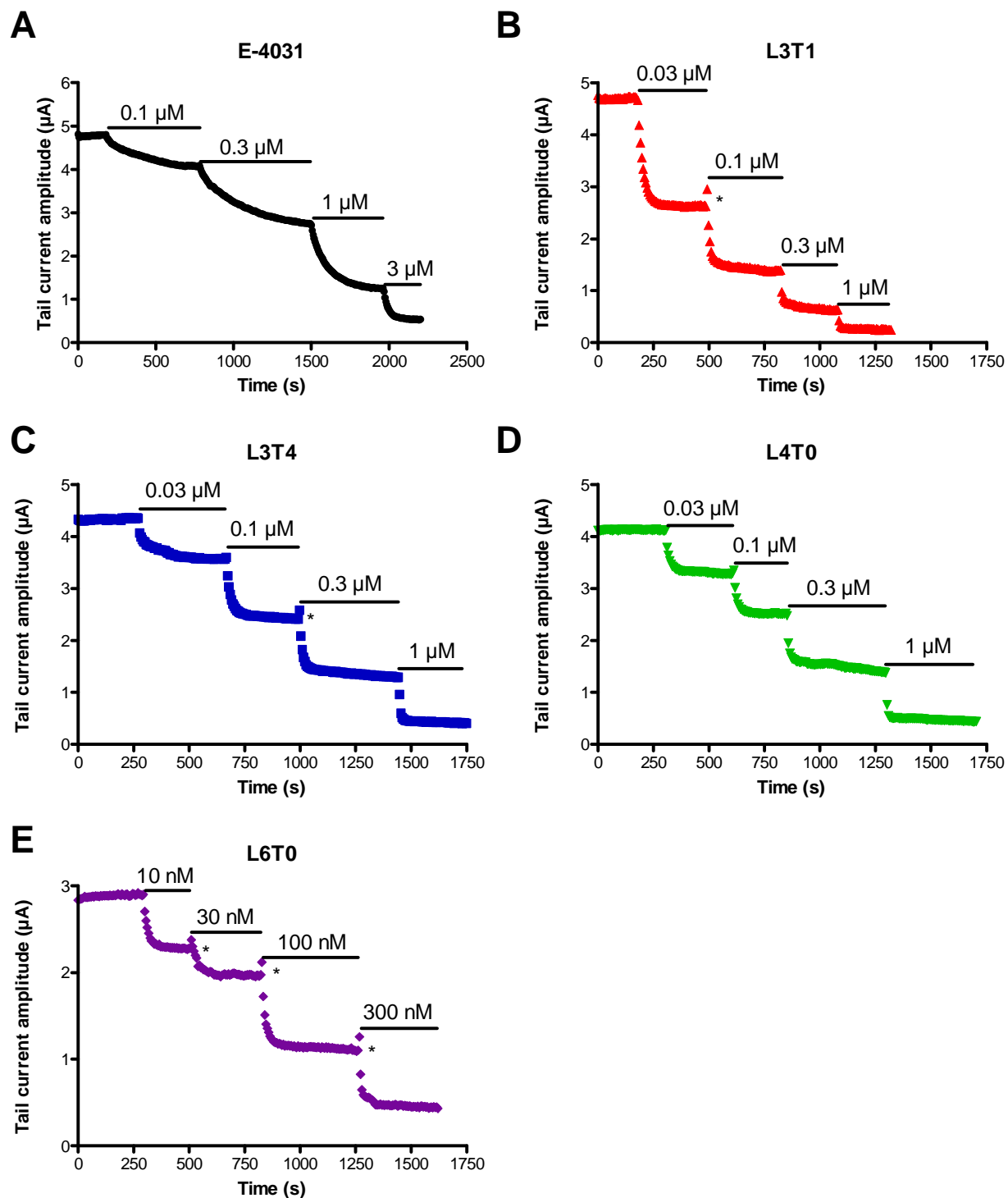


Figure 6.9: E-4031 derivatives have a fast onset of block compared to E-4031. Representative plots of the peak tail current amplitudes against time when exposed to cumulative concentrations of compound. Examples are shown for the longest and the shortest derivatives only. The amplitudes of the tails decrease in a concentration dependent fashion. Note the different time scale for E-4031 compared to the derivatives. The two minute interval when pulsing was stopped and solution was switched has been omitted from these plots. \* indicate the recovery from block when the pulsing was stopped.

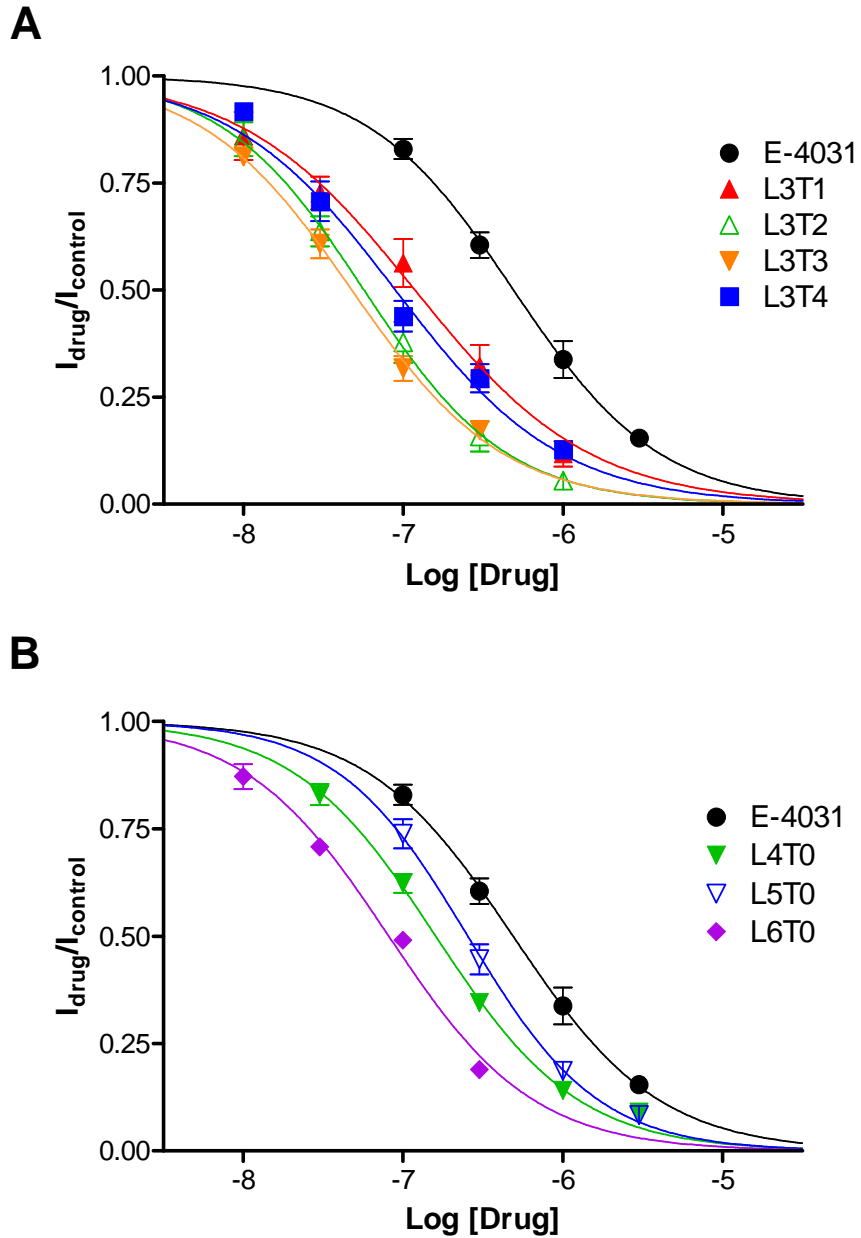


Figure 6.10: E-4031 derivatives all have higher potency than E-4031. Mean concentration-response relationships for inhibition of hERG tail currents by E-4031 and tail (A) and linker (B) extended derivatives. The points are fitted with a Hill function (solid line).  $n=5-9$

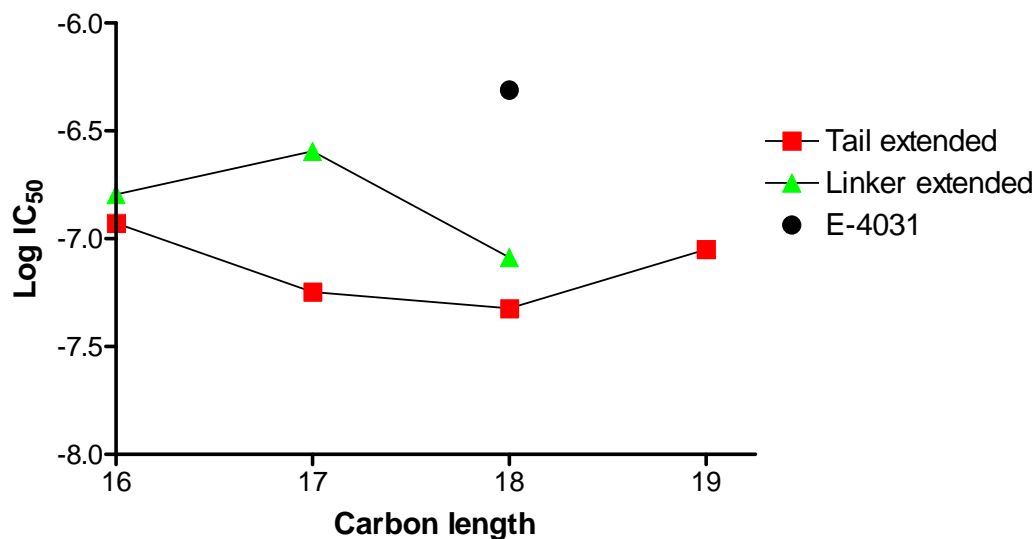


Figure 6.11: IC<sub>50</sub> of the derivatives varies with molecular length. The mean IC<sub>50</sub> of the derivatives was compared against an estimation of their length. The IC<sub>50</sub> of E-4031 is shown as a comparison. (n=5-9)

Drug	IC <sub>50</sub>	Hill slope	
E-4031	532.5 ± 1.1 nM	-1.00 ± 0.05	n=6
L3T1	125.6 ± 1.2 nM	-0.84 ± 0.10	n=7
L3T2	56.8 ± 1.1 nM	-1.01 ± 0.11	n=7
L3T3	47.5 ± 1.2 nM	-0.95 ± 0.14	n=9
L3T4	94.6 ± 1.3 nM	-0.89 ± 0.22	n=9
L4T0	159.1 ± 1.1 nM	-1.02 ± 0.09	n=7
L5T0	251.4 ± 1.1 nM	-1.10 ± 0.06	n=8
L6T0	81.3 ± 1.2 nM	-0.98 ± 0.15	n=7

Table 6.2: Comparisons of the IC<sub>50</sub> and slope values of E-4031 derivatives. Concentration-response experiments were carried out on WT hERG channels. The data are presented as means and S.E.M.

### ***Kinetics of drug block***

Once we had looked at the potency of the compounds, a more in depth study of the kinetics of drug block was performed to further characterise the inhibition. The longest (L3T4 and L6T0) and the shortest drug molecules (L3T1 and L4T0) were chosen for most of these studies as these would give the overall trend in kinetics. The initial focus of the study was to see if there was a difference between the derivatives in the rates for onset of block.

The kinetics of onset were studied using a single depolarising pulse for 60 s at -30, 0 and +30 mV. First a control recording was carried out and then a

recording with drug present was taken. An approximate 10 times  $IC_{50}$  concentration (1  $\mu$ M L3T1, L3T4 and L6T0) of the drug was perfused, this concentration was chosen to get close to maximum block, and so slight changes in concentration were negligible. The percentage inhibition was calculated by taking the ratios of the current blocked in presence and absence of drug. The degree of block was plotted against time and fitted with a single exponential to get a time course for block (figure 6.12).

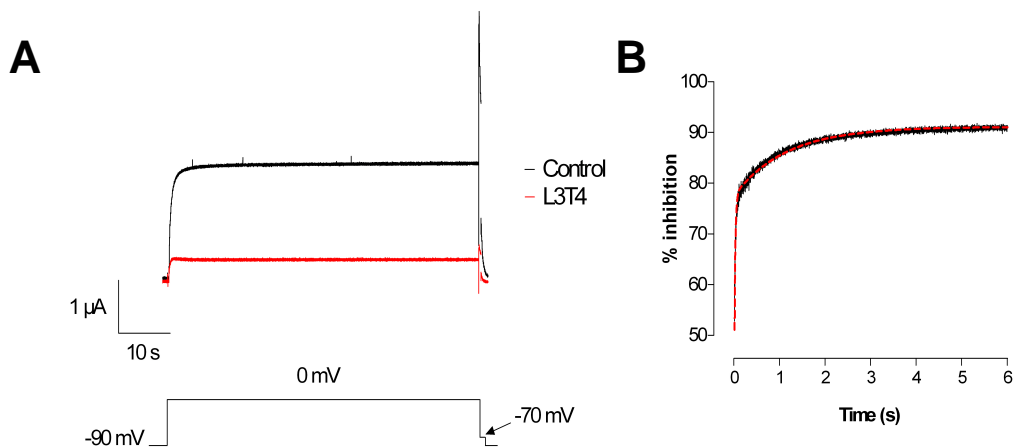


Figure 6.12: Time dependence of onset of WT hERG drug block. **A**, Representative trace of WT hERG in absence and presence of L3T4. The cell was depolarised to 0 mV for 60 s from a holding potential of -90 mV and tails recorded at -70 mV for 400 ms. **B**, The percentage of block was calculated as  $(100 \times (\text{Control} - \text{drug}) / \text{Control})$  and plotted against time, a single exponential was then fitted to get the time constant for the block of hERG current.

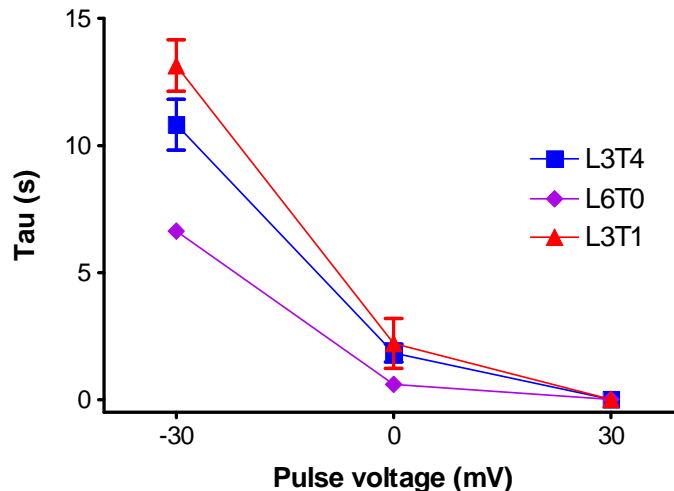


Figure 6.13: The voltage dependence of drug block. The time constants of block at -30, 0 and +30 mV were plotted against voltage. The rate of onset increases with voltage consistent with increased open probability. L3T1 n=5, L3T4 n=6 for L6T0 n=3

The onset of block kinetics displays voltage dependence (figure 6.13). As the membrane potential becomes more positive, the onset of block becomes more rapid. This is likely to be due to corresponding increases in channel activation and open probability. At more positive potentials there may also be more favourable electrostatic forces on the positively charged molecule as it moves across the membrane electric field into the inner cavity. The onset of block is fast, with a tau value from  $13.1 \pm 1.0$  s (L3T1) when depolarised at  $-30$  mV to  $0.01 \pm 0.001$  s at  $+30$  mV. The fast on rates could go some way to explain why the derivatives have a high potency.

There was not a statistical difference in the speed of onset of block between the short L3T1 and long L3T4 drug molecule. L3T4 had a slightly faster rate of onset. L6T0 was found to have a higher rate of block than L3T1 and L3T4, which is consistent with its higher potency.

It was noted during the concentration-response experiments that the current inhibition by the derivatives was decreased when the pulsing was stopped (figures 6.8-9), despite the continued presence of the blockers. This recovery from block indicated that the derivatives might not be trapped. This was an unexpected finding that was never observed with E-4031. We therefore carried out a detailed investigation into the voltage and time dependence of recovery when in the mostly closed state. To study this, the holding potential was set at either  $-120$ ,  $-90$  or  $-60$  mV to observe the affect it had on the recovery. To get an indication of the inhibition, a short pulse protocol was used. 50 ms pulses to  $+40$  mV followed by a step to  $-70$  mV for another 50 ms, this was repeated every 10 s. The length of the test pulse was chosen as it

opens the channels for a short enough time to measure current, but without time for much onset of block (figure 6.14).

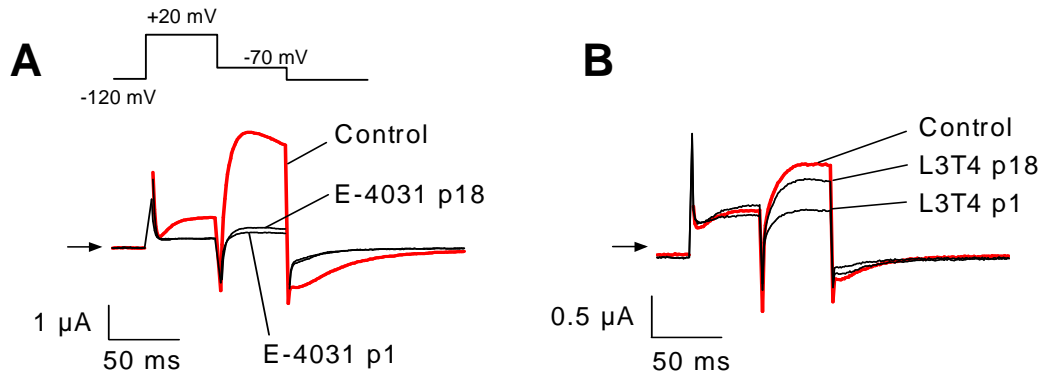


Figure 6.14: L3T4 exhibits rapid recovery from block of WT hERG. **A, B.** Representative WT hERG currents in absence of blockers (control) and during perfusion with either 5  $\mu$ M E-4031 (**A**) or 1  $\mu$ M L3T4 (**B**). Recovery from block was monitored with short (50 ms) depolarisations to +40 mV (to minimise open state block) from a holding potential of -120 mV. Tail currents were recorded at -70 mV for 50 ms. p1 and p18 refer to the first and eighteenth pulse respectively after attaining steady state block with 5 s depolarisations to 0 mV. (Arrows indicate zero current).

First, recordings of the short protocol were carried out as a control, then a 10 times  $IC_{50}$  concentration was introduced and steady state block was attained with repetitive application of 5 s pulses to 0 mV as per the concentration-response experiments. The recordings of the short protocol were then carried out again to observe the recovery at the different holding potentials. The tail current amplitudes from the recordings were measured, normalised to the control currents and plotted against time (figures 6.15A-16A). The recovery from block after 2 minutes was plotted against the holding potential (figures 6.15B-16B); this was used as an indicator of the rate of recovery from block. The results show that after 2 minutes, the E-4031 derivatives display a recovery from block which is voltage dependent. The recovery rate increases as the voltage becomes more negative. The recovery from block at -60 mV is much lower than at the other potentials; this may be due to increase in the

open probability at this potential allowing re-onset of block. The shorter compounds also recover from block at a slower rate than the longer ones, this maybe due to the size allowing for better retention in the cavity. Comparing this to E-4031, the results are consistent with the drug being trapped in the channel, it does not display recovery except at -60 mV. Again, this may be due to the increase in open probability allowing for the drug to escape. The

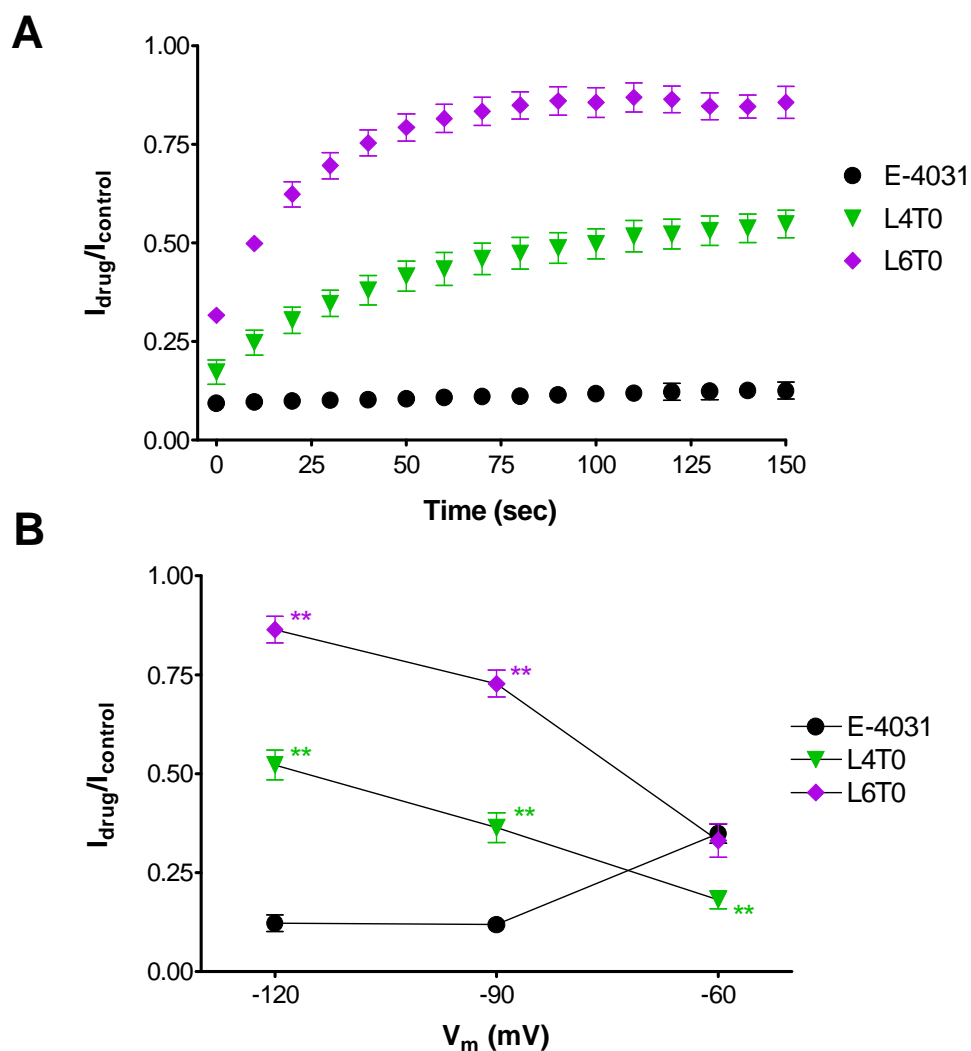


Figure 6.15: E-4031 derivatives show a rapid and voltage dependent recovery from block. **A** Peak tail current amplitudes in presence of linker modified compounds (1  $\mu$ M L6T0, 2  $\mu$ M L4T0) or 5  $\mu$ M E-4031 were normalised against control currents and plotted against time, the holding potential was set at  $-120$  mV. **B**, Mean normalised peak tail current amplitudes after 2 min of pulsing plotted against holding potential. The derivatives recover quickly even in presence of compound and at negative holding potentials, indicating neither of the drugs are trapped in the channel. In contrast, E-4031 recovery from block is slow, except at  $-60$  mV.  $n=3$  for E-4031,  $n=5-6$  for L4T0 and L6T0. \*\* indicates  $p<0.01$

results indicate that the derivatives do not display a drug trapping phenotype, as the compounds recover when the channels enter a mostly closed state, even with the compounds present. The compounds therefore favour binding to the open state compared to the closed state.

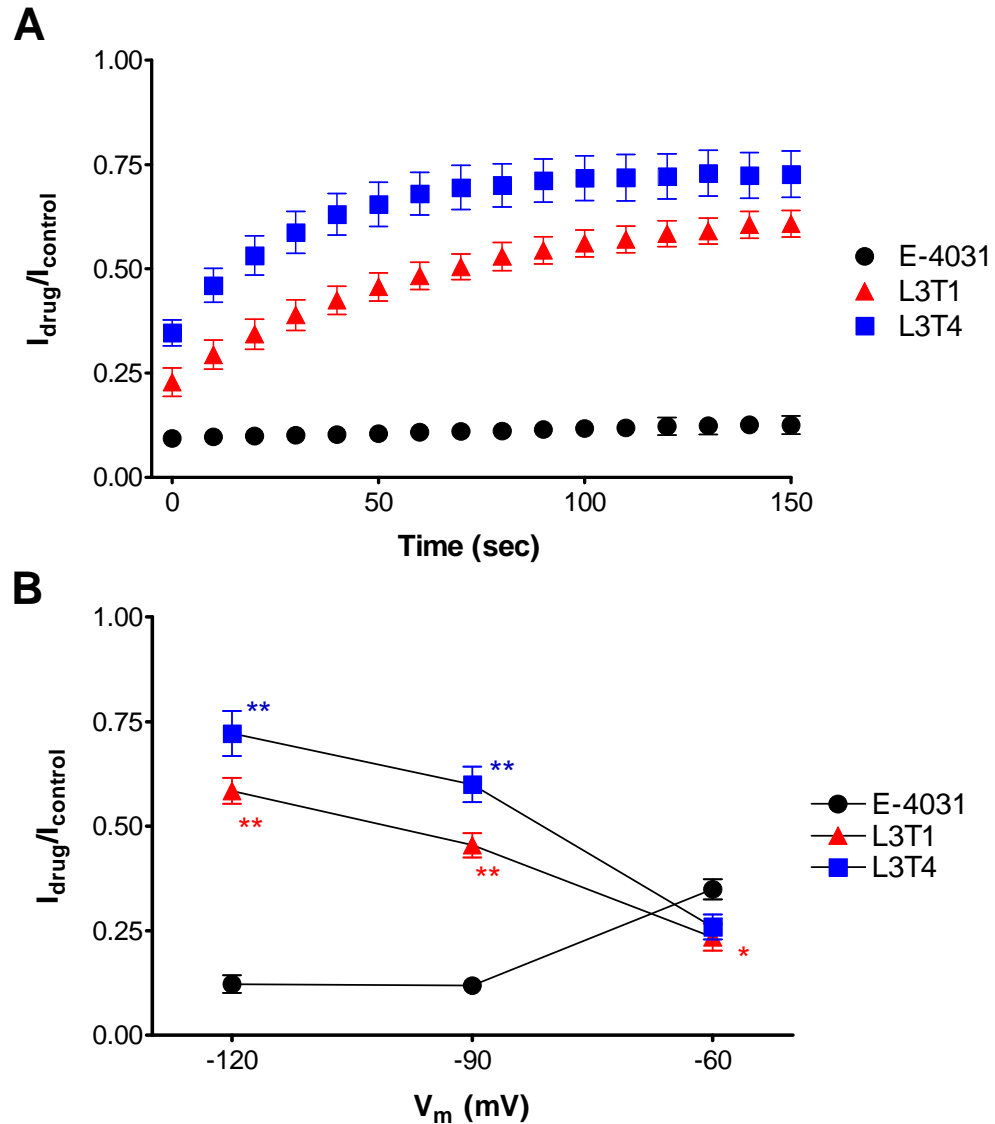


Figure 6.16: E-4031 derivatives show a rapid and voltage dependent recovery from block. The results were analysed as in figure 6.15. **A**, Peak tail current amplitudes in presence of the tail extended compounds (1  $\mu$ M L3T1 or L3T4) and plotted against time, with the holding potential at -120 mV. **B**, Mean normalised tail current amplitudes after 2 mins of recording  $n=3$  for E-4031,  $n=6-7$  for L3T1 and L3T4. \*\* indicates  $p<0.01$

### ***Do the derivatives exhibit a foot in the door phenotype?***

From the present results, the E-4031 derivatives have high potency for WT hERG, but it is highly state dependent. The derivatives bind well to the open state of the channel, but on closure, the compound is able to unbind from the channel. This would indicate that the compounds are not trapped.

Therefore, experiments were carried out to see if the drugs display a different phenotype of block, foot in the door. This type of block displays rapid recovery from block. This is due to the compounds inability to be trapped, so the closure of the channel is delayed by the presence of the compound. As explained in the introduction, the delay in the closure causes an apparent slowing of the deactivation.

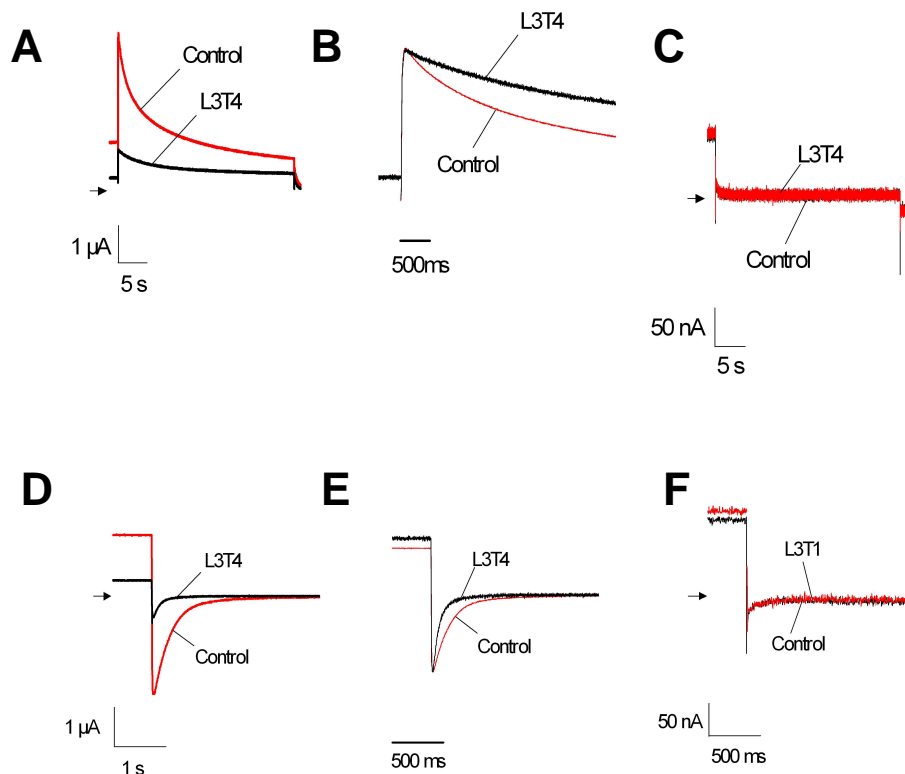


Figure 6.17: Recovery from block does not occur as channels deactivate. **A-F**, Representative traces of tail currents at -60 mV (**A-C**) or -120 mV (**D-F**) following a 5 s step to 0 mV. **A, D**, Representative WT hERG currents before and after reaching steady state inhibition by 1  $\mu$ M L3T4. **B, E**, Tail currents have been normalised to peak control amplitudes to display differences in time course. **C, F**, Current traces in DEPC H<sub>2</sub>O injected cells under the same recording conditions (Arrows indicates the zero current line)

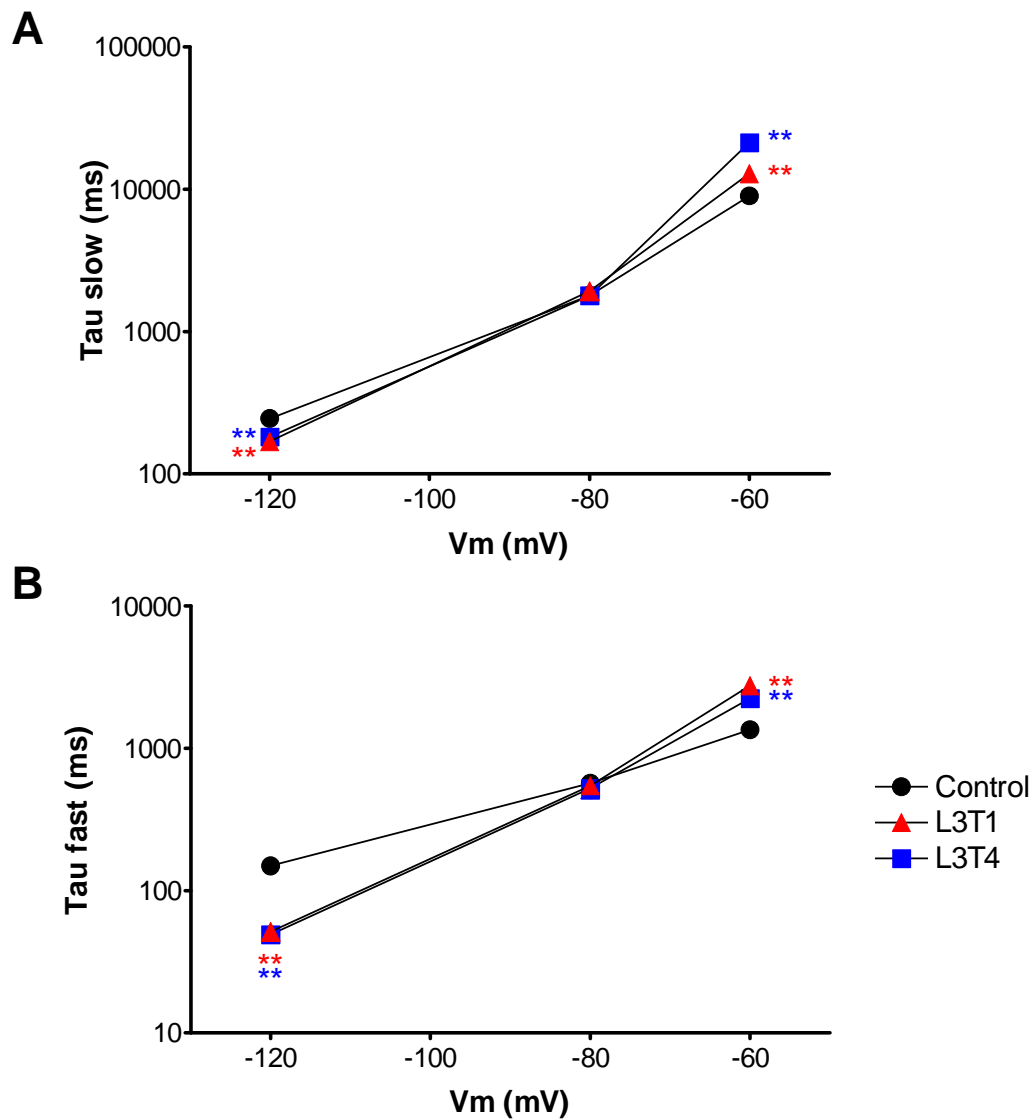


Figure 6.18: Slow (A) and fast (B) time constants for WT hERG deactivation in control solution and following block by either L3T1 or L3T4. Deactivating tails were measured at -120, -80 or -60 mV and fitted with a double exponential curve to obtain the time constants. The error bars present are not seen due to them being obscured by their small size n=4.

To test if the channels could only close once the E-4031 derivatives unbound, the kinetics of the deactivating tails were investigated. This used a protocol much like the fully activated tail protocol, the membrane potential was stepped from a holding potential of -90 mV to 0 mV for 30 s and then repolarised to either -60, -80 or -120 mV for another 30 s (figure 6.17). A brief 50 ms pulse

to -60, -80 or -120 mV at the start of the protocols was used to estimate the leak current in order for leak subtraction to be carried out. The tail currents were analysed to see if the compound slows deactivation, which would be an indication of foot in the door binding. Recordings were also made using DEPC H<sub>2</sub>O injected cells as a control, these recordings would show if there were any endogenous currents present that may introduce artefacts to the results. The tail currents were leak subtracted and then normalised to the peak control current and fitted with a double exponential in order to get the time constants for deactivation.

At -60 mV, the rate of deactivation is slower compared to the control (figure 6.18), but at -120 mV values there is an increase in the closure rate indicating that the derivatives interfere with closure of the channel. The longer drug appears to have a slightly greater affect on the closure of the channels. From these results, it is hard to say that there is a foot in the door phenotype, as the deactivation would be slowed at all potentials; which is not the case in these experiments. The data from the deactivation at -80 and -120 mV suggests that the channel is able to close with the compounds present. As the recovery from drug block is relatively fast, these experiments do not clearly explain how the closure can cause the recovery from drug block.

If the channels are unable to deactivate until the compound has unbound, then a mutation that accelerates channel deactivation should cause faster recovery from block and the effects on the apparent deactivation should be clearer, as the drug may interfere with deactivating channel. Therefore we investigated block of N-truncated hERG channels, a hERG channel with accelerated deactivation.

Drug	WT hERG		NTK hERG	
	L3T1	L3T4	L3T1	L3T4
IC <sub>50</sub>	125 ± 1.2 nM	94.6 ± 1.3 nM	60.9 ± 1.1 nM	50.6 ± 1.1 nM
Hill slope	-0.84 ± 0.10	-0.89 ± 0.22	-0.87 ± 0.08	-0.83 ± 0.08
	n=7	n=9	n=7	n=8

Table 6.3: Derivatives inhibit NTK channels more potently. Concentration-response experiments were carried out on NTK hERG channels Mean and S.E.M. data are presented here.  $p > 0.05$  therefore there was no significant difference

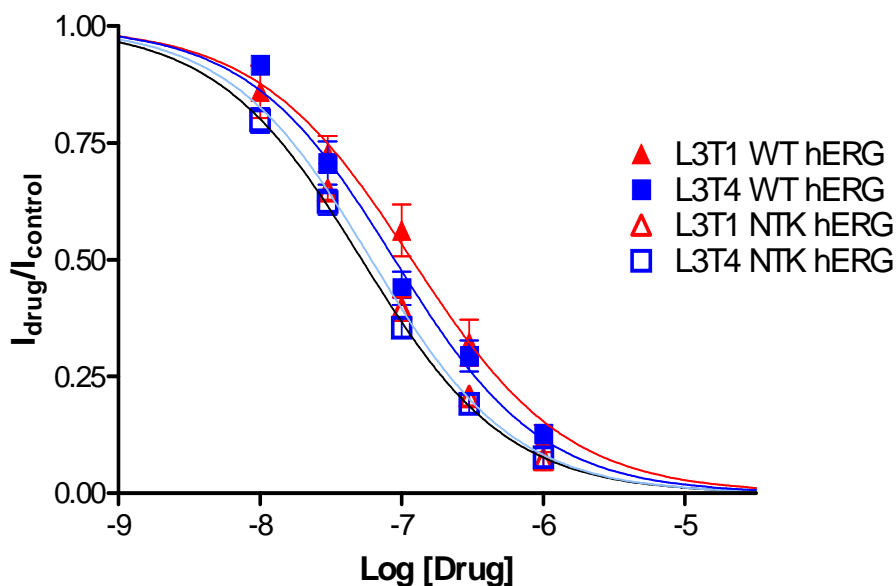


Figure 6.19: Mean concentration-response relationships of L3T1 and L3T4 inhibition of NTK hERG. Experiments were performed and analysed as described previously. Mean data were fit with a Hill function (solid line).  $n=7$

First, concentration-response experiments were carried out to determine the IC<sub>50</sub> of L3T1 and L3T4 compounds (figure 6.19). The results showed that the compounds were more potent inhibitors of NTK hERG than WT hERG currents. (See table 6.3). This increase in potency is a similar to results seen in chapter 4, where propafenone was used block NTK channels.

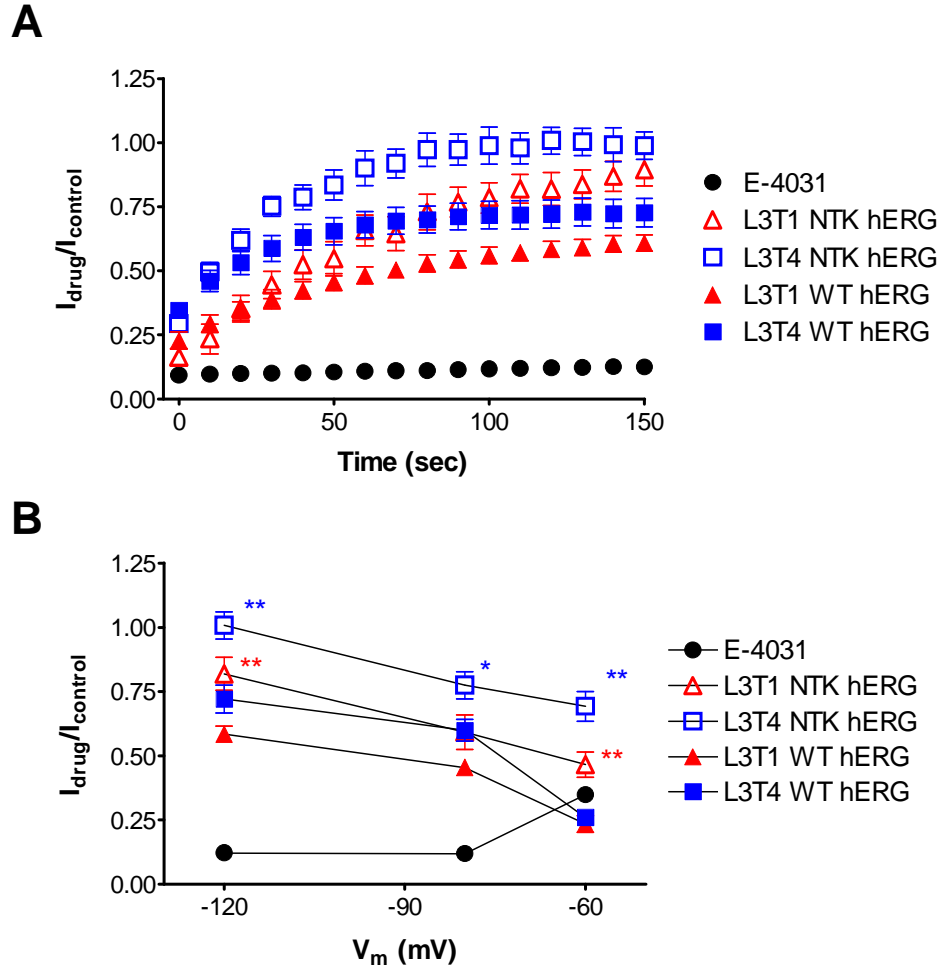


Figure 6.20: Recovery from block by E-4031 derivatives is faster for NTK hERG. The results were analysed as in figure 6.15. A, Peak tail currents in presence of the tail extended compounds (1  $\mu$ M L3T1 or L3T4) and plotted against time, with the holding potential set at -120 mV. B, Mean normalised tail current amplitudes after 2 mins of recording n=3 for E-4031, n=6-7 for L3T1 and L3T4. \* indicates  $p < 0.05$ , \*\* indicates  $p < 0.01$  compared to the WT hERG channel.

Using the  $10\times IC_{50}$  from the concentration-response experiments, the recovery from block experiments were repeated using the NTK hERG channels to see if the faster deactivating channel would trap the drugs. After achieving steady state block, the channels recovered quickly from inhibition (figure 6.20A). Compared to the WT hERG channels, the NTK hERG channels recovered to a greater degree (figure 6.20B), After two minutes held

at -120 mV, there was ~80% and ~100% recovery with L3T1 and L3T4 respectively. The recovery at -60 mV was greater in NTK hERG channels than in WT hERG, recovering from L3T1 inhibition by ~50% compared to ~30% respectively. This again reaffirms that the drugs are not trapped in the channel.

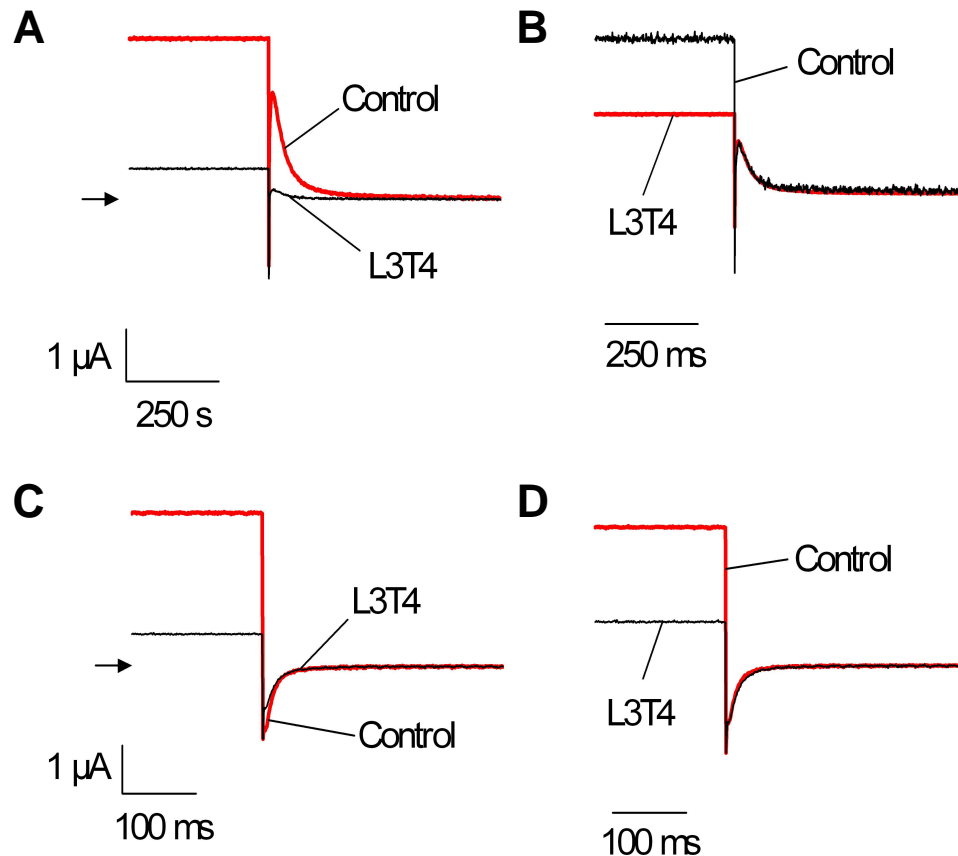


Figure 6.21: NTK hERG channels do not display a foot in the door phenotype. **A-D**, Representative traces of tail currents at -60 mV (**A, B**) and -120 mV (**C, D**). **A, C**, Representative NTK currents before and after reaching steady state block by 1 μM L3T4. **B, D**, Tail currents before and after block have been normalised to peak current amplitudes to display differences in time course. (Arrows indicate zero current)

The derivatives were next investigated to see if they displayed a foot in the door characteristic with the mutant channel (figure 6.21). The deactivation of the channel was examined to see if there was a slowing by the presence of the drug, a phenotype of foot in the door block. The tail currents show that in

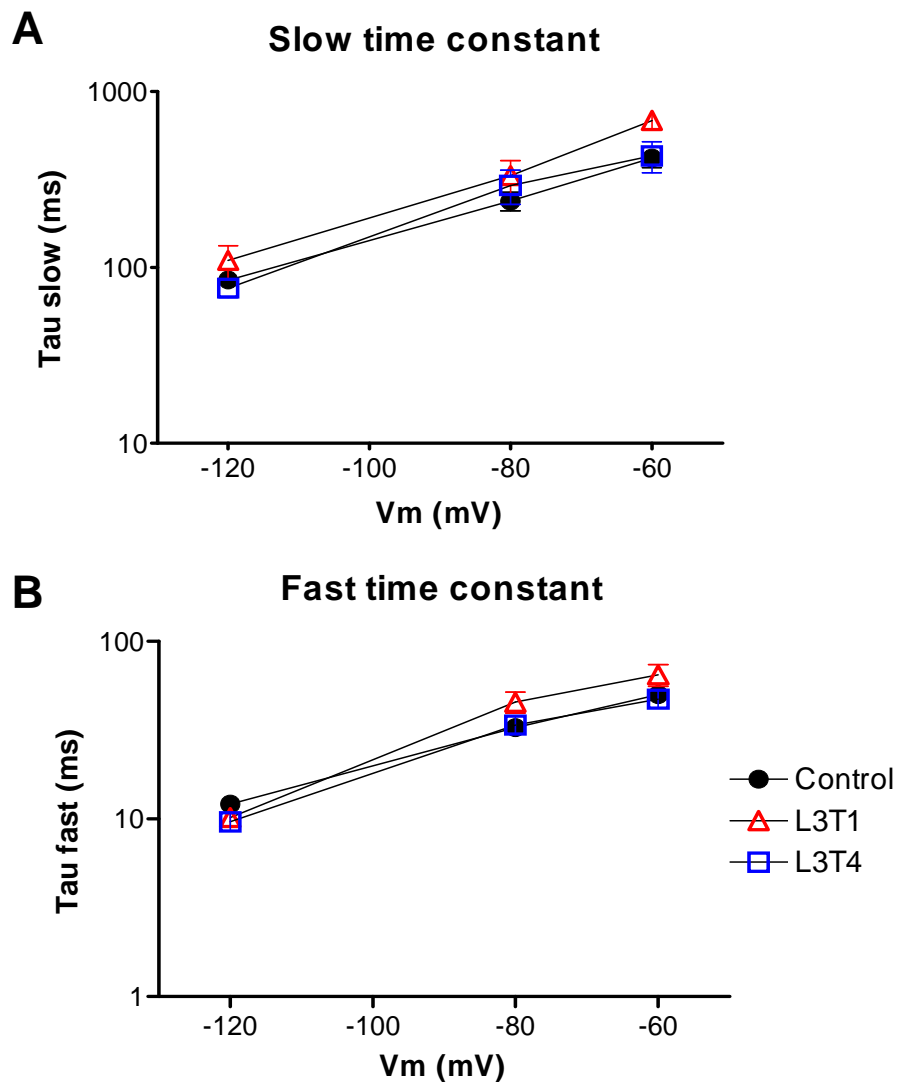


Figure 6.22: The derivatives do not slow the deactivation of the NTK hERG tail currents. Slow (A) and fast (B) time constants of NTK deactivation in control solution or in presence of L3T1 and L3T4. n=5-7.

presence of L3T1 there was a slight slowing of the deactivation at -60, -120 mV, but not at -80 mV (figure 6.22); this difference was not significantly different from the control currents. L3T4, however, did not show any slowing to the deactivation at any of the membrane potentials. It did show a slight increase in the deactivation rate at -120 mV, much like that seen in the WT hERG channels; but this was not significant from the control. The lack of

evidence of drug trapping and slowing of deactivation by the derivatives indicates that the drug is able to recover from block when the channels have entered a non conducting state.

### **Pharmacology of hERG channel mutants**

So far it has been assumed that the drugs bind to the inner cavity of the channel. However, the rapid kinetics of onset and recovery from block raised the possibility these compounds bind to a different site from E-4031. To test this hypothesis we investigated the impact of mutations of inner cavity residues on compound potency. A series of concentration-response experiments were carried out on these mutants. The mutants were chosen for this study due to their orientation (they face into the inner cavity) and their importance in altering drug potency in previous drug binding studies (Lees-Miller *et al.*, 2000; Perry *et al.*, 2004; Witchel *et al.*, 2004; Kamiya *et al.*, 2006).

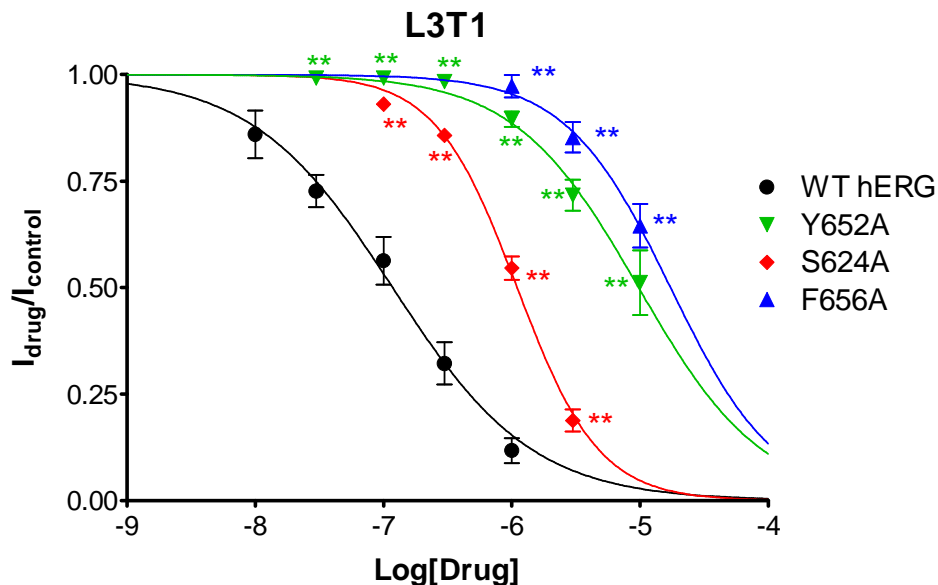


Figure 6.23: Phe656 and Tyr652 are critical drug binding site residue. Mean concentration-response relationships of mutant channels when blocked by L3T1. The experiments were performed and analysed as described previously.  $n=6-9$ . \*\* indicates  $p<0.01$  when compared to WT hERG.

Mutant	IC <sub>50</sub>	Hill slope	
WT hERG	0.13 ± 0.02 μM	-0.89 ± 0.22	n=8
Y652A	9.4 ± 1.9 μM **	-1.03 ± 0.15	n=5
S624A	1.1 ± 0.1 μM **	-1.38 ± 0.17 **	n=6
F656A	16.9 ± 3.5 μM **	-1.20 ± 0.26 **	n=5

Table 6.4: Comparisons of WT hERG and mutant channels blocked by L3T1. The data are displayed in mean and SEM form. \*\* indicates significant difference from WT hERG, with a p<0.01.

Three residues (F656A, Y652A and S624A) that have important implications to drug binding were studied when blocked by L3T1 and L3T4. The concentration-response experiments on the mutant channels were carried out as described previously, the mutations affect on the IC<sub>50</sub> and slope were analysed (table 6.4-5, figure 6.23-24).

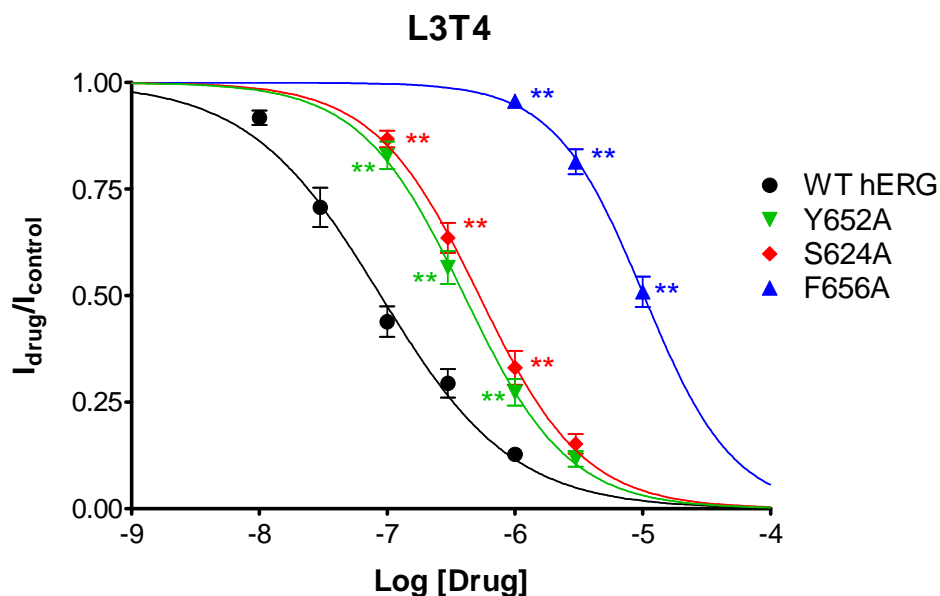


Figure 6.24: F656 is the critical drug binding site residue. Concentration-response relationships of mutant channels when blocked by L3T4. n=5-7. \*\* indicates p<0.01 compared to WT hERG.

It can be seen that the three mutations cause a loss in potency, mutating the residues Phe656 and Tyr652 to an alanine, causes a shift in IC<sub>50</sub> of over two log units (table 6.4, figure 6.23). S624A causes a smaller loss of potency, shifting the IC<sub>50</sub> by less than a log unit. The Hill slope for the S624A and F656A mutants were much steeper than that of the WT channel, this could

indicate there is some co-operative binding involved. The slope of F656A could be steeper as the data points do not cover the full curve, however, at higher concentrations the compound came out of solution.

The potency of L3T4 for the mutants differed from that of L3T1 (figure 6.24, table 6.5), the F656A mutant reduced the potency by 2 log units, but Y652A and S624A mutants resulted in less than 1 log unit reduction in potency. This suggests that the binding of these compounds differs, with L3T4 binding more strongly to the lower part of the cavity. The F656A again displays a steeper Hill slope, but this was again fitting a curve through points that cover only part of the curve.

Mutant	IC <sub>50</sub>	Hill slope	
WT hERG	0.09 ± 0.02 μM	-0.84 ± 0.22	n=10
Y652A	0.40 ± 0.04 μM **	-1.11 ± 0.10	n=5
S624A	0.53 ± 0.08 μM **	-1.08 ± 0.19	n=6
F656A	10.4 ± 1.0 μM **	-1.29 ± 0.15 **	n=5

Table 6.5: Comparisons of L3T4 blockade of WT hERG and mutant channels. The data are displayed in mean and SEM form. \*\* indicates  $p < 0.01$ .

What is apparent is that the Phe656 residue is important to the binding of the tail extended derivatives and that the derivatives do not bind in exactly the same fashion. To further investigate the residues important to binding, other mutant channels and the linker extended drugs were used. These would give further indication as to whether there were any other residues further down the cavity that were important to the derivatives binding and the differences in their importance for particular derivatives. In this case, the ten times IC<sub>50</sub> of the derivatives acting on wildtype channels were perfused on. (figure 6.25).

The results indicate that F656 is the main amino acid that is important to bind in all the drugs studied. Y652 also appears to be important in L3T1, L4T0 and L6T0 binding, mutation to an alanine causing the degree of block to drop to below 50% compared to approximately 85% block achieved when blocking

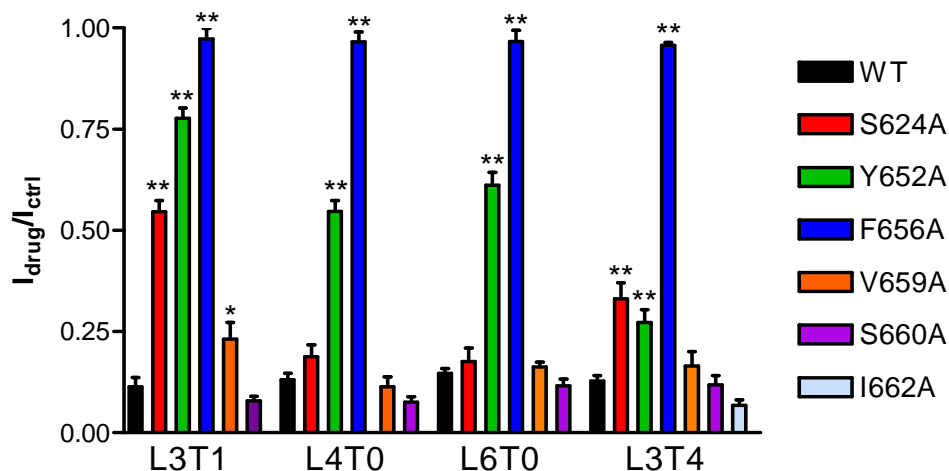


Figure 6.25: Further mutants of the hERG channel do not affect the drug binding. 10x IC<sub>50</sub> concentrations were used to analyse any change in the inhibition that mutations can cause. It seems that F656A and Y652A had any large affects to the inhibition by the drugs. n=5-8. \* indicates p<0.05, \*\* p<0.01 relative to WT hERG.

WT channels. L3T4 binding was not greatly affected by the mutation, as indicated by the concentration-response experiments before. The S624A mutation reduces L3T1 and L3T4 binding to approximately 45% and 70% respectively, while with the L4T0 and L6T0 binding does not significantly reduce the binding. Residues studied that line the lower part of the inner cavity, when mutated do not seem to have any affect on the binding of the drugs. Therefore the drugs mainly bind to F656 and in some cases Y652 and S624.

	WT	S624A	Y652A	F656A	V659A	S660A	I662A
L3T1	11.4 ± 2.3 % n=5	54.6 ± 2.8 % n=8**	77.7 ± 2.5 % n=7**	97.3 ± 2.7 % n=9**	23.1 ± 4.2 % n=5*	7.9 ± 1.1 % n=6	n.d.
L3T4	12.7 ± 1.4 % n=5	33.0 ± 4.0 % n=6**	11.7 ± 1.8 % n=5**	95.7 ± 0.7 % n=5**	16.5 ± 3.6 % n=5	11.8 ± 2.4 % n=6	6.7 ± 1.3 % n=5
L4T0	13.1 ± 1.5 % n=6	18.8 ± 2.9 % n=6	54.6 ± 2.7 % n=5**	96.5 ± 2.4 % n=5**	11.3 ± 2.5 % n=5	7.5 ± 1.3 % n=6	n.d.
L6T0	14.7 ± 1.2 % n=6	17.6 ± 3.3 % n=5	61.2 ± 3.2 % n=6**	96.6 ± 2.8 % n=6**	16.3 ± 1.2 % n=5	11.6 ± 1.6 % n=5	n.d.

Table 6.6: Comparisons of WT hERG and mutant channels blocked by 10x IC<sub>50</sub> concentrations. The percentage of the original currents is expressed as means and S.E.M. \* indicates p<0.05, \*\* indicates p<0.01 compared to WT hERG.

## Discussion

In this chapter we have used a set of derivatives of E-4031 to inhibit WT hERG channels in order to investigate the binding phenotype. Using this, it was hoped that the size of the inner cavity of the channel could be measured. From the experiments, it can be seen that small modifications in compound structure can have a profound affect on the binding of the molecules to the channel. This was first seen when examining the E-4031-A1 compound with the significant loss in potency. Investigations into further derivatives of E-4031 displayed an altered binding phenotype, they display high state dependence, with fast binding kinetics. The derivatives also display an unusual recovery from block that is not seen in previously published data.

### ***The methanesulphonamide intermediates have lower potency***

The first set of intermediates with the methanesulphonamide group displayed a lower potency to the WT hERG channel. The shorter molecules may have reduced potency through a decrease in hydrophobic interactions with amino acid residues in the channel, such as the F656 or V659 (Kamiya *et al.*, 2001; Fernandez *et al.*, 2004). These data would fit the pharmacophore model proposed by Cavalli *et al.* (2002), where they model an increase in potency with increased length of molecule.

The E-4031 A1 drug molecule that has the hydroxyl group replaced by a carbonyl group has an IC<sub>50</sub> which is 2 log units of concentration lower than with E-4031. This had not been predicted from in silico modelling of the drug binding to a homology model of WT hERG based on the closed KcsA, open MthK and KvAP channels (Doyle *et al.*, 1998; Jiang *et al.*, 2002; Jiang *et al.*,

2003; Kuo *et al.*, 2003) (Data not shown). The reason for the drop in potency could be due to the alteration of the electrostatic nature of the drug. As the carbonyl group is more electronegative than the hydroxyl group. The change in potency may also be due to the change in 3D structure, as the E-4031-A1 hydroxyl group has a tetrahedral structure compared to the planar structure of the carbonyl group in E-4031. Further studies would have to be carried out in order to understand this.

### ***E-4031 derivatives bind with high affinity within the inner cavity***

When hERG channel block by the E-4031 LxTy derivatives was studied, there are a number of differences compared with E-4031. The potency of all the drugs were more potent than E-4031. Up to a point, potency became greater with increasing length. This was possibly due to stronger hydrophobic interactions between the drug and the channel. This trend was observed in other studies and is consistent with the binding pocket being hydrophobic (Armstrong, 1971; Cavalli *et al.*, 2002), as seen in figure 6.1 with the Cavalli pharmacophore. If it is assumed that the chlorine group of the derivatives is at the C0 position of the pharmacophore, and the tail is at the C2 position. The model predicts the increase in the molecular volume at the C2 centroid will increase the binding affinity. However, the interaction does not follow a strict trend, which could indicate more complex mechanisms for binding are occurring.

A trend might become more apparent if there were further extensions to the length of the molecules. As only three linker extended molecules were studied, with which it is hard to spot a trend, particularly as the potency of the drug molecule went down then up. The tail extended derivatives may also display

more of a trend, as the longest drug displayed a slight decrease in the potency compared to the next longest. Extending the molecules length further may reveal if the maximum potency for the series was reached.

### ***The drugs bind to the channel inner vestibule***

It is apparent that, as with most other hERG blockers, the derivatives bind to the inner cavity of the channel. All of the compounds were potent and had relatively similar kinetics of block; this suggests that they bind to the channel in a similar manner. As the compounds were designed with differences in the linker and tail region, these results suggest that they do not have a significant role in binding with key residues in the inner cavity.

All four compounds studied were profoundly affected by the Phe656 mutation, the F656A mutation causing a shift in  $IC_{50}$  of over 2  $\log_{10}$  units when inhibited by L3T4 and L3T1. This reduction in potency by F656A has also been reported in previously published studies (Lees-Miller *et al.*, 2000; Milnes *et al.*, 2003; Fernandez *et al.*, 2004; Kamiya *et al.*, 2006).

Tyr652 also has an influence on binding, but its role is more variable, having a less of an effect on potency than Phe656. The L3T4 derivative is much less sensitive to the Y652A mutation compared to the other derivatives. The variability in the Tyr652 contribution to hERG block is seen in previously published data, where for some compounds, the Y652A mutation does not affect the binding for instance in the case of propafenone (Witchel *et al.*, 2004) or fluvoxamine (Milnes *et al.*, 2003). Whereas in some cases it is shown to affect the binding of compounds such as chloroquinone (Sanchez-Chapula *et al.*, 2002), quinidine (Sanchez-Chapula *et al.*, 2003), clofilium and ibutilide (Perry *et al.*, 2004).

Ser624 also has a role in the binding of the compounds. This has a weaker influence, as the mutation to an alanine does not decrease the inhibition to the level of F656A or Y652A. Within the series of derivatives, the tail extended compounds require S624 to bind more than the linker extended drugs. The variable contribution to binding of S624A is seen in other studies, in some cases the Ser624 mutant causes a significant reduction in the inhibition of the channel, as is the case for clofilium and vesinarinone (Kamiya *et al.*, 2001; Perry *et al.*, 2006). In other cases the mutation causes less of a reduction, in the case of MK-499 and propafenone (Mitcheson *et al.*, 2000b; Witchel *et al.*, 2004).

From these results it indicates that the residues higher up in the cavity involved in the binding of the derivatives, as mutations of these residues to alanine cause a reduction in inhibition; whilst the residues towards the intracellular end of the cavity do not alter the binding of the derivatives appreciably.

### ***The E-4031 derivatives display an unusual phenotype of block***

While carrying out this study it was seen that the drug potency is more heavily state dependent than E-4031, all the drugs derivatives studied bound to the open channel with high potency, while disassociated with the channel closure. This can be further seen in the recovery from block experiments. This contradicts the homology models of the hERG channel, which indicated that all but the longest derivatives should have been trapped in the channel.

The onset of hERG block by E-4031 derivatives is voltage dependent and displays fast kinetics, with time constants ranging from  $13.1 \pm 1.0$  s to  $0.01 \pm 0.001$  s. As the step potential becomes more positive, the time constant of

block onset becomes faster. This can be due to increased channel activation rates and open probability, allowing the compounds greater access to the inner cavity to bind. Also the voltage becomes more positive, the positively charged compounds will have more drive to cross the electric field of the membrane, thus are more likely to enter the channel to bind. The speed of block is more like lower potency drugs such as that seen with the onset of propafenone (Witchel *et al.*, 2004).

From the experiments to investigate the recovery from block, it can be seen that the drugs are not trapped, no matter the size of the molecule. The longest E-4031 derivatives (L6T0 and L3T4) were predicted to be too long to fit in a closed state homology model of hERG (data not shown), whilst other derivatives were predicted to fit within this cavity. However, none appear to be trapped, the drug molecules appear to leave the channel relatively quickly when it enters a closed state, indicated by the increasing current as the channels become unblocked, even in presence of compound. This is completely different from E-4031 and many other compounds previously studied, which are trapped in the channel (Carmeliet, 1993; Gessner & Heinemann, 2003; Perry *et al.*, 2004; Witchel *et al.*, 2004). These studies noted that the recovery from block required the compounds to be washed off and the channels also to be mainly in the open state, before they were able to recover from inhibition. Use of a mutant of the hERG channel D540K strengthens this evidence, it opens at positive potentials much like WT hERG, but at potentials negative of -90 mV the channels start to reopen. This mutant channel is able to recover from MK-499 inhibition when it is reopened at

negative potentials, whilst WT hERG fails to recover at these potentials when it is in a closed state (Mitcheson *et al.*, 2000b).

The recovery displays voltage dependence, when the resting membrane potential is set at -120 mV, the channels recover, whilst very little recovery occurs at -60 mV. This follows the trend of open probability, at -120 mV, when the open probability is low, there is a large degree of recovery. At a resting membrane potential of -60 mV there maybe some re-onset of block as the channels can flicker stochastically to the open state as it is close to the threshold of activation; therefore the recovery from block is much less. E-4031 displays the opposite of this, there is no recovery at the more negative holding potentials which is indicative of drug trapping. At a holding potential of -60 mV, the drug is able to escape as the channels flicker spontaneously to the open state.

If these derivatives are not trapped, then recovery from block might be seen at negative potentials, during the times that the channels are deactivating. This could be a foot in the door phenotype, where the compounds are not able to be retained in the closed channel need to unbind and exit before the channel is able to close. As the channels become unblocked, they may pass current before they deactivate, this would be recorded as an apparent slowing of the deactivating tails. In these experiments a double exponential was fit to the deactivating tails to obtain time constants for deactivation. These were analysed for changes that could be indicative of foot in the door phenotype.

The analysis of the deactivation rates in presence and absence of compound indicated the deactivation of the channels did not appear to be slowed. The compound presence did slow deactivation at -60 mV, this likely to be due to

the stochastic flickering of channel openings that can occur at this voltage at the threshold for channel activation. The openings could allow the compound to rebind to the channel, therefore it will slow the total unbinding rate and the closure of the channels and give the impression of a slower rate of deactivation. But at -120 mV the deactivation rate even increased slightly with the derivatives present. This would indicate that the derivatives have some influence on the closure of the channel. Not only at the more positive potentials where there is a flickering of channel openings, but also at negative potentials.

These results do not appear to correlate with the recovery from block which would suggest that there could be a foot in the door phenotype as seen in other studies (Armstrong, 1971; Holmgren *et al.*, 1997; Decher *et al.*, 2006). However, at the more negative potential of -120 mV the closure of the channel in presence of derivatives appears faster than in its absence. This appears contrary to the recovery from block data, where the channels recover from drug block faster at this potential. There is no slowing of deactivation that is predicted when compounds block with a foot in the door phenotype.

### ***Faster deactivating channels do not display foot in the door phenotype***

If the recovery from block occurs when the channels deactivate, it would be expected that channels with fast deactivation kinetics would show faster recovery from block. The rapid deactivation could also make the channel more sensitive to the foot in the door effect, as the closure of the channel may be affected to a larger degree by the presence of the derivative. Therefore,

the block of the faster deactivating NTK hERG channel was studied to see if there was an alteration of block phenotype.

Initial studies of the drug block of the NTK hERG mutant showed that the potency to the open channel is higher compared to WT hERG, an effect like that seen when blocking the channels with the drug propafenone (Chapter 4). This may be due to easier access for the drug to the pore region or an allosteric affect, where the loss of the N-terminus alters the binding site to allow higher affinity for the derivatives.

If the derivatives were trapped in the cavity, the faster deactivating channels would slow the recovery from block, as it should trap the molecule in the cavity. At all voltages the channels recover from block more completely over the same time period than when blocking WT hERG. However, this is not the case, at -120 mV, over 2 min, there is complete recovery for the long L3T4 derivative, and at -60 mV the channels recover by almost ~ 75 %. As the recovery from block is much greater, again showing that the derivatives are not trapped in the channel even when it closes faster than WT.

When examining the deactivating tail currents in presence and absence of derivatives for the foot in the door phenotype, they do not display a significant slowing of deactivation in the presence of the drug. The channels appear to deactivate at the same rate with or without drug present. This indicates that the derivatives do not block hERG with a foot in the door phenotype, where the presence of the derivatives would slow the rate of deactivation, as reported in previous studies (Armstrong, 1971).

### ***The derivatives block the hERG channel with an alternative model of block***

These results are not consistent with a drug trapping or foot in the door model of block. The models do not have an explanation for the recovery from block that occurs without altering the tail kinetics and from a closed state. It is unlikely that the channels can trap the drug and then pass current with the derivative present when it opens, as it is also unlikely for there to be space for both the ion and the derivative in the inner cavity.

There is a possibility that the derivatives causes an alternative closure of the channel, other than at the intracellular activation gate. The most likely position for a second gate would be at the selectivity filter, as this is another region of constriction in the pore (figure 6.26). The idea that the selectivity filter acts as a gate has been suggested before in other studies of KcsA channels (Blunck *et al.*, 2006), inwardly rectifying channels (Claydon *et al.*, 2003) and cyclic nucleotide gated channels (Flynn & Zagotta, 2003). It is known that the selectivity filter and turret region of hERG channels are important in the inactivation characteristics of the channel (Herzberg *et al.*, 1998; Ficker *et al.*, 2001; Liu *et al.*, 2002; Jiang *et al.*, 2005). Therefore, the derivatives binding may cause the channels to remain in a conformation which is similar to the inactivated state, where the selectivity filter becomes non-conducting, while the channel deactivates. The process of deactivation results in the reduced affinity, possibly due to the rotation of the S6 helices (Chen *et al.*, 2002). The reduced affinity of the derivatives for the channel allows it to diffuse away before the channel closes.

To conclude, the data in this chapter show that derivatives with similar structures can display quite drastic changes in the way that they bind and in the potency to the channel. This was seen with the analogues of E-4031, where the potency was dropped greatly when the carbonyl group was altered. When the structure was modified to produce further derivatives, the binding of the drugs to the channels changed completely. They had high potency for the hERG channel, were highly state dependent, strongly favouring the channel in the open state. None of the drug derivatives were trapped like E-4031 that they were based on. They also displayed much faster kinetics of block and were able to leave the channel when it entered a closed state. This

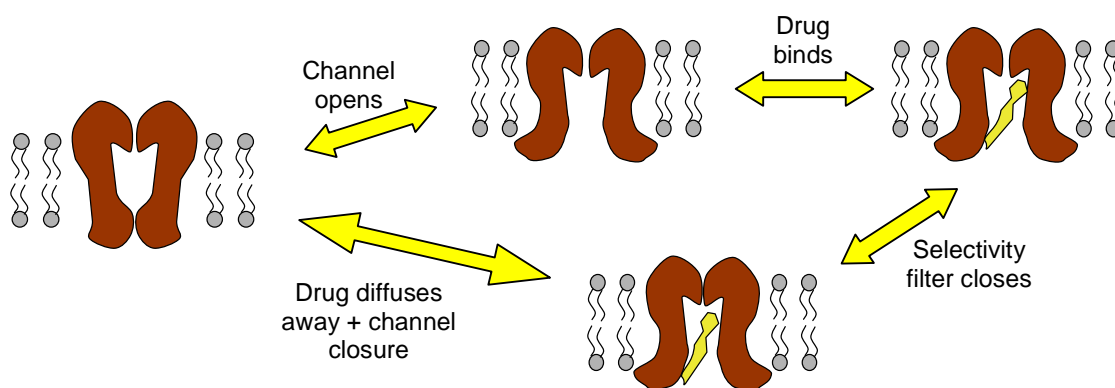


Figure 6.26: A schematic of a possible mechanism for the binding and unbinding of the E-4031 derivatives. The conventional mechanism is displayed in the top pathway, where the channel opens, a drug binds. On drug wash off the drug will unbind and then the channel closes. The alternate pathway is provided below this. The channels open and drugs bind to the channel. On repolarisation, the presence of the drug may cause the channels to close at an alternative region, likely the selectivity filter. This could allow the drug to unbind and channel to close without the passing of a current.

highlighted that drug trapping is not an important factor in the high potency drug block.

These effects were not something that could have been predicted from the present models of pharmacophores or in silico modelling of the drug binding. Therefore further study into the binding of drug molecules needs to be done in order for accurate predictions of potential clinical drug molecules which may

or may not block hERG channels as a side effect. It is important to look specifically at which residues bind to the particular structures in drugs, and if the structure of the molecules could be altered to change how the drugs can bind decreasing the affinity. Single channel recordings of the drug binding could also be carried out to look at the affinity of the E-4031 derivatives and whether they do actually leave the channel when the channel is in a closed state.

The effect of the different binding types could also be studied in relation to the cardiac action potential to see if this mode of blockade can also alter the QT interval. The data can further be used to create more detailed in silico model.

## **Chapter 7: General discussion and further experiments**

These studies investigated the structure-function relationship of the hERG channel in relation to gating and pharmacology. This project investigated the pharmacology of a series of drug analogues and derivatives of E-4031. The studies also investigated the rundown of hERG, the rundown of hERG/bEAG chimeras was also investigated. This was with the view to produce a chimera that had hERG voltage dependent and pharmacological characteristics but did not display rundown in activity. This channel could then be used in excised inside-out patch clamp experiments to directly apply compounds to the intracellular side of the channels and eliminate the factor of membrane permeability. The aim of this chapter is to summarise the findings reported in the preceding chapters and draw conclusions from these results and data other studies.

### **The termini of hERG and bEAG interact to alter the gating of hERG**

Chimeras of hERG and bEAG were created, where the intracellular termini of hERG were exchanged for one or both of the bEAG ones. All of the chimeric channels were functional, the expression was much lower than that of the WT hERG, WT bEAG and NTK hERG channels. The aim was to investigate if they had similar characteristics to WT hERG channels, so that they could be used to investigate the rundown of the channels when excised from the cell

membrane. These chimeras were first characterised using the TEVC technique, looking specifically at the voltage dependent characteristics.

### ***hERG deactivation gating***

If the termini of the hERG channel are modified, the kinetics of gating change. This is seen in previous studies where the termini of the channel are truncated (Schonherr & Heinemann, 1996; Wang *et al.*, 1997; Morais Cabral *et al.*, 1998; Aydar & Palmer, 2001; Gomez-Varela *et al.*, 2002).

When the PAS domain on the N-terminus was truncated or had certain residues mutated, the rate of deactivation was seen to increase (Schonherr & Heinemann, 1996; Spector *et al.*, 1996b; Wang *et al.*, 1997; Morais Cabral *et al.*, 1998). The effect of the increase in deactivation rate was reduced when PAS fragments were applied to the intracellular side of the channel (Morais Cabral *et al.*, 1998). It is thought that the N-terminus interacts with the S4-5 linker to stabilise the open state of the channel, slowing the rate of deactivation, as mutations to this region slow the rate of deactivation (Wang *et al.*, 1998; Sanguinetti & Xu, 1999). EAG also has a PAS domain, but lacks the proximal domain which lengthens the hERG N-terminus relative to the EAG one. Deletions to this domain in hERG, to make it more EAG like, resulted in an increase of the deactivation rate (Gomez-Varela *et al.*, 2003).

The C-terminus of hERG also modifies the deactivation rate. Truncations of the C-terminus resulted in an increase in the deactivation (Aydar & Palmer, 2001).

The results from the experiments in this chapter 3 show that exchanging the N- and/or C-terminus of the hERG channels for that of bEAG causes the increase in the rate of deactivation of the channels. These results indicate that

either the termini of hERG interact together to stabilise the open state, or exchanging the C-terminus of hERG causes the interference of the binding of the N-terminus to the S4-5 linker

### ***hERG activation gating***

When the N-terminus is truncated a positive shift in the  $V_{1/2}$  of activation was seen when compared to WT hERG (Schonherr & Heinemann, 1996; Spector *et al.*, 1996a; Vilorio *et al.*, 2000). The positive shift in the  $V_{1/2}$  of activation is seen in the NTK hERG, NHHBC and NBHHC chimeric channels, suggesting that there is an alteration of activation much like NTK hERG. The BHS16 chimeric channel displays a hyperpolarising shift in the  $V_{1/2}$  of activation, this channel behaviour is more like that of WT bEAG. It reflects the data reported by Valoria *et al.* (2000), who made deletions of the proximal domain between residues 138 and 373, which lead to a hyperpolarised shift in the  $V_{1/2}$ . The truncation of the proximal domain would make the N-terminus of the hERG channel more like that of bEAG.

The activation rates have also been altered when the termini were modified. The channels all display a slowing of the activation rate compared to WT hERG. This slowing of the activation rate is seen by Aydar *et al.* (2001), who truncated the N-terminus of hERG by 357 amino acids and saw a slight slowing of the activation. However other data show that smaller truncations of the N-terminus increases the rate of activation (Schonherr & Heinemann, 1996; Spector *et al.*, 1996a; Vilorio *et al.*, 2000). The difference may be due to the low n-numbers for these experiments. Further recordings will have to be done to confirm this.

### ***hERG Inactivation***

It is not clear whether the exchange of the termini alters the voltage dependence of inactivation. But it has not been eliminated, as seen from the I-V and fully activated experiments. These results reflect the findings of previous studies that show that the pore region between S5 and S6 domains hold the structures responsible for the fast inactivation properties. It is less likely to be influenced by the intracellular termini.

From these results it can be seen that the exchange of the termini causes alteration of the gating characteristics of the channel. The change is not a great shift from that of WT hERG, but needed to be taken into consideration when designing experiments to investigate their pharmacology. The protocols needed to be long enough to allow the channels to fully activate so they remain open for long enough for compound to bind to the inner cavity. The difference is small enough to allow for only require minor changes to the protocol used in the study of WT hERG.

Further studies will need to be done to quantify the voltage dependence of inactivation, to see if there is a change in the channel kinetics when the termini are exchanged. As the deactivation is fast in the chimeric channels, there maybe some contamination in TEVC recordings. The cut open oocyte recording technique could be used in to reduce contamination and artifacts in recordings (Costa *et al.*, 1994). This technique allows greater access to the intracellular side of the membrane, allowing the exchanging of intracellular solutions. Larger currents are able to be recorded and a faster, more stable

voltage clamp can be achieved. This method could more accurately record the voltage dependent kinetics of the channels in order to obtain time constants of inactivation and deactivation.

The influence of the termini can be further examined by producing partial exchanges of the termini. This may provide information on the region of the C-terminus which is responsible for the acceleration of deactivation rates.

### **Exchange of the C-terminus slows the rate of rundown**

The rundown of the WT hERG channels has been published in previous studies (Bian *et al.*, 2001; Cayabyab & Schlichter, 2002; Hirdes *et al.*, 2004). Through the addition of modulatory factors and kinase inhibitors, they have suggested that rundown is due to modulation by regulatory factors: PIP<sub>2</sub> binding, ATP and phosphorylation by protein kinases. However, the mechanism of rundown has not been studied in detail, so the mechanism of rundown and the location of the modulation sites are unclear.

My studies show that the rate and onset of rundown of WT hERG channels after excision from the membrane is quite variable, and occurring within a few minutes after excision. The rate and onset of rundown seemingly dependent on the characteristics of the excised patch, some displaying a delay before onset of rundown, whilst others display immediate rundown. The WT bEAG channels in contrast showed little rundown after excision. The chimeras show rundown, but the chimeras with the C-terminus exchanged with that of bEAG display a reduced rundown. The experiments suggest that there is some modulatory factors present in the cell that on excision is lost either by diffusion away from the patch or is metabolised and not replaced. As the patches excised are all different, the amount of these modulatory factors will be

variable and so lead to variation in the onset and rate of rundown. From the experiments with WT bEAG and C-terminal exchanged chimeras, the modulatory factor could bind with greater affinity than WT hERG, so being less susceptible to rundown.

Further recordings will have to be done to solidify the data that is seen in these results, particularly with the BHS16 chimeric channel. The role of possible modulation factors such as ATP, PIP<sub>2</sub> and certain protein kinases have to be investigated to discover if they are able to reduce the rundown of the channels. This can be done by altering the intracellular solution that is perfused onto the cytoplasmic side of the membrane. The experiments could also be run on mammalian cells transfected with the chimeric channels to analyse if a difference in the cell background affects the mechanism of rundown. The role of the C-terminus could be analysed in more detail to investigate the specific region that is responsible for maintenance of the channel activity. This can be through a series of point mutations to the predicted putative modulatory sites found on the C-terminus of hERG.

The act of excision does not appear to affect the voltage dependent deactivation of the hERG and chimeric channels. Much like the results in chapter 3, the deactivation rate of the chimeric channels is faster than WT hERG. However, there were some differences in the deactivation rate of the channels when compared to those recorded using the TEVC technique. This could be due to the difference in the recording solutions used. The TEVC technique keeps the intracellular conditions mostly intact, while the inside-out patch clamp technique changes the intracellular solutions. The alteration of which may alter the kinetics of the chimeric channels in a similar way as EAG

channels, where activation kinetics are altered by divalent ions (Terlau *et al.*, 1997; Schonherr *et al.*, 1999).

To conclude, the WT hERG channels display rapid rundown in excised inside-out patches that is not seen with WT bEAG channels. The NHHBC chimera exhibited stable currents over the course of several minutes, this channel could therefore be used in inside-out patch clamp experiments where the exchanges of intracellular solutions is required. It could be used to investigate the importance of membrane permeability on the potency of an inhibitor, by testing if there is an alteration in IC<sub>50</sub> compared those obtained in whole cell recordings. The channel may also be used in cysteine accessibility studies on intracellularly located amino acids.

## **hERG binding site**

### ***hERG channel inhibitors block hERG/bEAG chimeric channels in a similar fashion***

The basic pharmacology of the chimeric channels was studied using a series of different drugs. First a set of drugs were investigated, in order to make comparisons with the wildtype channels. With methanesulphonamide based drugs, E-4031 and dofetilide, the chimeras were found to have similar potency to wildtype channels and the data from the wildtype channels reflected results seen in previously studies (Ficker *et al.*, 1998; Herzberg *et al.*, 1998). The results in my study show that the structure that is important to methanesulphonamide drug binding is the pore forming region and little to do with the intracellular termini.

When the channels were blocked by a non-methanesulphonamide compound, propafenone, it was seen to inhibit the NTK hERG and chimeric currents to a greater extent than the wildtype hERG channel. The onset of the block and the washoff of propafenone were investigated to try and discover the basis of the difference. It was found that the rate of onset of block was slower in NTK hERG but the degree of block was much greater, suggesting that the off rate for WT hERG was also quicker. The results from the washoff experiments seem to also reflect this, after 2 minutes of washoff, the WT hERG currents recovered to a much greater degree than the NTK currents. Giving an indication that the slower off rates of the propafenone is the reason for the higher potency for NTK hERG channels. However, the change in potency caused by the alterations of the termini is probably an allosteric affect, as the amino acids lining the inner cavity create the drug binding site binding site (Mitcheson *et al.*, 2000a; Witchel *et al.*, 2004). The termini are present outside of this and so are unlikely to cause a direct interaction.

This study shows that the alterations of the termini affect the binding of compounds differently depending on their structure. It seems that the methanesulphonamide class is largely unaffected, while propafenone shows an increase in the potency to the chimeric channels. This could be further investigated by analysing which amino acids residues in the chimeric channels are important to the binding of compounds. By comparing these with those found to be important in WT hERG, it could uncover how some of the binding has altered. This could explain the small differences in the alterations in potency for E-4031 and propafenone. Further drug classes can also be

used to block the chimeric channels to investigate whether the change in potency is unique to propafenone binding.

The kinetics of propafenone binding could be further analysed to confirm whether the off rate of propafenone is the basis of an increase in the potency. This can be done through single channel recordings, comparing the single channel burst currents in presence and absence of propafenone can give a direct measurement of the off and on rates of block.

### ***E-4031 derivatives have high potency for hERG***

Studies have identified the inner cavity of the hERG channel as the main drug binding site (Mitcheson *et al.*, 2000a; Fernandez *et al.*, 2004). They mainly act by binding to the inner cavity, gaining access when the channels open and blocking the channel. The residues of the S6 and pore region are involved in the gating and the high affinity binding of compounds to hERG channels. This inner cavity is able to accommodate a large number of structurally diverse compounds that are able to block the channel with high affinity (Cavalli *et al.*, 2002; Aronov, 2005; Zunkler, 2006). Many attempts have been made to predict whether a novel compound is able to block the hERG channel, through the creation of pharmacophore models (Morgan & Sullivan, 1992; Cavalli *et al.*, 2002; Ekins *et al.*, 2002). These are able to predict the likelihood that a compound is able to bind to the hERG channel, but at present they are not able to accurately quantify the affinity of binding and there are also possibilities of false positives being reported.

Another method used is homology modelling to model the hERG channel in order to simulate the binding of compounds, highlighting potentially important interactions between the channel and compound. As these models are based

on a small number of crystal structures of voltage gated potassium channels, at present the models have not been used as an accurate predictive tool. These need to be refined by further experimental data.

This project attempted to characterise the size of the inner cavity of hERG, through the use of a series of varying length analogues based on E-4031. These analogues would have been used to test the hypothesis that as the compound length increased, the phenotype of block would change from one that was drug trapping to a foot in the door one.

Initial pharmacological experiments with E-4031 intermediates highlighted the importance of compound structure in their affinity to hERG. A change in the carbonyl group to a hydroxyl one in E-4031-A1 caused a 2  $\log_{10}$  unit drop in the  $IC_{50}$  that was not predicted with homology models. This could be due to changes in the electrostatic nature of the carbonyl compared to the hydroxyl groups, plus the change in 3D nature of the compound from a planar structure of E-4031 to a tetrahedral one of E-4031-A1.

When the derivatives of E-4031 were used to inhibit hERG channel, they were all found to have high potency, with  $IC_{50}$  values in the nM range. As the length of the derivatives was increased, there was a general trend for the potency to increase. This is consistent with the pharmacophore model by Cavalli *et al.* (2001). This predicts the volume increase will increase the potency of the compound. Further elongations of the series would have to be done to see if the potency will further follow this trend, or whether the increase had reached a maximum. As the tail extended derivatives displayed a slight decrease in potency of the longest compound compared to the next longest.

These derivatives all bind to the inner cavity with high affinity with similar kinetics, suggesting that they all bind in similar ways and that the tail region of derivatives have a minor role in binding to key residues. From mutagenesis data, the Phe656 residue is the most important to the binding of the derivatives to hERG. The role of Tyr652 in the binding is more variable, the sensitivity to the Y652A mutant varied with particular derivatives, L3T4 was much less sensitive to the mutation compared to other derivatives. This reflects previously studies where the sensitivity to the Y652A mutation is variable depending on the compound studied (Sanchez-Chapula *et al.*, 2002; Milnes *et al.*, 2003; Sanchez-Chapula *et al.*, 2003; Perry *et al.*, 2004; Witchel *et al.*, 2004). The S624 also has a weak influence on derivative binding, as the alanine mutation produce a smaller reduction in inhibition, it is greater contribution to the binding of the tail extended derivates than the linker extended ones, displaying a larger decrease in inhibition when the residue was mutated to an alanine. These residues were the only ones from those examined to show a decrease in inhibition when they were mutated to alanine, indicating that the derivatives bind to residues higher up in the cavity. While residues in the lower end of the cavity display little reduction in the inhibition.

### **The derivatives block hERG with an unusual phenotype**

The results show that the derivatives bind in a heavily state dependent manner. The derivatives bind with high affinity to the open channel, however they dissociate upon channel closure. The kinetics of block are rapid and voltage dependent. The derivatives display fast onset of hERG block, much like a lower potency hERG blocker propafenone (Witchel *et al.*, 2004). The rate of onset increased with more positive potentials, this is likely owing to the

corresponding increase in the activation rate and open probability of the channels. The more positive potential also favours the positively charged derivative molecule moving across the membrane electric field into the inner cavity of the channel.

The derivatives also display fast recovery from block that occurs when the channels are in the mostly closed state. The recovery from block was signified by the increase of current recorded briefly between closed states, this recovery from block does not require the compounds to be washed off. This indicated that the derivatives were not being trapped in the inner cavity of the channel when they closed. If they were trapped no recovery would be seen if the channels were closed, even with washoff, the inhibitor would remain in the cavity until the channels open allowing the compound to dissociate (Carmeliet, 1993; Gessner & Heinemann, 2003; Perry *et al.*, 2004; Witchel *et al.*, 2004).

As the derivatives did not block hERG channels with a drug trapping phenotype, the kinetics of deactivation in presence of derivatives were examined to see if they block hERG channels with a foot in the door phenotype. In this model the channels would not be able to close until after the compound unbinds and leaves the channel, during this time the channel is able to pass current before closing. This would be recorded as an apparent slowing of the deactivating tails. Comparing the deactivation rates of the tails in presence and absence of derivatives showed that at -60 mV the deactivating tails were slowed in presence of derivatives, but this may be due to the stochastic flickering of the channel at the threshold of activation. The openings may allow the derivatives to rebind to the channels, therefore giving an apparent slowing of the deactivation rates. At -120 mV there was no

slowing of the deactivation rate, in fact a slight increase in the deactivation rate was seen in presence of derivative. This would suggest that the derivatives have an influence on the closure of the channel, at both the more positive and negative potentials. These results do not indicate that the derivatives bind with a foot in the door phenotype that is seen in other previous studies (Armstrong, 1971; Holmgren *et al.*, 1997; Decher *et al.*, 2006).

The recovery from block was investigated further with the use of a fast deactivating NTK hERG channel. This investigated whether a foot in the door phenotype could be more clearly seen with the fast deactivation.

Initial studies found that the IC<sub>50</sub> was slightly higher than that found with WT hERG, similar to findings in experiments with propafenone. This effect is again probably due to increased access to the inner cavity or by an allosteric effect on the binding site of the derivatives.

Examining the deactivating tails, the currents deactivate at a similar rate in absence or presence of the derivatives. There is no slowing of deactivation that is associated with foot in the door type block. These results are not consistent with either a drug trapping or foot in the door phenotype of block. These models do not have an adequate explanation for how the derivatives are able to recover from block without altering the deactivation kinetics and when the channel is in a closed state. It is unlikely that the derivatives can remain in the channel on closure and then allow the passing of current when the channel reopens; as the space in the inner cavity is unlikely to accommodate both the derivative molecule and an ion.

The derivatives may cause an alternative closure of the channel at a region other than the intracellular activation gate. The most likely region would be the selectivity filter; this has been suggested as a point of gating in KcsA channels (Blunck *et al.*, 2006), inwardly rectifying channels (Claydon *et al.*, 2003) and cyclic nucleotide gated channels (Flynn & Zagotta, 2003). The selectivity filter and turret region of hERG is also involved in rapid inactivation properties of the channel (Herzberg *et al.*, 1998; Ficker *et al.*, 2001; Liu *et al.*, 2002; Jiang *et al.*, 2005). Therefore, the binding of the derivatives to the channel may cause it to remain in a conformation similar to the inactivated state, where the selectivity filter is non-conducting while the channel deactivates.

To conclude, the data presented demonstrate how structure of similar compounds can cause significant changes to the potency and binding mechanism for the channel, as seen with the E-4031-A1 analogue and the E-4031 derivatives. The derivatives have an unusual mechanism of block, they have high affinity for the hERG channel, with fast kinetics of block and high state dependence for the open state of the channel. The derivatives did not display any properties of drug trapping that E-4031, on which they are based, show. They also display recovery from block when the channels enter the closed state. Highlighting that drug trapping is not needed for high potency block.

These alterations in binding and potency are not able to be predicted with present models of pharmacophores or in silico modelling of drug binding. Therefore further studies of the binding of different compounds are needed to create more accurate models to predict the potential for clinical drugs to block the hERG channel as a side affect. The derivatives can be studied using

single channel recordings to measure the affinity of the derivatives for the hERG channel and also examine whether they are able to exit the channel when in the closed state. The different binding types can be used to investigate how they affect the cardiac action potential, investigating how they affect the QT interval.

A different series of analogues will have to be used to investigate whether increasing length of the molecule would alter the binding type from a drug trapping one to a foot in the door one.

### **Overall summary**

In this study the role of the intracellular termini of hERG channels in rundown was investigated. They were first characterised to examine whether the voltage dependent and pharmacological characteristics were altered. It was found that exchanging one or both of the termini altered the gating of the channels, accelerating the rate of deactivation and slowing the activation. It points to interactions between the N- and C-termini of hERG stabilising the open state. The inactivation remains, but this was not quantified properly. The pharmacological properties of the chimeras appear to be similar to those of WT hERG, though it may be dependent on the class of the compound, as methanesulphonamide drugs displayed similar  $IC_{50}$  values, while propafenone displayed smaller  $IC_{50}$  values.

In examinations of the rundown in activity of these channels it could be seen that the C-terminus may hold the modulatory sites that regulate the activity of the channel. The C-terminal swapped chimera could be used to discover where the modulation site for rundown is and lead to the creation of a channel that has more hERG like gating but with reduced rundown. This could then be

used to apply solutions to the intracellular side of the hERG channel without the problem of membrane permeability. This would aid in the understanding of the structure and pharmacology of the hERG channel.

A series of E-4031 derivatives were used to investigate the size of the inner cavity of hERG. However, it was found that they display an alternative mechanism of block than expected. The derivatives show that they may modify the way that the channel closes, allowing them to exit the channel when it is non-conducting. Further investigation will need to be carried out to discover the way that the derivatives exit the channels in a closed state. This would then be used to enhance the models of hERG blockers and their binding, in order to be able to predict potential side effects during the drug development process.

## Appendix

An alignment of the protein sequences of WT hERG (accession Q12809) and bEAG (O18965) are shown below, displaying the identical residues (\*), conservative residues (:) and semi-conserved (.). Gaps were inserted into the sequence to allow for better alignments. The S1-S6 transmembrane regions, along with the important structural domains of the PAS, CNBD, pore forming regions and selectivity filter are highlighted. The greatest sequence homology is in the PAS domain, the transmembrane domain and the CNBD. The greatest difference is in the length of the cytoplasmic N-terminus.

CLUSTAL 2.0.11 multiple sequence alignment

```

                                                    _____PAS domain_
sp|Q12809|hERG      ---MPVRRGHVAPQNTFLDTIIRKFEGQSRKFIIANARVENCAVIYCNDGFCELCGYSRA 57
sp|O18965|bEAG     MTMAGGRKGLVAPQNTFLENIVRRSNDTN--FVLGNAQIVDWPVIVYSNDGFCKLSGYHRA 58
                    *: * *****:.*:*: :. . *::.*:*: : :::*.*****:*.** **

                    _____
sp|Q12809|hERG     EVMQRPCTCDFLHGPRTQRRAAAQIAQALLGAEERKVEIAFYRKDGSCFLCLVDVVPVKN 117
sp|O18965|bEAG     EVMQKSSTCSFMYGELTDKDTIEKVRQTFENYEMNSFEILMYKKNRTPVWFFVKIAPIRN 118
                    ****:.*.*.*:* *:: : :: *:: . * ..** :*:*: : . :*:.:*:*

sp|Q12809|hERG     EDGAVIMFILNFEVVMKDMVGS PAHDTNHRGPPTSWLAPGRAKTFRLKLPALLALTARE 177
sp|O18965|bEAG     EQDKVVLFLCTFS-----DITAFK 137
                    *:. *:*:*: .* . :** :

sp|Q12809|hERG     SSVRSGGAGGAGAPGAVVVDVLT PAAPSSESLALDEVTAMDNHVAGLGAPEERRALVGP 237
sp|O18965|bEAG     QPIEDDSCKGWG----- 149
                    ..:..... * *

sp|Q12809|hERG     GSPPRSAPGQLPSRAHSLNPDASGSSCSLARTRSRESCASVRRASSADDIEAMRAGVLP 297
sp|O18965|bEAG     -----
```

```

sp|Q12809|hERG      PPRHASTGAMHPLRSGLLNSTSDSLVRYRTISKIPQITLNFVDLKGDPFLASPTS DRE 357
sp|O18965|bEAG     -----KFARLTRALTS SRGVLQQLAPS VQ-- 173
                    *:.:.* :. :.* :*: :
                    _____S1_____
sp|Q12809|hERG      IIAPKIKERTHNVTEKVTQVLSLGADVLP EYK LQAPRIHRWTILHYSPFKAVDWL LLLL 417
sp|O18965|bEAG     -----KGENVHKHSRLAEV LQLGSDILPQYKQ EAPKTPPHIILHYCVFKTTWDW IILIL 227
                    * . . : .: :.:*.**:*:*:*:* :*: * * * . * * . * * : * * :
                    _____S2_____
sp|Q12809|hERG      VIYTAVFTPYSA AFL LKETE EGPPATECGYACQPLAVVDLIVDIMFIVDILINFRTTYVN 477
sp|O18965|bEAG     TFYTAILVPYNV SFKTRQNN-----VAWLVDVSIVDVIFLVDIVLNFHTTFVG 275
                    .:***:.*.:.:* :.: : . * * * * * : : * * * : * * : * * :
                    _____S3_____
sp|Q12809|hERG      ANEEVVSHPGRIAVHYFKGWFLIDMVA AIPFDLLIFGS----- 515
sp|O18965|bEAG     PAGEVISDPK LIRMNYLKTWFVIDLLSCLPYDVINAFENVDEVS AFMGDPGKIGFADQIP 335
                    . * * : * . * * : * * * : : : : * * : .
                    _____S4_____ _____S5_____
sp|Q12809|hERG      -----GSEELIGLLKTARLLRLVRVARKLDRYSEYGAAVLFLLMCTFALIAHWLAC 566
sp|O18965|bEAG     PPLEGRESQG ISSLFSS LKVVRLRLGRVARKLDHYIEYGAAVLVLLVCVFGLA AHWMAC 395
                    * . . : . * * . * * * * * * * * * * * * * * * . * : * . * * * : * *
                    _____S6_____
sp|Q12809|hERG      IWY AIGNMEQPHMDSRIG---WLHNLGDQIGKPYNSSGLG-----GPSIKDKYV TALY 616
sp|O18965|bEAG     IWYSIGDYEIFDEDTKTIRNNSWLYQLAMDIGTPYQFNGSGSGK WEGGPSKNSVYISSLY 455
                    * * * : * * : * . : : * * : * . : * * * : * * * * * * * * * : . * * : * *
_Pore forming_____
sp|Q12809|hERG      FTFSSLTSVGFGNVSPNTNSEKIFSI CVMLIGSLMYASIFGNVSAIIQRLYSGTARYHTQ 676
Selectivity filter
sp|O18965|bEAG     FTMTSLTSVGFGN IAPSTDIEKIFAVAIMMIGSLLYATIFGNVTTIFQQMYANTNRYHEM 515
                    * * : * * * * * * * * : * . * : * * * : . : * * * * * * * * : * * : * * : * *
                    _____CNBD_____
sp|Q12809|hERG      LQHCKPFRGATKGLRALAMKFKTTHAPPGDTLVHAGDLLTALYFISRGSIEILRGDVVV 796
sp|O18965|bEAG     FKEHPAFRLASDG LRALAMEFQTVHCAPGD LIYHAGESVDSL CFVVGSL EVIQDDEVV 635
                    : . . . * * * : * * * * * * * * : * * . * . * * * : * * * : * * * : * * * : * * * : * *

```

```

sp|Q12809|hERG AILGKNDIFGEPLNLYARPGKSNQDVRALTYCDLHKIHRDDLLEVLDMYPEFSDHFWSSL 856
sp|O18965|bEAG AILKGDVFGDVFWEATLAQSCANVRALTYCDLHVIKRDALQKVLEFYTAFSHSFSRNL 695
*****.:***: : * .:* .:***** *:* * :*:* . * . * . *

sp|Q12809|hERG EITFNLRDNTMIPGSPGSTELEGGFSRQRKRKLSFRRRTDKDTEQPGEVSALGPGRAGAG 916
sp|O18965|bEAG ILTYNLRKRIVFRKISDVKREE--EERMKRKNEAPLILPPDHPVRLFRFRQKPEARL 752
.:***. .: . . . * .: *** . * . . : : .

sp|Q12809|hERG PSSRGRPGGPWGESPPSSGSPSESEDEGPRSSSPLRLVPFSSPRPPGEGEPLMED 976
sp|O18965|bEAG AAERGGRDLDDLVEKGSVLTEHSHHGLAKASVVTVRESPATPVAFPAAPAGLDHARL 812
.:** . : . . : * . . . : . . . * . * . * .

sp|Q12809|hERG CEKSSDTCNPLSG-AFSGVSNIFSWGDSRGRQYQELPRCPAPTPLLNIPLSSPGRPR 1035
sp|O18965|bEAG QAPGAEGLGPKAGGADCAKRGWARFKDACGQAEDWSKVSKAESMETLPERTKAAGEATL 872
.: : * : * * . . : : : * : * : . * : . * . : . * .

sp|Q12809|hERG GDVESRLDALQRQLNRLETR----LSADMATVLQLLQRQMTLVPPAYSAVTTPGPGTST 1091
sp|O18965|bEAG KKTDCDSGITKSDLRLDNVGEARSPQDRSPILAEVKHSFYPIPEQTLQAAVLEVKHELK 932
.:* .: : . ** . . * : : * : : : : * . . .

sp|Q12809|hERG SPLLPVSPPLPTLTLDLSQVSMACEELPPGAPELPQEGPTRRLSLPGQLGALTSQPLH 1151
sp|O18965|bEAG EDIKALSTKMTSIEKQLSEILRILTSRRSSQSPQELFEISRPQSPESERDIFGAS----- 987
. : :.* * . ** : : : . . . ** : . : . : : :

sp|Q12809|hERG RHGSDPGS 1159
sp|O18965|bEAG -----

```

## Bibliography

- ABBOTT, G. W., SESTI, F., SPLAWSKI, I., BUCK, M. E., LEHMANN, M. H., TIMOTHY, K. W., KEATING, M. T. & GOLDSTEIN, S. A. (1999). MiRP1 forms IKr potassium channels with HERG and is associated with cardiac arrhythmia. *Cell* **97**, 175-187.
- ARMSTRONG, C. M. (1971). Interaction of tetraethylammonium ion derivatives with the potassium channels of giant axons. *J Gen Physiol* **58**, 413-437.
- ARMSTRONG, D. & ECKERT, R. (1987). Voltage-activated calcium channels that must be phosphorylated to respond to membrane depolarization. *Proc Natl Acad Sci U S A* **84**, 2518-2522.
- ARNAOUT, R., FERRER, T., HUISKEN, J., SPITZER, K., STAINIER, D. Y., TRISTANI-FIROUZI, M. & CHI, N. C. (2007). Zebrafish model for human long QT syndrome. *Proc Natl Acad Sci U S A* **104**, 11316-11321.
- ARONOV, A. M. (2005). Predictive in silico modeling for hERG channel blockers. *Drug Discov Today* **10**, 149-155.
- AYDAR, E. & PALMER, C. (2001). Functional characterization of the C-terminus of the human ether-a-go-go-related gene K(+) channel (HERG). *J Physiol* **534**, 1-14.
- BARHANIN, J., LESAGE, F., GUILLEMARE, E., FINK, M., LAZDUNSKI, M. & ROMÉY, G. (1996). K(V)LQT1 and Isk (minK) proteins associate to form the I(Ks) cardiac potassium current. *Nature* **384**, 78-80.
- BIAN, J., CUI, J. & McDONALD, T. V. (2001). HERG K(+) channel activity is regulated by changes in phosphatidyl inositol 4,5-bisphosphate. *Circ Res* **89**, 1168-1176.
- BIAN, J. S., KAGAN, A. & McDONALD, T. V. (2004). Molecular analysis of PIP2 regulation of HERG and IKr. *Am J Physiol Heart Circ Physiol* **287**, H2154-2163.
- BICHET, D., HAASS, F. A. & JAN, L. Y. (2003). Merging functional studies with structures of inward-rectifier K(+) channels. *Nat Rev Neurosci* **4**, 957-967.
- BLUNCK, R., CORDERO-MORALES, J. F., CUELLO, L. G., PEROZO, E. & BEZANILLA, F. (2006). Detection of the opening of the bundle crossing in KcsA with fluorescence lifetime spectroscopy reveals the existence of two gates for ion conduction. *J Gen Physiol* **128**, 569-581.
- BRUNNER, M., PENG, X., LIU, G. X., REN, X. Q., ZIV, O., CHOI, B. R., MATHUR, R., HAJJIRI, M., ODENING, K. E., STEINBERG, E., FOLCO, E. J., PRINGA, E., CENTRACCHIO, J., MACHARZINA, R. R., DONAHAY, T., SCHOFIELD, L., RANA, N., KIRK, M., MITCHELL, G. F., POPPAS, A., ZEHENDER, M. & KOREN, G. (2008). Mechanisms of cardiac arrhythmias and sudden death in transgenic rabbits with long QT syndrome. *J Clin Invest* **118**, 2246-2259.
- CARMELIET, E. (1993). Use-dependent block and use-dependent unblock of the delayed rectifier K+ current by almokalant in rabbit ventricular myocytes. *Circ Res* **73**, 857-868.
- CAVALLI, A., POLUZZI, E., DE PONTI, F. & RECANATINI, M. (2002). Toward a pharmacophore for drugs inducing the long QT syndrome: insights from a CoMFA study of HERG K(+) channel blockers. *J Med Chem* **45**, 3844-3853.
- CAYABYAB, F. S. & SCHLICHTER, L. C. (2002). Regulation of an ERG K+ current by Src tyrosine kinase. *J Biol Chem* **277**, 13673-13681.

- CHEN, J., SEEBOHM, G. & SANGUINETTI, M. C. (2002). Position of aromatic residues in the S6 domain, not inactivation, dictates cisapride sensitivity of HERG and eag potassium channels. *Proc Natl Acad Sci U S A* **99**, 12461-12466.
- CHEN, J., ZOU, A., SPLAWSKI, I., KEATING, M. T. & SANGUINETTI, M. C. (1999). Long QT syndrome-associated mutations in the Per-Arnt-Sim (PAS) domain of HERG potassium channels accelerate channel deactivation. *J Biol Chem* **274**, 10113-10118.
- CHOI, B. R., JANG, W. & SALAMA, G. (2007). Spatially discordant voltage alternans cause wavebreaks in ventricular fibrillation. *Heart Rhythm* **4**, 1057-1068.
- CLARKE, C. E., HILL, A. P., ZHAO, J., KONDO, M., SUBBIAH, R. N., CAMPBELL, T. J. & VANDENBERG, J. I. (2006). Effect of S5P alpha-helix charge mutants on inactivation of hERG K<sup>+</sup> channels. *J Physiol* **573**, 291-304.
- CLAYDON, T. W., MAKARY, S. Y., DIBB, K. M. & BOYETT, M. R. (2003). The selectivity filter may act as the agonist-activated gate in the G protein-activated Kir3.1/Kir3.4 K<sup>+</sup> channel. *J Biol Chem* **278**, 50654-50663.
- COI, A., MASSARELLI, I., MURGIA, L., SARACENO, M., CALDERONE, V. & BIANUCCI, A. M. (2006). Prediction of hERG potassium channel affinity by the CODESSA approach. *Bioorg Med Chem* **14**, 3153-3159.
- COSTA, A. C., PATRICK, J. W. & DANI, J. A. (1994). Improved technique for studying ion channels expressed in *Xenopus* oocytes, including fast superfusion. *Biophys J* **67**, 395-401.
- CUI, J., KAGAN, A., QIN, D., MATHEW, J., MELMAN, Y. F. & McDONALD, T. V. (2001). Analysis of the cyclic nucleotide binding domain of the HERG potassium channel and interactions with KCNE2. *J Biol Chem* **276**, 17244-17251.
- CUI, J., MELMAN, Y., PALMA, E., FISHMAN, G. I. & McDONALD, T. V. (2000). Cyclic AMP regulates the HERG K(+) channel by dual pathways. *Curr Biol* **10**, 671-674.
- CURRAN, M. E., SPLAWSKI, I., TIMOTHY, K. W., VINCENT, G. M., GREEN, E. D. & KEATING, M. T. (1995). A Molecular Basis for Cardiac Arrhythmia: HERG Mutations Cause Long QT Mutations. *Cell* **80**, 795-803.
- DE PONTI, F., POLUZZI, E. & MONTANARO, N. (2000). QT-interval prolongation by non-cardiac drugs: lessons to be learned from recent experience. *Eur J Clin Pharmacol* **56**, 1-18.
- DE PONTI, F., POLUZZI, E. & MONTANARO, N. (2001). Organising evidence on QT prolongation and occurrence of Torsades de Pointes with non-antiarrhythmic drugs: a call for consensus. *Eur J Clin Pharmacol* **57**, 185-209.
- DECHER, N., KUMAR, P., GONZALEZ, T., PIRARD, B. & SANGUINETTI, M. C. (2006). Binding site of a novel Kv1.5 blocker: a "foot in the door" against atrial fibrillation. *Mol Pharmacol* **70**, 1204-1211.
- DEL CAMINO, D., HOLMGREN, M., LIU, Y. & YELLEN, G. (2000). Blocker protection in the pore of a voltage-gated K<sup>+</sup> channel and its structural implications. *Nature* **403**, 321-325.
- DOYLE, D. A., MORAIS CABRAL, J., PFUETZNER, R. A., KUO, A., GULBIS, J. M., COHEN, S. L., CHAIT, B. T. & MACKINNON, R. (1998). The structure of the potassium channel: molecular basis of K<sup>+</sup> conduction and selectivity. *Science* **280**, 69-77.
- DU, X., ZHANG, H., LOPES, C., MIRSHAHI, T., ROHACS, T. & LOGOTHETIS, D. E. (2004). Characteristic interactions with phosphatidylinositol 4,5-bisphosphate determine regulation of kir channels by diverse modulators. *J Biol Chem* **279**, 37271-37281.

- DUN, W., JIANG, M. & TSENG, G. N. (1999). Allosteric effects of mutations in the extracellular S5-P loop on the gating and ion permeation properties of the hERG potassium channel. *Pflugers Arch* **439**, 141-149.
- EKINS, S., CRUMB, W. J., SARAZAN, R. D., WIKEL, J. H. & WRIGHTON, S. A. (2002). Three-dimensional quantitative structure-activity relationship for inhibition of human ether-a-go-go-related gene potassium channel. *J Pharmacol Exp Ther* **301**, 427-434.
- FARID, R., DAY, T., FRIESNER, R. A. & PEARLSTEIN, R. A. (2006). New insights about HERG blockade obtained from protein modeling, potential energy mapping, and docking studies. *Bioorg Med Chem* **14**, 3160-3173.
- FERNANDEZ, D., GHANTA, A., KAUFFMAN, G. W. & SANGUINETTI, M. C. (2004). Physicochemical features of the HERG channel drug binding site. *J Biol Chem* **279**, 10120-10127.
- FICKER, E., JAROLIMEK, W. & BROWN, A. M. (2001). Molecular determinants of inactivation and dofetilide block in ether a-go-go (EAG) channels and EAG-related K(+) channels. *Mol Pharmacol* **60**, 1343-1348.
- FICKER, E., JAROLIMEK, W., KIEHN, J., BAUMANN, A. & BROWN, A. M. (1998). Molecular determinants of dofetilide block of HERG K+ channels. *Circ Res* **82**, 386-395.
- FLYNN, G. E. & ZAGOTTA, W. N. (2003). A cysteine scan of the inner vestibule of cyclic nucleotide-gated channels reveals architecture and rearrangement of the pore. *J Gen Physiol* **121**, 563-582.
- FRINGS, S., BRULL, N., DZEJA, C., ANGELE, A., HAGEN, V., KAUPP, U. B. & BAUMANN, A. (1998). Characterization of ether-a-go-go channels present in photoreceptors reveals similarity to IKx, a K+ current in rod inner segments. *J Gen Physiol* **111**, 583-599.
- GARG, D., GANDHI, T. & GOPI MOHAN, C. (2008). Exploring QSTR and toxicophore of hERG K+ channel blockers using GFA and HypoGen techniques. *J Mol Graph Model* **26**, 966-976.
- GESSNER, G. & HEINEMANN, S. H. (2003). Inhibition of hEAG1 and hERG1 potassium channels by clofilium and its tertiary analogue LY97241. *Br J Pharmacol* **138**, 161-171.
- GESSNER, G., ZACHARIAS, M., BECHSTEDT, S., SCHONHERR, R. & HEINEMANN, S. H. (2004). Molecular determinants for high-affinity block of human EAG potassium channels by antiarrhythmic agents. *Mol Pharmacol* **65**, 1120-1129.
- GOMEZ-VARELA, D., BARROS, F., VILORIA, C. G., GIRALDEZ, T., MANSO, D. G., DUPUY, S. G., MIRANDA, P. & DE LA PENA, P. (2003). Relevance of the proximal domain in the amino-terminus of HERG channels for regulation by a phospholipase C-coupled hormone receptor. *FEBS Lett* **535**, 125-130.
- GOMEZ-VARELA, D., DE LA PENA, P., GARCIA, J., GIRALDEZ, T. & BARROS, F. (2002). Influence of amino-terminal structures on kinetic transitions between several closed and open states in human erg K+ channels. *J Membr Biol* **187**, 117-133.
- HAACK, B., KUPKA, S., EBAUER, M., SIEMIATKOWSKA, A., PFISTER, M., KWIATKOWSKA, J., ERECINSKI, J., LIMON, J., OCHMAN, K. & BLIN, N. (2004). Analysis of candidate genes for genotypic diagnosis in the long QT syndrome. *J Appl Genet* **45**, 375-381.
- HERZBERG, I. M., TRUDEAU, M. C. & ROBERTSON, G. A. (1998). Transfer of rapid inactivation and sensitivity to the class III antiarrhythmic drug E-4031 from HERG to M-eag channels. *J Physiol* **511 ( Pt 1)**, 3-14.

- HILLMAN, E. M., BERNUS, O., PEASE, E., BOUCHARD, M. B. & PERTSOV, A. (2007). Depth-resolved optical imaging of transmural electrical propagation in perfused heart. *Opt Express* **15**, 17827-17841.
- HIRDES, W., HOROWITZ, L. F. & HILLE, B. (2004). Muscarinic modulation of erg potassium current. *J Physiol* **559**, 67-84.
- HOLMGREN, M., SMITH, P. L. & YELLEN, G. (1997). Trapping of organic blockers by closing of voltage-dependent K<sup>+</sup> channels: evidence for a trap door mechanism of activation gating. *J Gen Physiol* **109**, 527-535.
- HOLYOAKE, J., DOMENE, C., BRIGHT, J. N. & SANSOM, M. S. (2004). KcsA closed and open: modelling and simulation studies. *Eur Biophys J* **33**, 238-246.
- ISHII, K., NAGAI, M., TAKAHASHI, M. & ENDOH, M. (2003). Dissociation of E-4031 from the HERG channel caused by mutations of an amino acid results in greater block at high stimulation frequency. *Cardiovasc Res* **57**, 651-659.
- ABBOTT, G. W., SESTI, F., SPLAWSKI, I., BUCK, M. E., LEHMANN, M. H., TIMOTHY, K. W., KEATING, M. T. & GOLDSTEIN, S. A. (1999). MiRP1 forms IKr potassium channels with HERG and is associated with cardiac arrhythmia. *Cell* **97**, 175-187.
- ARMSTRONG, C. M. (1971). Interaction of tetraethylammonium ion derivatives with the potassium channels of giant axons. *J Gen Physiol* **58**, 413-437.
- ARMSTRONG, D. & ECKERT, R. (1987). Voltage-activated calcium channels that must be phosphorylated to respond to membrane depolarization. *Proc Natl Acad Sci U S A* **84**, 2518-2522.
- ARNAOUT, R., FERRER, T., HUISKEN, J., SPITZER, K., STAINIER, D. Y., TRISTANI-FIROUZI, M. & CHI, N. C. (2007). Zebrafish model for human long QT syndrome. *Proc Natl Acad Sci U S A* **104**, 11316-11321.
- ARONOV, A. M. (2005). Predictive in silico modeling for hERG channel blockers. *Drug Discov Today* **10**, 149-155.
- AYDAR, E. & PALMER, C. (2001). Functional characterization of the C-terminus of the human ether-a-go-go-related gene K(+) channel (HERG). *J Physiol* **534**, 1-14.
- BARHANIN, J., LESAGE, F., GUILLEMARE, E., FINK, M., LAZDUNSKI, M. & ROMEY, G. (1996). K(V)LQT1 and Isk (minK) proteins associate to form the I(Ks) cardiac potassium current. *Nature* **384**, 78-80.
- BIAN, J., CUI, J. & McDONALD, T. V. (2001). HERG K(+) channel activity is regulated by changes in phosphatidylinositol 4,5-bisphosphate. *Circ Res* **89**, 1168-1176.
- BIAN, J. S., KAGAN, A. & McDONALD, T. V. (2004). Molecular analysis of PIP2 regulation of HERG and IKr. *Am J Physiol Heart Circ Physiol* **287**, H2154-2163.
- BICHET, D., HAASS, F. A. & JAN, L. Y. (2003). Merging functional studies with structures of inward-rectifier K(+) channels. *Nat Rev Neurosci* **4**, 957-967.
- BLUNCK, R., CORDERO-MORALES, J. F., CUELLO, L. G., PEROZO, E. & BEZANILLA, F. (2006). Detection of the opening of the bundle crossing in KcsA with fluorescence lifetime spectroscopy reveals the existence of two gates for ion conduction. *J Gen Physiol* **128**, 569-581.
- BRUNNER, M., PENG, X., LIU, G. X., REN, X. Q., ZIV, O., CHOI, B. R., MATHUR, R., HAJJIRI, M., ODENING, K. E., STEINBERG, E., FOLCO, E. J., PRINGA, E., CENTRACCHIO, J., MACHARZINA, R. R., DONAHAY, T., SCHOFIELD, L., RANA, N., KIRK, M., MITCHELL, G. F.,

- POPPAS, A., ZEHENDER, M. & KOREN, G. (2008). Mechanisms of cardiac arrhythmias and sudden death in transgenic rabbits with long QT syndrome. *J Clin Invest* **118**, 2246-2259.
- CARMELIET, E. (1993). Use-dependent block and use-dependent unblock of the delayed rectifier K<sup>+</sup> current by almokalant in rabbit ventricular myocytes. *Circ Res* **73**, 857-868.
- CAVALLI, A., POLUZZI, E., DE PONTI, F. & RECANATINI, M. (2002). Toward a pharmacophore for drugs inducing the long QT syndrome: insights from a CoMFA study of HERG K(+) channel blockers. *J Med Chem* **45**, 3844-3853.
- CAYABYAB, F. S. & SCHLICHTER, L. C. (2002). Regulation of an ERG K<sup>+</sup> current by Src tyrosine kinase. *J Biol Chem* **277**, 13673-13681.
- CHEN, J., SEEBOHM, G. & SANGUINETTI, M. C. (2002). Position of aromatic residues in the S6 domain, not inactivation, dictates cisapride sensitivity of HERG and eag potassium channels. *Proc Natl Acad Sci U S A* **99**, 12461-12466.
- CHEN, J., ZOU, A., SPLAWSKI, I., KEATING, M. T. & SANGUINETTI, M. C. (1999). Long QT syndrome-associated mutations in the Per-Arnt-Sim (PAS) domain of HERG potassium channels accelerate channel deactivation. *J Biol Chem* **274**, 10113-10118.
- CHOI, B. R., JANG, W. & SALAMA, G. (2007). Spatially discordant voltage alternans cause wavebreaks in ventricular fibrillation. *Heart Rhythm* **4**, 1057-1068.
- CLARKE, C. E., HILL, A. P., ZHAO, J., KONDO, M., SUBBIAH, R. N., CAMPBELL, T. J. & VANDENBERG, J. I. (2006). Effect of S5P alpha-helix charge mutants on inactivation of hERG K<sup>+</sup> channels. *J Physiol* **573**, 291-304.
- CLAYDON, T. W., MAKARY, S. Y., DIBB, K. M. & BOYETT, M. R. (2003). The selectivity filter may act as the agonist-activated gate in the G protein-activated Kir3.1/Kir3.4 K<sup>+</sup> channel. *J Biol Chem* **278**, 50654-50663.
- COI, A., MASSARELLI, I., MURGIA, L., SARACENO, M., CALDERONE, V. & BIANUCCI, A. M. (2006). Prediction of hERG potassium channel affinity by the CODESSA approach. *Bioorg Med Chem* **14**, 3153-3159.
- COSTA, A. C., PATRICK, J. W. & DANI, J. A. (1994). Improved technique for studying ion channels expressed in *Xenopus* oocytes, including fast superfusion. *Biophys J* **67**, 395-401.
- CUI, J., KAGAN, A., QIN, D., MATHEW, J., MELMAN, Y. F. & McDONALD, T. V. (2001). Analysis of the cyclic nucleotide binding domain of the HERG potassium channel and interactions with KCNE2. *J Biol Chem* **276**, 17244-17251.
- CUI, J., MELMAN, Y., PALMA, E., FISHMAN, G. I. & McDONALD, T. V. (2000). Cyclic AMP regulates the HERG K(+) channel by dual pathways. *Curr Biol* **10**, 671-674.
- CURRAN, M. E., SPLAWSKI, I., TIMOTHY, K. W., VINCENT, G. M., GREEN, E. D. & KEATING, M. T. (1995). A Molecular Basis for Cardiac Arrhythmia: HERG Mutations Cause Long QT Mutations. *Cell* **80**, 795-803.
- DE PONTI, F., POLUZZI, E. & MONTANARO, N. (2000). QT-interval prolongation by non-cardiac drugs: lessons to be learned from recent experience. *Eur J Clin Pharmacol* **56**, 1-18.
- DE PONTI, F., POLUZZI, E. & MONTANARO, N. (2001). Organising evidence on QT prolongation and occurrence of Torsades de Pointes with non-antiarrhythmic drugs: a call for consensus. *Eur J Clin Pharmacol* **57**, 185-209.

- DECHER, N., KUMAR, P., GONZALEZ, T., PIRARD, B. & SANGUINETTI, M. C. (2006). Binding site of a novel Kv1.5 blocker: a "foot in the door" against atrial fibrillation. *Mol Pharmacol* **70**, 1204-1211.
- DEL CAMINO, D., HOLMGREN, M., LIU, Y. & YELLEN, G. (2000). Blocker protection in the pore of a voltage-gated K<sup>+</sup> channel and its structural implications. *Nature* **403**, 321-325.
- DOYLE, D. A., MORAIS CABRAL, J., PFUETZNER, R. A., KUO, A., GULBIS, J. M., COHEN, S. L., CHAIT, B. T. & MACKINNON, R. (1998). The structure of the potassium channel: molecular basis of K<sup>+</sup> conduction and selectivity. *Science* **280**, 69-77.
- DU, X., ZHANG, H., LOPES, C., MIRSHAHI, T., ROHACS, T. & LOGOTHETIS, D. E. (2004). Characteristic interactions with phosphatidylinositol 4,5-bisphosphate determine regulation of kir channels by diverse modulators. *J Biol Chem* **279**, 37271-37281.
- DUN, W., JIANG, M. & TSENG, G. N. (1999). Allosteric effects of mutations in the extracellular S5-P loop on the gating and ion permeation properties of the hERG potassium channel. *Pflugers Arch* **439**, 141-149.
- EKINS, S., CRUMB, W. J., SARAZAN, R. D., WIKEL, J. H. & WRIGHTON, S. A. (2002). Three-dimensional quantitative structure-activity relationship for inhibition of human ether-a-go-go-related gene potassium channel. *J Pharmacol Exp Ther* **301**, 427-434.
- FARID, R., DAY, T., FRIESNER, R. A. & PEARLSTEIN, R. A. (2006). New insights about HERG blockade obtained from protein modeling, potential energy mapping, and docking studies. *Bioorg Med Chem* **14**, 3160-3173.
- FERNANDEZ, D., GHANTA, A., KAUFFMAN, G. W. & SANGUINETTI, M. C. (2004). Physicochemical features of the HERG channel drug binding site. *J Biol Chem* **279**, 10120-10127.
- FICKER, E., JAROLIMEK, W. & BROWN, A. M. (2001). Molecular determinants of inactivation and dofetilide block in ether a-go-go (EAG) channels and EAG-related K(+) channels. *Mol Pharmacol* **60**, 1343-1348.
- FICKER, E., JAROLIMEK, W., KIEHN, J., BAUMANN, A. & BROWN, A. M. (1998). Molecular determinants of dofetilide block of HERG K<sup>+</sup> channels. *Circ Res* **82**, 386-395.
- FLYNN, G. E. & ZAGOTTA, W. N. (2003). A cysteine scan of the inner vestibule of cyclic nucleotide-gated channels reveals architecture and rearrangement of the pore. *J Gen Physiol* **121**, 563-582.
- FRINGS, S., BRULL, N., DZEJA, C., ANGELE, A., HAGEN, V., KAUPP, U. B. & BAUMANN, A. (1998). Characterization of ether-a-go-go channels present in photoreceptors reveals similarity to IK<sub>x</sub>, a K<sup>+</sup> current in rod inner segments. *J Gen Physiol* **111**, 583-599.
- GARG, D., GANDHI, T. & GOPI MOHAN, C. (2008). Exploring QSTR and toxicophore of hERG K<sup>+</sup> channel blockers using GFA and HypoGen techniques. *J Mol Graph Model* **26**, 966-976.
- GESSNER, G. & HEINEMANN, S. H. (2003). Inhibition of hEAG1 and hERG1 potassium channels by clofilium and its tertiary analogue LY97241. *Br J Pharmacol* **138**, 161-171.
- GESSNER, G., ZACHARIAS, M., BECHSTEDT, S., SCHONHERR, R. & HEINEMANN, S. H. (2004). Molecular determinants for high-affinity block of human EAG potassium channels by antiarrhythmic agents. *Mol Pharmacol* **65**, 1120-1129.
- GOMEZ-VARELA, D., BARROS, F., VILORIA, C. G., GIRALDEZ, T., MANSO, D. G., DUPUY, S. G., MIRANDA, P. & DE LA PENA, P. (2003). Relevance of the proximal domain in the amino-terminus of HERG channels for regulation by a phospholipase C-coupled hormone receptor. *FEBS Lett* **535**, 125-130.

- GOMEZ-VARELA, D., DE LA PENA, P., GARCIA, J., GIRALDEZ, T. & BARROS, F. (2002). Influence of amino-terminal structures on kinetic transitions between several closed and open states in human erg K<sup>+</sup> channels. *J Membr Biol* **187**, 117-133.
- HAACK, B., KUPKA, S., EBAUER, M., SIEMIATKOWSKA, A., PFISTER, M., KWIATKOWSKA, J., ERECINSKI, J., LIMON, J., OCHMAN, K. & BLIN, N. (2004). Analysis of candidate genes for genotypic diagnosis in the long QT syndrome. *J Appl Genet* **45**, 375-381.
- HERZBERG, I. M., TRUDEAU, M. C. & ROBERTSON, G. A. (1998). Transfer of rapid inactivation and sensitivity to the class III antiarrhythmic drug E-4031 from HERG to M-eag channels. *J Physiol* **511 ( Pt 1)**, 3-14.
- HILLMAN, E. M., BERNUS, O., PEASE, E., BOUCHARD, M. B. & PERTSOV, A. (2007). Depth-resolved optical imaging of transmural electrical propagation in perfused heart. *Opt Express* **15**, 17827-17841.
- HIRDES, W., HOROWITZ, L. F. & HILLE, B. (2004). Muscarinic modulation of erg potassium current. *J Physiol* **559**, 67-84.
- HOLMGREN, M., SMITH, P. L. & YELLEN, G. (1997). Trapping of organic blockers by closing of voltage-dependent K<sup>+</sup> channels: evidence for a trap door mechanism of activation gating. *J Gen Physiol* **109**, 527-535.
- HOLYOAKE, J., DOMENE, C., BRIGHT, J. N. & SANSOM, M. S. (2004). KcsA closed and open: modelling and simulation studies. *Eur Biophys J* **33**, 238-246.
- ISHII, K., NAGAI, M., TAKAHASHI, M. & ENDOH, M. (2003). Dissociation of E-4031 from the HERG channel caused by mutations of an amino acid results in greater block at high stimulation frequency. *Cardiovasc Res* **57**, 651-659.
- JIANG, M., ZHANG, M., MASLENNIKOV, I. V., LIU, J., WU, D. M., KOROLKOVA, Y. V., ARSENIYEV, A. S., GRISHIN, E. V. & TSENG, G. N. (2005). Dynamic conformational changes of extracellular S5-P linkers in the hERG channel. *J Physiol* **569**, 75-89.
- JIANG, Y., LEE, A., CHEN, J., CADENE, M., CHAIT, B. T. & MACKINNON, R. (2002). The open pore conformation of potassium channels. *Nature* **417**, 523-526.
- JIANG, Y., LEE, A., CHEN, J., RUTA, V., CADENE, M., CHAIT, B. T. & MACKINNON, R. (2003). X-ray structure of a voltage-dependent K<sup>+</sup> channel. *Nature* **423**, 33-41.
- KAMIYA, K., MITCHESON, J. S., YASUI, K., KODAMA, I. & SANGUINETTI, M. C. (2001). Open channel block of HERG K(+) channels by vesnarinone. *Mol Pharmacol* **60**, 244-253.
- KAMIYA, K., NIWA, R., MITCHESON, J. S. & SANGUINETTI, M. C. (2006). Molecular Determinants of hERG Channel Block. *Mol Pharmacol*.
- KUO, A., GULBIS, J. M., ANTCLIFF, J. F., RAHMAN, T., LOWE, E. D., ZIMMER, J., CUTHBERTSON, J., ASHCROFT, F. M., EZAKI, T. & DOYLE, D. A. (2003). Crystal structure of the potassium channel KirBac1.1 in the closed state. *Science* **300**, 1922-1926.
- LEES-MILLER, J. P., DUAN, Y., TENG, G. Q. & DUFF, H. J. (2000). Molecular determinant of high-affinity dofetilide binding to HERG1 expressed in *Xenopus* oocytes: involvement of S6 sites. *Mol Pharmacol* **57**, 367-374.
- LIU, J., ZHANG, M., JIANG, M. & TSENG, G. N. (2002). Structural and functional role of the extracellular s5-p linker in the HERG potassium channel. *J Gen Physiol* **120**, 723-737.
- LONG, S. B., CAMPBELL, E. B. & MACKINNON, R. (2005). Crystal structure of a mammalian voltage-dependent Shaker family K<sup>+</sup> channel. *Science* **309**, 897-903.

- LONG, S. B., TAO, X., CAMPBELL, E. B. & MACKINNON, R. (2007). Atomic structure of a voltage-dependent K<sup>+</sup> channel in a lipid membrane-like environment. *Nature* **450**, 376-382.
- MADEJA, M., LEICHER, T., FRIEDERICH, P., PUNKE, M. A., HAVERKAMP, W., MUSSHOFF, U., BREITHARDT, G. & SPECKMANN, E. J. (2003). Molecular site of action of the antiarrhythmic drug propafenone at the voltage-operated potassium channel Kv2.1. *Mol Pharmacol* **63**, 547-556.
- MCDONALD, T. V., YU, Z., MING, Z., PALMA, E., MEYERS, M. B., WANG, K. W., GOLDSTEIN, S. A. & FISHMAN, G. I. (1997). A minK-HERG complex regulates the cardiac potassium current I(Kr). *Nature* **388**, 289-292.
- MCNICHOLAS, C. M., WANG, W., HO, K., HEBERT, S. C. & GIEBISCH, G. (1994). Regulation of ROMK1 K<sup>+</sup> channel activity involves phosphorylation processes. *Proc Natl Acad Sci U S A* **91**, 8077-8081.
- MILNES, J. T., DEMPSEY, C. E., RIDLEY, J. M., CROCIANI, O., ARCANGELI, A., HANCOX, J. C. & WITCHEL, H. J. (2003). Preferential closed channel blockade of HERG potassium currents by chemically synthesised BeKm-1 scorpion toxin. *FEBS Lett* **547**, 20-26.
- MITCHESON, J. S. (2003). Drug binding to HERG channels: evidence for a 'non-aromatic' binding site for fluvoxamine. *Br J Pharmacol* **139**, 883-884.
- MITCHESON, J. S., CHEN, J., LIN, M., CULBERSON, C. & SANGUINETTI, M. C. (2000a). A structural basis for drug-induced long QT syndrome. *Proc Natl Acad Sci U S A* **97**, 12329-12333.
- MITCHESON, J. S., CHEN, J. & SANGUINETTI, M. C. (2000b). Trapping of a methanesulfonanilide by closure of the HERG potassium channel activation gate. *J Gen Physiol* **115**, 229-240.
- MORAIS CABRAL, J. H., LEE, A., COHEN, S. L., CHAIT, B. T., LI, M. & MACKINNON, R. (1998). Crystal structure and functional analysis of the HERG potassium channel N terminus: a eukaryotic PAS domain. *Cell* **95**, 649-655.
- MORGAN, T. K., JR. & SULLIVAN, M. E. (1992). An overview of class III electrophysiological agents: a new generation of antiarrhythmic therapy. *Prog Med Chem* **29**, 65-108.
- OSTERBERG, F. & AQVIST, J. (2005). Exploring blocker binding to a homology model of the open hERG K<sup>+</sup> channel using docking and molecular dynamics methods. *FEBS Lett* **579**, 2939-2944.
- PEARLSTEIN, R. A., VAZ, R. J., KANG, J., CHEN, X. L., PREOBRAZHENSKAYA, M., SHCHEKOTIKHIN, A. E., KOROLEV, A. M., LYSENKOVA, L. N., MIROSHNIKOVA, O. V., HENDRIX, J. & RAMPE, D. (2003). Characterization of HERG potassium channel inhibition using CoMSiA 3D QSAR and homology modeling approaches. *Bioorg Med Chem Lett* **13**, 1829-1835.
- PERRY, M., DE GROOT, M. J., HELLIWELL, R., LEISHMAN, D., TRISTANI-FIROUZI, M., SANGUINETTI, M. C. & MITCHESON, J. S. (2004). Structural determinants of HERG channel block by clofilium and ibutilide. *Mol Pharmacol* **66**, 240-249.
- PERRY, M., STANSFELD, P. J., LEANEY, J., WOOD, C., DE GROOT, M. J., LEISHMAN, D., SUTCLIFFE, M. J. & MITCHESON, J. S. (2006). Drug binding interactions in the inner cavity of HERG channels: molecular insights from structure-activity relationships of clofilium and ibutilide analogs. *Mol Pharmacol* **69**, 509-519.
- PROKS, P., CAPENER, C. E., JONES, P. & ASHCROFT, F. M. (2001). Mutations within the P-loop of Kir6.2 modulate the intraburst kinetics of the ATP-sensitive potassium channel. *J Gen Physiol* **118**, 341-353.

- RANGANATHAN, R., LEWIS, J. H. & MACKINNON, R. (1996). Spatial localization of the K<sup>+</sup> channel selectivity filter by mutant cycle-based structure analysis. *Neuron* **16**, 131-139.
- RODEN, D. M., BALSER, J. R., GEORGE, A. L., JR. & ANDERSON, M. E. (2002). Cardiac ion channels. *Annu Rev Physiol* **64**, 431-475.
- SANCHEZ-CHAPULA, J. A., FERRER, T., NAVARRO-POLANCO, R. A. & SANGUINETTI, M. C. (2003). Voltage-dependent profile of human ether-a-go-go-related gene channel block is influenced by a single residue in the S6 transmembrane domain. *Mol Pharmacol* **63**, 1051-1058.
- SANCHEZ-CHAPULA, J. A., NAVARRO-POLANCO, R. A., CULBERSON, C., CHEN, J. & SANGUINETTI, M. C. (2002). Molecular determinants of voltage-dependent human ether-a-go-go related gene (HERG) K<sup>+</sup> channel block. *J Biol Chem* **277**, 23587-23595.
- SANGUINETTI, M. C., CURRAN, M. E., SPECTOR, P. S. & KEATING, M. T. (1996). Spectrum of HERG K<sup>+</sup>-channel dysfunction in an inherited cardiac arrhythmia. *Proc Natl Acad Sci U S A* **93**, 2208-2212.
- SANGUINETTI, M. C., JIANG, C., CURRAN, M. E. & KEATING, M. T. (1995). A mechanistic link between an inherited and an acquired cardiac arrhythmia: HERG encodes the IKr potassium channel. *Cell* **81**, 299-307.
- SANGUINETTI, M. C. & TRISTANI-FIROUZI, M. (2006). hERG potassium channels and cardiac arrhythmia. *Nature* **440**, 463-469.
- SANGUINETTI, M. C. & XU, Q. P. (1999). Mutations of the S4-S5 linker alter activation properties of HERG potassium channels expressed in *Xenopus* oocytes. *J Physiol* **514** ( Pt 3), 667-675.
- SCHONHERR, R., HEHL, S., TERLAU, H., BAUMANN, A. & HEINEMANN, S. H. (1999). Individual subunits contribute independently to slow gating of bovine EAG potassium channels. *J Biol Chem* **274**, 5362-5369.
- SCHONHERR, R. & HEINEMANN, S. H. (1996). Molecular determinants for activation and inactivation of HERG, a human inward rectifier potassium channel. *J Physiol* **493** ( Pt 3), 635-642.
- SHRIVASTAVA, I. H. & BAHAR, I. (2006). Common mechanism of pore opening shared by five different potassium channels. *Biophys J* **90**, 3929-3940.
- SMITH, P. L., BAUKROWITZ, T. & YELLEN, G. (1996). The inward rectification mechanism of the HERG cardiac potassium channel. *Nature* **379**, 833-836.
- SPECTOR, P. S., CURRAN, M. E., KEATING, M. T. & SANGUINETTI, M. C. (1996a). Class III antiarrhythmic drugs block HERG, a human cardiac delayed rectifier K<sup>+</sup> channel. Open-channel block by methanesulfonanilides. *Circ Res* **78**, 499-503.
- SPECTOR, P. S., CURRAN, M. E., ZOU, A., KEATING, M. T. & SANGUINETTI, M. C. (1996b). Fast inactivation causes rectification of the IKr channel. *J Gen Physiol* **107**, 611-619.
- STANSFELD, P. J., GEDECK, P., GOSLING, M., COX, B., MITCHESON, J. S. & SUTCLIFFE, M. J. (2007). Drug block of the hERG potassium channel: insight from modeling. *Proteins* **68**, 568-580.
- STANSFELD, P. J., GROTTESI, A., SANDS, Z. A., SANSOM, M. S., GEDECK, P., GOSLING, M., COX, B., STANFIELD, P. R., MITCHESON, J. S. & SUTCLIFFE, M. J. (2008). Insight into the mechanism of inactivation and pH sensitivity in potassium channels from molecular dynamics simulations. *Biochemistry* **47**, 7414-7422.

- TAMARGO, J., CABALLERO, R., GOMEZ, R., VALENZUELA, C. & DELPON, E. (2004). Pharmacology of cardiac potassium channels. *Cardiovasc Res* **62**, 9-33.
- TANG, X. D. & HOSHI, T. (1999). Rundown of the hyperpolarization-activated KAT1 channel involves slowing of the opening transitions regulated by phosphorylation. *Biophys J* **76**, 3089-3098.
- TERLAU, H., HEINEMANN, S., STUHMER, W., PONGS, O. & LUDWIG, J. (1997). Amino terminal-dependent gating of the potassium channel rat eag is compensated by a mutation in the S4 segment. *J Physiol (Lond)* **502**, 537-543.
- THOMAS, D., ZHANG, W., WU, K., WIMMER, A. B., GUT, B., WENDT-NORDAHL, G., KATHOFER, S., KREYE, V. A., KATUS, H. A., SCHOELS, W., KIEHN, J. & KARLE, C. A. (2003). Regulation of HERG potassium channel activation by protein kinase C independent of direct phosphorylation of the channel protein. *Cardiovasc Res* **59**, 14-26.
- TORRES, A. M., BANSAL, P. S., SUNDE, M., CLARKE, C. E., BURSILL, J. A., SMITH, D. J., BAUSKIN, A., BREIT, S. N., CAMPBELL, T. J., ALEWOOD, P. F., KUCHEL, P. W. & VANDENBERG, J. I. (2003). Structure of the HERG K<sup>+</sup> channel S5P extracellular linker: role of an amphipathic alpha-helix in C-type inactivation. *J Biol Chem* **278**, 42136-42148.
- TRISTANI-FIROUZI, M. & SANGUINETTI, M. C. (1998). Voltage-dependent inactivation of the human K<sup>+</sup> channel KvLQT1 is eliminated by association with minimal K<sup>+</sup> channel (mink) subunits. *J Physiol* **510 ( Pt 1)**, 37-45.
- TRUDEAU, M. C., WARMKE, J. W., GANETZKY, B. & ROBERTSON, G. A. (1995). HERG, a human inward rectifier in the voltage-gated potassium channel family. *Science* **269**, 92-95.
- TSENG, G. N. (2001). I(Kr): the hERG channel. *J Mol Cell Cardiol* **33**, 835-849.
- TSENG, G. N. (2006). Linkage between 'disruption of inactivation' and 'reduction of K<sup>+</sup> selectivity' among hERG mutants in the S5-P linker region. *J Physiol* **577**, 459-460; author reply 461-452.
- VILORIA, C. G., BARROS, F., GIRALDEZ, T., GOMEZ-VARELA, D. & DE LA PENNA, P. (2000). Differential effects of amino-terminal distal and proximal domains in the regulation of human erg K(+) channel gating. *Biophys J* **79**, 231-246.
- WANG, J., MYERS, C. D. & A., R. G. (2000). Dynamic Control of Deactivation Gating by a Soluble Amino-Terminal Domain in HERG K<sup>+</sup> Channels. *J. Gen. Physiol.* **115**, 749-758.
- WANG, J., TRUDEAU, M. C., ZAPPIA, A. M. & ROBERTSON, G. A. (1998). Regulation of deactivation by an amino terminal domain in human ether-a-go-related gene potassium channels. *J Gen Physiol* **112**, 637-647.
- WANG, S., LIU, S., MORALES, M. J., STRAUSS, H. C. & RASMUSSEN, R. L. (1997). A quantitative analysis of the activation and inactivation kinetics of HERG expressed in *Xenopus* oocytes. *J Physiol* **502 ( Pt 1)**, 45-60.
- WATANABE, E., YASUI, K., KAMIYA, K., YAMAGUCHI, T., SAKUMA, I., HONJO, H., OZAKI, Y., MORIMOTO, S., HISHIDA, H. & KODAMA, I. (2007). Upregulation of KCNE1 induces QT interval prolongation in patients with chronic heart failure. *Circ J* **71**, 471-478.
- WEERAPURA, M., NATTEL, S., CHARTIER, D., CABALLERO, R. & HEBERT, T. E. (2002). A comparison of currents carried by HERG, with and without coexpression of MiRP1, and the native rapid delayed rectifier current. Is MiRP1 the missing link? *J Physiol* **540**, 15-27.

- WILLIAMS, G. B., MCARDLE, C. A. & NAHORSKI, S. R. (1998). Acute desensitization of phospholipase C-coupled muscarinic M3 receptors but not gonadotropin-releasing hormone receptors co-expressed in alphaT3-1 cells: implications for mechanisms of rapid desensitization. *Biochem J* **333** ( Pt 2), 301-308.
- WITCHEL, H. J., DEMPSEY, C. E., SESSIONS, R. B., PERRY, M., MILNES, J. T., HANCOX, J. C. & MITCHESON, J. S. (2004). The low-potency, voltage-dependent HERG blocker propafenone--molecular determinants and drug trapping. *Mol Pharmacol* **66**, 1201-1212.
- YANG, B. F., XU, D. H., XU, C. Q., LI, Z., DU, Z. M., WANG, H. Z. & DONG, D. L. (2004). Inactivation gating determines drug potency: a common mechanism for drug blockade of HERG channels. *Acta Pharmacol Sin* **25**, 554-560.
- ZAGOTTA, W. N., OLIVIER, N. B., BLACK, K. D., YOUNG, E. C., OLSON, R. & GOUAUX, E. (2003). Structural basis for modulation and agonist specificity of HCN pacemaker channels. *Nature* **425**, 200-205.
- ZUNKLER, B. J. (2006). Human ether-a-go-go-related (HERG) gene and ATP-sensitive potassium channels as targets for adverse drug effects. *Pharmacol Ther* **112**, 12-37.
- JIANG, M., ZHANG, M., MASLENNIKOV, I. V., LIU, J., WU, D. M., KOROLKOVA, Y. V., ARSENIYEV, A. S., GRISHIN, E. V. & TSENG, G. N. (2005). Dynamic conformational changes of extracellular S5-P linkers in the hERG channel. *J Physiol* **569**, 75-89.
- JIANG, Y., LEE, A., CHEN, J., CADENE, M., CHAIT, B. T. & MACKINNON, R. (2002). The open pore conformation of potassium channels. *Nature* **417**, 523-526.
- JIANG, Y., LEE, A., CHEN, J., RUTA, V., CADENE, M., CHAIT, B. T. & MACKINNON, R. (2003). X-ray structure of a voltage-dependent K<sup>+</sup> channel. *Nature* **423**, 33-41.
- KAMIYA, K., MITCHESON, J. S., YASUI, K., KODAMA, I. & SANGUINETTI, M. C. (2001). Open channel block of HERG K(+) channels by vesnarinone. *Mol Pharmacol* **60**, 244-253.
- KAMIYA, K., NIWA, R., MITCHESON, J. S. & SANGUINETTI, M. C. (2006). Molecular Determinants of hERG Channel Block. *Mol Pharmacol*.
- KUO, A., GULBIS, J. M., ANTCLIFF, J. F., RAHMAN, T., LOWE, E. D., ZIMMER, J., CUTHBERTSON, J., ASHCROFT, F. M., EZAKI, T. & DOYLE, D. A. (2003). Crystal structure of the potassium channel KirBac1.1 in the closed state. *Science* **300**, 1922-1926.
- LEES-MILLER, J. P., DUAN, Y., TENG, G. Q. & DUFF, H. J. (2000). Molecular determinant of high-affinity dofetilide binding to HERG1 expressed in *Xenopus* oocytes: involvement of S6 sites. *Mol Pharmacol* **57**, 367-374.
- LIU, J., ZHANG, M., JIANG, M. & TSENG, G. N. (2002). Structural and functional role of the extracellular s5-p linker in the HERG potassium channel. *J Gen Physiol* **120**, 723-737.
- LONG, S. B., CAMPBELL, E. B. & MACKINNON, R. (2005). Crystal structure of a mammalian voltage-dependent Shaker family K<sup>+</sup> channel. *Science* **309**, 897-903.
- LONG, S. B., TAO, X., CAMPBELL, E. B. & MACKINNON, R. (2007). Atomic structure of a voltage-dependent K<sup>+</sup> channel in a lipid membrane-like environment. *Nature* **450**, 376-382.
- MADEJA, M., LEICHER, T., FRIEDERICH, P., PUNKE, M. A., HAVERKAMP, W., MUSSHOF, U., BREITHARDT, G. & SPECKMANN, E. J. (2003). Molecular site of action of the antiarrhythmic drug propafenone at the voltage-operated potassium channel Kv2.1. *Mol Pharmacol* **63**, 547-556.
- MACKINNON, R. (2003). Potassium channels. *FEBS Lett* **555**, 62-65.

- MCDONALD, T. V., YU, Z., MING, Z., PALMA, E., MEYERS, M. B., WANG, K. W., GOLDSTEIN, S. A. & FISHMAN, G. I. (1997). A minK-HERG complex regulates the cardiac potassium current I(Kr). *Nature* **388**, 289-292.
- MCNICHOLAS, C. M., WANG, W., HO, K., HEBERT, S. C. & GIEBISCH, G. (1994). Regulation of ROMK1 K<sup>+</sup> channel activity involves phosphorylation processes. *Proc Natl Acad Sci U S A* **91**, 8077-8081.
- MILNES, J. T., DEMPSEY, C. E., RIDLEY, J. M., CROCIANI, O., ARCANGELI, A., HANCOX, J. C. & WITCHEL, H. J. (2003). Preferential closed channel blockade of HERG potassium currents by chemically synthesised BeKm-1 scorpion toxin. *FEBS Lett* **547**, 20-26.
- MITCHESON, J. S. (2003). Drug binding to HERG channels: evidence for a 'non-aromatic' binding site for fluvoxamine. *Br J Pharmacol* **139**, 883-884.
- MITCHESON, J. S., CHEN, J., LIN, M., CULBERSON, C. & SANGUINETTI, M. C. (2000a). A structural basis for drug-induced long QT syndrome. *Proc Natl Acad Sci U S A* **97**, 12329-12333.
- MITCHESON, J. S., CHEN, J. & SANGUINETTI, M. C. (2000b). Trapping of a methanesulfonanilide by closure of the HERG potassium channel activation gate. *J Gen Physiol* **115**, 229-240.
- MORAIS CABRAL, J. H., LEE, A., COHEN, S. L., CHAIT, B. T., LI, M. & MACKINNON, R. (1998). Crystal structure and functional analysis of the HERG potassium channel N terminus: a eukaryotic PAS domain. *Cell* **95**, 649-655.
- MORGAN, T. K., JR. & SULLIVAN, M. E. (1992). An overview of class III electrophysiological agents: a new generation of antiarrhythmic therapy. *Prog Med Chem* **29**, 65-108.
- OSTERBERG, F. & AQVIST, J. (2005). Exploring blocker binding to a homology model of the open hERG K<sup>+</sup> channel using docking and molecular dynamics methods. *FEBS Lett* **579**, 2939-2944.
- PEARLSTEIN, R. A., VAZ, R. J., KANG, J., CHEN, X. L., PREOBRAZHENSKAYA, M., SHCHEKOTIKHIN, A. E., KOROLEV, A. M., LYSENKOVA, L. N., MIROSHNIKOVA, O. V., HENDRIX, J. & RAMPE, D. (2003). Characterization of HERG potassium channel inhibition using CoMSiA 3D QSAR and homology modeling approaches. *Bioorg Med Chem Lett* **13**, 1829-1835.
- PERRY, M., DE GROOT, M. J., HELLIWELL, R., LEISHMAN, D., TRISTANI-FIROUZI, M., SANGUINETTI, M. C. & MITCHESON, J. (2004). Structural determinants of HERG channel block by clofilium and ibutilide. *Mol Pharmacol* **66**, 240-249.
- PERRY, M., STANSFELD, P. J., LEANEY, J., WOOD, C., DE GROOT, M. J., LEISHMAN, D., SUTCLIFFE, M. J. & MITCHESON, J. S. (2006). Drug binding interactions in the inner cavity of HERG channels: molecular insights from structure-activity relationships of clofilium and ibutilide analogs. *Mol Pharmacol* **69**, 509-519.
- RANGANATHAN, R., LEWIS, J. H. & MACKINNON, R. (1996). Spatial localization of the K<sup>+</sup> channel selectivity filter by mutant cycle-based structure analysis. *Neuron* **16**, 131-139.
- RODEN, D. M., BALSER, J. R., GEORGE, A. L., JR. & ANDERSON, M. E. (2002). Cardiac ion channels. *Annu Rev Physiol* **64**, 431-475.
- SANCHEZ-CHAPULA, J. A., FERRER, T., NAVARRO-POLANCO, R. A. & SANGUINETTI, M. C. (2003). Voltage-dependent profile of human ether-a-go-go-related gene channel block is influenced by a single residue in the S6 transmembrane domain. *Mol Pharmacol* **63**, 1051-1058.

- SANCHEZ-CHAPULA, J. A., NAVARRO-POLANCO, R. A., CULBERSON, C., CHEN, J. & SANGUINETTI, M. C. (2002). Molecular determinants of voltage-dependent human ether-a-go-go related gene (HERG) K<sup>+</sup> channel block. *J Biol Chem* **277**, 23587-23595.
- SANGUINETTI, M. C., CURRAN, M. E., SPECTOR, P. S. & KEATING, M. T. (1996). Spectrum of HERG K<sup>+</sup>-channel dysfunction in an inherited cardiac arrhythmia. *Proc Natl Acad Sci U S A* **93**, 2208-2212.
- SANGUINETTI, M. C., JIANG, C., CURRAN, M. E. & KEATING, M. T. (1995). A mechanistic link between an inherited and an acquired cardiac arrhythmia: HERG encodes the IKr potassium channel. *Cell* **81**, 299-307.
- SANGUINETTI, M. C. & TRISTANI-FIROUZI, M. (2006). hERG potassium channels and cardiac arrhythmia. *Nature* **440**, 463-469.
- SANGUINETTI, M. C. & XU, Q. P. (1999). Mutations of the S4-S5 linker alter activation properties of HERG potassium channels expressed in *Xenopus* oocytes. *J Physiol* **514 ( Pt 3)**, 667-675.
- SCHONHERR, R., HEHL, S., TERLAU, H., BAUMANN, A. & HEINEMANN, S. H. (1999). Individual subunits contribute independently to slow gating of bovine EAG potassium channels. *J Biol Chem* **274**, 5362-5369.
- SCHONHERR, R. & HEINEMANN, S. H. (1996). Molecular determinants for activation and inactivation of HERG, a human inward rectifier potassium channel. *J Physiol* **493 ( Pt 3)**, 635-642.
- SHRIVASTAVA, I. H. & BAHAR, I. (2006). Common mechanism of pore opening shared by five different potassium channels. *Biophys J* **90**, 3929-3940.
- SMITH, P. L., BAUKROWITZ, T. & YELLEN, G. (1996). The inward rectification mechanism of the HERG cardiac potassium channel. *Nature* **379**, 833-836.
- SPECTOR, P. S., CURRAN, M. E., KEATING, M. T. & SANGUINETTI, M. C. (1996a). Class III antiarrhythmic drugs block HERG, a human cardiac delayed rectifier K<sup>+</sup> channel. Open-channel block by methanesulfonanilides. *Circ Res* **78**, 499-503.
- SPECTOR, P. S., CURRAN, M. E., ZOU, A., KEATING, M. T. & SANGUINETTI, M. C. (1996b). Fast inactivation causes rectification of the IKr channel. *J Gen Physiol* **107**, 611-619.
- STANSFELD, P. J., GEDECK, P., GOSLING, M., COX, B., MITCHESON, J. S. & SUTCLIFFE, M. J. (2007). Drug block of the hERG potassium channel: insight from modeling. *Proteins* **68**, 568-580.
- STANSFELD, P. J., GROTTESI, A., SANDS, Z. A., SANSOM, M. S., GEDECK, P., GOSLING, M., COX, B., STANFIELD, P. R., MITCHESON, J. S. & SUTCLIFFE, M. J. (2008). Insight into the mechanism of inactivation and pH sensitivity in potassium channels from molecular dynamics simulations. *Biochemistry* **47**, 7414-7422.
- TAMARGO, J., CABALLERO, R., GOMEZ, R., VALENZUELA, C. & DELPON, E. (2004). Pharmacology of cardiac potassium channels. *Cardiovasc Res* **62**, 9-33.
- TANG, X. D. & HOSHI, T. (1999). Rundown of the hyperpolarization-activated KAT1 channel involves slowing of the opening transitions regulated by phosphorylation. *Biophys J* **76**, 3089-3098.
- TERLAU, H., HEINEMANN, S., STUHMER, W., PONGS, O. & LUDWIG, J. (1997). Amino terminal-dependent gating of the potassium channel rat eag is compensated by a mutation in the S4 segment. *J Physiol (Lond)* **502**, 537-543.

- THOMAS, D., ZHANG, W., WU, K., WIMMER, A. B., GUT, B., WENDT-NORDAHL, G., KATHOFER, S., KREYE, V. A., KATUS, H. A., SCHOELS, W., KIEHN, J. & KARLE, C. A. (2003). Regulation of HERG potassium channel activation by protein kinase C independent of direct phosphorylation of the channel protein. *Cardiovasc Res* **59**, 14-26.
- TORRES, A. M., BANSAL, P. S., SUNDE, M., CLARKE, C. E., BURSILL, J. A., SMITH, D. J., BAUSKIN, A., BREIT, S. N., CAMPBELL, T. J., ALEWOOD, P. F., KUCHEL, P. W. & VANDENBERG, J. I. (2003). Structure of the HERG K<sup>+</sup> channel S5P extracellular linker: role of an amphipathic alpha-helix in C-type inactivation. *J Biol Chem* **278**, 42136-42148.
- TRISTANI-FIROUZI, M. & SANGUINETTI, M. C. (1998). Voltage-dependent inactivation of the human K<sup>+</sup> channel KvLQT1 is eliminated by association with minimal K<sup>+</sup> channel (minK) subunits. *J Physiol* **510 ( Pt 1)**, 37-45.
- TRUDEAU, M. C., WARMKE, J. W., GANETZKY, B. & ROBERTSON, G. A. (1995). HERG, a human inward rectifier in the voltage-gated potassium channel family. *Science* **269**, 92-95.
- TSENG, G. N. (2001). I(Kr): the hERG channel. *J Mol Cell Cardiol* **33**, 835-849.
- TSENG, G. N. (2006). Linkage between 'disruption of inactivation' and 'reduction of K<sup>+</sup> selectivity' among hERG mutants in the S5-P linker region. *J Physiol* **577**, 459-460; author reply 461-452.
- VILORIA, C. G., BARROS, F., GIRALDEZ, T., GOMEZ-VARELA, D. & DE LA PENNA, P. (2000). Differential effects of amino-terminal distal and proximal domains in the regulation of human erg K(+) channel gating. *Biophys J* **79**, 231-246.
- WANG, J., MYERS, C. D. & A., R. G. (2000). Dynamic Control of Deactivation Gating by a Soluble Amino-Terminal Domain in HERG K<sup>+</sup> Channels. *J. Gen. Physiol.* **115**, 749-758.
- WANG, J., TRUDEAU, M. C., ZAPPIA, A. M. & ROBERTSON, G. A. (1998). Regulation of deactivation by an amino terminal domain in human ether-a-go-go-related gene potassium channels. *J Gen Physiol* **112**, 637-647.
- WANG, S., LIU, S., MORALES, M. J., STRAUSS, H. C. & RASMUSSEN, R. L. (1997). A quantitative analysis of the activation and inactivation kinetics of HERG expressed in *Xenopus* oocytes. *J Physiol* **502 ( Pt 1)**, 45-60.
- WATANABE, E., YASUI, K., KAMIYA, K., YAMAGUCHI, T., SAKUMA, I., HONJO, H., OZAKI, Y., MORIMOTO, S., HISHIDA, H. & KODAMA, I. (2007). Upregulation of KCNE1 induces QT interval prolongation in patients with chronic heart failure. *Circ J* **71**, 471-478.
- WEERAPURA, M., NATTEL, S., CHARTIER, D., CABALLERO, R. & HEBERT, T. E. (2002). A comparison of currents carried by HERG, with and without coexpression of MiRP1, and the native rapid delayed rectifier current. Is MiRP1 the missing link? *J Physiol* **540**, 15-27.
- WILLIAMS, G. B., MCARDLE, C. A. & NAHORSKI, S. R. (1998). Acute desensitization of phospholipase C-coupled muscarinic M3 receptors but not gonadotropin-releasing hormone receptors co-expressed in alphaT3-1 cells: implications for mechanisms of rapid desensitization. *Biochem J* **333 ( Pt 2)**, 301-308.
- WITCHEL, H. J., DEMPSEY, C. E., SESSIONS, R. B., PERRY, M., MILNES, J. T., HANCOX, J. C. & MITCHESON, J. S. (2004). The low-potency, voltage-dependent HERG blocker propafenone--molecular determinants and drug trapping. *Mol Pharmacol* **66**, 1201-1212.

- YANG, B. F., XU, D. H., XU, C. Q., LI, Z., DU, Z. M., WANG, H. Z. & DONG, D. L. (2004). Inactivation gating determines drug potency: a common mechanism for drug blockade of HERG channels. *Acta Pharmacol Sin* **25**, 554-560.
- ZAGOTTA, W. N., OLIVIER, N. B., BLACK, K. D., YOUNG, E. C., OLSON, R. & GOUAUX, E. (2003). Structural basis for modulation and agonist specificity of HCN pacemaker channels. *Nature* **425**, 200-205.
- ZUNKLER, B. J. (2006). Human ether-a-go-go-related (HERG) gene and ATP-sensitive potassium channels as targets for adverse drug effects. *Pharmacol Ther* **112**, 12-37.